

Middlesex University Research Repository:

an open access repository of
Middlesex University research

<http://eprints.mdx.ac.uk>

Baria, Roy, 1986.
The Use of Seismic Techniques to Identify Hazardous
Ground Conditions Associated with Cavities.
Available from Middlesex University's Research Repository.

Copyright:

Middlesex University Research Repository makes the University's research available electronically.

Copyright and moral rights to this thesis/research project are retained by the author and/or other copyright owners. The work is supplied on the understanding that any use for commercial gain is strictly forbidden. A copy may be downloaded for personal, non-commercial, research or study without prior permission and without charge. Any use of the thesis/research project for private study or research must be properly acknowledged with reference to the work's full bibliographic details.

This thesis/research project may not be reproduced in any format or medium, or extensive quotations taken from it, or its content changed in any way, without first obtaining permission in writing from the copyright holder(s).

If you believe that any material held in the repository infringes copyright law, please contact the Repository Team at Middlesex University via the following email address:
eprints@mdx.ac.uk

The item will be removed from the repository while any claim is being investigated.

THE USE OF SEISMIC TECHNIQUES TO IDENTIFY HAZARDOUS
GROUND CONDITIONS ASSOCIATED WITH CAVITIES

A thesis submitted by Roy Baria, BSc, CEng, MIEE
in partial fulfilment of the requirements
for the degree of Master of Philosophy
of the Council for National Academic Awards

March 1986

Sponsoring Establishment:

Middlesex Polytechnic
Bounds Green Road
LONDON N11 2NQ

Collaborating Establishment:

British Geological Survey
Nicker Hill
KEYWORTH
Nottingham NG12 5GG

ac8007A

DECLARATION

THIS IS TO CERTIFY that the work submitted for the degree of Master of Philosophy under the title "The use of seismic techniques to identify hazardous ground conditions associated with cavities" is the result of the candidate's own investigation. All authors and assistance received has been acknowledged.

Signed A. Baria Candidate

Signed A.F. Goldspink Director of Studies

Signed D.V. McLann Industrial Supervisor

This work has not already been accepted in substance for any degree, and is not being concurrently submitted in candidature for any other degree.

Signed A. Baria Candidate

CONTENTS

		PAGE
	ABSTRACT	1
1	INTRODUCTION	2
2	CAVITIES	4
2:1	Man-made cavities	4
2:1:1	Mining tunnels and excavations	4
2:1:2	Solution mines	6
2:2	Natural cavities	8
3	SEISMIC WAVES IN SEDIMENTS AND SOFT ROCKS	10
3:1	Relationship between elastic constants and seismic velocity	11
3:2	Wave propagation theories for suspensions	13
3:3	Wave propagation theories for porous solids	16
3:4	Wave propagation theories for granular media	17
3:5	Compression wave measurements in sediments and soft rocks	18
3:6	Attenuation measurements in sediments and soft rocks	20
3:7	Conclusions	21
4	SURFACE SEISMIC METHODS	23
4:1	Seismic refraction method	24
4:1:1	Theory and principles	25
4:1:2	Seismic refraction survey at Cocking	29
4:1:3	Results and discussion	38
4:1:4	Development of the Time Delay image Enhancement method (TIDE)	43
4:2	Seismic reflection method	63
4:2:1	Theory and principles	64
4:2:2	Case histories	69
4:3	Seismic resonance method	78
4:3:1	Theory and principles	78
4:3:2	Case histories	79
5	BOREHOLE SEISMIC METHODS	86
5:1	Interborehole seismic method	86
5:1:1	Experimental procedures for interborehole seismics	87
5:1:2	Interborehole seismics at Cocking	92
5:1:3	Interborehole seismics at Maidstone	105
5:2	Surface to borehole seismic method	117
5:2:1	Theory and principles	118
5:2:2	Experimental procedure for surface to borehole seismic method	121
5:2:3	Surface to borehole seismics at Cocking	122
6	DEVELOPMENT OF SINGLE HOLE METHOD (ACDER)	129
6:1	Laboratory model study	133
6:1:1	Seismic source	136
6:1:2	Directional receiver	161
6:1:3	Instrumentation and display	179
6:1:4	The effect of a cylindrical obstruction/target on a propagating seismic pulse	187

	PAGE	
6:2	Borehole sparker source	193
6:2:1	High resolution sparker probe (HRSP)	196
6:2:2	Free field measurements	198
6:2:3	Radiation patterns from a seismic source in a borehole	209
6:3	Field trial of the single hole method	213
6:3:1	Geology and borehole configuration	213
6:3:2	In-situ compressional wave velocity structure	215
6:3:3	Field trial of the ACDER system	215
6:3:4	Interborehole measurements	219
7	DISCUSSION	225
7:1	Surface seismic methods	226
7:2	Borehole seismic methods	229
7:3	Single hole method	231
8	CONCLUSIONS	234
9	RECOMMENDATIONS	236
10	ACKNOWLEDGEMENTS	238
11	REFERENCES	239
APPENDIX		
I	Fracture log of cores from borehole No 3 (Cocking site)	252
II	Seismic resonance survey	255
III	Design of a high voltage capacitor discharge unit	259
IV	List of DIPRAT program	269

ABSTRACT

The identification of civil engineering hazards such as cavities, mine shafts, etc., is an integral part of site investigations carried out prior to the construction of roads, tunnels and other civil engineering structures. The use of geophysical methods to identify these hazards is becoming increasingly important.

An investigation into the effectiveness of three seismic methods to delineate the possible anomalous ground conditions associated with the presence of cavities has been evaluated. The three methods are: surface, interborehole and a single hole method.

The surface seismic method (refraction) was used successfully over a disused railway tunnel to identify the presence of a cavity, and a technique was developed to generate images of a theoretical model, which can be compared to a field survey.

The interborehole seismic method was used across a disused railway tunnel to study the effect of a cavity on changes in seismic parameters, such as compressional wave velocity and attenuation. Both of these parameters were sensitive to the presence of a large cavity, and the successful application of the technique is demonstrated in the Maidstone survey, where the presence of loosely packed sand (due to sinkholes in the vicinity) was located under a house.

The use of the single hole method for detecting cavities is a new technique (ACDER) in seismics, and it is analogous to methods of radar detection. A sparker source, directional receiver and associated instrumentation were developed in the laboratory before field trials at East Fleet.

Of the three methods, the interborehole technique was the most successful, followed by the surface method. The single hole method looks promising but requires further work in the design of directional receiving transducers, followed by more field trials.

1 INTRODUCTION

With the increasing demand for suitable land, areas which have been previously considered dangerous for fear of subsidence, as a result of hazardous ground conditions associated with the presence of a cavity, are becoming important. Tunnels are often required wherever the topography is unsuitable for surface routes or where the ground surface is already occupied by existing works. Thus tunnels for roads or railways are required to be driven under rivers or beneath areas of urban development. The scope for a conventional civil engineering site investigation is severely limited by the same physical conditions which render a surface route impractical.

The extraction of raw material such as coal, ironstone etc by underground mining has always been a hazardous occupation. The possibility of a disaster occurring if the tunnelling or mining machine intersects a disused tunnel or cavity is always present, especially if the disused tunnels or cavities are filled with water or slurry. An example of this type of disaster occurred at the Lofthouse Colliery, where a disused mine shaft was penetrated by the face cutters, causing the flooding of the mine face and the loss of lives.

Geophysical techniques (Refs 1, 2) have been used successfully to delineate large geological discontinuities such as faults, oil reservoirs or mineral ore deposits. The effectiveness of most geophysical techniques diminishes as the physical dimensions of the discontinuity become smaller. In particular the geological variations within the stratified deposits may have greater influence on geophysical measurements than the presence of a small discontinuity. The extraction of useful information from the background geological variations will depend on the selection of an appropriate geophysical technique to enhance the identification of the discontinuity from perturbations generated by the geological variations.

Of all the geophysical techniques available for investigating small geological discontinuities, the seismic method appears to lend itself most readily for manipulation because of the number of seismic propagation parameters available for interpretation, such as velocity, amplitude, reflection etc of compressional and shear waves.

The possibility of adopting standard seismic site investigation techniques to the working face in mines and tunnels has been discussed previously (Baria, 1974; Ref 3). It was suggested that it may be possible to use the customary exploratory horizontal boreholes on the cutting face to carry out interborehole seismic, borehole to cutting face seismic, and the development of a single hole reflection seismic technique. These methods have been investigated in this research programme and the single hole method has also been partially developed.

2 CAVITIES

Cavities by definition are hollow spaces in a geological formation, formed either by natural processes or by man. Cavities can be air filled or infilled; in the latter case in particular a great danger may be presented to the safety in a mining environment. Near-surface cavities can be hazardous for civil engineering installations, in particular, when large structures are constructed above or near it. Severe change in weather, such as a very dry summer followed by a torrential rain, or excessive loading above an unknown cavity, may cause the ground to subside and create a hazardous situation. The discussion on cavities is classified in terms of their formation, as either man-made or natural.

2:1 Man-made cavities

Man-made cavities are generally created by mining for raw materials or civil engineering works such as tunnels and basements. Legislation to register plans of mine workings was not made compulsory until 1872 (Littlejohn, 1979; Ref 4) and it is estimated that over 30 000 unrecorded workings exist from operations carried out before the legislation. Old civil engineering structures can be demolished without legislation to compel registration of the plans of the demolished work, which also poses a great danger to subsequent civil engineering construction on the same site.

2:1:1 Mining tunnels and excavations

The need for valuable earth materials has produced numerous underground workings over the centuries. Not until 1872 was it made compulsory in Britain for detailed plans of mine workings and shafts to be submitted to the local authorities; up until this time, it has been estimated that a total of 4 000 000 000 tons of coal, ironstone and other economic materials have been extracted. Removal of such large quantities has left many areas where workings are liable to collapse, producing subsidence at surface. Unfortunately, these workings are the most difficult to locate because no records of their existence survive, and are hazardous because in these early times workings were necessarily shallow (Table 2:1).

TABLE 2:1 RECORD OF COLLIERY SHAFTS IN THE EASTERN DISTRICT OF SCOTLAND IN 1873 (AFTER MAXWELL, 1975)

Depth of shaft (m)	Downcast (f)	Shaft (%)	Upcast (f)	Shaft (%)	Total (%)
< 30	60	16	69	22	19
30-60	116	33	91	29	31
60-90	67	18	64	21	20
90-120	49	13	36	12	13
>120	71	20	45	16	17

Coal mining development in Britain was likely to have followed closely that of Scotland, of which Maxwell (1971; Ref 5) has made an extensive study. The earliest known method of working coal (apart from open cast) was pillar and room, and it was not until 1867 that an improved method, introduced from Newcastle, was in general use. For the Newcastle method, large pillars were left behind by a first working, and then systematically reduced by a second working, for greater coal yield. Both methods were similar and left numerous interconnected voids, but the Newcastle rooms were consistently larger than those of the older method (Table 2:2). This meant that the smaller pillars remaining in the Newcastle method were in many cases unable to support the roof of the working, with subsequent collapse.

Once a mine could no longer produce coal economically the shaft was abandoned and sealed, and the colliery area was levelled by filling in any small pits. It was common practice to block the shaft just below the surface with a wooden platform, and fill the remaining small space with waste material.

The popular use of steam engines after about 1725 at colliery works produced large quantities of ash, which are magnetic, probably because of their iron content and heat of formation. Fortunately, the extensive use of this magnetic material for capping the shaft, and its shallowness, make it possible to locate abandoned shafts with geophysical methods (Maxwell, 1975, Ref 6; Jackson and Suddaby, 1979,

Ref 7). A magnetometer is used to measure variation in the earth's magnetic field influenced by the magnetic infill. In Scotland, the majority of mine shafts were wooden lined, whereas those of England and Wales were usually brick lined, and these bricks can aid detection of each shaft because of their magnetic content.

TABLE 2:2 PROBABLE AREA OF GROUND WORKED BY PILLAR AND ROOM METHODS IN SCOTLAND PRIOR TO 1873 (AFTER MAXWELL, 1975)

	Prior to 1760	1760- 1800	1800- 1850	1850- 1872
Conjectural output (tonnes x 10)	30	30	145	260
Conjectural output of pillar and room workings (tonnes x 10)				
i Old method	30	25	100	0
ii Newcastle method	0	0	20	130
Conjectural area of pillar and room workings (hectares)				
i Old method	3000	2500	10000	0
ii Newcastle method	0	0	1100	7000
Conjectural area of pillar and room workings <120 m deep (hectares)				
i Old method	3000	2500	9000	0
ii Newcastle method	0	0	500	2000
Assumptions:		Average thickness of seam worked (m)	Amount of seam extracted (%)	
i Old method		1.25	-60	
ii Newcastle method		1.75	+80	

2:1:2 Solution mines

Controlled solution mining is popular in many countries for obtaining valuable minerals from the evaporite horizons; Cheshire is the most important salt producing area in Britain. The basic method (Collins, 1969; Ref 8) is to introduce water under sufficient pressure into

evaporite horizons to dissolve it and raise the evaporite solution to surface. The pumping is carefully monitored for cavities of predetermined size and shape to be formed, so that the remaining shaft will produce sufficient support for the overburden and thus prevent collapse. Each cavity is developed over several years and left free of saturated brine once the maximum size for safety is reached. The size and spacing of these solution cavities is related to the thickness of beds being worked, and it is claimed that they can be made permanently stable.

The knowledge gained in controlled solution mining has been utilised in another equally important field of storing toxic materials. Environmental pressures to dispose safely of toxic waste (including radioactive substances) have led to new methods of waste disposal (Horner, 1971; Ref 9). Cavities are now produced artificially in evaporite horizons so that they can be used for the storage of fluid and toxic waste. Salt is ideal for storage because of its high impermeability, and the formation of cavities can be carefully controlled.

Before the introduction of controlled solution mining, the method of salt extraction consisted of mining and wild brine pumping; in Cheshire only one salt mine is still active and wild brine pumping has been discontinued because of its often catastrophic results.

Salt mines prior to the twentieth century had a life expectancy of thirty or forty years, and flooding and eventual collapse followed their abandonment.

Wild brine pumping consisted of sinking wells to where the circulation of natural groundwater dissolved the salt at the wet rock head, often at depths greater than 70 m; the brine was then pumped to the surface. With the increasing demand for salt, water was pumped down to increase the dissolution. Unfortunately, this often led to uncontrolled cavity formation, much of which became extensive; and without the required overburden support, subsidence at the surface often resulted.

Frequent collapse as a result of mining and pumping operations was common by the end of the eighteenth century in the industrialised salt extraction centres of Cheshire. The last catastrophic collapse in Cheshire was at the Adelaide mine in 1928; since then, the increased safety standards and improved methods of salt extraction have greatly reduced serious subsidence, although gentle settling occurs in some areas.

2:2 Natural cavities

The predominant form of natural cavity results from solution of suitable deposits. Cavities in limestone (eg, Carboniferous limestone of South Wales) and chalk are formed by percolating groundwater acting as a carrier of dissolved oxygen and carbon dioxide, together with various acids and organic products derived from the soil. The acidity of such solutions derives mainly from the dissolved carbon dioxide, which slowly dissolves in turn the calcium carbonate, to be removed as sodium bicarbonate. Over extensive periods, the continual passage of acidic groundwater along joints and bedding planes can create extremely large cavities (eg Victoria Cave, Yorkshire). The surface opening to the passage of underground water often becomes enlarged in favourable areas and funnel shaped holes, known as swallow or sink holes, are developed. Limestone areas which have been extensively eroded by solution, with large depressions resulting from the collapse of cave roofs, and underground drainage in places of surface streams, are known as karst regions.

Cavities may be produced in evaporite deposits as a result of the action of circulating groundwater to dissolve and remove large amounts of the evaporite. The prolonged dissolution of such deposits is usually accompanied by a gradual settling of the overburden to produce large surface depressions which, in Cheshire, may be as large as 600 ft in diameter. Colley (1963; Ref 10) has noted topographical depressions in parts of Iraq several miles across and sometimes over 40 m deep, which are considered to be the result of the leaching away of anhydrite, followed by the collapse of the cave roof; it is possible that large cavities in the same area exist which have not collapsed.

A form of natural cavity which does not result from solution is the lava tube. As lava flows down a slope, it loses heat from its surface by radiation until eventually a crust forms. Flow continues beneath the forming crust and, in some cases, molten lava may flow completely away, leaving a thin crust covering a tubular cavity known as a lava tube. The formation of large lava tubes is fairly rare, but some have been known to be over 1 km in length.

It has been noted that cavity collapse can be related in some cases to the falling of the water level of an area, with the result that the void of the roof can no longer support the overburden. Cases have been reported in South Wales (Waller, 1972; Ref 11), for example, where regions which have previously been unaffected have suddenly been prone to cavity collapse, because the groundwater level had been lowered to enable limestone to be quarried nearby. Similar disastrous effects have been noted (Snowdowne, 1968; Ref 12) following the drainage of mining levels some 1000 m deep in South Africa. The drainage accelerated the collapse of cavities in dolomite near the water table some 100 m below the surface. Ten years after the pumping commenced, large depressions began to appear at the surface, the largest of which was 120 m in diameter and 40 m deep.

3 SEISMIC WAVES IN SEDIMENTS AND SOFT ROCKS

The word 'seismic' is derived from the Greek word 'seiein', which means 'to shake', and as the word implies seismics is a discipline of geophysics which deals with vibrations associated with an elastic body. A major proportion of seismic theory was developed before sufficiently sensitive instruments were available to permit significant measurements to be made.

Earthquake seismology preceded its applications in the exploration field. Attempts to measure seismic velocities were made by Mallet as early as 1845, while Knott developed the theory of refraction and reflection at an interface in 1899, and Zoeppritz and Wichert published their findings on wave theory in 1907.

Applied seismology is used primarily for exploration of natural resources, such as oil and gas reservoirs in sedimentary regions, but it also offers an effective and most economical tool for evaluation of dynamic elastic moduli, as well as measuring the thickness of different geological layers of ground required for site investigation in civil engineering.

Velocities of seismic wave propagation in the field can be determined by measuring travel times of single elastic pulses along well defined wave paths, using refraction, reflection or borehole transmission techniques.

The simplest type of wave propagated in a homogeneous, infinite, elastic medium consists of alternating compressions and rarefactions, during which process adjacent particles along any line in the direction of the waves are, respectively, closer together or farther apart than normal. Such waves are referred to as compressional waves, and their particle motion is in the direction of propagation.

For shear waves, particle motion is perpendicular to the direction of propagation. Shear waves can be polarised in both vertical and horizontal directions. Those produced by particle motion in the vertical mode are called vertical shear (SV), while shear waves with particle motion in the horizontal mode are called horizontal shear (SH).

In addition to body waves, there are also surface waves which in principle are plane waves, in which strain energy travels along the geological interface. Surface waves are defined as either Rayleigh waves or Love waves. The distinction between the two is in their particle motion: in Love waves it is horizontally polarised and transverse to wave propagation, whilst in Rayleigh waves it is elliptical and retrograde with respect to propagation, and vertically polarised.

There are two fundamental parameters for seismic wave propagation. The first is the time taken for a P wave to travel a specific distance, referred to as the velocity of propagation, and the second is the loss of energy over a specific distance, which is loosely grouped under the heading of attenuation.

Both of these parameters are affected by geological variations, discontinuities and relative geometry of the geological formation. Variations in seismic properties may be used to identify zones of discontinuity by selection of an appropriate source and receiver geometry.

3:1 Relationship between elastic constants and seismic velocity

Derivation of compressional and shear wave velocity using Hooke's law for elastic solids has been comprehensively discussed by Telford et al (1976; Ref 13), White (1965; Ref 14), Dobrin (1976; Ref 15), Grant and West (1965; Ref 16) and many others.

Seismic velocity depends mainly on compressibility and shear resistivity of the propagating medium, which is the geological formation. Two types of elastic waves propagate through an infinite, homogeneous, isotropic, perfectly elastic medium: compressional and shear waves. Velocities of these waves are related to their dynamic properties by

$$V_p = \sqrt{(\lambda + 2\mu) / \rho} \quad - (3.1)$$

and

$$V_s = \sqrt{\mu / \rho} \quad - (3.2)$$

where V_p = compressional wave velocity
 λ = Lamé's constant
 μ = shear modulus of the medium
 ρ = density of the medium

The bulk modulus k is given by

$$k = \lambda + \frac{2}{3}\mu \quad - (3.3)$$

Substituting equation (3.3) into (3.1) gives V_p in terms of k and μ

$$V_p = \sqrt{(k + (4/3)\mu)/\rho} \quad - (3.4)$$

For a given fluid media where the shear modulus (μ) is zero, the compressional wave velocity in fluid V_f can be expressed by

$$\begin{aligned} V_f &= \sqrt{(k/\rho)} \\ &= \sqrt{(1/\beta\rho)} \end{aligned} \quad - (3.5)$$

For a fluid $\mu=0$ in which case $k=\lambda$ from equation (3.3) and

$$V_f = \sqrt{\lambda/\rho} \quad - (3.6)$$

V_p and V_s can also be related to Young's modulus and Poisson's ratio. Lamé's constant is related to Young's modulus and Poisson's ratio by equations

$$E = \frac{\mu(3\lambda + 2\mu)}{(\lambda + \mu)} \quad - (3.7)$$

and
$$\nu = \frac{0.5\lambda}{(\lambda + \mu)} \quad - (3.8)$$

where E = Young's modulus
 ν = Poisson's ratio

From equation (3.2)

$$\mu = V_s^2 \rho \quad - (3.9)$$

Using equations (3.4) and (3.2)

$$k = \rho (V_p^2 - (4/3)V_s^2) \quad - (3.10)$$

From equations (3.3), (3.7), (3.8) and (3.9)

$$v = \frac{(V_p/V_s)^2 - 2}{2(V_p/V_s)^2 - 1} \quad - (3.11)$$

Following the derivation of the relationship of the seismic waves in an isotropic elastic medium, the theories which attempt to describe the propagation of seismic waves (and/or acoustic) of natural materials have been reviewed on the basis of three distinct approaches. The first approach considers the velocity of compressional waves propagating in a fluid containing suspended solid particles of variable size and concentrations. The second approach considers a porous, solid medium consisting of a solid framework with pores. Finally, the wave propagation through the material has been examined by considering a 'model' packing of elastic spheres in contact.

3:2 Wave propagation theories for suspensions

The seismic velocity through a fluid medium is related to the elastic constants of the medium as defined by equation 3.5. Solid particles suspended in a fluid behave like a fluid as long as these particles do not interact with each other either by contact or electrochemical forces. As the shear modulus in a suspension system approaches zero, the equations (3.5 & 3.6) used for defining the compressional wave velocity through a fluid are also applicable to suspensions.

An equation relating acoustic velocity to suspensions was originally developed by Wood (1940 Ref 17). Wood's equation for acoustic velocity replaces bulk density and compressibility by component terms for the water and mineral fractions, each component contributing to the bulk compressibility and bulk density of the suspension in proportion to its volume concentration in the suspension.

$$\rho = n\rho_w + (1-n)\rho_m \quad - (3.12)$$

$$\beta = n\beta_w + (1-n)\beta_m \quad - (3.13)$$

where

- ρ_m = mineral density
- β_m = mineral compressibility
- ρ_w = water density
- β_w = water compressibility
- n = fraction porosity

When equations (3.12) and (3.13) are substituted into equation (3.5), the acoustic velocity in suspension becomes

$$V_f = \left[\frac{1}{(n\beta_w + 1-n\beta_m)(n\rho_w + 1-n\rho_m)} \right]^{\frac{1}{2}} \quad - (3.14)$$

Equation 3.14 predicts that the acoustic velocity of a suspension can be lower than the individual components (ie water and minerals). Equation 3.14 is known as Wood's emulsion equation. The validity of Wood's equation was demonstrated by Urick (1947; Ref 18, 1948; Ref 19) and Urick and Ament (1949; Ref 20) by laboratory measurements using low concentration suspensions of kaolinite. Hamilton (1956; Ref 21) carried out in-situ measurements at sea which showed that the velocity through the high porosity muds were three percent lower than in the overlying water. Although the above measurements agree with the concept of Wood's equation, the measured velocity was found to be higher than predicted by the equation other than for very high porosity sediments. This suggests a possible lower limit for the acoustic velocity through most sediments rather than describing it.

The absorption of sound in a suspension of immobile particles was reviewed by Epstein (1941; Ref 22). He concluded that Sewell's (1910; Ref 23) treatise on fogs was inapplicable to aqueous suspensions because of the greater particle densities involved. Sewell's treatise were extended by Lamb (1945; Ref 24) for rigid, incompressible particles, able to move freely within the sound field. An equation for the attenuation of a compressional wave in a suspension of equal diameter spherical particles was derived by Urick (1948, Ref 19) as follows

$$2 = C_0 \left[\frac{k^4 r^3}{6} + k \left\{ \frac{\rho_s}{\rho_w} - 1 \right\}^2 \cdot \frac{S}{S^2 + ((\rho_s/\rho_w) + \tau)^2} \right] - (3.15)$$

where

- r = particle radius
- C₀ = concentration (number of particles per unit volume)
- k = wave number (2π/λ)
- λ = wavelength
- S = (9/4Br)(1+(1/Br))
- τ = ½+(9/4Br)
- B = √(ω/2q)
- ω = angular frequency
- q = kinematic viscosity of fluid

The above equation was applied by Urick (op.cit.) to homogeneous, aqueous suspensions of sand and kaolinite, of various sizes, concentrations and viscosities, and in a frequency of 1-15 MHz range. The absorption can be explained by the viscous losses at the surface of the particles because of the relative motion of the solid and fluid phases, represented by the second term on the right of the above equation, and scattering losses generated as the wavelength approaches the particle size. The scattering losses are represented by the first term on the right of the above equation.

At high frequencies, large particles remained almost stationary in the sound field and produced a loss which was proportional to the square root of frequency. At low frequency the small particles tended to move with the fluid to generate a loss proportional to frequency squared.

Ahuja (1974; Ref 25) reviewed the work relating to the derivation of relationships describing the acoustic properties of deflocculated liquid-solid mixtures with a porosity of 60-100 percent. The properties considered were compressibility, density, thermal conductivity, shear viscosity and surface tension. The suspension theories described here only take into consideration the losses attributed to the viscous interaction between the solid and liquid component of the mixture.

During early developments, Urick and Ament (1949; Ref 26) found a discrepancy between the theory and the experimental result as the particle concentration of the suspension increased above 30 percent. The failure of equations (3.14) and (3.15) was caused by inter-particle contact and acoustic dissipation by inter-particle friction. Urick's (1948; Ref 19) absorption equation has been the basis of the discussion by McCann (1969; Ref 27) and Gultepe et al (1977; Ref 28) for clay suspensions of high concentration.

3:3 Wave propagation theories for porous solids

The theories relating to the propagation of acoustic waves in porous media was provided in a quantitative basis by Lord Rayleigh (1878; Ref 29). The early theories (Morse & Bolt, 1944; Ref 30, Scott, 1945; Ref 31, Beranek, 1947; Ref 32, Zwicker & Kosten, 1949; Ref 33) were mainly concerned with room acoustics and the acoustic attributes of various porous materials.

Biot (1956a; Ref 34; and 1956b; Ref 35) gave the first comprehensive theory describing the propagation of elastic waves in the fluid-saturated porous solid. The theory discusses a range of systems in which water within the pore spaces either did or did not move in response to the stress induced by the passage of an acoustic wave. Elastic moduli of the solid, the fluid and the porous skeleton were combined to describe the couple motion of two phases. Biot (1956a; Ref 34) initially considered low frequency propagation and assumed that the flow through the pores was Poiseuille type. The theory predicts the presence of two compressional waves and one shear wave. The phase velocity of the first type of compressional wave had negligible dependence on frequency with an absorption coefficient proportional to the square of the frequency. The second type of compressional wave was highly attenuated when the pore fluid was of low compressibility. The propagation of this wave was considered to be that of a diffusion wave and analagous to heat conduction. The phase velocity of the shear wave increased slightly with frequency and absorption coefficient was as above.

In the second paper he extended the mathematical treatment to high frequency at which Poiseuille flow is not considered to be applicable. A

'structure factor' concept was introduced into the treatment which represented the effect of sinusoidality and the shape of the pores. The phase velocity was found to increase with frequency for the first type of compressional wave with the absorption coefficient proportional to the square root of the frequency. The shear wave velocity was also found to be more frequency dependent than the low flow case. The absorption coefficient was found to be proportional to the square root of the frequency.

In subsequent papers Biot (1962a; Ref 34; 1962b; Ref 35) extended his acoustic propagation theory in porous media to include inter-particle, viscoelastic and isotropic media. Biot's work was verified by numerous researchers (Geertsma and Smith, 1961; Ref 36, Wyllie et al, 1962; Ref 37) and was also used as a basis for further theoretical analysis of porous solids (Hsieh and Yew, 1973; Ref 38, Mengi and Niven, 1977; Ref 39).

3:4 Wave propagation theories for granular media

Biot's theory on the static and dynamic response of porous material was discussed in the previous chapter. Gassmann (1951; Ref 40), based on the earlier theory of porous solids, considered the elasticity of a hexagonal matrix of closely packed spheres which were deformed at points of contact because of the applied stress. The velocities of elastic waves for packing, which was considered as anisotropic and inhomogeneous, were calculated for interspaces either evacuated, filled with fluid or gas under two sets of conditions.

In the first condition, which was regarded as an 'open system', the hydrostatic pressure of the pores was considered to be constant but the pore fluid was allowed to circulate through the pores. The second condition, which was regarded as a 'closed system', did not allow pore fluid to circulate and was analogous to stress variations in the earth's interior due to earthquake waves. Gassmann's theory obtained an expression relating sound velocity to the sixth root of the depth of burial which predicts the variation of velocity with depth. This was also observed experimentally by Faust (1960; Ref 41).

Gassmann's theory was extended by White and Sengbush (1953; Ref 42) and Duffy and Mindlin (1957; Ref 43) to include tangential forces between spheres. Brandt (1955; Ref 44 and 1960; Ref 45) developed theoretical equations for acoustic velocity to include the effect of pressure and liquid saturation in an aggregate of randomly arranged spherical particles of different sizes.

White (1966; Ref 46) modified the expression derived by Duffy and Mindlin (1957; Ref 43) to include both static and dynamic friction (sticking and sliding) of spheres at the point of contact. The attenuation coefficient was shown to be a function of the tangential forces between the spheres and directly proportional to frequency. Gassmann's theory on the 'closed system' was used by Hamilton (1971a; Ref 47, 1971b; Ref 48, and 1972; Ref 49) to predict the acoustic properties of water saturated marine sediments using an elastic or nearly viscoelastic model.

3:5 Compressional wave measurements in sediments and soft rocks

Considerable amounts of data have been published in laboratory and field studies of compressional waves through sediments (Laughton, 1954; Ref 50 and 1957; Ref 51, Hunter et al, 1961; Ref 52, Morgan, 1969; Ref 53, Shumway, 1960a; Ref 54, 1960b; Ref 55, Hampton, 1967; Ref 56, McCann and McCann, 1969; Ref 57, McCann, 1972; Ref 58, Buchan et al, 1972; Ref 59, Akal, 1972; Ref 60, Hamilton, 1970; Ref 61, 1972; Ref 49, 1976; Ref 62, and Jackson et al, 1980; Ref 63).

Laughton (1954; Ref 50, and 1957; Ref 51) made laboratory measurements of compressional wave propagation in marine sediments and found a vertical gradient in the acoustic velocity with compaction pressure in deep-sea cores. Acoustic measurements made in the laboratory by Shumway (1956; Ref 64) and in-situ by Hamilton et al (1956; Ref 21), on shallow-water fine sands and silts, showed that generally the acoustic velocity decreased with decreasing grain size and increasing porosity. Shumway (1960a; Ref 54, and 1960b; Ref 55) obtained acoustic measurements on 111 unconsolidated marine samples which range from deep-sea clays to shallow-water sands. The range of velocities obtained were from 1474 m/s for red medium clay to 1785 m/s for medium sand.

The most significant parameter affecting the variation in the acoustic velocity was found to be the porosity, which varied between 36 to 86 percent for the above samples. Sediment rigidity, related to the predominance of coarse grains in samples, was found to be the second most important parameter. The analysis also considered other parameters such as pressure, the compressibility of the grain aggregate and temperature.

Other parameters such as the confining pressure, the grain characteristics of the sand size materials and the moisture content were considered by Brandt (1960; Ref 44), Harding and Richart (1963; Ref 65) and Gardner et al (1964; Ref 66), who concluded that porosity was the most significant parameter which determined the acoustic velocity in sediments. Hamilton (1968; Ref 67), after the assessment of laboratory test data for shallow and deep-sea samples from the North Pacific and Caribbean area, suggested that a generalised curve which relates acoustic velocity to various sedimentary parameters should be superseded by curves and equations involving specific environments. McCann (1968; Ref 68), Schreiber (1968; Ref 69) and Morgan (1969; Ref 53) also concluded from a multivariate statistical analysis of core data that sediment porosity was the most significant parameter affecting the acoustic velocity.

The porosity of the core samples for the above study varied from approximately 35 to 85 percent covering a range from fine sand to silty clay. The change in the acoustic velocity with porosity followed the curvilinear trend as represented by Wood's (1940; Ref 17) equation (eqn. 3.14); this correlation has been observed by several authors. Other parameters which indirectly affect the acoustic velocity and are linked with porosity are the grain size, sorting, shape and the interrelationships between sediment particles.

The acoustic velocity and porosity relationship was confirmed by Horn et al (1968; Ref 70) for fine sand to clay sized materials. The 22 core samples used were from the Mediterranean Sea and the Norwegian Basin. The sorting, the skewness and kurtosis of the grain size frequency distribution were shown to be useful tools in predicting the acoustic velocity with bimodal sediments, although the acoustic transmission was not directly affected by these parameters. The correlation between

compressional wave velocity and either dry sediment density or shear strength was found to be insignificant. The statistical appraisal of a large amount of data by Buchan et al (1972; Ref 59), Anderson (1974; Ref 71), Taylor Smith (1974; Ref 72) and Hamilton (1975; Ref 73) concluded that variability of sediment acoustic velocity and impedance generally required consideration of a number of geotechnical parameters (such as sorting, porosity grain size, specific gravity of solids, carbonate content, liquid and plastic limits, shear strength etc) in a multivariate solution, although the most predominant parameters affecting the acoustic velocity were considered to be sample porosity and sediment grain size.

3:6 Attenuation measurements in sediments and soft rocks

Hamilton (1956; Ref 21) reported the attenuation coefficient for silt and fine sand to be 1.5 dB/m and 16 dB/m respectively at 30 kHz. The attenuation results, in sand sediment alone, did not appear to be related to porosity or mean grain diameter. Compressional wave attenuation (at 1 MHz) was found to be relatively greater in coarse grained sediments than in sediments of smaller particle size by Sutton et al (1957, Ref 74), Hunter et al (1961; Ref 75) and Hall and Richart (1963; Ref 76). The absorption maximum of sediments of intermediate porosity (45 to 60 percent) and intermediate grain size (2ϕ to 5ϕ) reported by Shumway (1960a; Ref 54) was confirmed by McCann and McCann (1969; Ref 57).

The values of constant K were investigated by Hamilton (1972; Ref 49) for various porosities and mean grain size; the relationship was

$$\alpha = Kf^n \quad - (3.16)$$

where

- α = absorption coefficient (in dB/m)
- f = frequency in kHz
- n = exponent of frequency

The attenuation (K) increases with decreasing grain size in sands, reaching a maximum between 3.50ϕ to 4.50ϕ and then decreasing in silts and clays. The variation of K with porosity was similar to the grain size. The highest K values were found in sands and silts, with the porosity

range between 50 and 54 percent. A correlation between the attenuation coefficient and the percentage of sand sized particles was reported by Shumway (1960b; Ref 55) and Buchan et al (1972; Ref 59), although in the early work Buchan et al (1967; Ref 26) suggested that the attenuation of a compressional wave in marine sediments was susceptible to a change in a complete range of parameters rather than in only a single parameter.

3:7 Conclusions

Acoustic waves through water saturated sediments are affected by the mechanical properties of the fluid, the individual sediment particles and the skeleton formed by these particles. In suspension, when the particles are not in contact, the acoustic velocity is described by the product of the compressibilities and densities of the solid particles and the pore fluid, multiplied by their respective proportional volume in the total volume.

When the particle concentration is increased, the particles either make physical contact (eg. non-cohesive sands and silts) or are joined by electromechanical forces such as clay minerals. The interaction of sediment particles generates a rigidity modulus and a frame modulus into the velocity equation. This is in excess of the bulk modulus computed from the suspension component alone (Hamilton 1971b; Ref 48). The two rigidity components, associated with particle interaction, comprise the 'effective rigidity' (Shumway 1960b; Ref 55), and are affected by the sediment packing, the type of inter-particle contact, and the degree of interlocking and friction between particles. Therefore, the most important parameters that describe the sediment and the acoustic velocity variation, at a given confining pressure, are sample porosity, grain size, mineralogy, and the angularity and sphericity of particles.

Attenuation in marine sediments can be generally attributed to three mechanisms. These are: Rayleigh scattering, solid-friction attenuation and viscous energy losses. Rayleigh scattering occurs when the wavelength approaches the grain size diameter. The attenuation caused by scattering is related to the fourth power of the frequency. The solid-friction attenuation is caused by inter-grain movement, similar to the losses in polycrystalline rocks (Mavko and Nur, 1979; Ref 77; Toksoz et al, 1979a; Ref 78; 1979b; Ref 79). These losses are represented by a

linear variation of the attenuation coefficient with frequency. Viscous losses are derived from the relative movement of solid and liquid particles in the sediment and water mixture. Attenuation caused by viscous losses is related to the frequency squared or the square root of the frequency, depending on the size of the pore-space (Biot, 1956a; Ref 34, and 1956b; Ref 35).

In sediments, viscous and solid-friction loss mechanisms are expected to operate to a varying degree (Buchan et al, 1972; Ref 59). The overall effect is an apparent increase in attenuation, over a range of grain size from coarse sands to clays, reaching a maximum around 4.0ϕ to 5.0ϕ . The attenuation caused by solid-friction is reduced in relation to a reduction in sediment rigidity. Further reduction in grain size can complicate the issue as inter-particle attraction occurs, which reduces the relative motion between the solid particles and the fluid, causing a reduction in the contribution to the viscous dissipation. McCann and McCann (1969, Ref 57) found 6ϕ as the grain size at which inter-particle forces became dominant.

4 SURFACE SEISMIC METHODS

Surface seismic methods are widely used in oil exploration and civil engineering site investigations. In oilfield exploration, they have been developed to a high degree of sophistication for the selection of sites for exploratory oil wells. Their main advantage over other geophysical methods is that they are capable of achieving greater penetration coupled with higher resolution and precision. Their main use in the civil engineering field is the determination of the depth to the bedrock and the mechanical properties of the first 50-100 m of the natural material, in order to establish the safe loading on the foundation for the installation of large structures such as a tall building, nuclear power station, a dam etc.

The two predominant surface seismic techniques used are the refraction and the reflection methods. Of the two methods, refraction is the most common method used in civil engineering site investigation because the data acquisition, processing and interpretation is relatively less complex. The results are cost effective for the relatively small area normally investigated.

Surface seismic methods can on occasions suffer from high attenuation caused by the surface deposits, which in some cases exhibit compressional wave velocities less than that of water. This is caused by the presence of air in the pores influenced by the geology, water table and other local drainage conditions. This lower velocity layer is sometimes called a weathered zone and may vary from a few to 50 m in depth. Weathering of natural materials is very complex and beyond the scope of this thesis but one of the predominant interactions is between the soluble oxygen or the free hydrogen ions in the water and the minerals in rocks and sediments, causing alterations in the mineral constituents and the fabric.

Weathered zones can also be responsible for the loss of energy at high frequencies. Similarly, an intrusive structure (such as an air or sludge-filled cavity) in a homogeneous rock mass exhibits an effective increase in bulk porosity in the path of a propagating wave, which in turn exhibits a slower velocity for that particular path, depending on source wavelength, velocity in formation and source receiver geometry.

Whenever a seismic wave encounters a sudden change in elastic properties, as when it arrives at a surface separating two geological beds, part of the energy is reflected and remains in the same medium as the original energy; the remaining energy is refracted into the second medium (with higher velocity), with an immediate change in direction of propagation occurring at the interface. Refraction and reflection seismics are used extensively in exploration seismology, but inter-borehole seismics is also gaining popularity, particularly in engineering seismics where more detailed seismic results are achieved by moving away from the weathered zone on the surface.

4:1 Seismic refraction method

As early as 1923, the seismic refraction technique was responsible for the spectacular success of geophysics in finding a great number of shallow Gulf Coast salt domes associated with oil deposits (Dobrin, 1976; Ref 15). The first seismic technique used in petroleum prospecting was the refraction method, although seismic refraction principles had been applied for some time by earthquake seismologists in determining the structure of the Earth's interior from earthquake records.

The use of the seismic refraction method has diminished in the oil industry over the years, but the method has found increasing use in engineering geophysics for site investigation. The method becomes a valuable investigative tool when used in conjunction with information from exploratory drilling.

The refraction survey method is well established and interpretation of the data is reasonably straightforward for most cases. The layout of the geophone array can be changed to allow judgment and imagination in obtaining and handling of raw data. Like other indirect methods of subsurface exploration, there are no rigid, inflexible approaches to making sense of data, nor are there any handbooks that can infallibly direct a geophysicist to the correct answer. Knowledge of the site conditions and understanding of what is geologically plausible will always help in deriving a meaningful interpretation from the data.

Various authors (Black et al, 1962, Ref 80; Bush and Schwarz, 1965, Ref 81; Hobson, 1970, Ref 82; Grainger et al, 1973, Ref 83; Cratchley et al,

1976, Ref 84) and others have successfully used seismic refraction techniques to assess geological stratification, large weathered zones within the rock mass and other larger geological variations for civil engineering site investigation.

4:1:1 Theory and principles

The refraction method consists of measuring (at known points along the ground surface) travel times of compressional waves generated by an impulse energy source. The energy source could be a small explosive, drop weight or any impulse source that imparts seismic energy into the ground. Received seismic energy at each sensor on the surface is amplified and recorded using an analogue or digital refraction instrument. The raw data therefore consists of travel times and distances, and this time-distance information is then manipulated to convert it into a format based on velocity variations with depth.

Propagation of seismic energy through the rock mass is described essentially by the same laws that govern light ray propagation through transparent media. The refraction or angular deviation that a light ray or seismic pulse undergoes when passing from one medium to another depends upon the ratio of the transmission velocity of the two materials. The fundamental law that describes refraction is Snell's Law which, with the phenomenon of critical incidence, forms the foundation of seismic refraction surveys. Snell's Law and critical incidence are shown in Fig 4:1:1, which illustrates a medium with velocity V_1 overlaid by a medium with a higher velocity V_2 . Until the critical angle of incidence is reached, almost all compressional energy is transmitted (refracted) into the higher velocity medium. When the critical angle is exceeded, the energy is almost totally reflected, and no energy is refracted into the high-speed layer. This phenomenon takes into account only compressional waves, ignoring shear wave energy and the transformation of a portion of a compressional wave into a shear wave that can occur at boundaries.

Critically refracted rays travel along the boundary between the two media at the higher of the two velocities, continually generating seismic waves in the lower-velocity (upper) layer that depart from the

boundary at an angle of critical incidence. These waves are normally referred to as head waves.

Construction of time/distance graphs, and their interpretation using different techniques, has been discussed by various authors - Dobrin (1960; Ref 15), Musgrave (1969; Ref 85), Telford et al (1976; Ref 13) and others, but a derivation of a general equation is shown below.

A formula is derived expressing arrival time in terms of geophone spacing, depth and velocities for a simple case of the two-layer medium, as shown in Fig 4:1:2. Telford et al (1976; Ref 13) has shown that for a geophone at a point R, the travel time t can be expressed as

$$t = (x/V_2) + t_1 \quad - (4.1)$$

where $t_1 = (2z \cos \theta_1)/V_1$
and $\theta_1 = \sin^{-1}(V_1/V_2)$

A generalised equation that can be applied to any number of layers was developed by Telford et al (1976; Ref 13) from a consideration of the three-layer case. The horizontally three-layered model, with compressional wave velocities of V_1 , V_2 and V_3 respectively, is shown in Fig 4:1:2.

It can be demonstrated that for a geophone at point R, the travel time t can be expressed as:

$$t = (x/V_3) + (2z_2/V_2)\cos\theta + (2z_1/V_1)\cos\theta_1 \quad - (4.2)$$

where $V_3 > V_2 > V_1$

The equation can be generalised for n beds in the form:

$$t = (x/V_n) + \sum_i (2z_i/V_i)\cos\theta_i \quad - (4.3)$$

where $\theta_i = \sin^{-1}(V_i/V_n)$

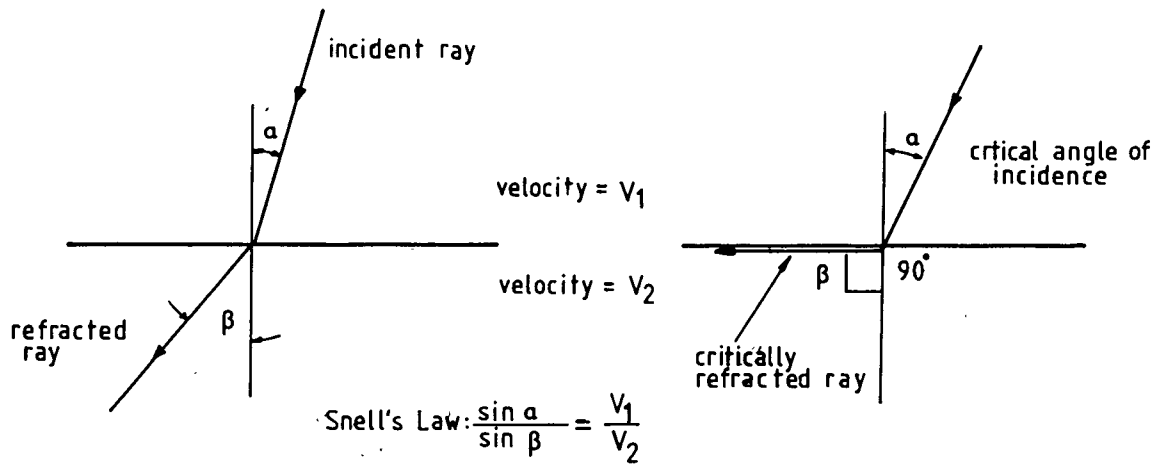


FIG. 4:1:1 SNELL'S LAW & REFRACTION AT AN INTERFACE

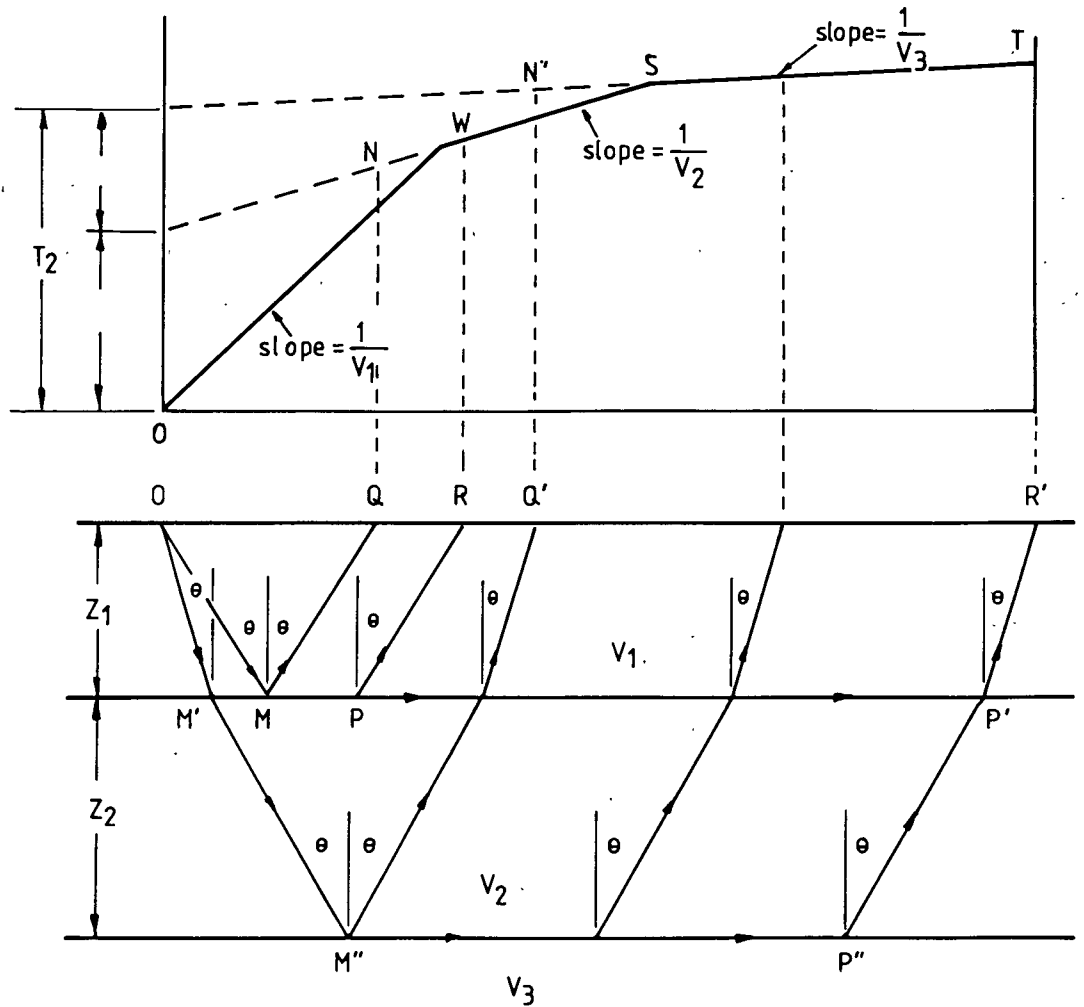


FIG. 4:1:2 TRAVEL-TIME GRAPH FOR TWO LAYER MODEL

(after Telford et al, 1976; Ref 13)

Equation 4.3 can be used to calculate the thickness of a series of horizontal refracting beds, each with a constant velocity increasing with depth. Each bed must make a sufficient contribution to the time/distance graph to enable its velocity to be determined from the slope of the appropriate straight line section of the graph. The generalised equation does not include the effect of a dipping interface, which has a considerable influence on the time/distance graph - a comprehensive treatment of this more complex situation is given in Telford et al (1976; Ref 13) and Dobrin (1976; Ref 15).

The geological situation described by equation (4.3), where the beds are horizontal and have a constant velocity and thickness, very rarely arises in practice. In many situations large thicknesses of non-uniform drift deposits overlie the geological strata of interest and this results in a reduction in the resolution that can be obtained with a standard seismic refraction survey. Many modifications have been applied to the standard interpretation method based on equation (4.3) and the following approaches are of particular interest:

- a Thornburgh's wavefront diagrams (Thornburgh, 1930; Ref 86)
- b Gardner's constituent delay time construction (Gardner, 1939; Ref 87)
- c Barthelmes' continuous profiling analysis (Barthelmes, 1946; Ref 88)
- d Slotnick's multilayer refraction analysis (Slotnick, 1950; Ref 89)
- e Baumgarte's graphical ray-stretching method (Baumgarte, 1955; Ref 90)
- f Hales' and Tarrant's tangent plotting of varying refractor interfaces (Hales, 1958; Ref 91 and Tarrant, 1956; Ref 92)
- g Hagedoorn's plus-minus method using reversed refraction profiles (Hagedoorn, 1959; Ref 93)

4:1:2 Seismic refraction survey at Cocking

A disused railway tunnel was selected as an air-filled cavity to examine how this type of discontinuity in the rock mass affects seismic and other geophysical techniques.

The selected site is about 1.5 km southwest of Cocking village in Sussex (grid reference 870 160 on 1:50 000 sheet 197). Access to the site was via a lane off the A216 Cocking to Chichester road (Fig 4:1:3).

The geology of the area is characterised by a fractured chalk bedrock with an overlay of loamy soil about 0.25 m in depth; fracturing of the chalk decreases with depth below the surface. The tunnel is about 14 m below the surface, 5 m wide and 5 m high (Fig 4:1:4). Initial investigations had shown that the tunnel was constructed by a boring technique, so that it was positioned in a rock mass consisting of fairly solid chalk. However, further investigations carried out when the geophysical results did not fit the above model showed that the southern end section of the tunnel, over which most of the geophysical investigations had been carried out, was constructed by the cut and fill method.

The state of the rock mass in the immediate vicinity of the tunnel in this section was thus more complex to determine than initially envisaged, because of the heterogeneous nature of the mixture of chalk and clay in the backfill material. This is evident in the fracture log of the cores obtained from the borehole drilled for the interborehole acoustic measurements which are shown in appendix I. These show fine clay bands up to a depth of 15 m and other gradations of chalk structure up to a depth of 19 m.

Seismic refraction surveys were carried out in parallel and across the centre line of the tunnel at Cocking to assess the rock mass condition in the vicinity of the tunnel.

The survey was carried out with a 24-channel ABEM seismic set with a falling weight seismic source. Three seismic lines were selected, as shown in Fig 4:1:5. Seismic lines SL1 and SL3 were in parallel with the tunnel, while line 4 was perpendicular to the tunnel.

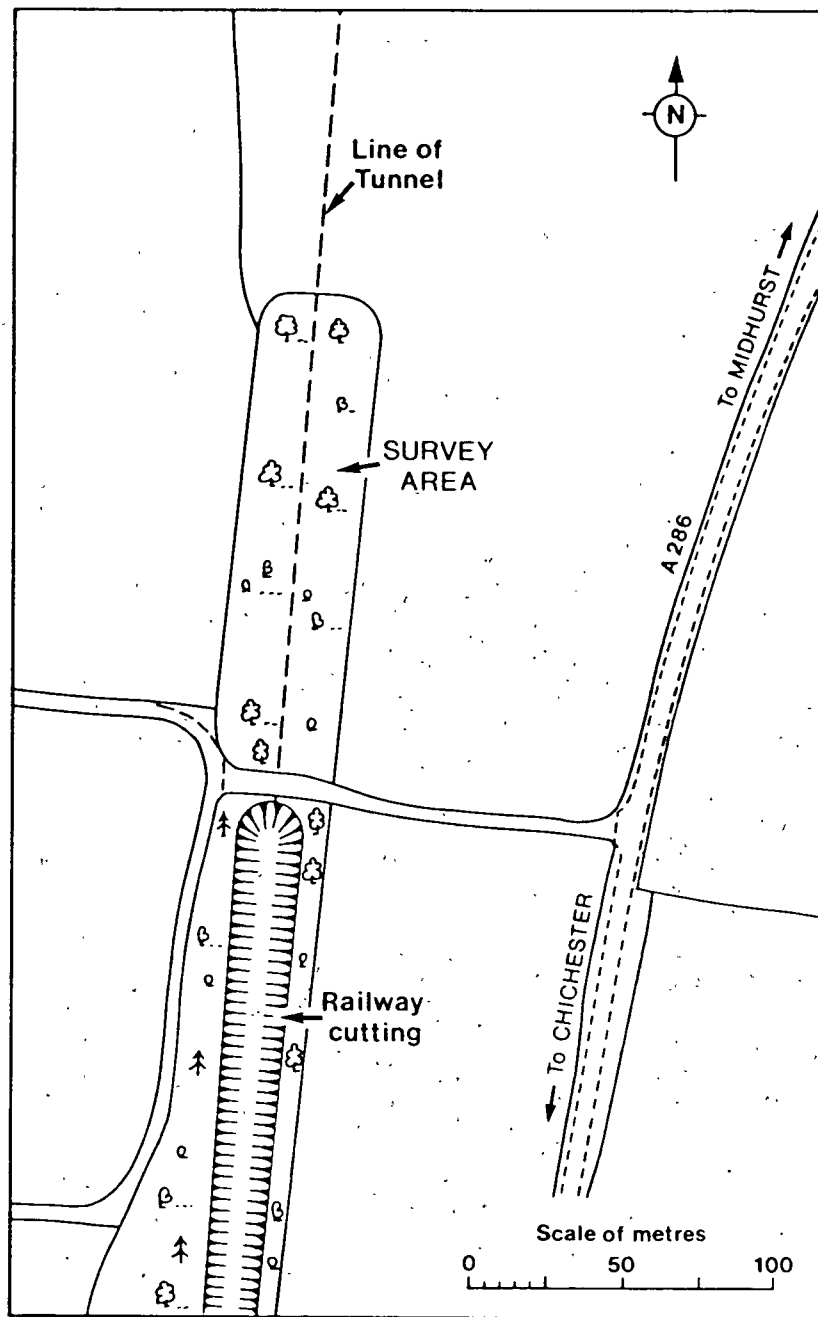
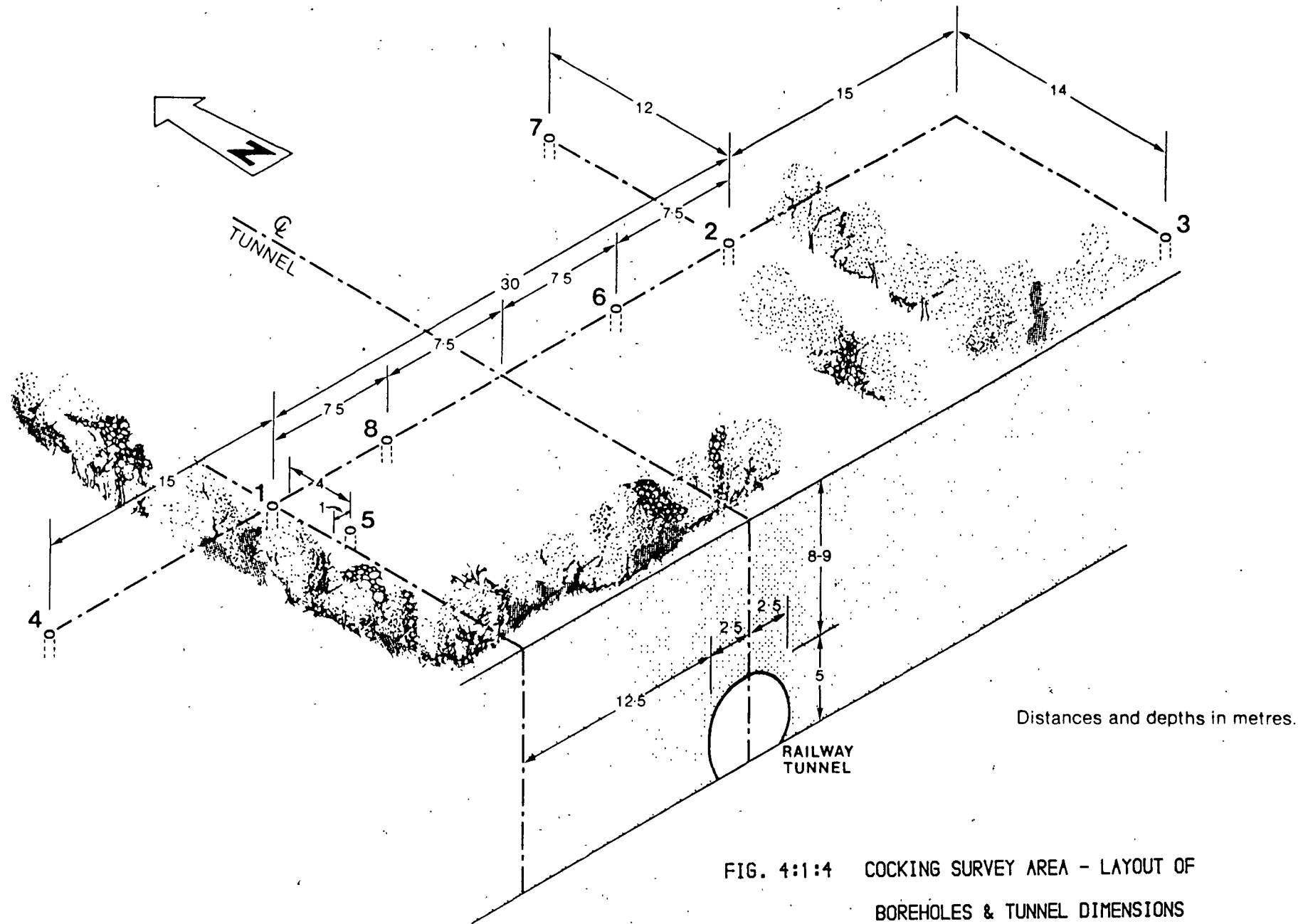


FIG. 4:1:3 COCKING SURVEY AREA



Distances and depths in metres.

FIG. 4:1:4 COCKING SURVEY AREA - LAYOUT OF BOREHOLES & TUNNEL DIMENSIONS

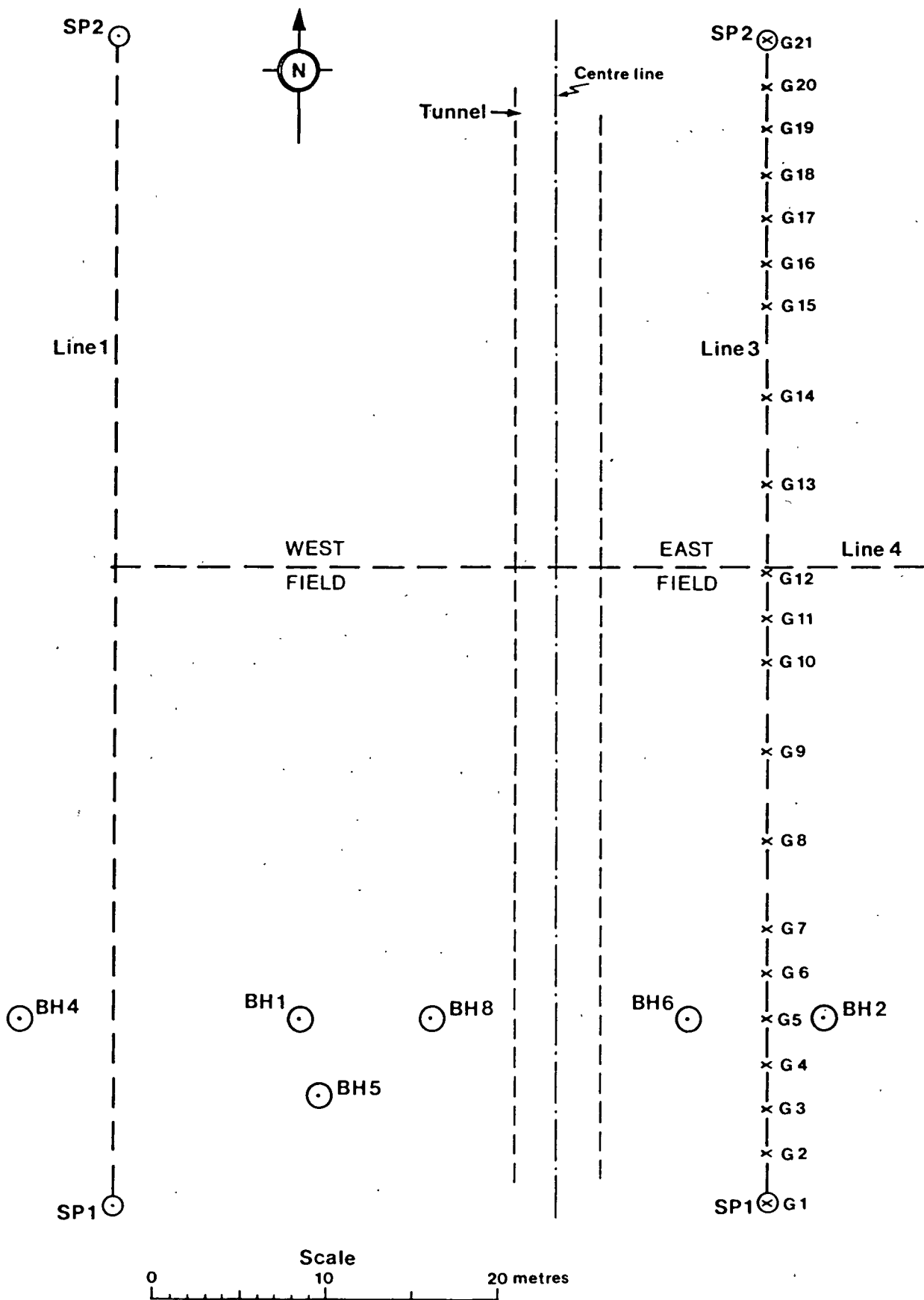


FIG. 4:1:5 COCKING TEST SITE - POSITION AND LAYOUT OF SURFACE SEISMIC LINES

Seismic lines 1 and 3 were 24 m west and 12 m east respectively of the centre line of the tunnel. The geophone spacing for seismic lines SL1 and SL3 were identical, as shown in Fig 4:1:6. Twenty-one geophones were used, with shot points SP1 and SP2 for each line occupying geophones G1 and G2 respectively. The geophones were buried just below the surface to reduce the environmental noise, while the strike plate was placed at the bottom of an 18 cm deep hole to provide good coupling to the rock mass.

Seismic line SL4 was perpendicular to the centre line of the tunnel. The line covered 23 m on either side of the tunnel with geophone spacings of 2 m. Twenty-four geophones were used, with shot points SP1 (at east) to SP24 (at west) occupying geophones G1 to G24 respectively, as shown in Fig 4:1:6.

A seismograph record of each shot point for a given line was obtained and the time break for each of the traces on the seismogram was measured for each series of shots. The results were used to plot time/distance graphs, as shown in Figs 4:1:7, 4:1:8 and 4:1:9. The slope of each line section gave the compressional wave velocity for each seismic layer ($1/v = t/d$). The thickness of each layer was calculated from the measured velocities and the line intercept value obtained, extrapolating each straight line (representing a velocity) until it cuts the time axis.

The generalised equation (4.3) describing the time/distance curve for n layers was used to find the thickness of each of a series of horizontal refracting beds, each of constant velocity.

For the three layer case, it can be shown that:

$$Z_1 = [V_1 T_1 / 2] [1 - (V_1 / V_2)^2]^{1/2} \quad - (4.4)$$

$$Z_2 = [(V_3 T / 2) - Z_1 ((V_3 / V_1)^2 - 1)^{1/2}] / [(V_3 / V_2)^2 - 1]^{1/2} \quad - (4.5)$$

where

Z_1 = thickness of layer 1

Z_2 = thickness of layer 2

V_1 = compressional wave velocity in layer 1

V_2 = compressional wave velocity in layer 2

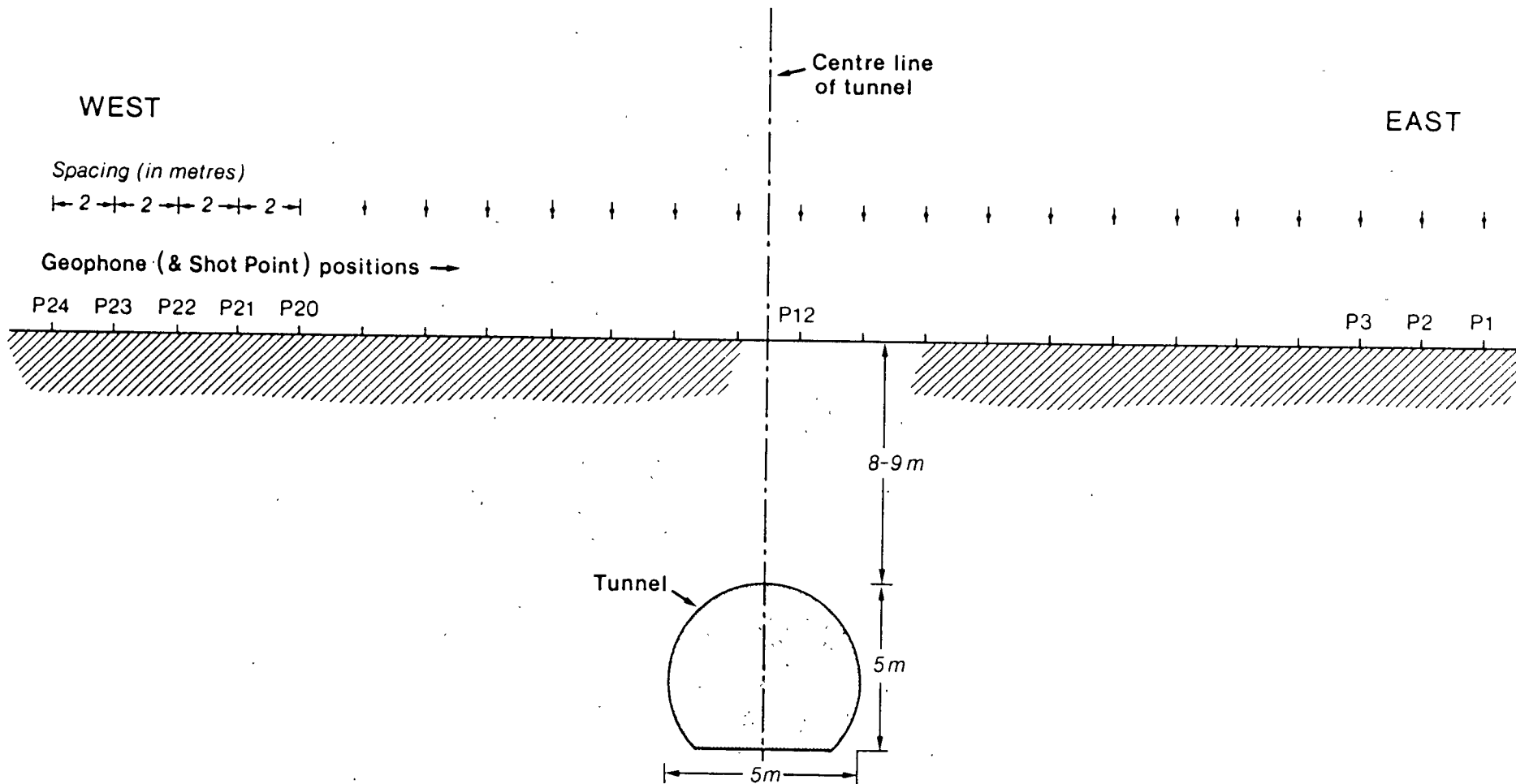


FIG. 4:1:6 COCKING TEST SITE - GEOPHONE & SHOT POINT
POSITION ON SEISMIC LINE 4 ACROSS THE TUNNEL

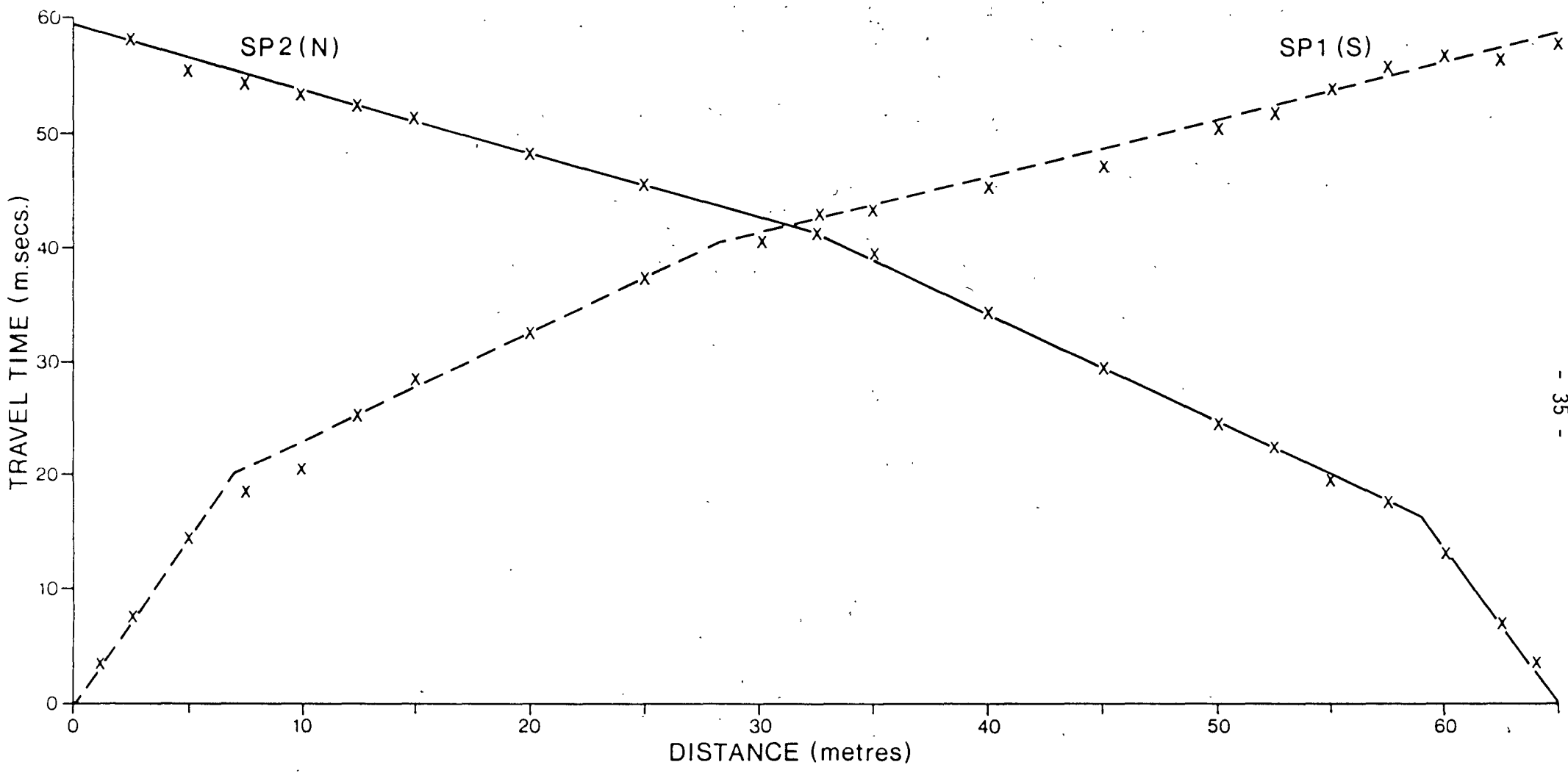


FIG. 4:1:7 COCKING SURVEY - SEISMIC LINE 3
 (east of tunnel centre line)

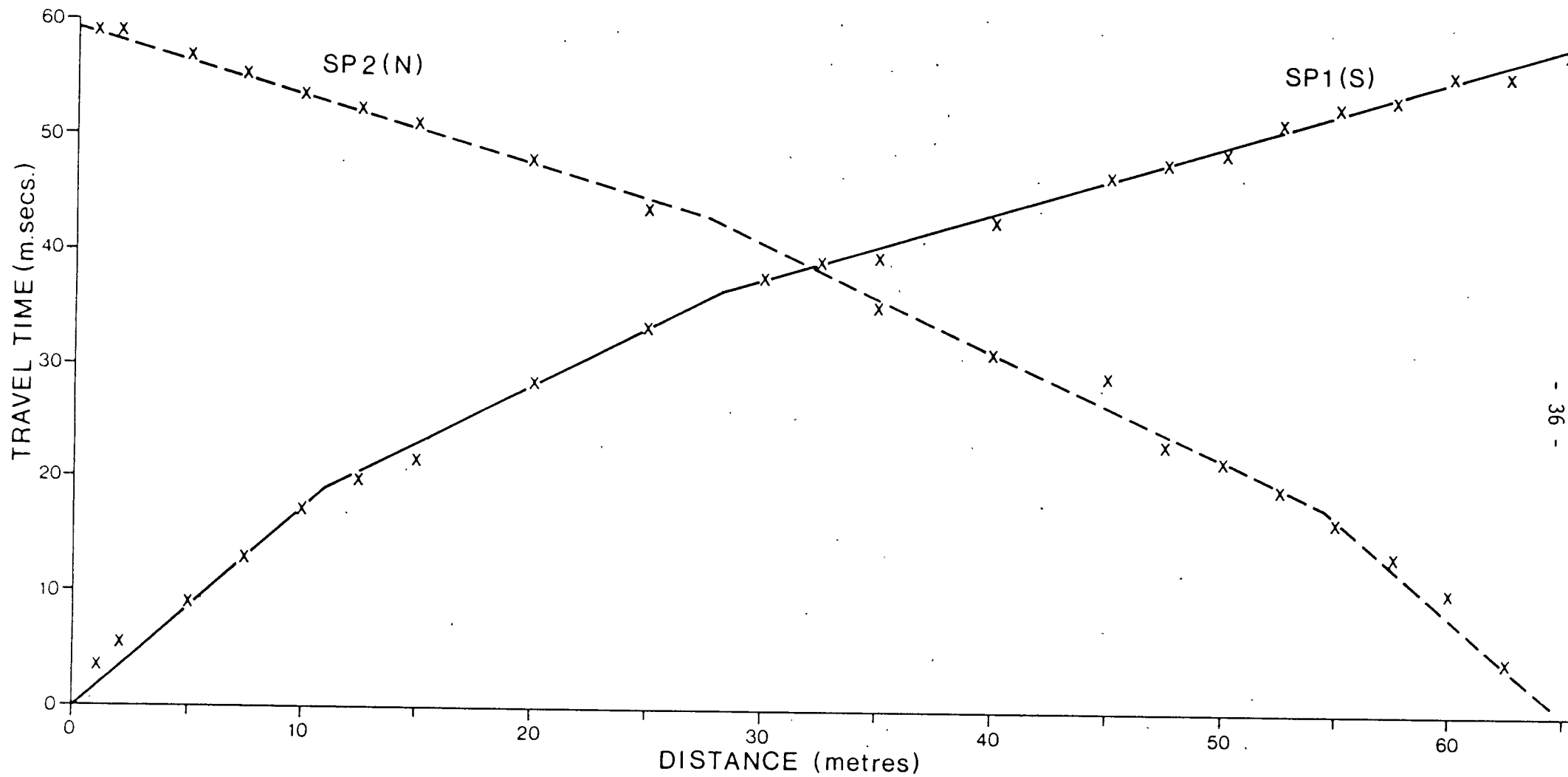


FIG. 4:1:8 COCKING SURVEY - SEISMIC LINE 1
 (west of tunnel centre line)

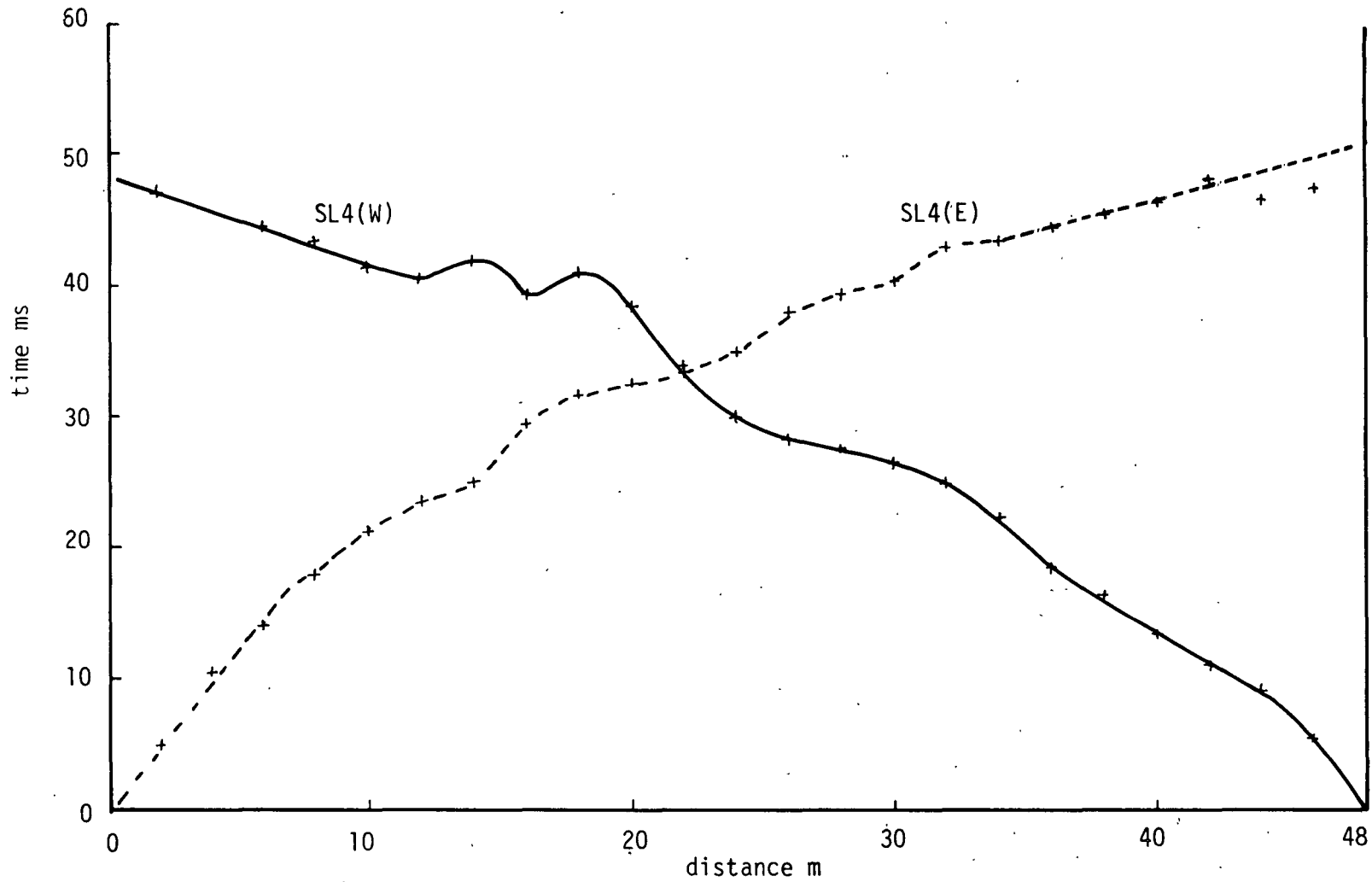


FIG. 4:1:9 COCKING SURVEY - SEISMIC LINE 4
(across tunnel)

- V_3 = compressional wave velocity in layer 3
 T_1 = time intercept for layer 1
 T_2 = time intercept for layer 2

Substituting the above equation for shot points SP1 and SP2 for seismic lines SL1 and SL3, the following models for the chalk mass beneath the shot points were computed.

4:1:3 Results and discussion

The models of the chalk mass as computed from the refraction surveys for the two seismic lines SL1 and SL3 are given below (Table 4:1).

Seismic records indicate that there are lateral variations in the chalk mass.

TABLE 4:1

Seismic line	Shot point	Depth to interface (m)	Compressional wave velocity V_p (km/s)
1	SP1 (south)	2.79	0.59
		9.29	0.97
	SP2 (north)	2.76	0.58
		11.26	1.08
3	SP1 (south)	3.30	0.420
		11.31	1.09
	SP2 (north)	2.89	0.47
		10.52	1.05
			1.89
			2.06
		1.89	

Records for seismic line SL1, which is 24 m west of the centre line of the tunnel, show that surface material varies in thickness from 2.79 m (at south) to 2.76 m (at north) with compressional wave velocities of 0.59 km/s and 0.58 km/s respectively. The second interface of the fractured chalk is at 9.29 m (at south) to 11.25 m (at north), with

compressional wave velocities of 0.97 km/s and 1.08 km/s respectively. The compressional wave velocity below the second interface varies from 1.71 km/s (at south) to 1.87 km/s (at north).

Seismic line SL3 is only 12 m east of the centre line of the tunnel and is therefore more representative of the rock mass in the vicinity of the tunnel. Records show that the surface material varies in thickness from 3.3 m (at south) to 2.89 m (at north), with compressional wave velocities of 0.42 km/s and 0.47 km/s respectively. The second interface of the fractured chalk is at 11.31 m (at south) to 10.52 m (at north), with compressional wave velocities of 1.09 km/s and 1.05 km/s respectively. Compressional wave velocity below the second interface varies between 2.06 km/s (at south) to 1.89 km/s (at north).

The result of the seismic refraction lines 1 and 3 show that the near surface chalk mass behaved like a three layer velocity case. The P wave velocity layers are related to the engineering grades as discussed by Ward et al (1964; Ref 94) and not bedding or any other stratigraphical features. The engineering classification of the chalk established by Ward et al (1968; Ref 94) is given in Table 4:2. Grainger et al (1973; Ref 83) correlated the P wave velocity layers with the engineering chalk grades based on the seismic refraction survey data as shown in Table 4:3.

The result of the refraction survey line SL1, which was 24 m west of the centre line of the tunnel, shows three velocity layers. The average velocities of the three layers are 0.6 km/s, 1.0 km/s and 1.8 km/s respectively and are comparable with those identified by Grainger et al (1973; Ref 83), ie 0.7 km/s, 1.1 km/s and 1.7 km/s respectively. The result from refraction line SL3, which was 12 m east and therefore relatively closer, also shows similar average velocity layers except for the marginal reduction in the value of the first layer to about 0.45 km/s. This may have been caused by the inhomogeneity of the rock mass above the tunnel or better drainage conditions influenced by the presence of the tunnel.

TABLE 4:2
(after Ward et al 1968; Ref 94)

A description of the grade of chalk shown on the sections

V	Structureless melange. Unweathered and partially-weathered angular chalk blocks and fragments set in a matrix of deeply-weathered remoulded chalk. Bedding and jointing are absent.
IV	Friable to rubbly chalk. Unweathered or partially-weathered chalk with bedding and jointing present. Joints and small fractures closely spaced, ranging from 10 mm apart to about 60 mm apart. Joints commonly open up to 20 mm and infilled with weathered debris and small unweathered chalk fragments.
III	Rubbly to blocky chalk. Unweathered medium to hard chalk with joints 60 mm to 200 mm apart. Joints open up to 3 mm, sometimes with secondary staining and fragmentary infillings.
II	Medium hard chalk with widely spaced closed joints. Joints more than 200 mm apart. When dug out for examination purposes this material does not pull away along the joint faces but fractures irregularly.
I	Hard, brittle chalk with widely-spaced, closed joints. Details as for Grade II but here the chalk is harder.

TABLE 4:3
(after Grainger et al 1973; Ref 83)

A correlation of the velocity layers with the engineering chalk grades, based on seismic lines 1-3 and 6-10

Velocity layer	Range of values Km/s	Mean value Km/s	Chalk grade
v ₁	0.65 - 0.75	0.7	V
v ₂	1.0 - 1.2	1.1	IV
v ₃	1.6 - 1.8	1.7	III
v ₄	2.2 - 2.3	2.3	II

Grainger et al (1973; Ref 83) also observed that the reduction in the depth of the water table increased the velocity of the P wave from 0.7-1.1 km/s for the unsaturated state to 1.95 km/s for the saturated state. Therefore, in a porous material such as chalk, the depth of the water table significantly influences the P wave velocity. The water table at the Cocking site was below 30 m, as observed during the drilling of the first four boreholes, and it was estimated that the level dropped as low as 70 m during the exceptionally dry summer of 1976. In this case, the influence of the water table on the measured P wave velocity layers may be marginal as the the depth of investigation was considerably shallower, although the inhomogeneous nature of the infill and the local drainage conditions (because of the presence of the cavity) may influence the P wave velocity. Clearly there is a need for care in the interpretation of seismic velocity solely in terms of the state of fracture.

Seismic line SL4 was laid perpendicular to the tunnel on the surface, with 12 geophones on each side of the centre line of the tunnel. This gave a reasonable spread of geophones to study the effect of the tunnel on the seismic refraction survey. Twenty-four shot points were taken, with each shot point replacing a geophone in turn. Shot point SP1 was on the east of the line replacing geophone 1, while shot point SP24 replaced geophone 24 on the west side of the line. A seismogram of each shot point was obtained and the time break for each of the traces on the seismogram was measured. Results were used to plot time/distance graphs.

The time/distance graphs from the seismic line in parallel with the tunnel (SL3) were compared with the seismic line across the tunnel (SL4), as shown in Fig 4:1:10. The figure shows that the data from the seismic line that is parallel with the tunnel fall on a section of the straight line, as expected in the normal refraction survey, but data from the seismic line across the tunnel (SL4) only partially fall on the straight line sections. Comparisons of the time/distance graphs for SL3 and SL4 are reasonably good at points closer to the shot point and the far end but the travel time graph for SL4 clearly indicates that the travel times associated with the geophones in the middle of the lines are affected by the tunnel and the surrounding rock mass. It is interesting to note the comparison made by McCann et al (1982; Ref 95) using resistivity traverses on line SL4 and lines 100 m further north

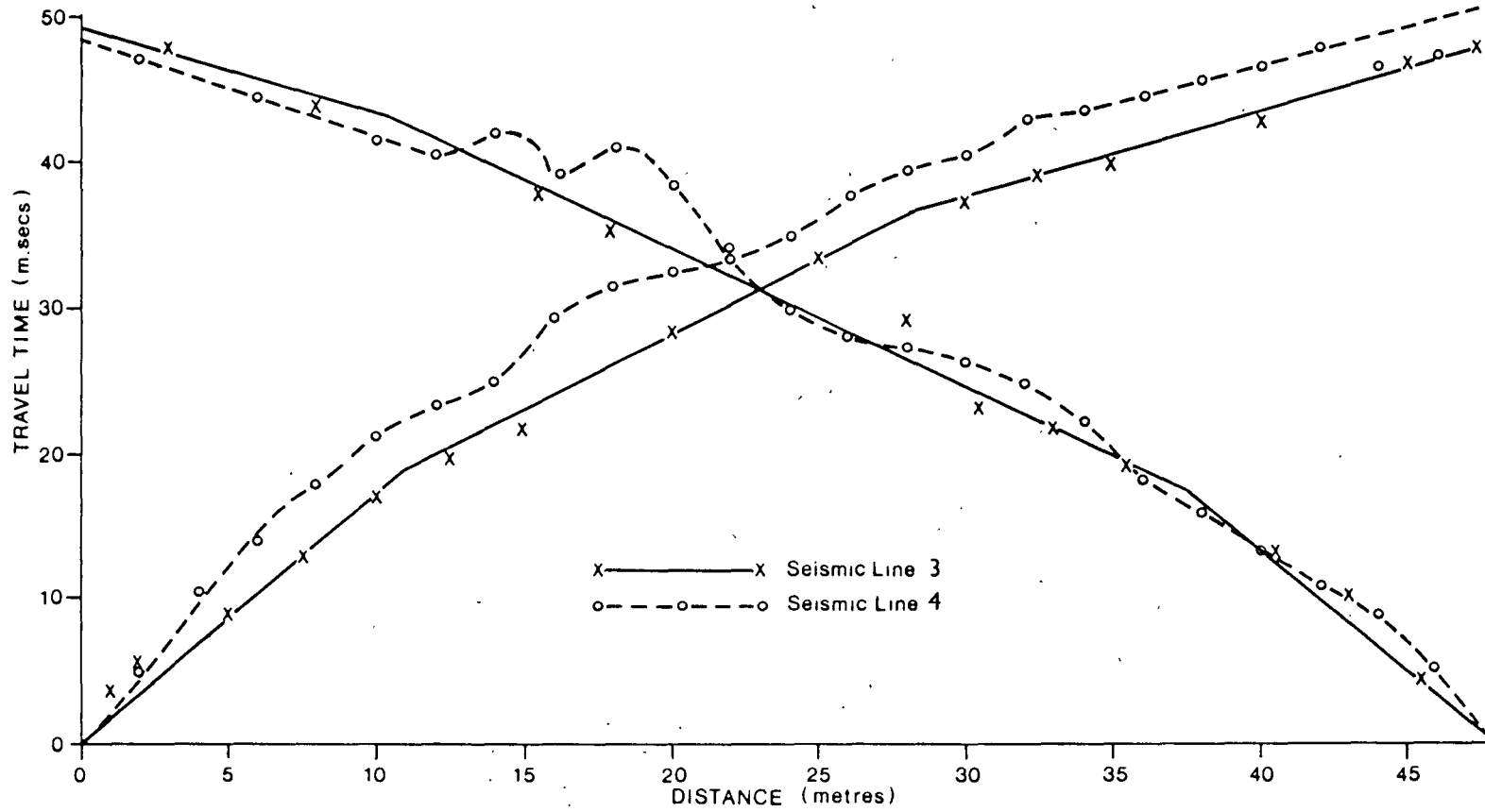


FIG. 4:1:10 COCKING SURVEY - SEISMIC LINE 3 & 4

(parallel & across tunnel)

(Fig 4:1:11), which show that there was a greater reduction in the background noise on the lines 100 m away from SL4 (Figs 4:1:12 and 4:1:13), indicating that the chalk mass below these lines had not been excavated. The authors concluded that the greater background noise in the resistivity measurements near the mouth of the tunnel may have been caused by the variation in the water content of the infill material, as might be expected for a cut and fill site.

Although the standard method does give an indication of the presence of the cavity and the disturbed ground associated with it when used in a comparative mode, the presentation is not satisfactory because of the effect that the superficial deposit could have on the data. Two separate approaches were attempted, to unravel the effect of the superficial deposit from that caused by the presence of the tunnel on the refraction survey. The first method is the time delay image enhancement method, which was devised so that a micro-computer can be used to smooth out the surface variation and present the delay caused by the tunnel as on a contour map. The second method was the seismic velocity profile calculated from the interborehole work to generate a seismic model, from which the geophones affected by the delay caused by the tunnel are identified using the ray tracing technique.

4:1:4 Development of the Time Delay image Enhancement method (TIDE).

This method describes a technique of processing the data from a seismic refraction line of n geophones using n shot points, where each shot point replaces a geophone position in turn.

The time break for each geophone is displayed as a function of the position of geophone number and shot location to form a matrix.

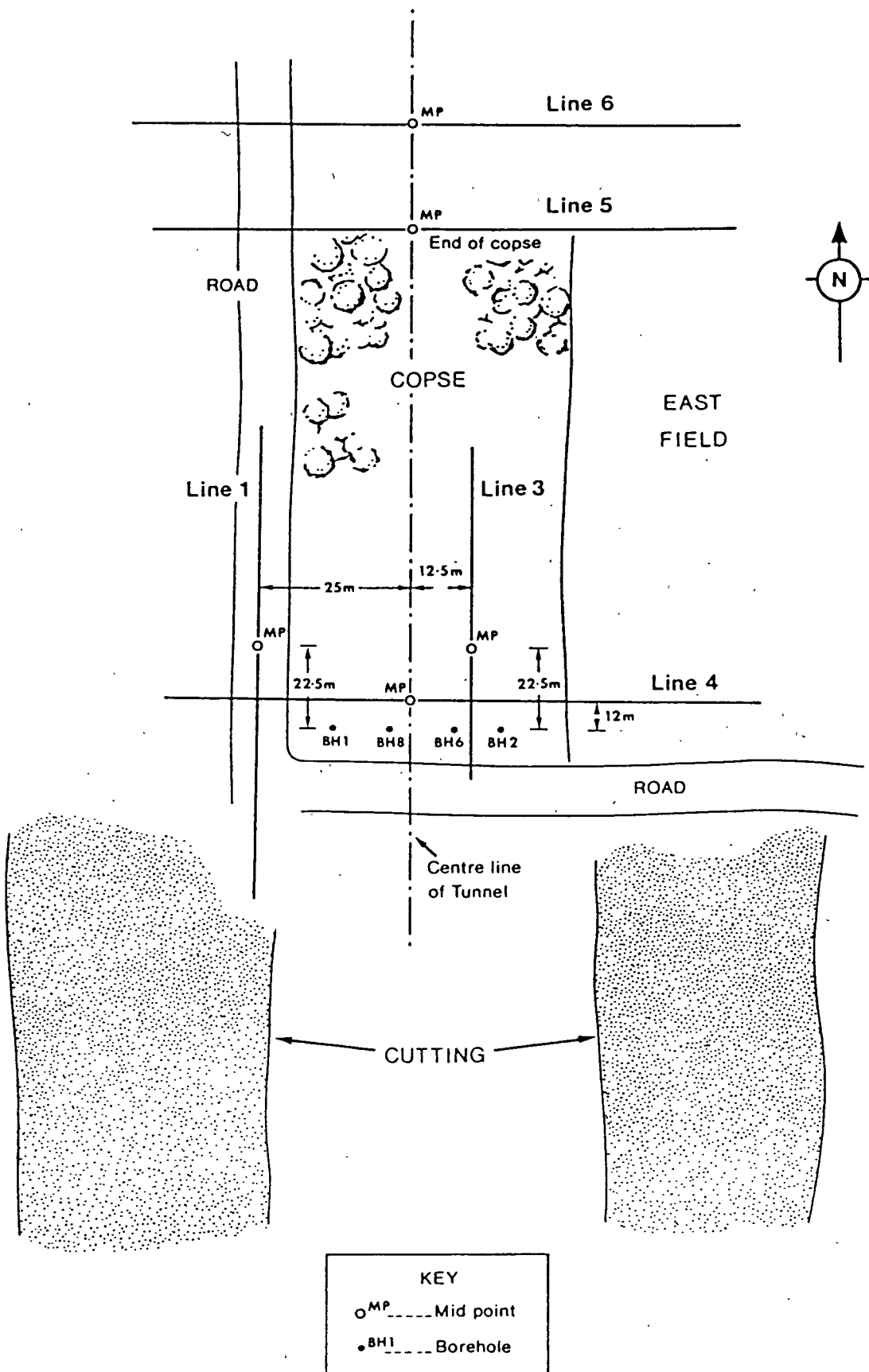


FIG. 4:1:11 THE COCKING SITE SHOWING THE LINES USED FOR RESISTIVITY TRAVERSING (after McCann et al 1982; Ref 95)

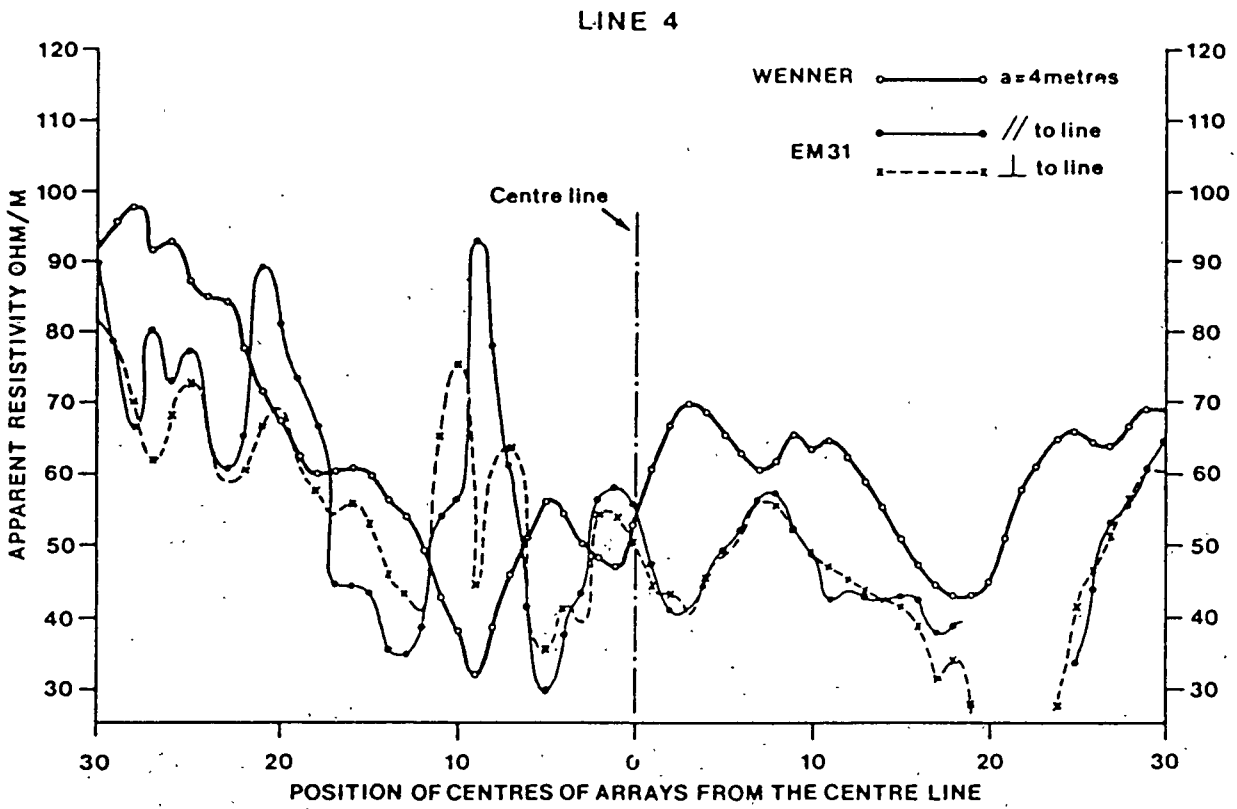


FIG. 4:1:12 COCKING SURVEY - LOW INDUCTION NUMBER ELECTROMAGNETIC TRAVERSES ACROSS LINE 4 COMPARED WITH A WENNER TRAVERSE (after McCann et al. 1982; Ref 95)

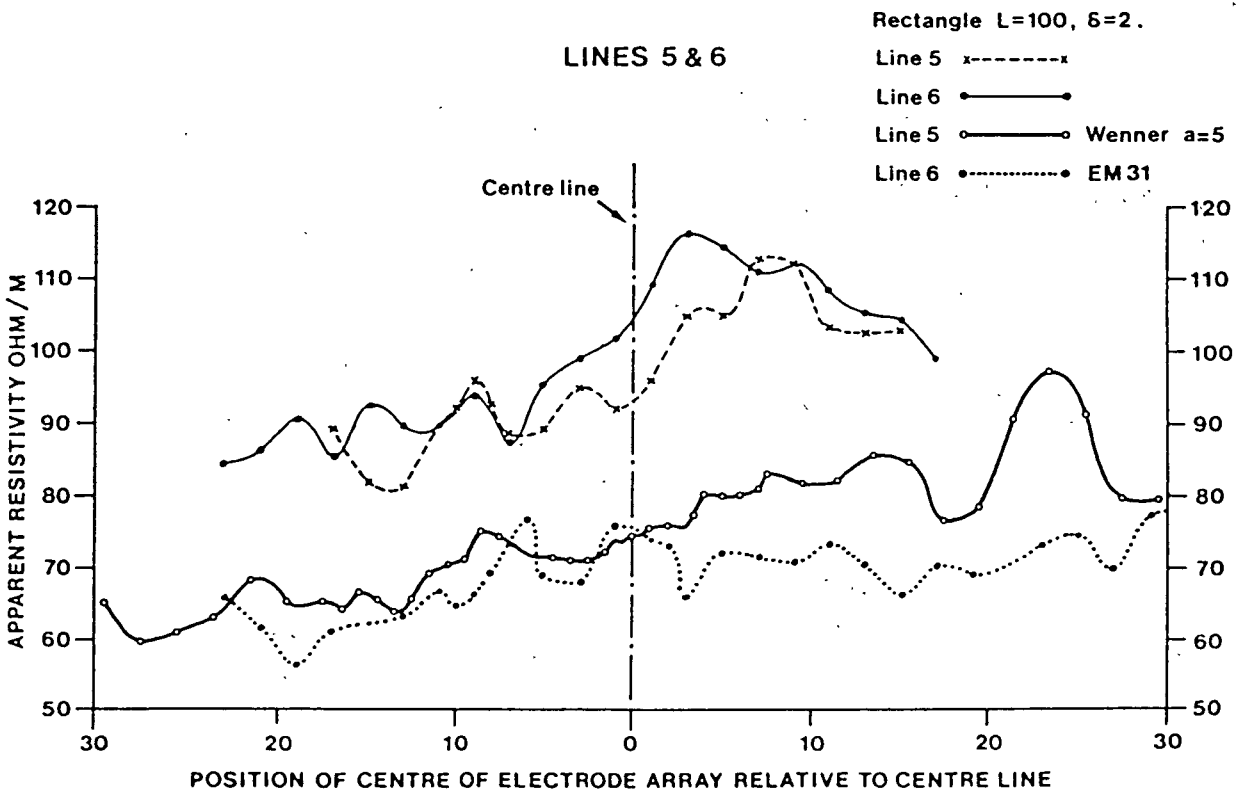


FIG. 4:1:13 COCKING SURVEY - A COMPOSITE PLOT OF TRAVERSES MADE ALONG LINES 5 AND 6 TO THE NORTH OF THE MAIN SITE (see Fig. 4:1:11; after McCann et al 1982; Ref 95)

TABLE 4:4

GEOPHONE LOCATION

		G ₁	G ₂	G ₃	G _u	G _n
SHOT LOCATION	S ₁	T ₁₁	T ₂₁	T ₃₁	T ₄₁	T _{n1}
	S ₂	T ₁₂	T ₂₂	T ₃₂	T ₄₂	T _{n2}
	S ₃	T ₁₃	T ₂₃	T ₃₃	T ₄₃	T _{n3}
	
.		
.		
	S _m	T _{1m}	T _{2m}	T _{3m}	T _{nm}

where n represents geophone number, m represents shot number and T is the time break.

For example,

T₂₁ = time break from geophone number 2 from shot one position in G₁ position

T₄₃ = time break from geophone number 4 from shot three position in place of geophone G₃.

The diagonal of the matrix (ie T₁₁, T₂₂, T₃₃ ... T_{nm}) represents zero time break as the shot point replaces that particular geophone.

Now, if the time delay occurring in the superficial material is constant, the matrix will be symmetrical about the diagonal, ie

$$T_{31} = T_{13}$$

In practice this is not the case, because superficial material may not be a constant thickness and may also be subject to lateral variations. This error can be highlighted by subtracting the column from the rows to form a new matrix (error matrix).

TABLE 4:5

		GEOPHONE LOCATION				G _n
		G ₁	G ₂	G ₃	G ₄	
SHOT LOCATION	S ₁	0	(T ₂₁ -T ₁₂)	(T ₃₁ -T ₁₃)	(T ₄₁ -T ₁₄)	(T _{n1} -T _{1n})
	S ₂		0	(T ₃₂ -T ₂₃)	(T ₄₂ -T ₂₄)	(T _{n2} -T _{2n})
	S ₃			0	(T ₄₃ -T ₃₄)	(T _{n3} -T _{3n})
	S _m				0	(T _{nm} -T _{nm})

Since the two halves of the matrix differ only in sign, it is only necessary to consider one half. Now, if errors are random, the summation of each row should be zero for a large sample, but any non-zero value would imply a system error, such as an incorrect geophone location, etc.

Therefore, for row 1 the numerical error K is

$$K_1 = \sum_{n=1}^{n=\infty} (T_{n1}-T_{1n})/n \quad - (4.6)$$

and for row 2

$$K_2 = \sum_{n=1}^{n=\infty} (T_{n2}-T_{2n})/n \quad - (4.7)$$

A generalised equation for each row is

$$K_n = \sum_{n=1}^{n=\infty} (T_{nm}-T_{mn})/n \quad - (4.8)$$

where

n = number of geophone locations

m = number of shot locations

K_n = average error for a row of n geophones.

Once K_n is established, a two-stage data smoothing process is carried out to enhance in-phase values but attenuate random values. The first stage subtracts the average random error value from the original row values to smooth random variation within a row (ie for a particular shot point), while the second stage makes use of the first stage smoothed

values to average the value of the geophones' position of its mirror images in subsequent shot locations.

Therefore, the first stage of smoothing can be presented as:

TABLE 4:6

		GEOPHONE LOCATION				
		G ₁	G ₂	G ₃	G ₄	G _n
SHOT LOCATION	S ₁	0	T ₂₁ -K ₁	T ₃₁ -K ₁	T ₄₁ -K ₁	T _{n1} -K ₁
	S ₂	T ₁₂ -K ₂	0	T ₃₂ -K ₂	T ₄₂ -K ₂	T _{n2} -K ₂
	S ₃	T ₁₃ -K ₃	T ₂₃ -K ₃	0	T ₄₃ -K ₃	T _{n3} -K ₃
	S ₄	T ₁₄ -K ₄	T ₂₄ -K ₄	T ₃₄ -K ₄	0	T _{n4} -K ₄
	S _m	T _{1m} -K _m				T _{nm} -K _m

The second and final step in the smoothing of the data using the two diagonal halves of the matrix (mirror images):

TABLE 4:7

		GEOPHONE LOCATION				
		G ₁	G ₂	G ₃	G ₄	G _n
SHOT LOCATION	S ₁	0	$\frac{(T_{21}-K_1)+(T_{12}-K_2)}{2}$	$\frac{(T_{31}-K_1)+(T_{13}-K_3)}{2}$	$\frac{(T_{41}-K_1)+(T_{14}-K_4)}{2}$	$\frac{(T_{n1}-K_1)+(T_{1n}-K_n)}{2}$
	S ₂		0	$\frac{(T_{32}-K_2)+(T_{23}-K_3)}{2}$	$\frac{(T_{42}-K_2)+(T_{24}-K_4)}{2}$	$\frac{(T_{n2}-K_2)+(T_{2n}-K_n)}{2}$
	S ₃			0	$\frac{(T_{43}-K_3)+(T_{34}-K_4)}{2}$	$\frac{(T_{n3}-K_3)+(T_{3n}-K_n)}{2}$
	S ₄				0	$\frac{(T_{n4}-K_4)+(T_{4n}-K_n)}{2}$
	S _m					0

When the smoothed set of values is plotted as a half matrix, the time delay due to a seismic discontinuity is accentuated as a series of high values, and overall scatter in the values should be eliminated.

The new value is represented as 't' and the new matrix will appear as shown:

TABLE 4:8

		GEPHONE LOCATION					
		G ₁	G ₂	G ₃	G ₄		G _n
SHOT LOCATION	S ₁	0	t ₂₁	t ₃₁	t ₄₁		tn ₁
	S ₂		0	t ₃₂	t ₄₂		tn ₂
	S ₃			0	t ₄₃		tn ₃
							tn _m

The above smoothed data can be used to compare data generated from a theoretical model to show the effect of any irregularities in field data. The theoretical model is constructed from the field data, but only follows the general straight line contours of the time/distance graph.

This theoretical model can now be used to generate a matrix to represent expected head wave arrival time (M) at each geophone as shown:

TABLE 4:9

		GEPHONE LOCATION					
		G ₁	G ₂	G ₃	G ₄		G _n
SHOT LOCATION	S ₁	0	M ₂₁	M ₃₁	M ₄₁		Mn ₁
	S ₂		0	M ₃₂	M ₄₂		Mn ₂
	S ₃			0	M ₄₃		Mn ₃
	S _m				0		Mnm

The comparative test is carried out between theoretical data and smoothed field data by subtracting smoothed field data from theoretical data to form a new 'comparative' matrix.

TABLE 4:10

		GEOPHONE LOCATION				
		G ₁	G ₂	G ₃	G ₄	G _n
S ₁		0	M ₂₁ -t ₂₁	M ₃₁ -t ₃₁	M ₄₁ -t ₄₁	M _{n1} -t _{n1}
S ₂			0	M ₃₂ -t ₃₂	M ₄₂ -t ₄₂	M _{n2} -t _{n2}
S ₃				0	M ₄₃ -t ₄₃	M _{n3} -t _{n3}
S _m					0	M _{nm} -t _{nm}

If data from the theoretical model and the field data are the same the matrix will show zero numerical values, but if there is some variation in head wave arrival times due to a discontinuity in velocity structure, the comparison matrix will show non-zero values at the relevant geophone position. Colour coding or contouring of the final triangle formed by the half matrix will give a good representation of any anomaly.

A few examples are computed to show the effect of the time delay enhancement processing method (TIDE plot) on various models. The simple case of the three layer model is considered, but other models can be used without difficulty.

Case 1

This case (Fig 4:1:14) considers the effect of a different velocity value for the superficial layers of the field and theoretical model respectively. The field model (which represents the field data) consists of a three layer case with VF1 = 0.55 km/s, VF2 = 0.72 km/s and VF3 = 1.84 km/s. The first layer is 3.5 m thick and the second layer is 8 m thick. The theoretical model used for comparison is also a three layer case with VT1 = 0.45 km/s, VT2 = 0.72 km/s and VT3 = 1.84 km/s.

The thickness of the first and the second layers are identical to the field model. Fig 4:1:14 shows the TIDE plot computed by subtracting field data from theoretical data. The diagonal of the matrix triangle represents the superficial layer and the apex of the matrix represents the bottom layer. The difference between the two models lies only in the velocity of the superficial layer and this is confirmed by the TIDE plot, since the contour gradient falls off towards the apex of the matrix triangle.

Case 2

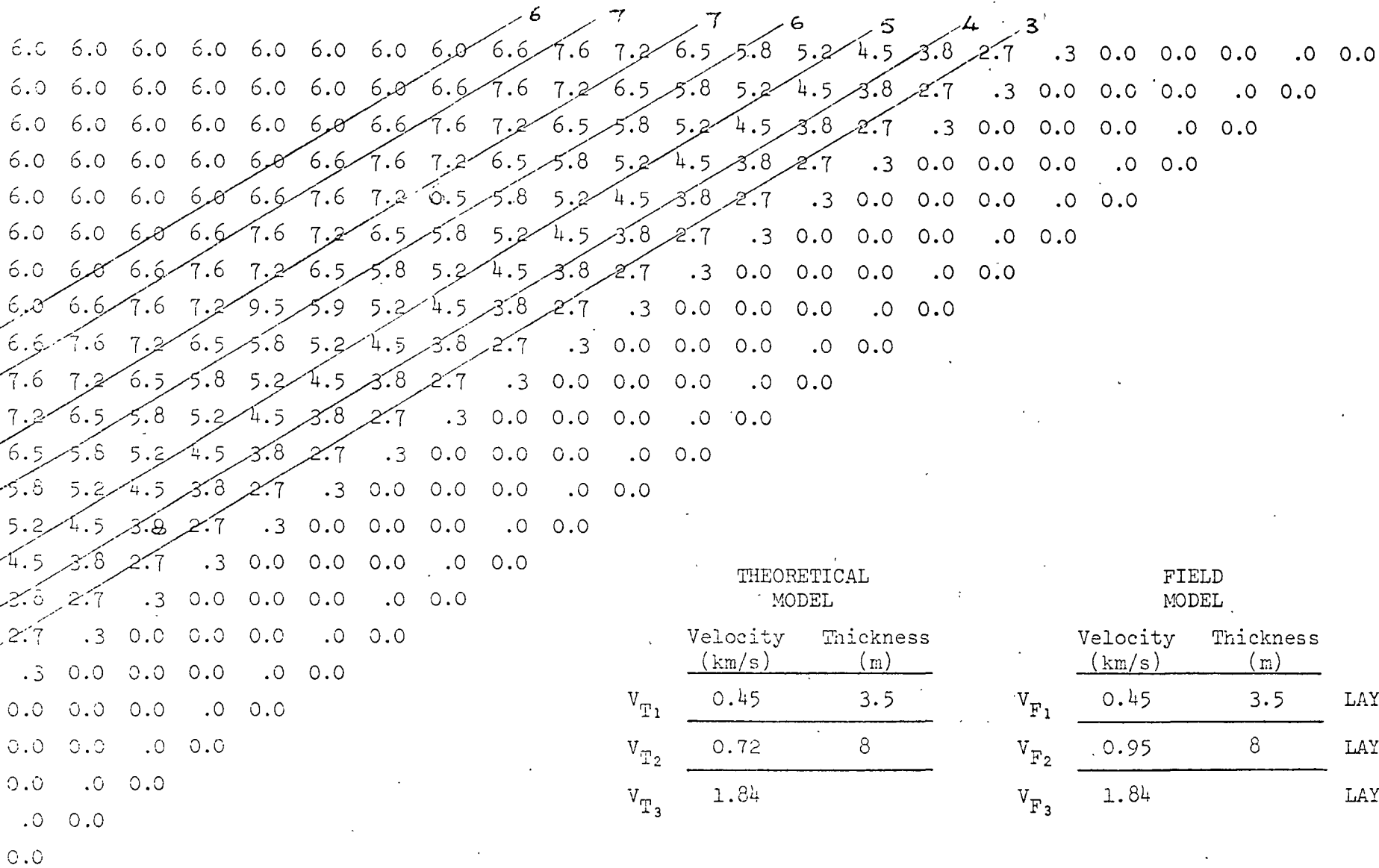
In this case (Fig 4:1:15), the only difference between theoretical and field model is the compressional wave velocity of layer 2 in the theoretical model. The TIDE plot (Fig 4:1:15) shows that there is an agreement between top layers and bottom layer, but the second layer is not comparable. The identical values of velocity in layer 1 are represented on the diagonal of the TIDE plot by zero values. The different velocity values in layer 2 are represented by increasing values on the contour, while the identical values of velocity in layer 3 result in constant delay values (ie 6 m/s) towards the apex of the triangle.

Case 3

In this case, the velocity values in the third layer are different in the two models. This results in increasing values towards the apex of the TIDE plot (Fig 4:1:16).

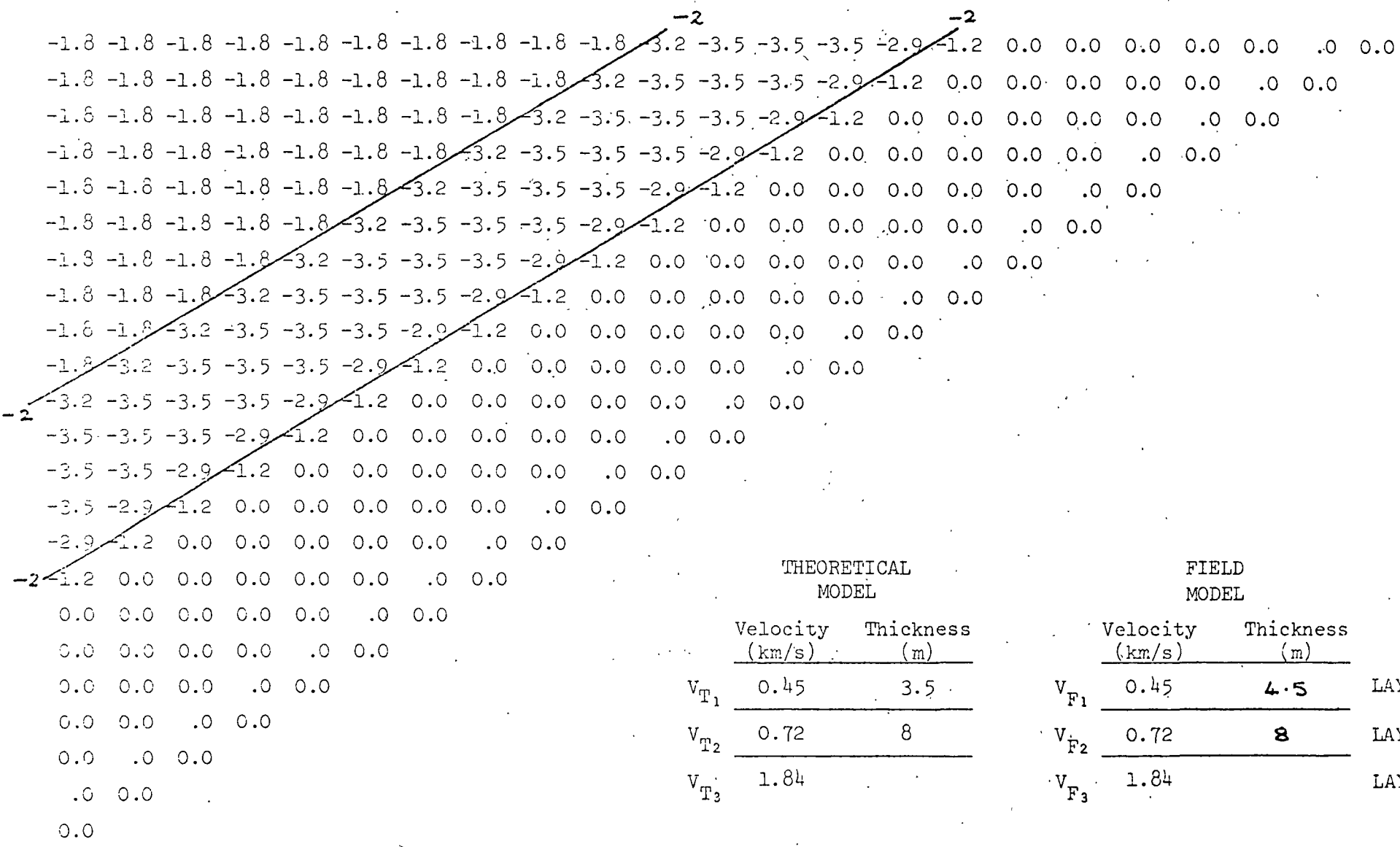
Cases 4 and 5

In these two cases, the three layer model is still under consideration, but the thickness of the first and second layers is varied while velocity values remain the same. The TIDE plots for these two cases are shown in Figs 4:1:17 and 4:1:18 respectively.



	THEORETICAL MODEL		FIELD MODEL		
	Velocity (km/s)	Thickness (m)	Velocity (km/s)	Thickness (m)	
V_{T1}	0.45	3.5	V_{F1}	0.45	LAYER 1
V_{T2}	0.72	8	V_{F2}	0.95	LAYER 2
V_{T3}	1.84		V_{F3}	1.84	LAYER 3

FIG. 4:1:15 CASE 2 TIDE PLOT VF2 > Vt2



THEORETICAL MODEL		FIELD MODEL		
Velocity (km/s)	Thickness (m)	Velocity (km/s)	Thickness (m)	
V_{T1}	0.45	3.5	4.5	LAYER 1
V_{T2}	0.72	8	8	LAYER 2
V_{T3}	1.84	1.84		LAYER 3

FIG. 4:1:17 CASE 4 TIDE PLOT TF1 > Tt1

Case 6

This case illustrates the effect of a simple fault on the field data and hence the derived field model, as shown in Fig 4:1:19. The contour lines are not parallel with the diagonal of the TIDE plot, indicating that there is a discontinuity in the velocity structure just below the superficial layer. In general, the effect of incorrect substitution of the velocity value in the theoretical model creates a relatively large spread in delayed time values in parallel with the diagonal, but an incorrect substitution of the thickness of a layer is displayed as a very narrow spread in delayed time values in parallel with the diagonal.

The geophones' positions are represented by the position of delayed time values on the diagonals, and the depth from surface to bottom layer is represented by the distance from diagonal to apex of the triangle. However, the relationship between the geophone position and a particular discontinuity at depth in the field model has not been studied to give a correlation between the field and the theoretical models.

If irregular contours are to be identified as the effect of cavities, then the theoretical model has to be adjusted so that parallel contouring is eliminated. Banding in the direction of 90 to the diagonal would represent such features as faulting, dykes, etc. The above method is most suitable for processing on micro-computers, which are used increasingly for on line field analysis.

The TIDE method was used on the data obtained from the Cocking site. Data from the seismic line in parallel with the tunnel (SL3) was compared with the seismic line across the tunnel (SL4). SL3 was used for the theoretical model, since it was the closest seismic line to the tunnel and hence represented the velocity structure of the infill and bedrock material. SL4, which was used as field data, had a geophone spacing of 2 m, but SL3 had a different geophone separation. The TIDE method requires geophone spacing to be the same, and it was therefore necessary to take relevant travel times for a 2 m geophone spacing from the travel time graph for SL3.

Fig 4:1:20 shows the TIDE plot of results obtained when SL4 is compared with SL3. The contour map of the TIDE plot shows that there is some

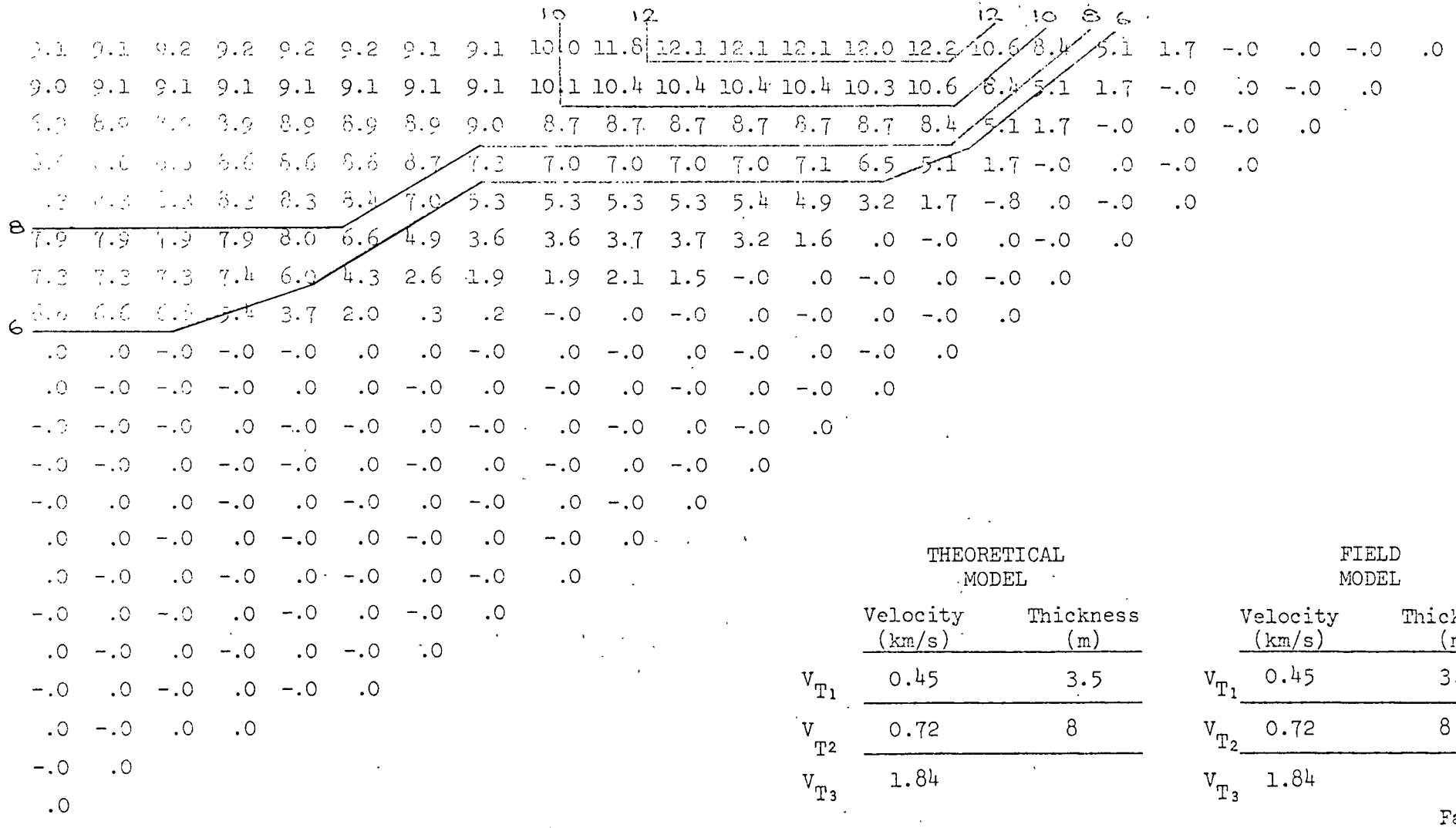


FIG. 4:1:19 CASE 6 TIDE PLOT FOR A MODEL OF FIELD SURVEY ACROSS A FAULT

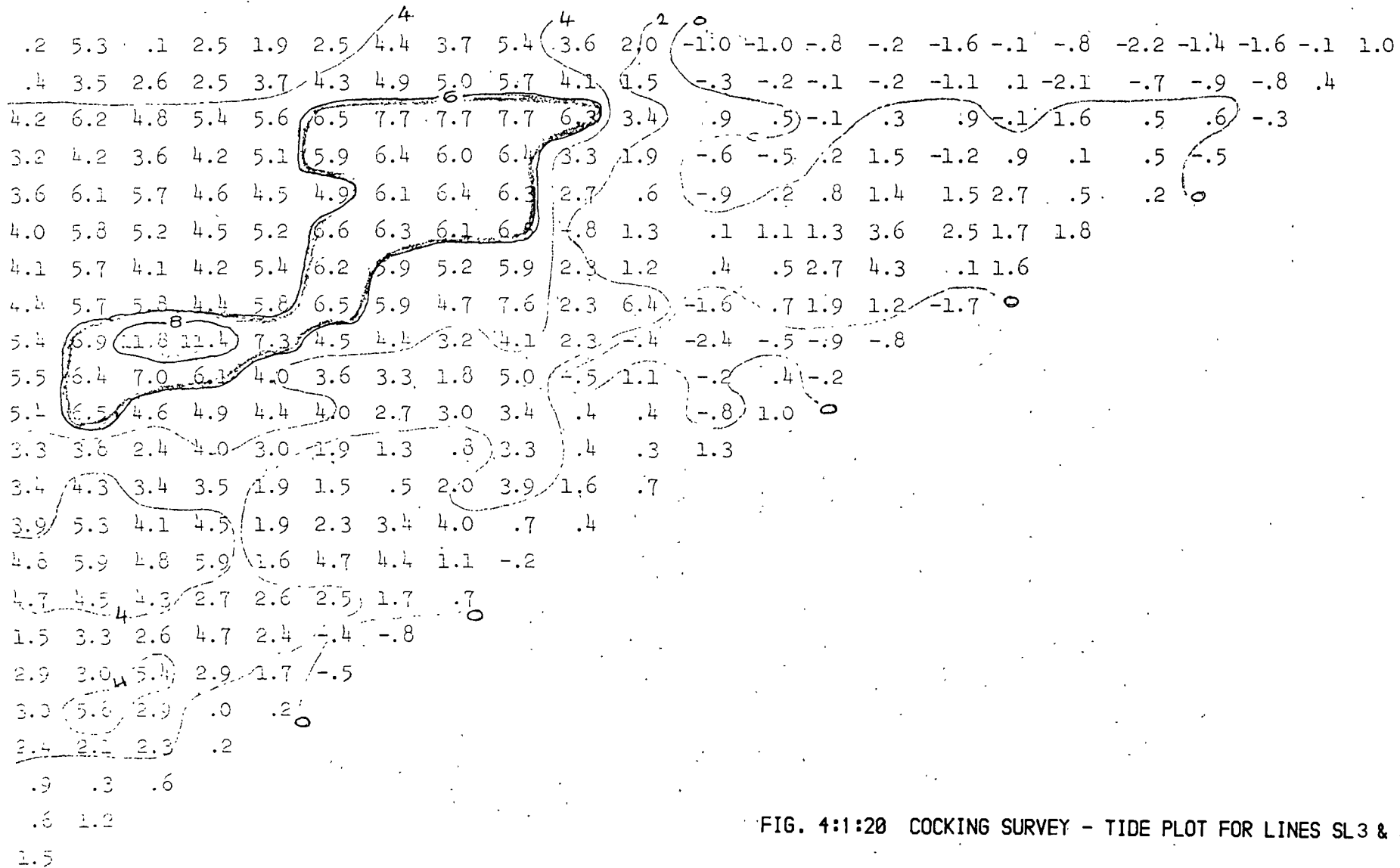


FIG. 4:1:20 COCKING SURVEY - TIDE PLOT FOR LINES SL3 & SL4

variation in delay caused by superficial material from the two seismic lines, represented by the variation in the numerical values at the base of the triangle on the longest side. There is a group of high numerical values contoured in the centre of the TIDE plot and numerical values reduce towards the edge of the TIDE triangle. The higher numerical contour values are presumed to reflect delays caused by the presence of the tunnel and its effect on the surrounding mass.

Data smoothing process of the TIDE method (using matrices up to Table 4:7) was used on the data from SL4 (across the tunnel) and SL1 (parallel with the tunnel). The smoothed data was plotted as time/distance curves, as shown in Fig 4:1:21. The two curves follow similar paths until at geophone position G13, where the seismic line across the tunnel shows a considerable delay due to the effect of the presence of the cavity on the propagation of the seismic pulse. Here again, a comparison is made between the data with the cavity in its path to that without it, with the data obtained within the confinement and constraints of the site. This approach enhances and highlights the differences in the two data sets.

A ray tracing method was used to assess which geophone will be the first to encounter the delay caused by the presence of the tunnel. The result shown in Fig 4:1:22 indicates that G14 was the first geophone to 'see' the delay, which is in agreement with the experimental data (Fig 4:1:21).

This method is in its infancy and considerably more work is needed to understand and improve its representation, but it does provide a very useful method of producing an image of gross variations in the rock mass which is relatively easy to visualise.

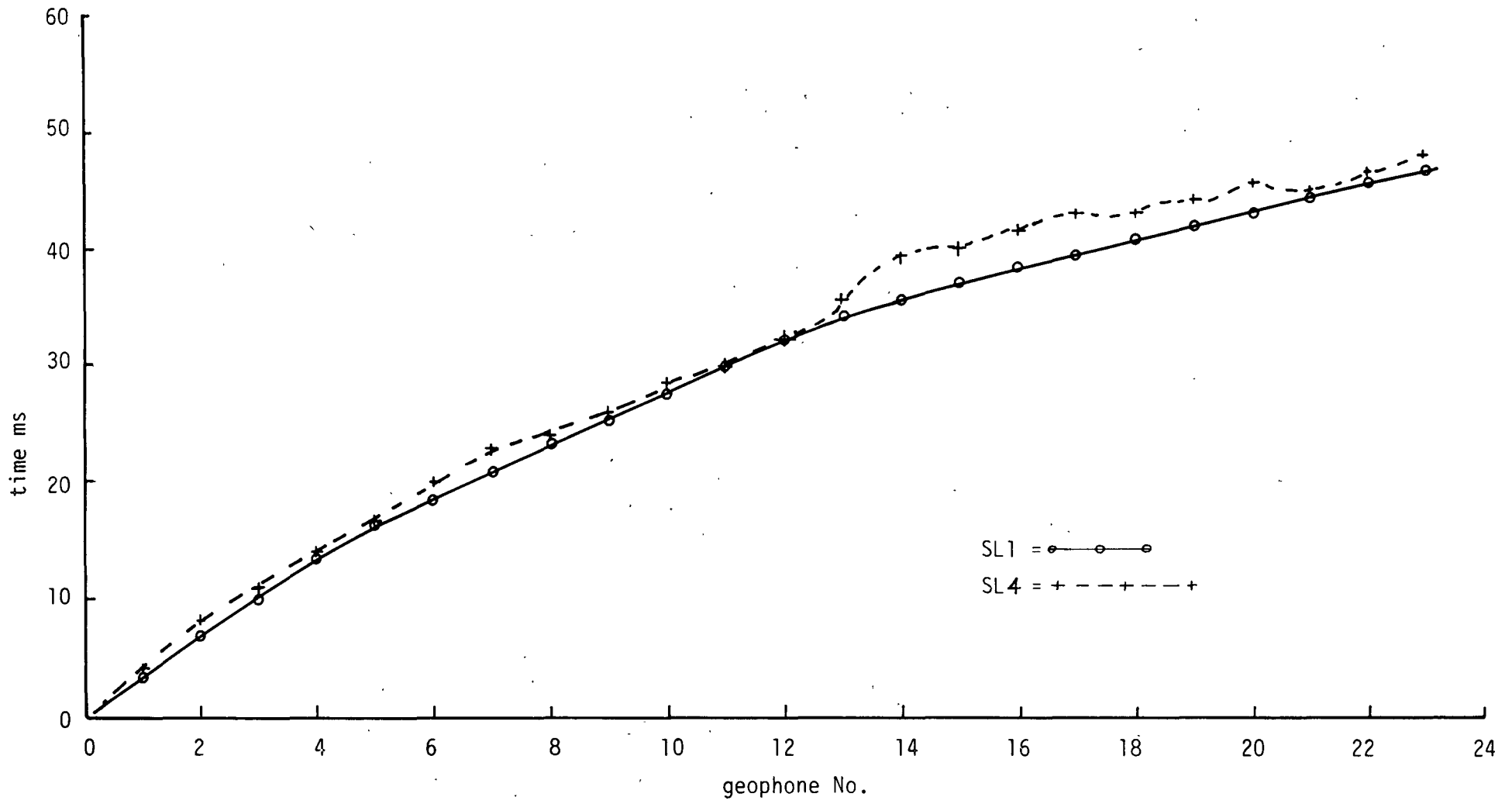


FIG. 4:1:21 COCKING SURVEY - PROCESSED DATA
FROM SEISMIC LINE 1 & 4

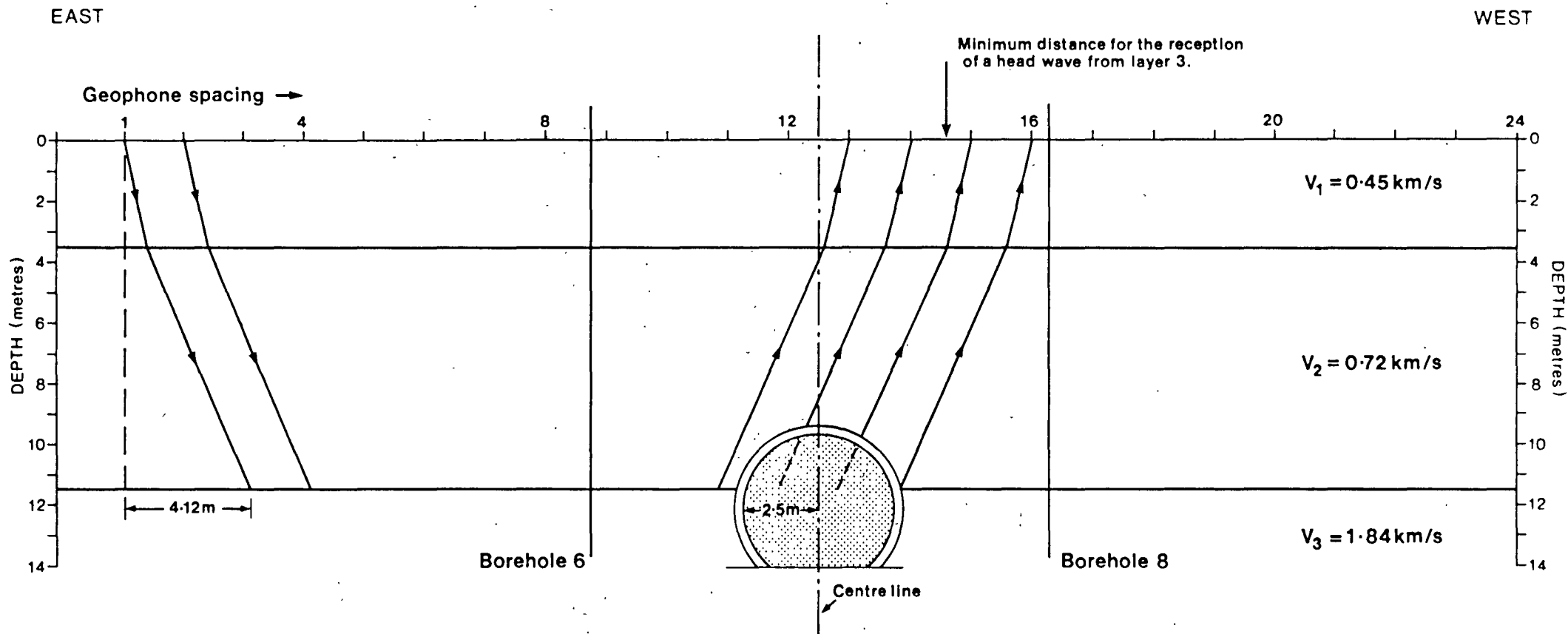


FIG. 4:1:22 RAY PATH DIAGRAM FOR A THEORETICAL SEISMIC MODEL
OF THE ROCK MASS AROUND THE COCKING TUNNEL

4:2 Seismic reflection method

The seismic reflection method is by far the most widely used geophysical technique, particularly in the hydrocarbon field, for the determination of lithology and structure at great depths from velocity and attenuation data (Dobrin 1976) and for the detection of gas deposits on the basis of reflection amplitudes. The method has been developed to a very high degree of sophistication since the modern survey requires the use of multiple geophone arrays, tape recording, analogue to digital converters, complex digital filtering systems and computer analysis.

The seismic reflection method comes closer than most geophysical techniques to providing a structural cross-section of the sub-surface geology, which can readily be interpreted by the geologist. Its development and use in the field of civil engineering is, therefore, extremely worthwhile since if the practical difficulties mentioned briefly below could be overcome there is no doubt that the method could provide information that could be directly applied in a site investigation. Hence, the method is considered in some detail even though its current application for the location of geological hazards, such as cavities, is somewhat limited.

The major problem associated with the use of the seismic reflection method in shallow engineering problems is the balance between optimum resolution and penetration. The penetration of the seismic pulse is controlled by the attenuating properties of the material and this is frequency dependent. Thus, for deep penetration a fairly low frequency seismic source should be used, such as explosives or an air-gun. This, however, inevitably results in an increase in the pulse length, which will result in a decrease in the resolution that can be achieved. If the thickness of a layer is less than half the wave length of the incident seismic energy, interference will take place between the seismic pulse reflected from the top and bottom interfaces of the layer and it will not be resolved.

Most seismic reflection surveys are based on continuous coverage of the reflecting horizon and the geophone spread must be laid out relative to the source such that the reflected signal is enhanced in some way to make it stand out, firstly on the seismic record and, secondly, in the final digital computation.

4:2:1 Theory and principles

The principle of seismic reflection has been discussed comprehensively by Dobrin (1976; Ref 15) and Telford (1976; Ref 13) using Huygens' principle and Snell's Law, which is normally associated with optics.

Applying Huygens' principle to the case of a plane longitudinal wave impinging obliquely upon an interface between two elastic media having longitudinal velocities of V_1 and V_2 , transverse velocities of V_{S1} and V_{S2} , and densities of ρ_1 and ρ_2 , respectively (Fig 4:2:1). An incident wave front AB would produce a longitudinal wave reflection which will have an angle of reflection r_L equal to the angle of incidence i , and a transverse wave which will make angle r_T with the interface, determined by the relation

$$\sin r_T = (V_{S1}/V_1)\sin i \quad - (4.9)$$

In the case of normal incidence, the reflection coefficient R is given by

$$\begin{aligned} R &= A_2/A_1 = (P_2V_2 - P_1V_1)/(P_2V_2 + P_1V_1) \\ &= (Z_2 - Z_1)/(Z_2 + Z_1) \end{aligned} \quad - (4.10)$$

where

- A_1 = incident wave amplitude
- A_2 = reflected wave amplitude
- Z = acoustic impedance, the product of PV

Reflected amplitude in this case depends on the contrast in the product of density and velocity (acoustic impedance) on opposite sides of the interface, from which the incident wave approaches. When the medium containing the incident wave has a smaller acoustic impedance than the medium across the interface, there is no phase change on reflection. When the opposite is true there is a 180° phase shift. Thus, a compression becomes a rarefaction upon reflection from a medium having a lower product of seismic velocity and density.

Standard seismic reflection methods used for mapping geological structures, and interpretation of these methods, are discussed comprehensively by Telford et al (1976; Ref 13) and Dobrin (1976; Ref 15).

Geological structures are mapped using seismic reflection surveys by measuring arrival times of pulses which have been reflected from interfaces between regions of different impedance. The general objective of the reflection method is to determine layer thicknesses and depths as well as associated irregularities.

The seismic reflection method can best be explained by the example of a horizontal sedimentary layer overlying a basement rock of different thickness, as shown in Fig 4:2:2. When a seismic pulse is applied at shot point 0, the pulse reflected at depth h and measured with respect to initiation time for geophone offset distance x , the wave path is governed by two parametric equations:

- a a relationship between reflector depth h and geophone offset distance x :

$$x = 2h \tan \alpha \quad - (4.11)$$

- b an expression for travel time t :

$$t = 2h / (V \cos \alpha) \quad - (4.12)$$

Therefore, if angle α of emergence is known, depth h and velocity V of the stratum can be determined. When the geophone is placed close to the shot and the offset distance is very small, then vertical travel time (t_0) is of special importance.

Velocity V in the first layer can be determined using equation (4.12) and with $\alpha = 0$:

$$V = 2h / t_0 \quad - (4.13)$$

Time delay Δt between uphole time t_0 and arrival time t , as a function of offset distance x (Fig 4:2:3), is known as the normal moveout. Many velocity analysis methods use normal moveout intervals, assuming straight line wave propagation within each layer of the ground. Considerable information on velocity anomalies, departures from parallel stratifications and multiple reflections can be obtained from the normal moveout measurements.

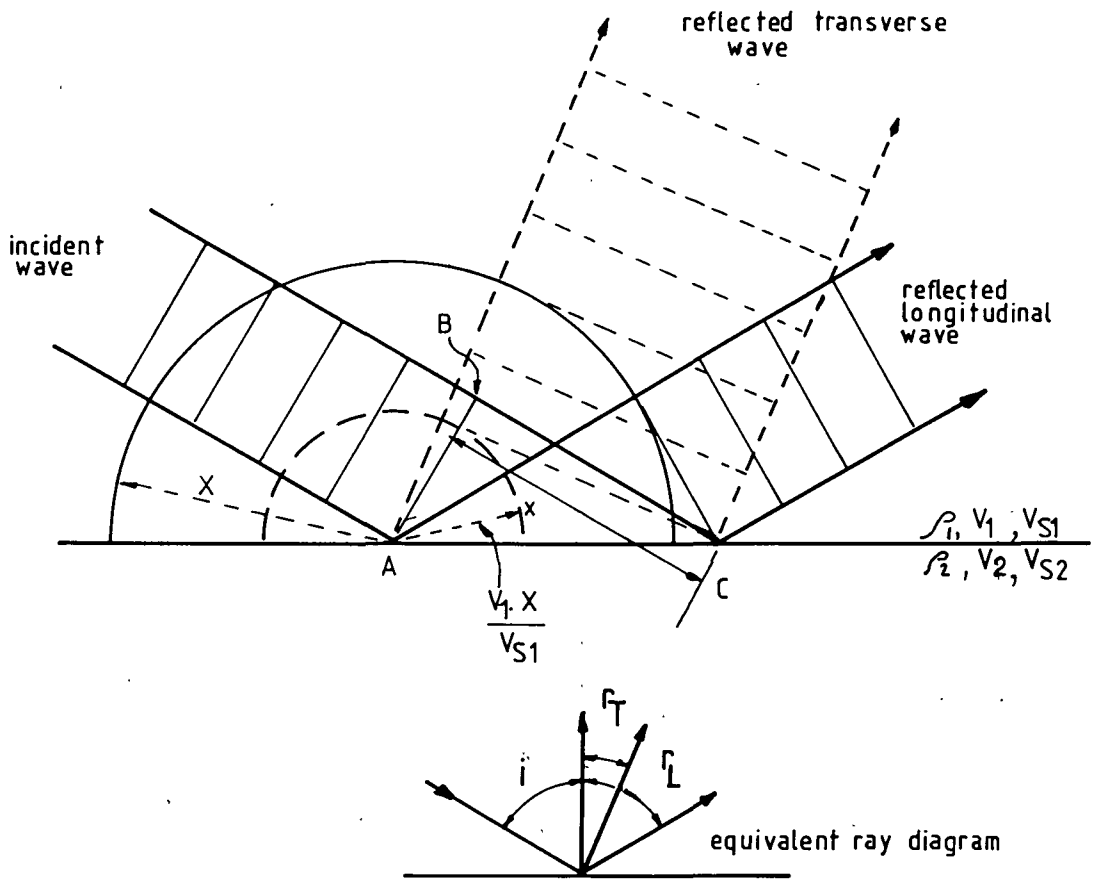


FIG. 4:2:1 REFLECTION OF PLANE ELASTIC WAVE AT INTERFACE

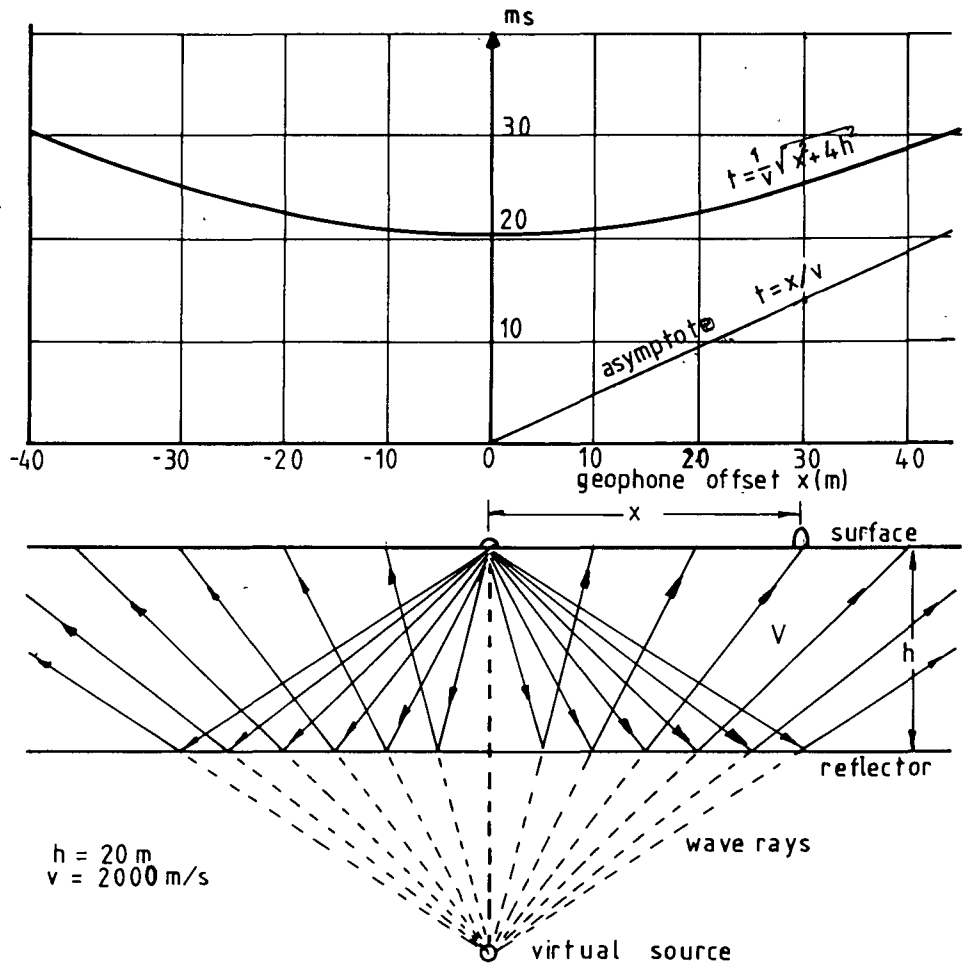


FIG. 4:2:2 WAVE RAYS AND TIME/DISTANCE DIAGRAM FOR REFLECTION FROM TWO LAYER CASE

The normal moveout time delay Δt can be derived using Fig 4:2:3 as

$$\Delta t = t - t_0 \quad - (4.14)$$

where $t^2 = t_0^2 + (x/v)^2 \quad - (4.15)$

giving $\Delta t = (1/(t + t_0))(x/v)^2 \approx (1/2t)(x/v)^2 \quad - (4.16)$

and $v \approx x/(2t\Delta t)^{\frac{1}{2}} \quad - (4.17)$

The velocity-time layer can be obtained by plotting x^2 against t^2 , as shown in Fig 4:2:4, where $1/v^2$ is the slope of a straight line passing through the t^2 axis at point t_0^2 .

For a dipping interface, as shown in Fig 4:2:5, the time-distance plot is obtained by using the reflection laws of optics, which gives

$$t^2 = t_0^2 + (x \cos i/v)^2 \quad - (4.18)$$

$$\Delta t = 1/2t(x \cos i/v)^2 \quad - (4.19)$$

$$v = x \cos i/(2t\Delta t)^{\frac{1}{2}} \quad - (4.20)$$

where $i =$ inclination angle

For a stratified geological structure generating multiple reflections, as shown in Fig 4:2:6, a set of general equations can be shown as

$$t_{0,n} = 2\sum_{i=1}^n (h_i/v_i) \quad - (4.21)$$

$$t_n = 2\sum_{i=1}^n (h_i/v_i^*) \quad - (4.22)$$

where $V_i^* = V_i \cos \alpha_i$
 $n =$ number of layers
 $t_{0,n} =$ travel time of vertically reflected waves from the bottom of the nth layer
 $t_n =$ arrival time of slant reflections from the same interface

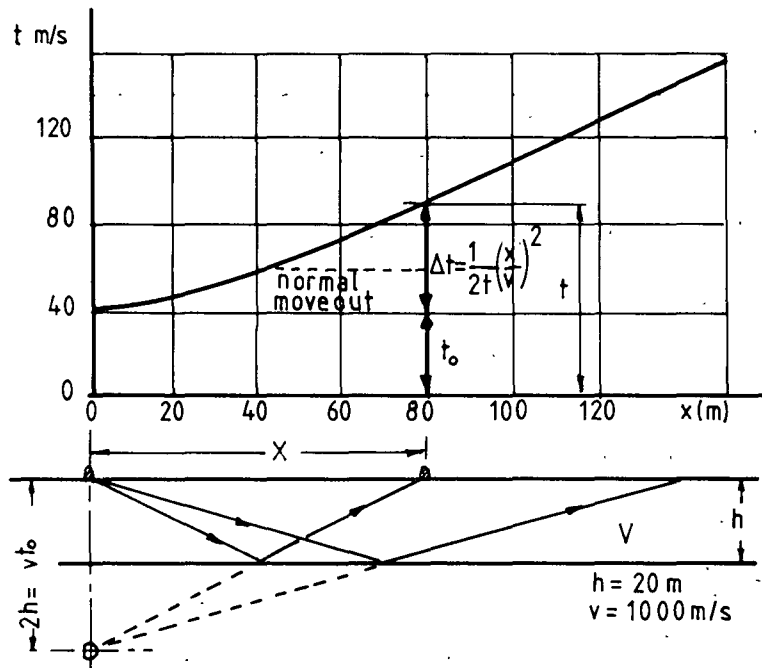


FIG. 4:2:3 NORMAL MOVEOUT (Δt) AS A FUNCTION OF GEOPHONE OFFSET (x)

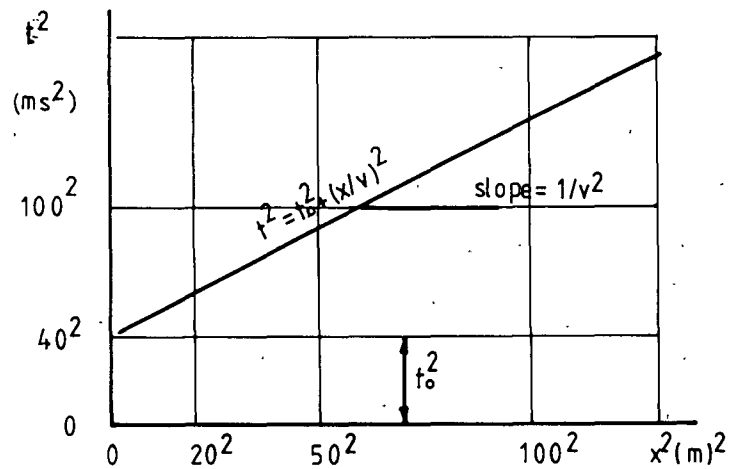


FIG. 4:2:4 NORMAL MOVEOUT ($x^2 - t^2$)

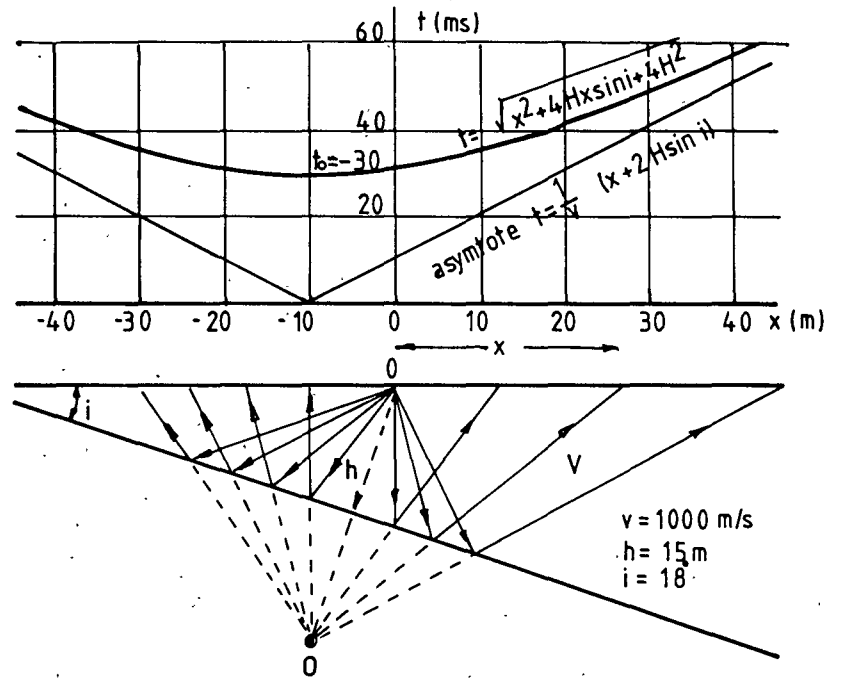


FIG. 4:2:5 RAY-PATH CONSTRUCTION AND TIME/DIST. DIAG. FOR REFLECTIONS FROM A DIPPING INTERFACE

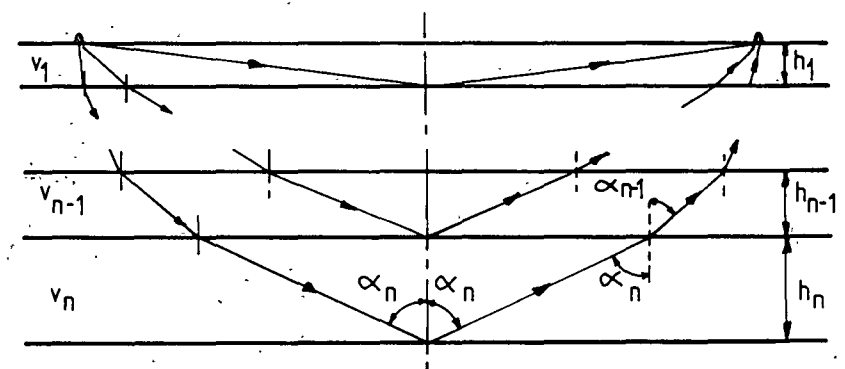


FIG. 4:2:6 MULTILAYER REFLECTION

Offset distance x will be related to the horizontal travel path by

$$x = 2\sum_{i=1}^n h_i \tan \alpha_i \quad - (4.23)$$

Vertical delay time Δt_n between vertical reflection time $t_{o,n}$ and slant time t_n can be approximated to

$$\Delta t_n = x^2 / \sum_{i=1}^n (4h_i V_i) \quad - (4.24)$$

The corresponding time delay t_{n-1} for reflection from the bottom of the (n-1) layer is given by

$$\Delta t_{n-1} = x^2 / \sum_{i=1}^{n-1} (4h_i V_i) \quad - (4.25)$$

Using equations (4.24) and (4.25), we can obtain

$$V_n = (x^2 / 4h_n) [(1/\Delta t_n) - (1/\Delta t_{n-1})] \quad - (4.26)$$

The nth layer thickness h_n can be eliminated by use of the vertical reflection times $t_{o,n}$ and $t_{o,n-1}$

$$h_n = 0.5 V_n (t_{o,n} - t_{o,n-1}) \quad - (4.27)$$

The latter two equations allow computation of velocity V_n and thickness h_n , when reflection arrival time and delay time data are given for n successive reflections.

4:2:2 Case histories

The use of the method for the location of cavities and other types of anomalous ground conditions is limited by the available seismic sources. When the wavelength of the incident seismic energy is greater than the cavity diameter very little energy will be reflected back to the surface (see chapter 6:1:4 for experimental result). In a shallow survey, reflections from the near surface interface are often completely obscured by the large amplitude of surface wave arrivals and are consequently difficult to identify.

Nevertheless, considerable effort has been made over the past decade to develop this method for use in the civil engineering field down to depths of 30 m. McCann et al (1982; Ref 92) suggest that a high frequency energy source, operating in a 700-1500 Hz bandwidth used in conjunction with common depth point reflection processing, does have considerable potential. Greater resolution could be achieved with the use of multiple geophone or accelerometer arrays used in conjunction with digital stacking.

Two case histories are briefly described to illustrate the problems associated with the seismic reflection method when looking at shallow reflections. However, the overall usefulness of the method for studying deeper reflection should also be noted.

a Standard seismic reflection survey at Onley

As has been mentioned above, the seismic reflection method is not widely used in the engineering geological context and suitable case histories (McCann et al, 1982; Ref 95) illustrating the use of the method are difficult to find. However, a standard seismic reflection survey carried out at Onley near Rugby, Northamptonshire, will be briefly described to illustrate the complexity of the basic survey procedure.

The disused track of the old Great Central Railway to the south of Rugby was used for a standard seismic reflection survey to compare the performance of seismic sources, such as a borehole air gun, a gas gun, and a sparker, with that of gelignite. A complete description of the work is given by Andrew (1979; Ref 96) and only the results of the surveys using gelignite are discussed. The profile was marked out as shown in Fig 4:2:7 and the common depth point surveying method was used.

The data recorded during the survey were processed by Seismograph Services (England) Limited using their standard package on the Phoenix computer; the resulting time section is shown in Fig 4:2:8. This shows a very strong reflection at a two way time of about 140 ms, another strong reflection above it at 85 ms and several minor reflections, continuous above but somewhat broken below 140 ms, but all essentially associated

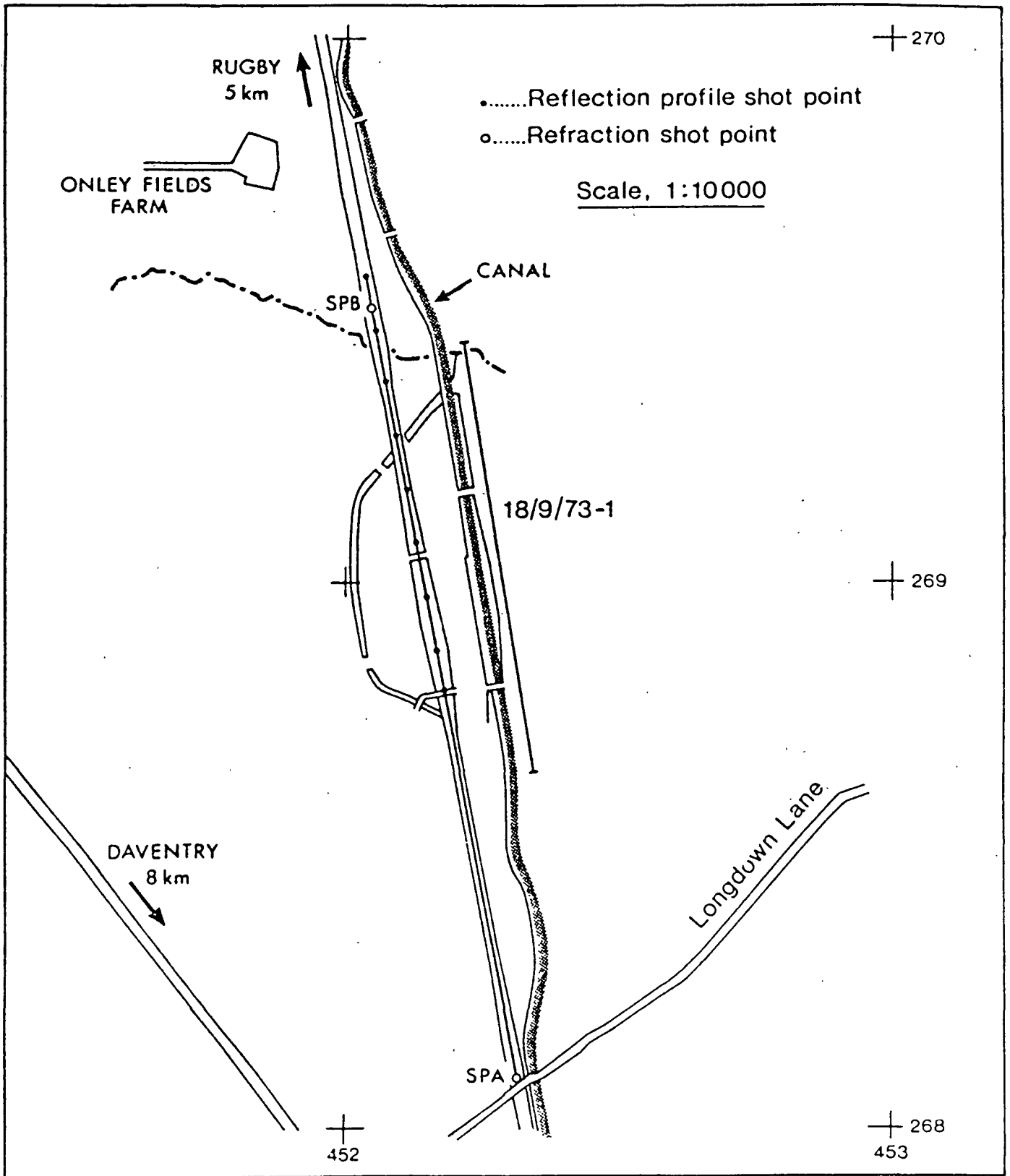


FIG. 4:2:7 MAP OF THE ONLEY AREA SHOWING THE POSITIONS OF THE SEISMIC REFLECTION PROFILES ON THE DISUSED RAILWAY TRACK & THE CANAL (after McCann et al 1982; Ref 95)

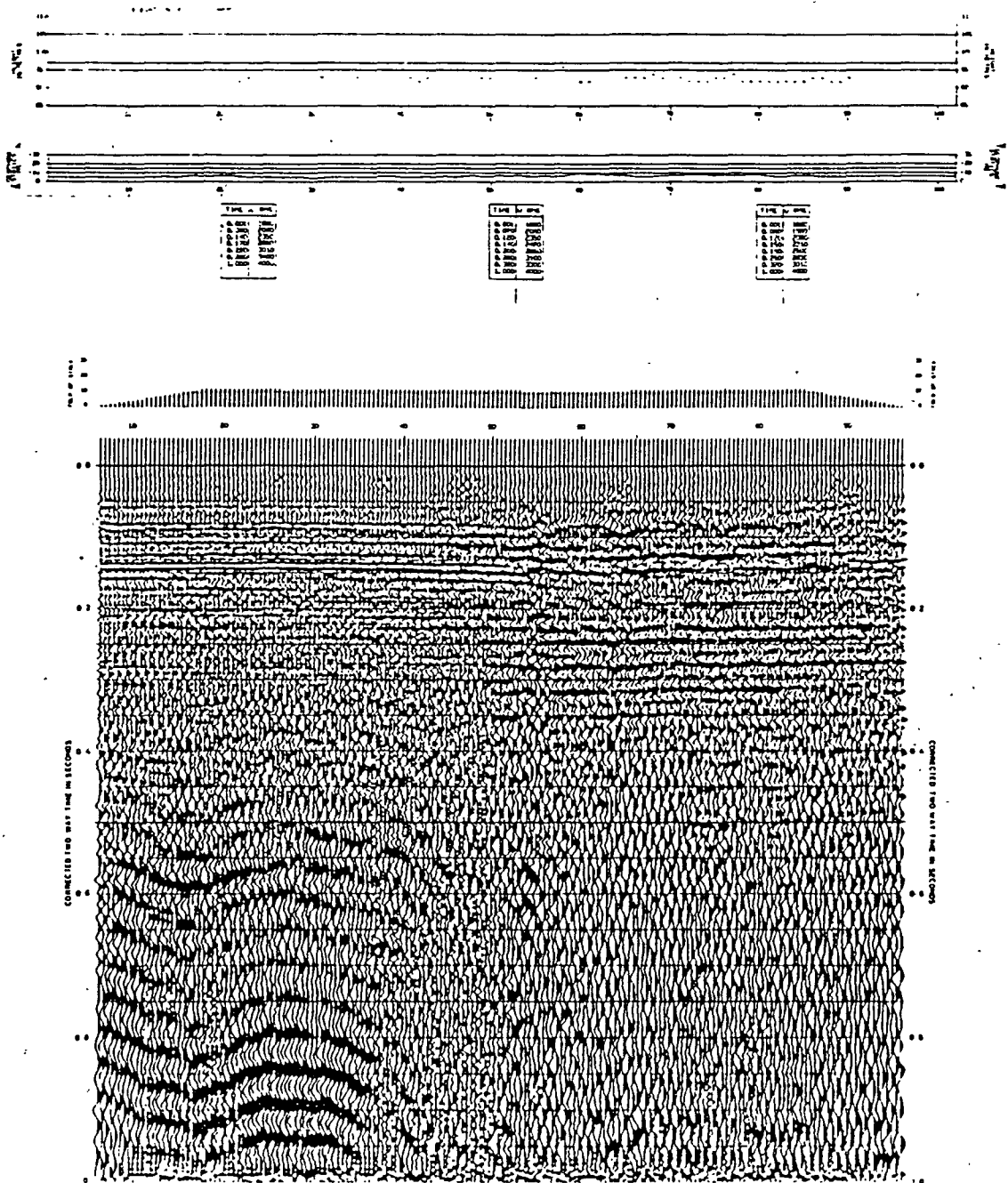


FIG. 4:2:8 COMPUTED TIME SECTION FROM THE ONLEY SEISMIC REFLECTION PROFILE WITH GELIGNITE AS THE SEISMIC SOURCE (after Andrew, 1979; Ref 96)

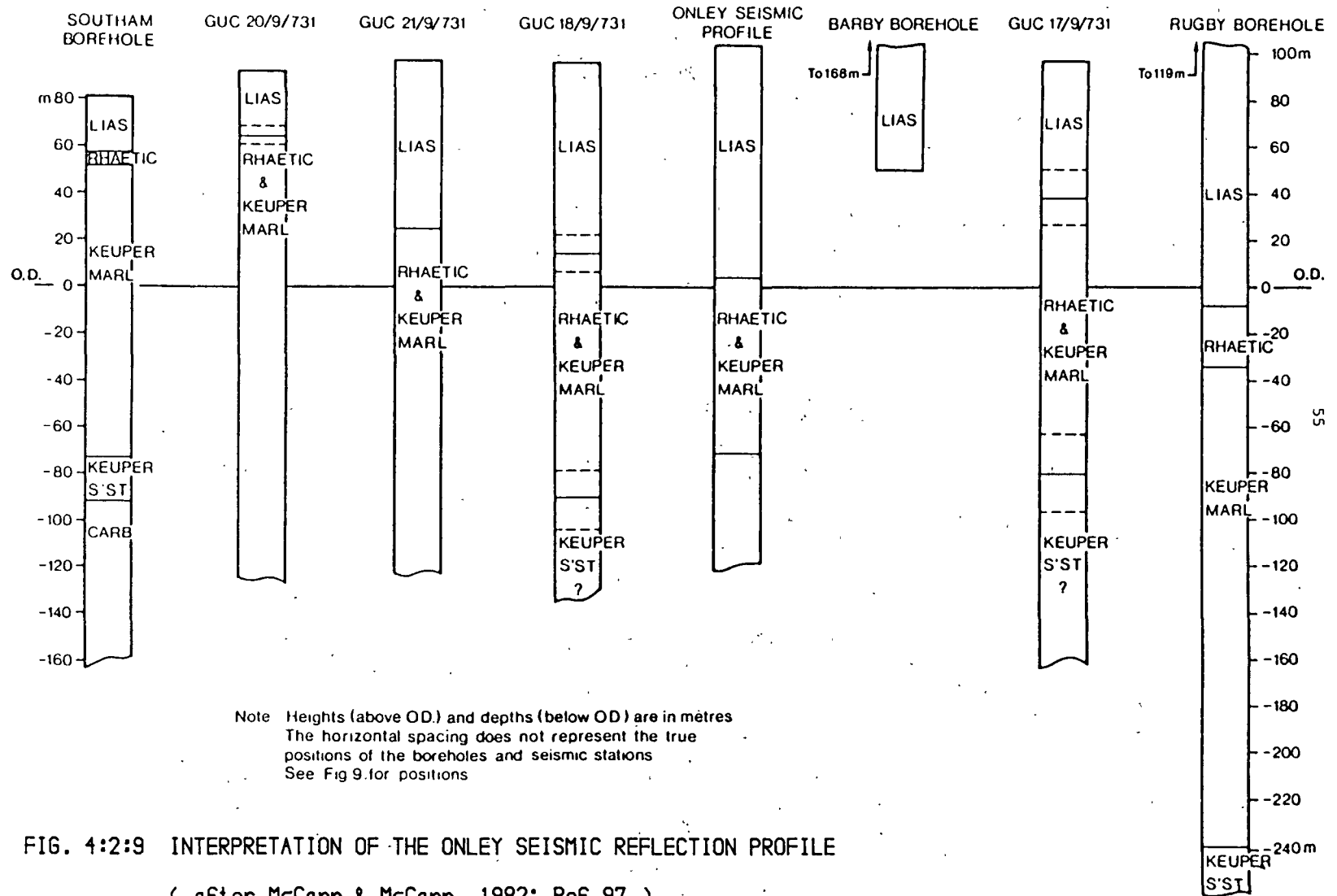
with horizontal reflectors beneath the southern half of the line. The character and clarity of these reflections change dramatically under the northern half of the line, the high frequency content having been lost. On the southern part of the line a low frequency event is observed below about 0.35 sec two way time.

The presence of very strong reflectors at 86 ms and 136 ms two way time is confirmed by the profile obtained on the adjacent canal (McCann and McCann, 1983; Ref 97). The authors surmise that the reflector at 86 ms is, in fact, from the top of the Liassic basal limestone, known as the White Lias, at a depth of 17 m above O.D. The authors suggest that the deeper reflection is not a multiple and the overburden velocity is too high. It is, therefore, reasonable to identify this as the Keuper/Palaeozoic boundary at a depth of 81 m below O.D. Two other reflectors, at 108 ms and 129 ms two way time, are indicated at 23 m and 51 m below O.D. respectively. The lower one may well be the top of the Keuper sandstone, giving only 60 m for the thickness of the Rhaetic and the Keuper Marl. All the seismic and geological information from this area is summarised in Fig 4:2:9 which is taken from McCann and McCann (1983; Ref 97).

The survey described above illustrates the complex nature of the seismic reflection method and the difficulties in applying it in the civil engineering field. The lack of high frequency energy associated with most standard seismic sources limits the resolution that can be achieved in the top 30 m and would prevent the detection of most anomalous zones in the superficial deposits.

b Seismic reflection survey over known cavities

The results of several seismic reflection surveys have led Cook (1965; Ref 98) to believe that the variation in amplitude attenuation can successfully delineate suitable brine cavities in bedded salt at depths up to 500 m. Originally Cook expected to delineate the brine cavity by searching the seismic records for anomalous amplitudes associated with the cavity (Fig: 4:2:10). Due to the marked difference in reflection and transmission coefficients between the brine cavity and the surrounding undissolved material, strong amplitude reflections from the flat-topped cavity, and severe amplitude attenuation ('seismic shadow')



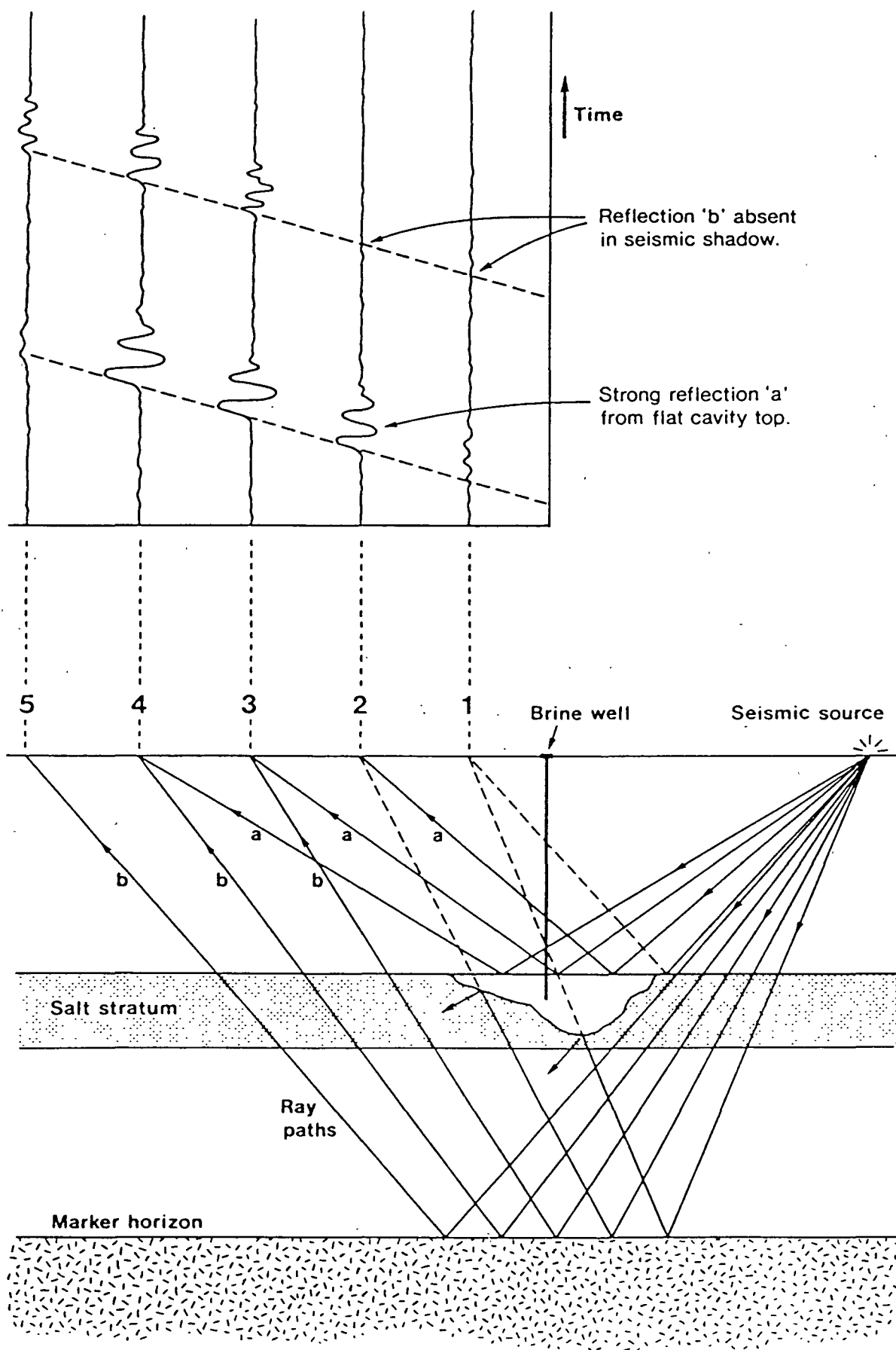


FIG. 4:2:10 IDEALISED SEISMOGRAM AND SOLUTION CAVITY, SHOWING
 EXPECTED RESULTS (after Cook, 1965; Ref 98)

for those waves travelling through the brine solution, were expected.

A special plate charge was devised to deliver horizontally polarised shear waves into the ground. It was hoped that the high reflectivity for the shear waves at the brine interface would improve the chances of locating the cavity. Unfortunately, the seismic reflections obtained from the top of the salt horizon proved disappointing, chiefly because of predominant reverberation noise. Possible strong reflections were noted by Cook which could have resulted from reflection at the top of the interface of the brine cavity, but better results are needed for reliable interpretation.

Cook made a detailed study of seismic records showing strong reflections obtained from another solution-mining area. Three strong reflections were noticeable and were designated A, B and C: reflection B was thought to correspond to the solution mining horizon at an approximate depth of 500 m. Various techniques were employed to see if there was a consistent amplitude variation in the reflections which would correlate with the presumed position of the brine cavities.

By far the most promising results were obtained when the amplitude ratio for reflections A and C were computed for each seismic trace with no automatic gain control applied. On plotting the amplitude ratio A/C against geophone location, anomalous values were found to coincide with the approximate position of the brine well (Fig 4:2:11). This was as predicted by simple theory, and was taken to represent 'shadowing' of the underlying reflector C by a seismically opaque object.

In the mined out, flooded areas, the ratio A/C is highly variable, and Cook attributed this to diffraction from irregularities in the brine cavities roof and the possible local variations in longitudinal P wave transmissivity due to the presence of air pockets. Cook claims that this method attains a lateral resolution of 5 m (approximately $\frac{1}{4}\lambda$) for a cavity at a depth of 500 m, where λ is the wavelength of the incident seismic wave.

The size of the cavity may have been underestimated because the laboratory experiment discussed in Chapter 6:1:4 indicates that the diameter of the obstruction in the path of a wave has to be over a half

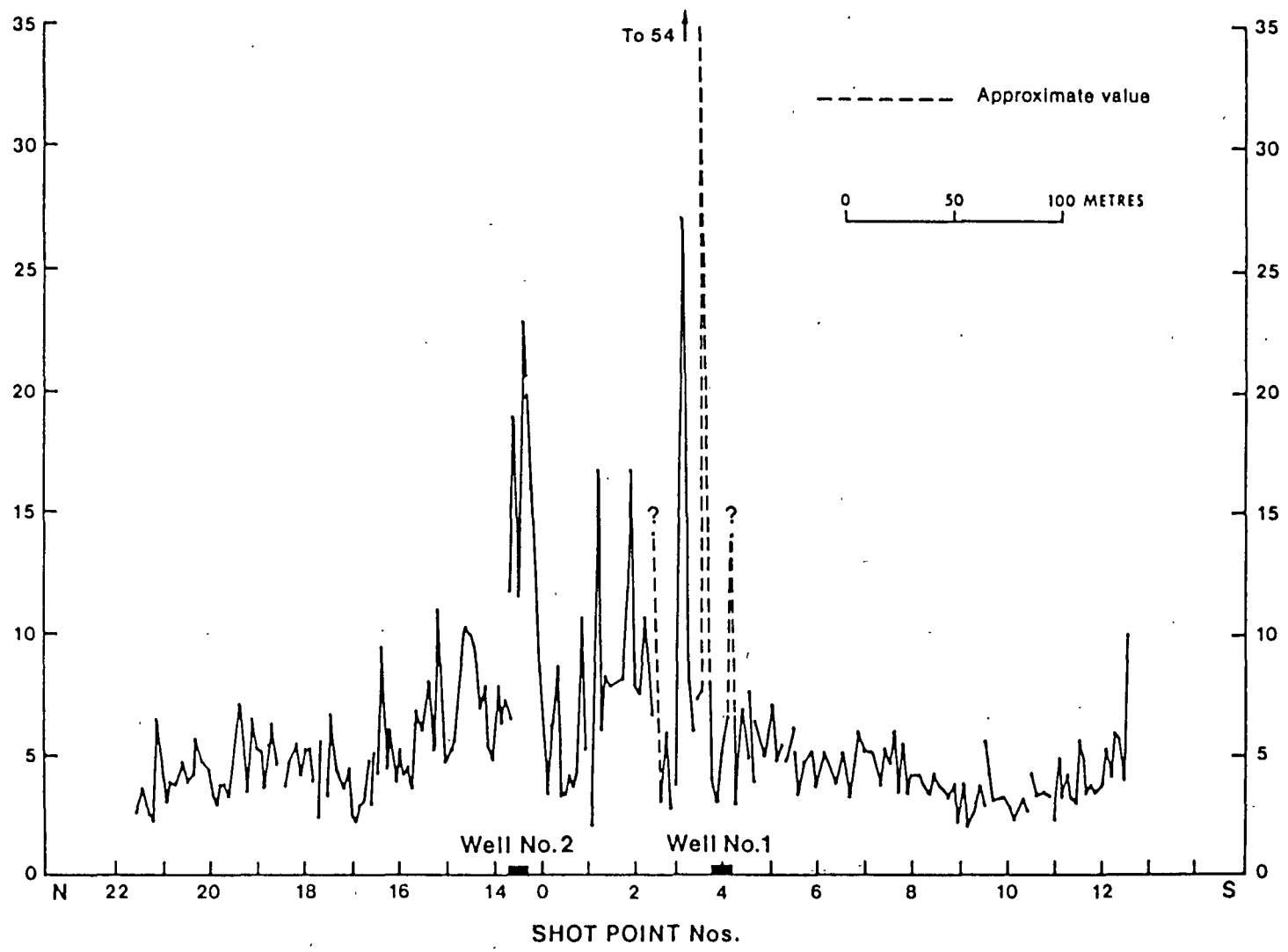


FIG. 4:2:11 PLOT OF NORMALISED REFLECTION "C" ALONG TRAVERSE SHOWING
'SEISMIC SHADOW' ANOMALY NEAR WELLS (after Cook, 1965; Ref 98)

wavelength to produce a noticeable attenuation in the amplitude.

Despite the success of the method, it is seldom used because the field procedure for the resolution required for reflection from shallow boundaries is uneconomical; the geophone spacing must be small compared to the depth of penetration, which would ultimately limit the area covered.

4:3 Seismic resonance method

All systems possessing mass and elasticity are capable of relative motion. If the motion of such systems repeat itself after a given interval of time, such a period motion is known as vibration. When an external force is applied to the system, it will oscillate at its natural frequency. But when the frequency of excitation is equal to the natural frequency of the system, resonance occurs and the amplitude of vibration will increase without bounds, being governed only by the amount of damping present in the system.

Long refraction seismic records in the vicinity of cavities frequently exhibit constant frequency oscillations for periods up to four seconds after the shot instant. According to Watkins et al (1967; Ref 101), following several field investigations, this phenomenon is a result of oscillations being excited in the cavity walls by an explosion near the ground surface. Unfortunately, the exact mechanism of the seismic resonance phenomenon is not fully understood, and it is likely that present theories will undergo constant amendment as more knowledge is gained.

4:3:1 Theory and principles

Initial interpretation of the cavity resonance phenomenon was based on theoretical work by Biot (1952; Ref 102). Biot showed, by consideration of radial oscillations in a cylindrical hole in an infinite solid, that minimum dispersion occurs for a wavelength approximately equal to one and a half times the cavity diameter (Fig 4:3:1). The sharp frequency cut-off shown in Fig 4:3:1 suggests that several comparisons can be made between the characteristics of the cavity and electrical analogue circuits (Kinsler and Frey, 1962; Ref 103). It is a property of sharp

cut-off filters that ringing (reverberation) occurs in response to a step input pulse. By further analogy, the more rapid the energy loss from a cavity by radiation (ie for large dispersion), the wider is the frequency spectrum radiated from it. In order to maintain the resonant frequency within a narrow bandwidth, the cavity must be driven with a harmonic source of that frequency.

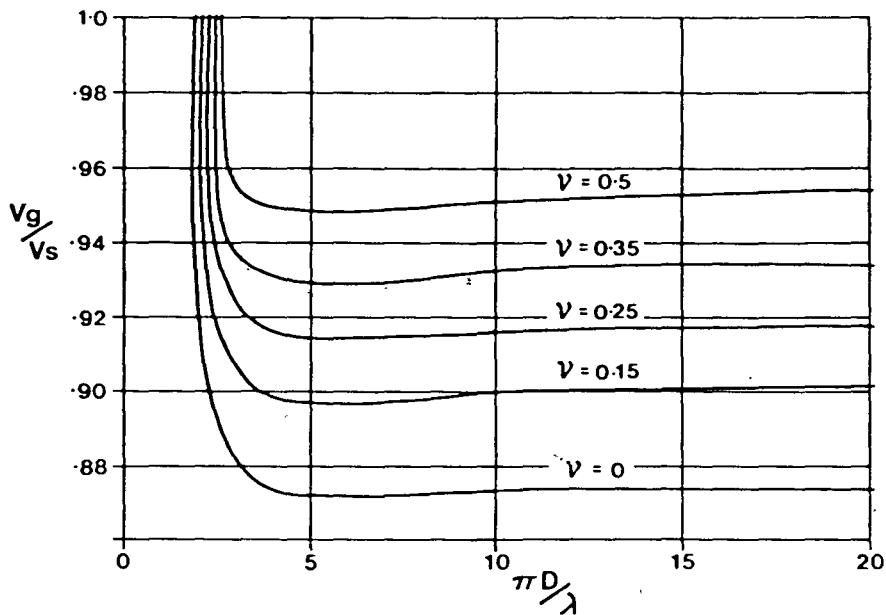
According to the theoretical considerations of Biot (1952; Ref 102), the diameter of a cavity D (m), a shear wave velocity V_s (ms) and a resonance frequency f are related in the following manner, for a cylindrical hole in an infinite solid:

$$D = V_s / 1.55 f \quad - (4.28)$$

Although actual cavities are seldom of this idealised form, an estimate of the size can be made if the frequency data are successfully retrieved from the field record, and provided the shear wave velocity is known, or can be calculated. However, determination of the resonant frequency requires that electronic filtering and automatic gain control (AGC) should not be used, as this may remove the characteristics of resonance which contain the useful information. Because of the relatively long duration and narrow frequency band of the cavity oscillations, it has been suggested that the signal enhancement technique be applied to the field records so that the oscillations may be identified, even in a noisy background.

4:3:2 Case histories

Initial experiments investigating seismic resonance were carried out over known cavities by Watkins et al (1966; Ref 101), and an outline of the field procedure and the results are given below. A large array of geophones were laid perpendicular to, and centred over, the longitudinal axis of a small lava tube. An explosive source, with a broad frequency spectrum, induced oscillations in the walls of the cavity, which were recorded on these geophones in the vicinity of the cavity. The seismic records show that the dominant frequency associated with cavity wall oscillations is relatively uniform with time, but due to the masking effect of the initial 'ground roll' they are not observable until approximately one and a half seconds after the shot instant (Fig 4:3:2).



V_g = group velocity; V_s = shear velocity; D = hole diameter; λ = wave length; ν = Poisson's ratio.

FIG. 4:3:1 GROUP VELOCITY FOR AN EMPTY CYLINDRICAL HOLE
(after Biot, 1952; Ref 102)

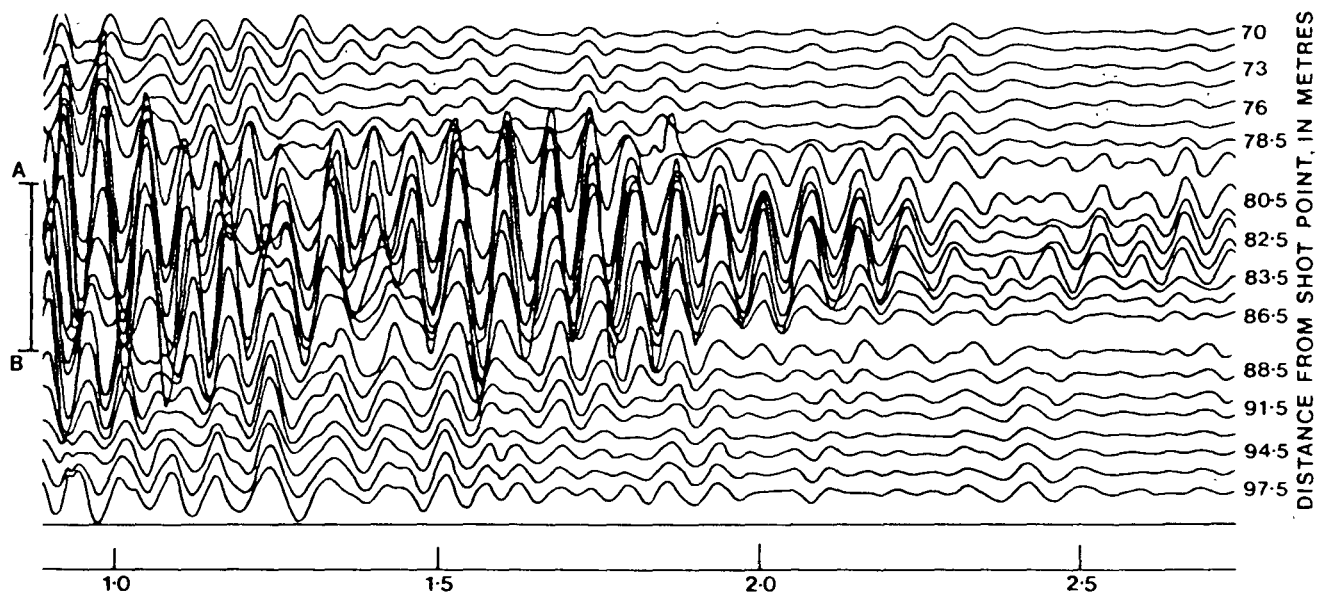


FIG. 4:3:2 PART OF A SEISMOGRAM SHOWING RESONANCE IN THE VICINITY OF
A CAVITY. A-B INDICATES THE LOCATION AND THE WIDTH OF
THE CAVITY (after Watkins et al, 1967; Ref 101)

Based on the above relationship between diameter and resonant frequency, the diameters of the two cavities investigated (lava tubes) were calculated from seismic records and compared to their known value. In both cases the calculated diameter was three times larger than the actual size. Of course, errors are to be expected, because cavities do not take the idealised form used in Biot's theory. Also, small errors are possible in the experimental data, and it has been estimated that there is a possible 5% error in frequency at both sites, and as much as a 15% error in the shear wave velocity. Despite the calculable errors, it is still difficult to account for the 300% difference between the known and calculated diameters.

A seismic resonance survey was carried out to determine the competency of a reservoir site, and the results interpreted in conjunction with a gravity survey of the same area (Godson and Watkins, 1968; Ref 104). The area was covered with a series of geophone spreads at 30.5 m (100 ft) intervals on a grid system; each spread consisted of 24 geophones at intervals of 7.6 m (25 ft). Variations in size and depth of the explosive charges indicated that cavity resonance appeared to be induced more frequently from a small shallow source than from a large deep source. As shallow charges are thought to generate larger Raleigh waves, these surface waves are interpreted as the possible triggering mechanism that excites resonance. By careful examination of seismic records, traces showing cavity vibrations were graded poor (P), fair (F) or good (G) on the basis of magnitude of amplitude and duration of response. These grades were plotted on the gravity map of the area, and were found to coincide roughly with the gravity anomaly (Fig 4:3:3). The presence of a surface crack in this region was thought to be the result of faulting, suggesting that cavity formation was associated with fault zones.

A further investigation of the seismic resonance method was made by Richtien and Stewart (1975; Ref 105), who carried out a controlled experiment over a near surface cavern with the principal objective of obtaining a spatial definition of the associated cavity resonance phenomenon. The work of Watkins et al (1967; Ref 101) and Godson and Watkins (1968; Ref 104) used only vertical geophones, and it is interesting to note that Richtien and Stewart (1975; Ref 105) did not record any events on their seismic records from the vertical geophones,

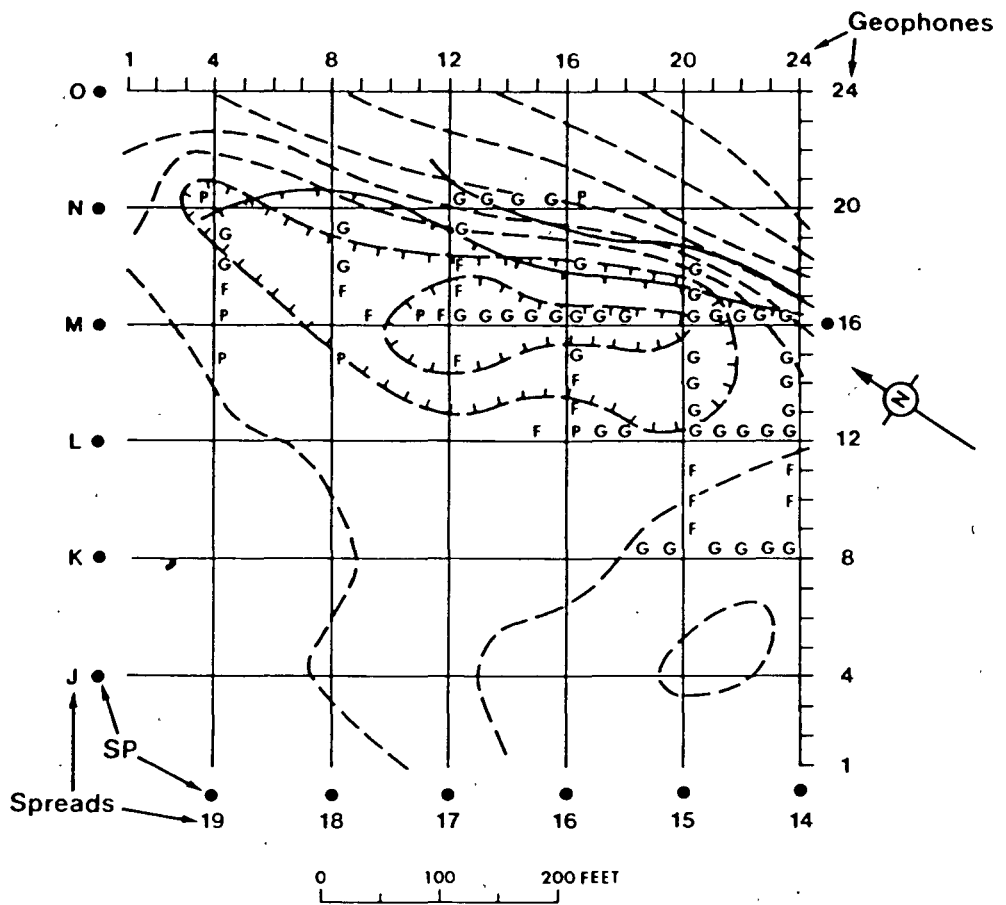


FIG. 4:3:3 LOCATIONS OF RESONANCE PHENOMENA (labelled G, good; F, Fair; P, poor) IN RELATION TO THE SURFACE CRACK, TO THE TRACE AT A DEPTH OF ABOUT 20 FT OF A SUSPECTED FAULT, AND TO THE BOUGUER GRAVITY LOW (after Godson and Watkins, 1968; Ref 104)

which could not be identified as standard wave modes of seismic wave transmission. It was noticed, however, that only horizontally polarised motion in the latter part of the seismic record could possibly be associated with a resonance phenomenon. It was therefore concluded that, while seismic resonance was a promising and attractive method for cavity location, further work should be carried out in the light of the different findings of Watkins et al (1967; Ref 101) and Richtien and Stewart (1975; Ref 105).

In the experiments described above, explosives were used on both occasions to excite the underground cavity. This is a transient seismic source, which acts, in practice, as a step input to the cavity so that it 'rings' at its natural resonant frequency. It is not unknown for this to happen, since reverberations of this type have been observed during seismic surveys using a hammer and a plate seismic source over areas where cavities are known to exist. Small cavities behind tunnel linings, particularly on railways, are also located using the principle of listening to the ring of a hammer blow on the brick lining. During the interborehole measurements in the vicinity of a disused tunnel at Cocking, (Chapter 5:1:2) 'ringing' or reverberation of the tunnel was induced by a sparker source when it was operated in a borehole close to the tunnel. It would, however, seem preferable to use a variable frequency continuous seismic source, since it is then possible to resonate a cavity over a narrow bandwidth.

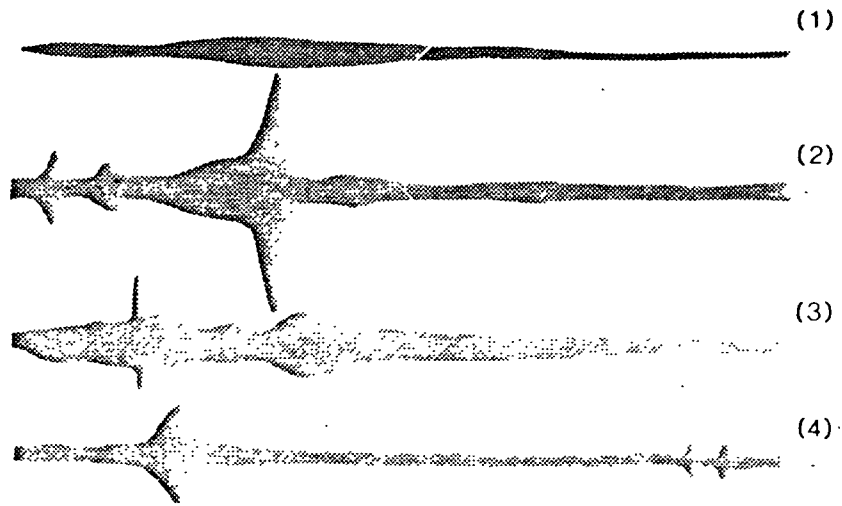
Very little information has appeared to date in the scientific literature on the practical use of the seismic resonance technique in the location of cavities. The apparent conflict between the result of Godson and Watkins (1968; Ref 104) and Richtien and Stewart (1975; Ref 105), using a transient source, does not seem to have been resolved. It has, however, been suggested above that these resonant seismic events can be observed on seismic records and are used in practice to examine railway tunnel linings. A later paper by Ballard (1982; Ref 106) draws particular attention to the seismic resonance technique and refers to its practical use in a number of site investigations.

The only commercial organisation in the UK who use the resonance phenomenon to detect cavities is Search Engineering Limited of Leatherhead. The system is called the 'SHRIMP' system (Savage and

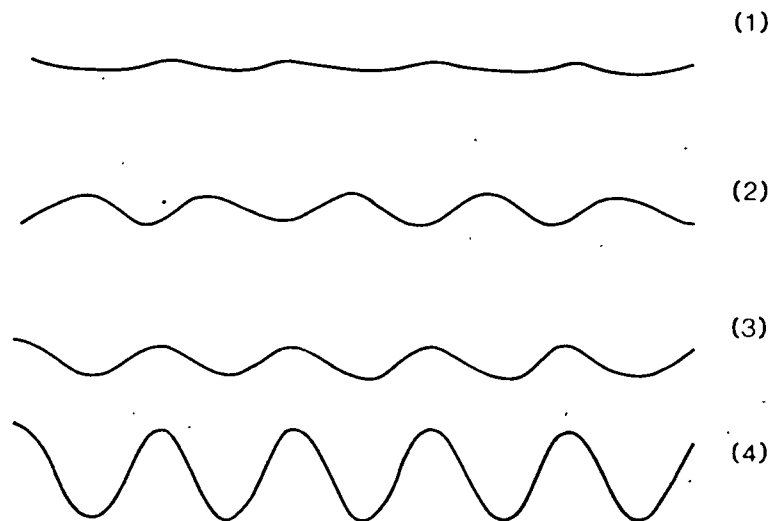
Heierli Resonant Investigation Method - Patented) and uses a continuously sweeping seismic source instead of an explosive source. A brief description of the system and the method is given in Appendix II.

The 'SHRIMP' system was evaluated for site investigation by Baria (1977; Ref 107) during a field demonstration, and it was concluded that the technique was promising but was very slow and labour intensive. During the demonstration two cavities were apparently detected, as shown in Fig 4:3:4a. Fig 4:3:4b shows a cavity in resonance at a discrete frequency of 28 Hz. However, the presence of these cavities was not confirmed by drilling into the formation after the demonstration.

It was claimed that a cavity of 1 m in diameter can be located at a maximum depth of about 25 m, but larger cavities may be detected at up to depth of 50 m. The only published reference to the use of this system in a practical site investigation is in Arrowsmith and Rankilor (1981; Ref 108). In this instance, the method was used to attempt to locate and record mine shafts and workings along the proposed route of the Dalton bypass. The results obtained are reported to have been inconclusive and the work was terminated. It is, however, quite possible that the infilling within the mineshafts and cavities resulted in a reduction of the peak amplitude at the resonance frequency, so that it was difficult to decide whether a resonant point was reached in the frequency scan.



(a) Signals from 4 Accelerometers with Vibrator in Sweep Mode (3 - 120 Hz)



(b) Signals from the Same 4 Accelerometers with Vibrator Tuned to Resonant Frequency of No. 4 Accelerometer (28 Hz)

FIG. 4:3:4 TYPICAL FIELD SURVEY RESULTS FROM THE SYSTEM

(after Baria, 1977; Ref 107)

5 BOREHOLE SEISMIC METHODS

One of the difficulties associated with surface seismic methods is that it is often very difficult to carry out the required surveys because of obstructions on the ground surface. This is a particular problem in redevelopment areas, where substantial disturbance of the near surface geological strata may have occurred in the past. Associated with this is the presence of old foundations, large buildings, etc., which often hinder the use of surface seismic methods.

Thus, the location of cavities, mine workings or anomolous ground conditions in this type of environment is not very practical with the majority of surface seismic methods. However, most site investigations carried out for civil engineering development are based on the drilling of boreholes to collect samples for engineering testing in the laboratory, to determine the geological structure beneath the ground surface. The availability of boreholes on a site gives an access to investigation of the rock mass beneath the surface obstructions using borehole seismic methods.

Information can be obtained on the engineering characteristics of the rock mass in situ using standard geophysical logging methods, and it is possible to extend the effective range of some of the geophysical tools used by making measurements between adjacent boreholes or from surface to boreholes. Interborehole and surface to borehole seismic studies carried out at the BGS test site at Cocking are considered in this chapter. In addition, a survey in connection with cavity detection on a housing estate in Maidstone, Kent, using interborehole seismic measurement, is also discussed.

5:1 Interborehole seismic method

The interborehole seismic method involves the transmission of a seismic pulse between a pair of boreholes. The time taken for the seismic pulse to travel the distance between the two boreholes can be used to calculate the velocity. The seismic velocity and other seismic propagation properties can be used to assess the mechanical properties of the rock mass.

Interborehole seismic measurements have been used in the field of civil engineering over the past decade, and it has been the subject of considerable development. Bois et al (1971, Ref 109; 1972, Ref 110) carried out interborehole seismic measurements using explosives to determine seismic velocity. La Porte et al (1973; Ref 111) extended the method to investigate rock properties between galleries in a mine for civil engineering purposes. Stokoe and Woods (1972; Ref 112) McCann et al (1975; Ref 113), Cratchley et al (1976; Ref 84), Green et al (1975; Ref 114), Baria (Ref 115), and Albright and Harold (1976; Ref 116) have all used interborehole seismic techniques for site investigation and to determine dynamic mechanical properties of the rock mass.

Dressen (1973; Ref 117) and Baria et al (1978; Ref 118) have used interborehole methods to study the effect of cavities on seismic wave propagation. Baria et al (in press; Ref 119) have also used interborehole seismic measurements, to identify the fractured zone caused by artificial stimulation using explosives in an igneous rock mass, for the hot dry rock geothermal project.

Two case studies are discussed to demonstrate the use of interborehole seismic measurements in the location of cavities. The first case history is of an experimental site at Cocking in Sussex, which was used to carry out various geophysical measurements and observe the effect of the proximity of a disused railway tunnel on these measurements. The second case history is a practical application of the above technique in the investigation of possible cavities beneath a housing estate in Maidstone, Kent.

5:1:1 Experimental procedures for interborehole seismics

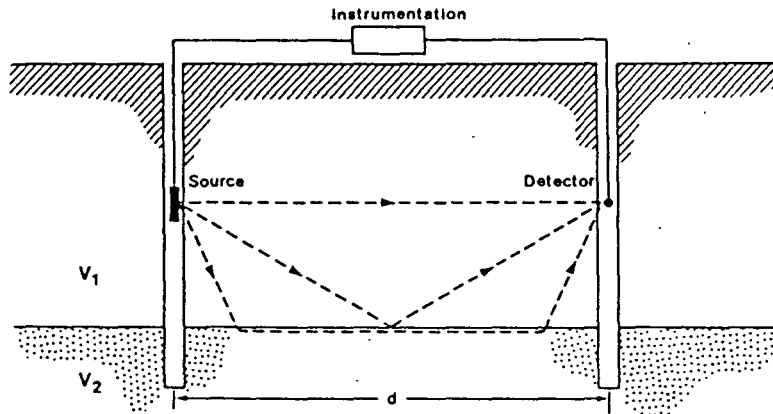
a Instrumentation

Interborehole seismic measurements are carried out by transmitting a seismic pulse through the rock mass between two adjacent boreholes. A high power seismic source and detector are lowered to the same depth in adjacent boreholes. The transmitter emits a pulse at a rate of one pulse every two or three seconds and the travel time of the pulse is measured. The apparent seismic velocity at the depth is calculated using the measured travel time and the distance between the boreholes. The term

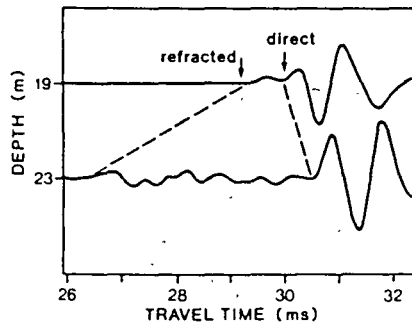
'apparent seismic velocity' is used since the first recorded signal can either be a direct arrival through material or a refracted one from an underlying material with faster seismic velocity. A reflected arrival may also often be observed on the received pulse train. An interesting example showing all three arrivals on a received pulse train is given by McCann et al (1975; Ref 113) and is reproduced in Fig 5:1:1. In Fig 5:1:1(b) the refracted arrival from the Thanet Sand/Chalk interface clearly separates out from the direct arrival through the Thanet Sand as the transmitter and the receiver approach the interface. In Fig 5:1:1(c), the reflected arrival from the interface starts to interfere with the direct arrival as the transmitter and receiver approach the interface.

The field instrumentation for interborehole seismic measurements based on a high power sparker source has been comprehensively described by McCann et al (1975; Ref 113). A block diagram of the instrumentation is shown in Fig 5:1:2. The sparker probe is connected across a capacitor bank (charged to 4KV) and the application of a positive trigger pulse to the trigger control unit causes the capacitor bank to discharge through the spark gap and electrolyte in the probe, so that a short seismic pulse is emitted. The received seismic pulse is detected by a hydrophone array, summed and transmitted to the surface where it is amplified by the low-noise instrumentation amplifier. The signal is then displayed on a storage oscilloscope after the bandwidth is limited by a filter, if necessary. The storage oscilloscope is triggered externally by a trigger pulse used for controlling the firing rate of the sparker source. The transit time of the seismic pulse is measured using the delay time base facility of a storage oscilloscope and a counter timer.

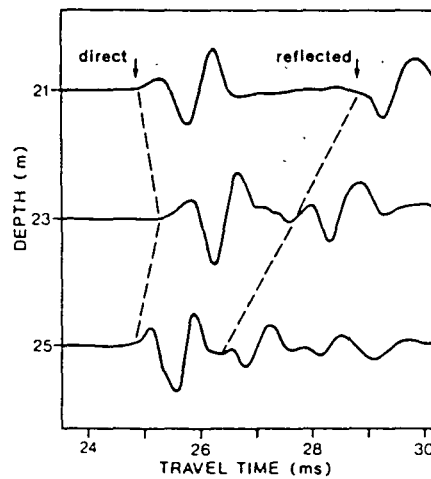
Most of the interborehole data was obtained using the above method, but the data acquisition method was subsequently improved using digital techniques. Here, the signal from the main signal amplifier is digitised using a transient recorder, which is also triggered by the pulse used for controlling the firing rate of the sparker. The digitised data is then stored in an array on a microcomputer memory. Each subsequent signal is digitised and the new array is added to the one in the computer memory and then averaged, the resultant array being kept in the memory. This method of processing the data is called stacking or



(a) Wave Paths between Transmitter and Receiver.



(b) Typical Refracted Arrivals from Thanet Sand/Chalk Interface.



(c) Typical Reflected Arrivals from Thanet Sand/Chalk Interface.

FIG. 5:1:1 INTERBOREHOLE SEISMIC MEASUREMENTS
(after McCann et al, 1975; Ref 113)

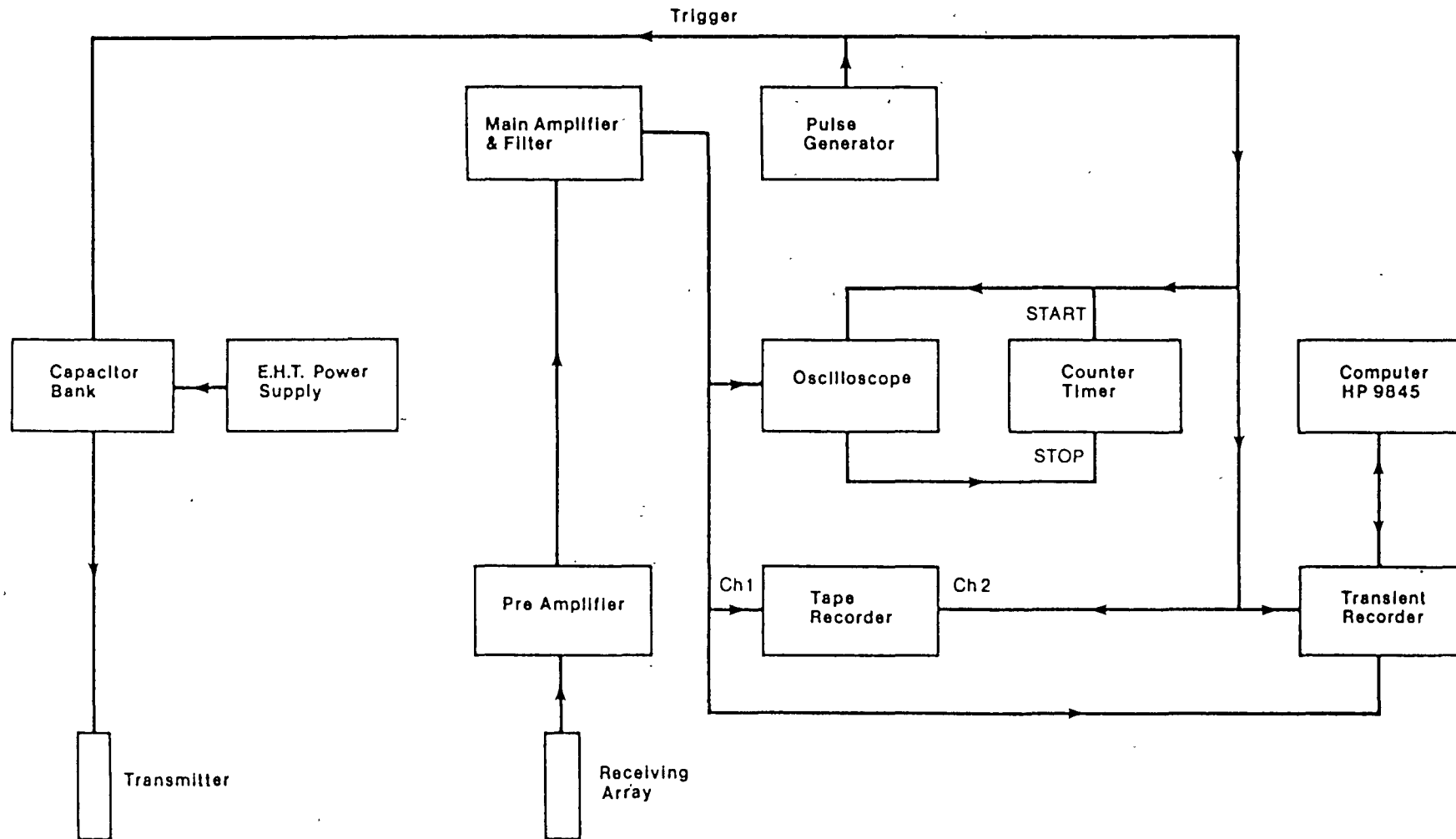


FIG. 5:1:2 BLOCK DIAGRAM OF INSTRUMENTATION FOR INTERBOREHOLE SEISMIC MEASUREMENTS INCORPORATING SIGNAL STACKING AND WAVEFORM ANALYSIS CAPABILITY

digital averaging. Stacking or averaging, when correctly used, enhances the signals and depletes the environmental noise. It is a useful and powerful method of identifying signals in a noisy environment. The measurement of the travel time and amplitude of the received signals is carried out using a cursor on the HP45B screen, and the relevant part of the wave form is plotted out using the digital plotter.

The raw data, the trigger pulse and the voice commentary is recorded on a magnetic tape recorder for further analysis at a later date. The travel time of the first arrival is measured, which may be a direct pulse or a refracted pulse, depending on the lithology and the geometry of the transmitter and receiver.

b Seismic sources and receivers

Various types of borehole seismic sources are available for interborehole seismic measurements. For many years explosives have been the main energy source for general seismic surveys and also for the initial interborehole seismic (acoustic) scanning. Explosives provide a compact package of concentrated energy and a very simple means of rapid and almost instantaneous release of energy. Although explosives are fairly reliable and a simple seismic source for interborehole work, they do present problems in terms of the possibility of damaging the borehole casing, inconsistent energy output, the inherent delay in the firing of the normal seismic detonators and the political and dangerous nature of its use in populated environments. The borehole air gun can also be used as a borehole source.

The borehole sparker is another seismic source which is useful for interborehole surveys. It was originally developed as a marine seismic source by EG&G International, who still produce all the high voltage equipment needed to generate the seismic pulse. A seismic pulse is generated by charging a capacitor bank to a potential of 3000-5000V and discharging it between electrodes under the sea. The borehole sparker works on the same principle, but the electrolyte is retained in a chamber (McCann et al 1975; Ref 113). The basic advantage of using the sparker for the interborehole work is that the energy output and the bandwidth from the source is constant and the pulse shape is repetitive.

Three types of sensors are available for detecting seismic signals in boreholes. These are hydrophones, well geophones and borehole accelerometers. The hydrophone is a pressure sensing device, which requires fluid in a borehole to provide seismic coupling to the rock mass. A well geophone measures the particle velocity of the seismic wave and is normally clamped to the wellbore. The accelerometer is sensitive to particle acceleration and also requires to be clamped to the wellbore for the optimum performance.

5:1:2 Interborehole seismics at Cocking

The geology, size of tunnel and general information on the site was discussed in section 4:1:2.

A total of eight boreholes were drilled at the Cocking site, as shown in Fig 4:1:4. The first four boreholes (numbers 1 to 4 respectively) were drilled in the summer of 1976 to a depth of 30 m, but were found to be inadequate for interborehole seismic measurements, as the grouting of the plastic casing to the rock mass proved unsuccessful. This unsuccessful grouting of the four boreholes may well be attributed to a fall in the water table by about 70 m during the prolonged drought in the summer of 1976, resulting in the near surface rock mass' becoming extremely dry. This could have caused the grouting to crack, and thus loosened the firm bonding required for efficient transmission of the seismic pulse.

The second four boreholes (numbers 5 to 8 respectively) were drilled in the late summer of 1977 using the foam flush method. A new technique was devised by Baria et al (1978; Ref 118) to overcome the above borehole coupling problem. A layer of 1000 gauge polythene tubing was pulled over a perforated P.V.C. corrugated pipe (100 mm OD) and deployed in the open boreholes. The polythene tubing was then filled with a weak solution of bentonite mud to reduce any leaks and provide good seismic coupling. It was thought that the flexible corrugated P.V.C. borehole liner (casing) would help to prevent the generation of standing waves.

The later boreholes (numbers 5 to 8 respectively) were drilled to a depth of 20 m, but later collapsed at 13 m, 16 m, 8 m and 15 m respectively. These boreholes, however, were open long enough to enable a programme of seismic measurements to be made.

a Initial survey

Interborehole seismic measurements were carried out on boreholes numbers 1, 2, 3 and 4 after grouting the casings in the boreholes. Instrumentation used for interborehole seismic measurements was as used by McCann et al (1975; Ref 113), but on subsequent surveys more sensitive hydrophones, a wide-band sparker (HRSP) and a data stacking facility were developed and introduced into the system.

Before the start of the survey, amplitude calibration tests were carried out to check the gain required to obtain the best dynamic range on the Fenlow tape recorder. This was normally achieved by firing a few shots between the surface and the bottom of the borehole, with transmitter and receiver moving together at the same depth but in separate boreholes. The above calibration procedure was first carried out for boreholes numbers 2 and 3, but could not be accomplished as no seismic energy was detected. The electrical power into the transmitter (sparker) was doubled to 1000 J and maximum gain applied to the hydrophone amplifier, but no improvement in signal level was achieved. After carrying out various other test procedures, it became apparent that either the casings had not been grouted successfully or there was an acoustic discontinuity between boreholes numbers 2 and 3.

Similar calibration procedures were carried out on boreholes numbers 1 and 4, which showed that weak seismic signals were detectable at depths of 6 m and 29 m. Figs 5:1:3 and 5:1:4 show signals obtained from the parallel interborehole seismic measurements carried out between boreholes numbers 4 and 1, with the transmitter in BH4 and the receiver in BH1, for a scan depth of up to 15 m from the surface, and an electrical input energy of 500 J and 1000 J respectively.

Figs 5:1:3 and 5:1:4 show that the signals are very poor (almost in the background noise level), with practically no apparent signals below the depth of 10 m on Fig 5:1:3 and about 12 m on Fig 5:1:4. This may be attributed to poor seismic coupling between the casing and the formation. Doubling of the electrical input energy to the sparker did improve the received signals marginally but not significantly.

Depth

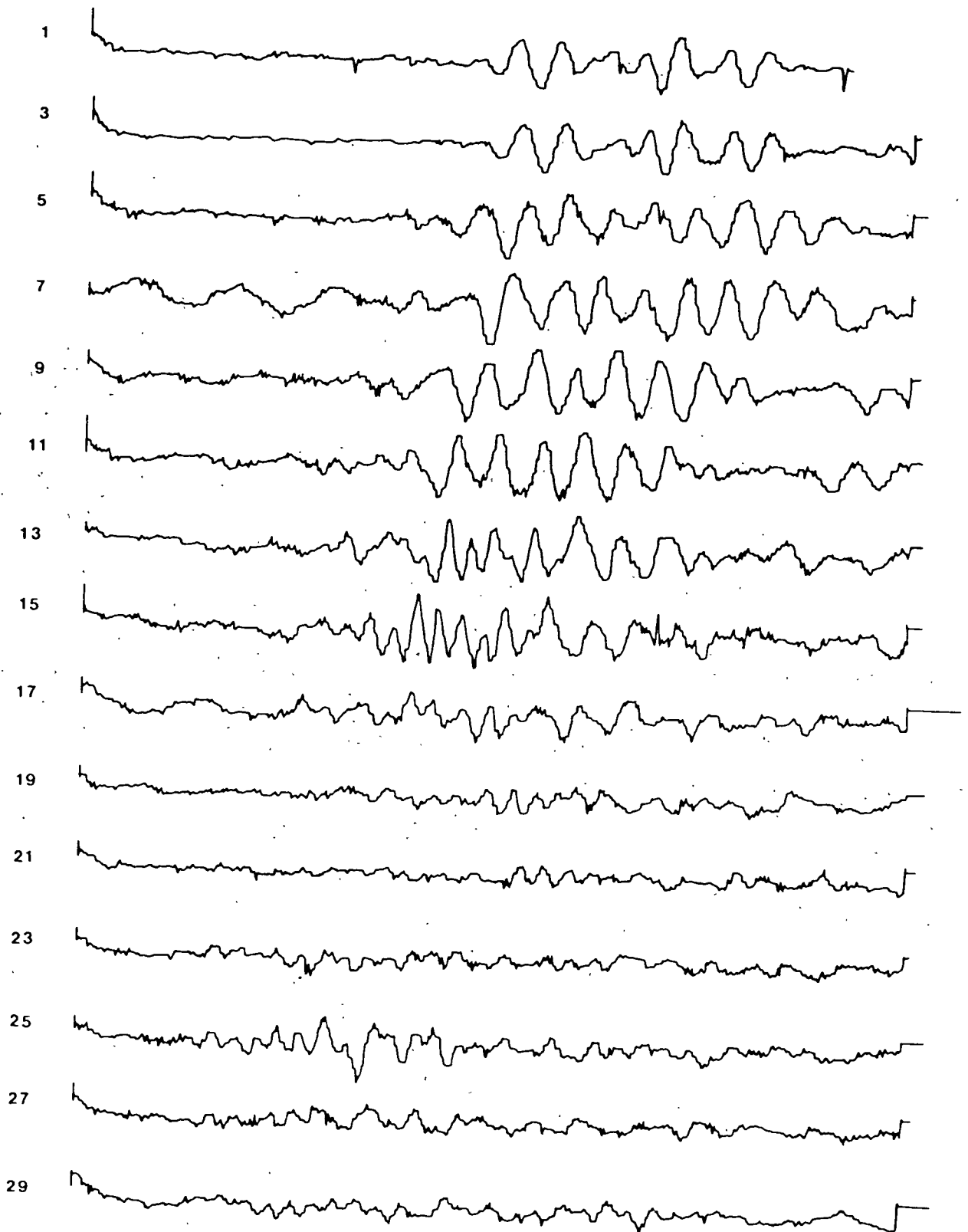


FIG. 5:1:3 COCKING SURVEY - SEISMIC SCAN 4/1

(diagonal measurements with transmitter
stationary at 29 m in borehole 4)

Depth

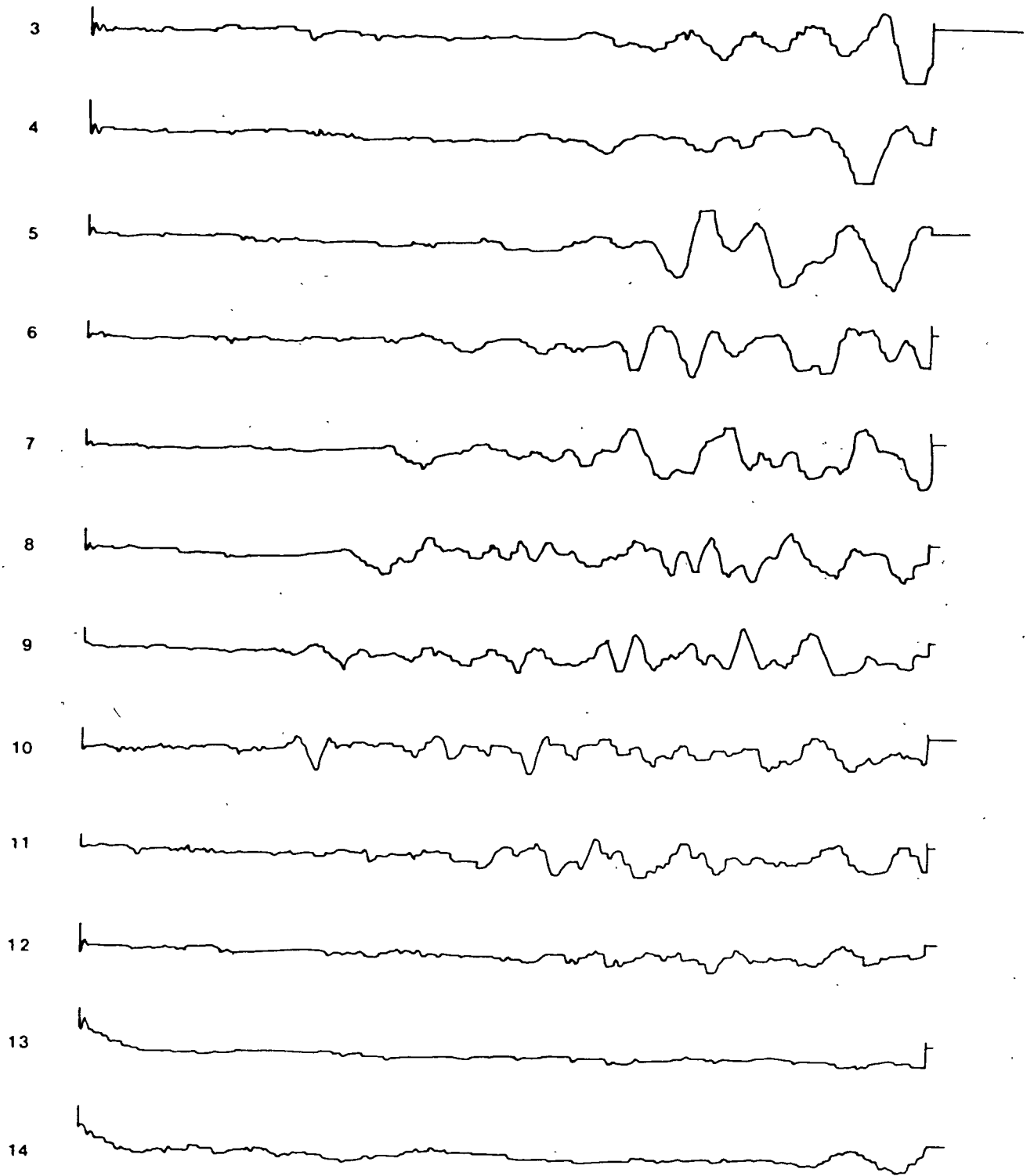


FIG. 5:1:4 COCKING SURVEY - SEISMIC SCAN 4/1

1000 J SPARKER SOURCE

It was concluded that the bottom of the borehole must be reasonably coupled, as the grouting procedure pumps the cement down the inside of the pipe and extrudes it up between the outside of casing and formation. In view of this, diagonal scans were carried out with the sparker resting at the bottom of borehole BH4 and the hydrophone moving down from the surface in steps of 2 m. Fig 5:1:5 shows seismic signatures of the scans, and it is apparent that there was a reasonable transmission of seismic energy between the bottom of borehole BH4 and the top of borehole BH1 (ie, over a distance of approximately 32 m), but poor transmission across the bottom of the boreholes over a distance of 15 m (ie, the bottoms of boreholes BH4 and BH1). It is difficult to explain this result other than by a poor coupling at the bottom.

The initial calibration scans had shown that there were reasonable signals transmitted at a depth of 5 m from surface. A diagonal scan was carried out with the sparker stationary at 5 m from the surface in BH4, with the hydrophone moving down from the surface in steps of 2 m in BH1. The received seismic signature from the diagonal scan is shown in Fig 5:1:6. This scan does not show the expected increase in amplitude of signatures near the surface, although the transmission distance has been reduced from 30 m to about 15 m, compared with the previous diagonal scan (Fig 5:1:5). Signatures show that the coupling is not particularly good, especially at a depth of 19-23 m.

A further experiment was carried out by reversing the function of the two boreholes, so that the transmitter was kept stationary in BH1 at 5 m and the receiver was moved down in BH4 from the surface in steps of 2 m. Fig 5:1:7 shows the seismic signatures obtained in this scan, and it is apparent that very little energy is transmitted from below 14 m in BH4. When Fig 5:1:7 is compared with Fig 5:1:6, it is possible to conclude that coupling in BH1 is better than that in BH4, since the sparker vibrates the casing and even expands it momentarily by a small amount, which bridges the gap in the micro-annulus and is thus able to introduce some energy into the formation. However, if the roles are reversed, the sparker may transmit considerable energy into the ground but the receiver will not be able to detect any signals, as it is not able to bridge the gap in the micro-annulus and consequently not coupled to the rock mass.

Depth

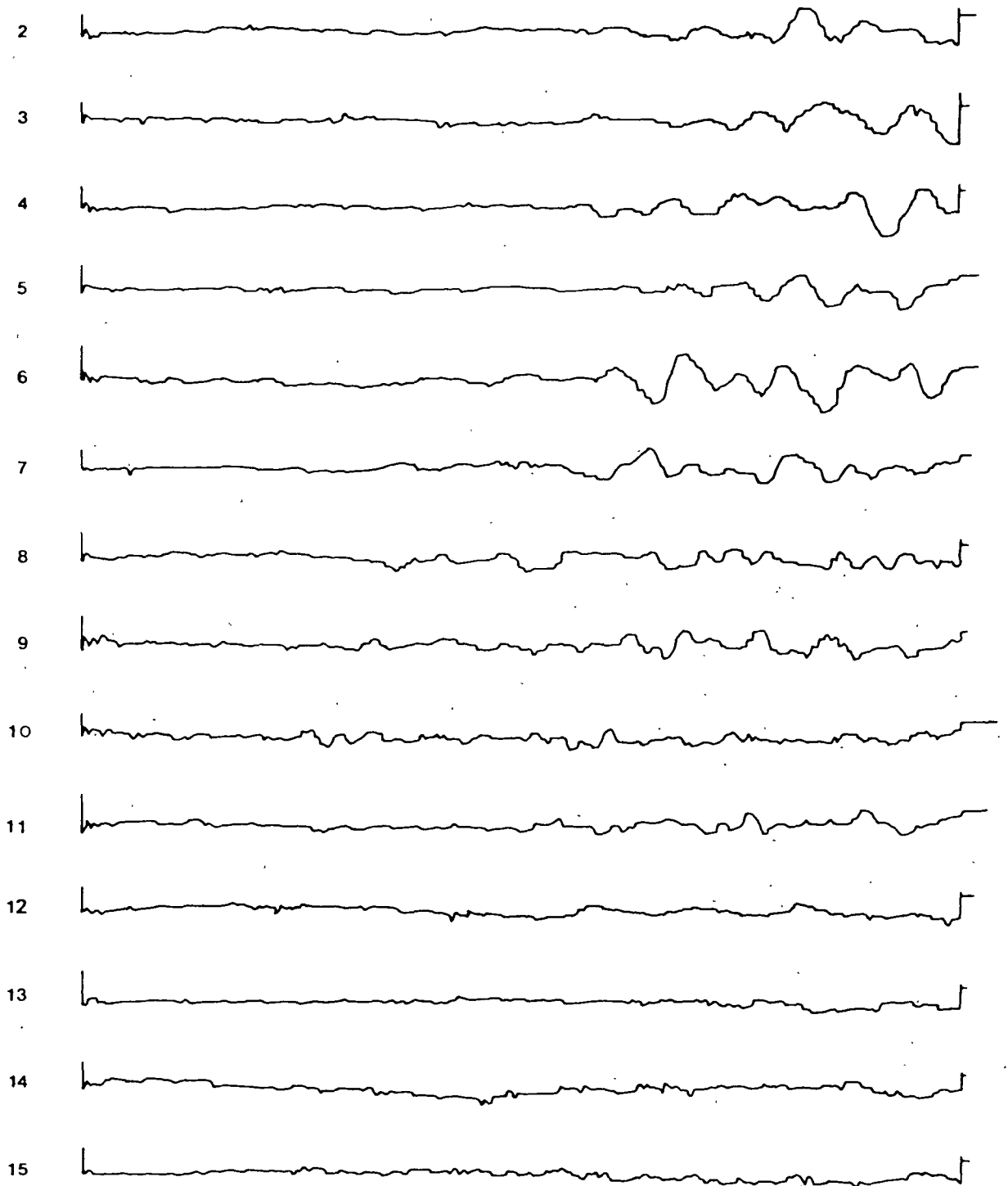


FIG. 5:1:5 COCKING SURVEY - SEISMIC SCAN 4/1

Depth

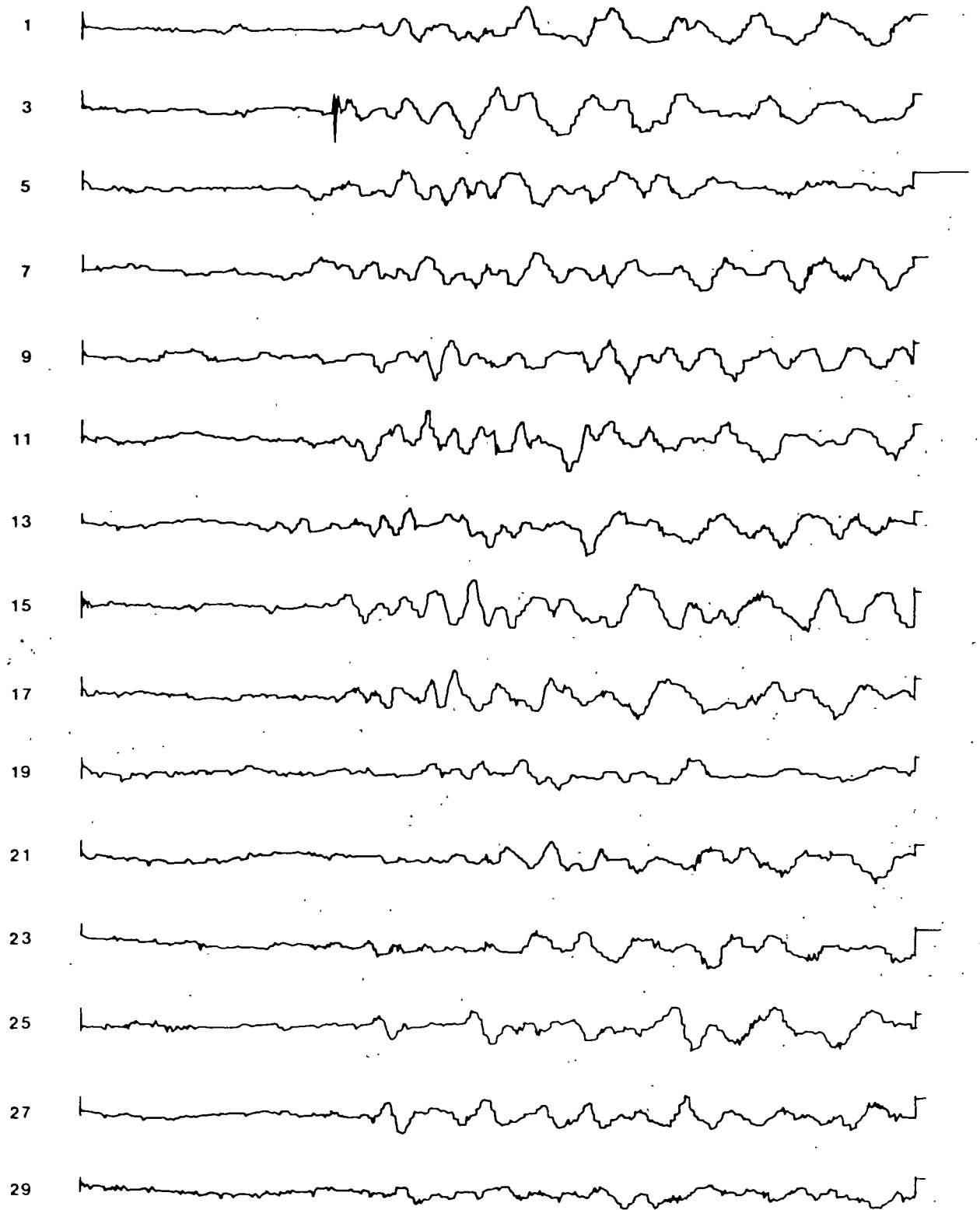


FIG. 5:1:6 (diagonal measurements with transmitter
stationary in borehole 4 at 5 m)

Depth

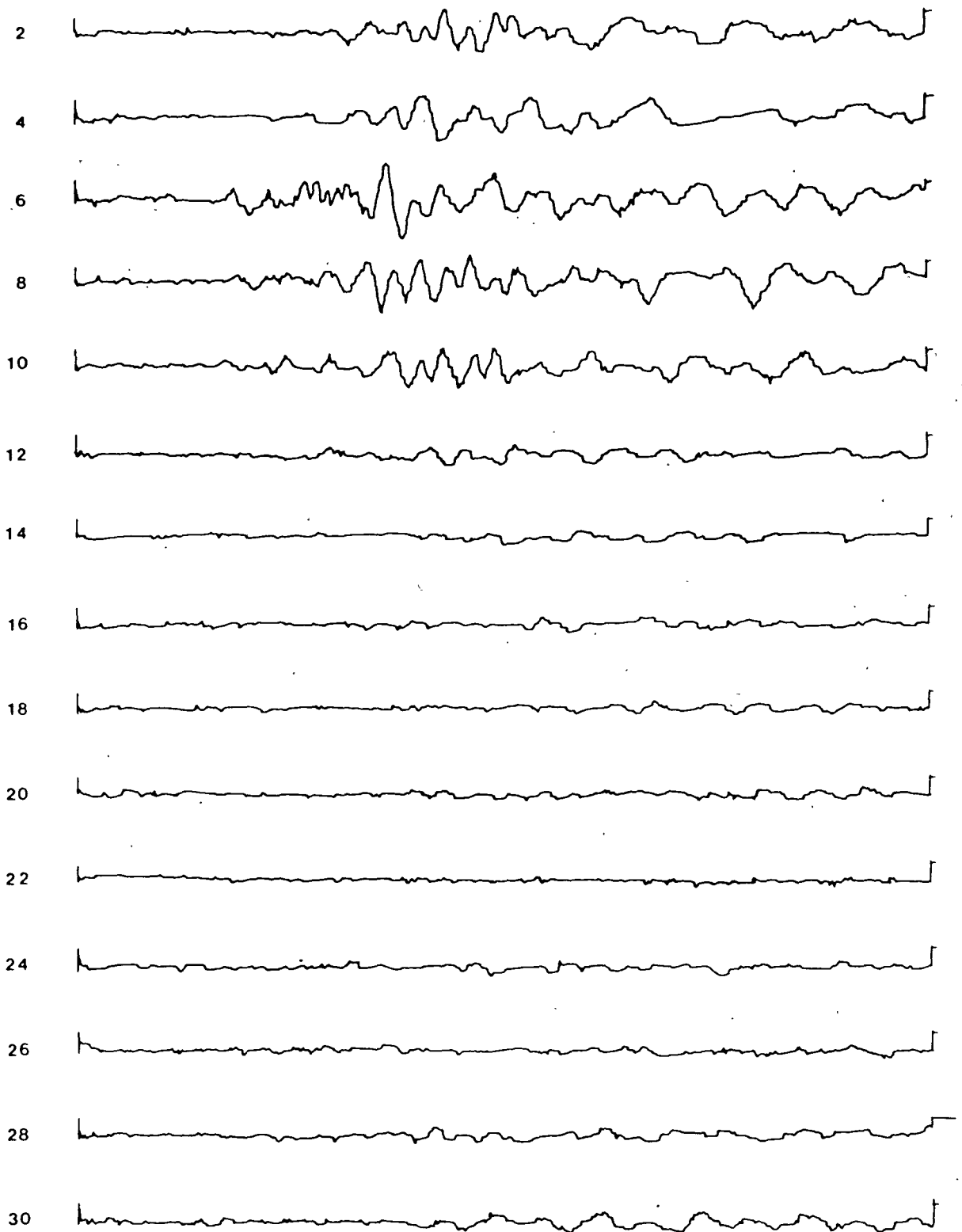


FIG. 5:1:7 COCKING SURVEY - SEISMIC SCAN 1/4
(diagonal measurements with transmitter
stationary in borehole 1 at 5 m)

Listening tests were also carried out (Baria, 1976; Ref 74) whereby the sparker was placed at 13 m depth in each borehole in sequence, and an observer listened to the acoustic signal inside the tunnel. No sound was heard inside the tunnel when the sparker was placed in BH2 and BH3. However, the acoustic pulse was nearly audible when the sparker was placed in BH4, and just audible when the sparker was placed in BH1. It is difficult to quantify between the sound intensity from BH4 and BH1 due to the increase in distance (from 12.5 m to 27.5 m), but it is reasonable to compare the sound from BH2 and BH3 with BH1 and BH4 because they are symmetrically positioned from the centre of the tunnel. It can be concluded that some form of weak grouting existed between the formation and BH4 and BH1 at the depth of 13 m for energy to be imparted into the rock mass, whilst in BH2 and BH3 the energy was not imparted into the rock mass. This was most probably caused by the air gap between the formation and the casing, causing the casing to resonate.

The above experiment shows that it is essential to have good and sound coupling between the borehole casing and the formation for a successful interborehole survey. Proper planning has to be carried out in this field when investigating a soft rock such as chalk, since the formation is not sufficiently soft to collapse and bridge the gap between casing and formation.

b Main survey

In view of the impractical nature of the available four drilled and cased boreholes, new boreholes were drilled and a new method of casing the boreholes was developed (Baria et al, 1978; Ref 118). Four new boreholes were drilled using an EGU drilling rig. Of the four new boreholes (numbers 5, 6, 7 and 8), only numbers BH6 and BH8 were suitable for seismic measurements. Borehole BH5 partially collapsed during the programme of seismic measurements, limiting the use of standard borehole hydrophones to the depth of the restriction, and borehole BH7 failed to retain the bentonite drilling fluid.

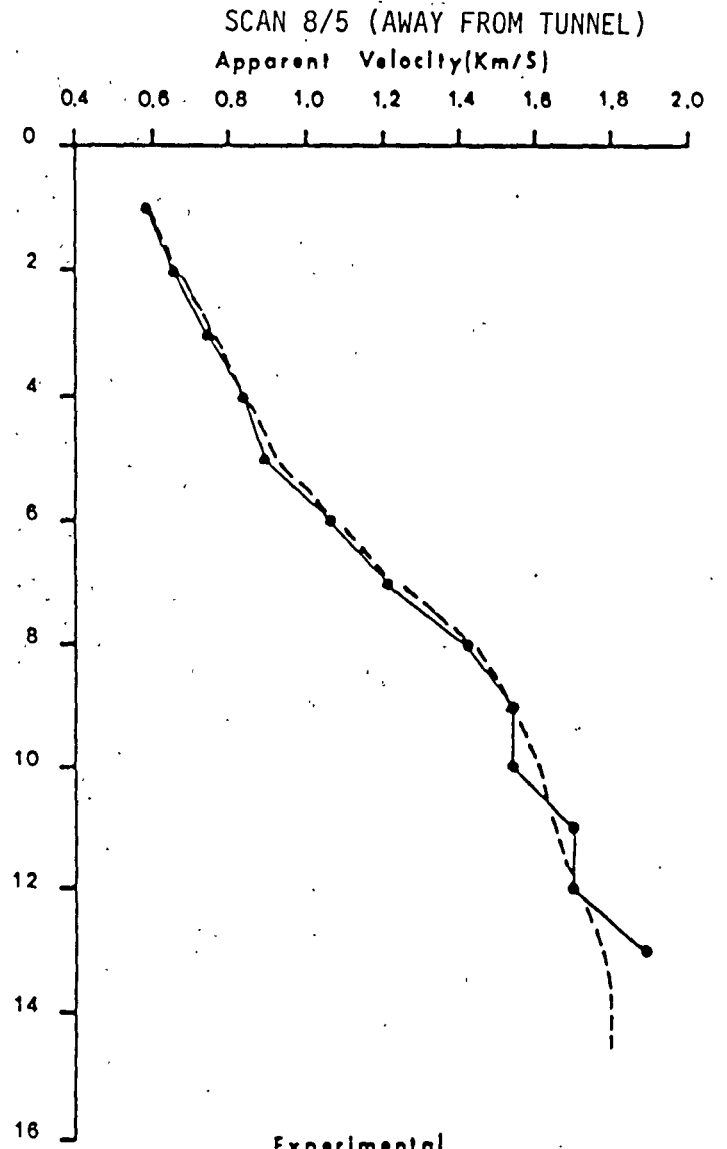
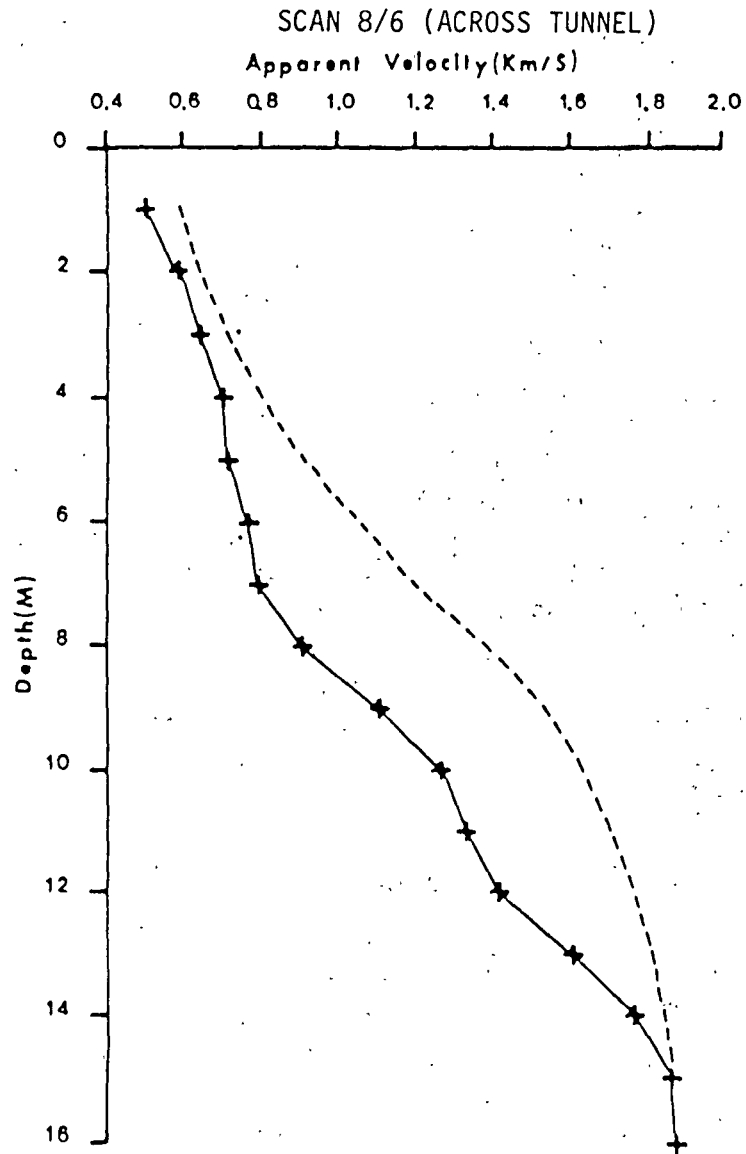
Interborehole seismic measurements were carried out with a sparker source and hydrophone array between boreholes BH5, BH6 and BH8 (scans 8/5 and 8/6 respectively).

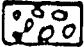

Each scan was carried out with source and receiver positioned at identical depths in the two boreholes, measured at intervals of 1 m from the ground surface to the bottom of the boreholes. The maximum depth of investigation for scan 8/6 (with the tunnel between the boreholes) was 16 m, approximately 2 m below the tunnel. Scan 8/5 was carried out up to the depth of the restriction in BH5, which was 13 m.

A model of the undisturbed section of the ground between boreholes 8 and 5 was developed for scan 8/5, and the theoretical scan 8/5 computed from this model is shown in Fig 5:1:8. The model was also used for the computation of a theoretical scan 8/6, in which the presence of the cavity (or tunnel) between the two boreholes was ignored. A comparison of the theoretical and experimental scans 8/6 clearly shows the effect of the presence of the tunnel on the experimental results between 8 m and 13 m depth. The disturbed nature of the material above the tunnel and its effect on the drainage conditions is also evident in the experimental results.

The above discussion only relates the changes in the apparent velocity due to the presence of a tunnel in the path of a propagating acoustic pulse. The energy received can be assessed by the amplitude of the received pulse for a given wavelength, and therefore the amplitude of signatures from different surveys can be compared in terms of energy transmitted through the rock mass, provided the traces are normalised for the gain settings.

Figs 5:1:9 and 5:1:10 are the received acoustic signatures for parallel scans 8/6 and 8/5. These signatures are normalised for gain, and therefore represent amplitude values which can be compared with other normalised traces. In Figs 5:1:9 the amplitude increases with depth until it reaches a depth of 8 m, where it begins to diminish. The amplitude stays at this very low level until it reaches 13 m depth where it begins to increase, and this trend is continued to the maximum depth scanned, 16 m. Scan 8/5 represents an acoustic scan between two boreholes, BH8 and BH5, without the tunnel in between. Signatures of the scan 8/5 (Fig 5:1:10) shows that the amplitude of the signature generally increases with depth as fracturing in the rock mass reduces. There is no indication of the amplitudes diminishing over a specified depth, as shown on Figs 5:1:9.



 Disturbed Rock Mass Above Tunnel
 Tunnel

— Experimental
 - - - Theoretical

FIG. 5:1:8 COCKING SURVEY - VELOCITY SCANS ACROSS (8/6) AND AWAY FROM TUNNEL (8/5)

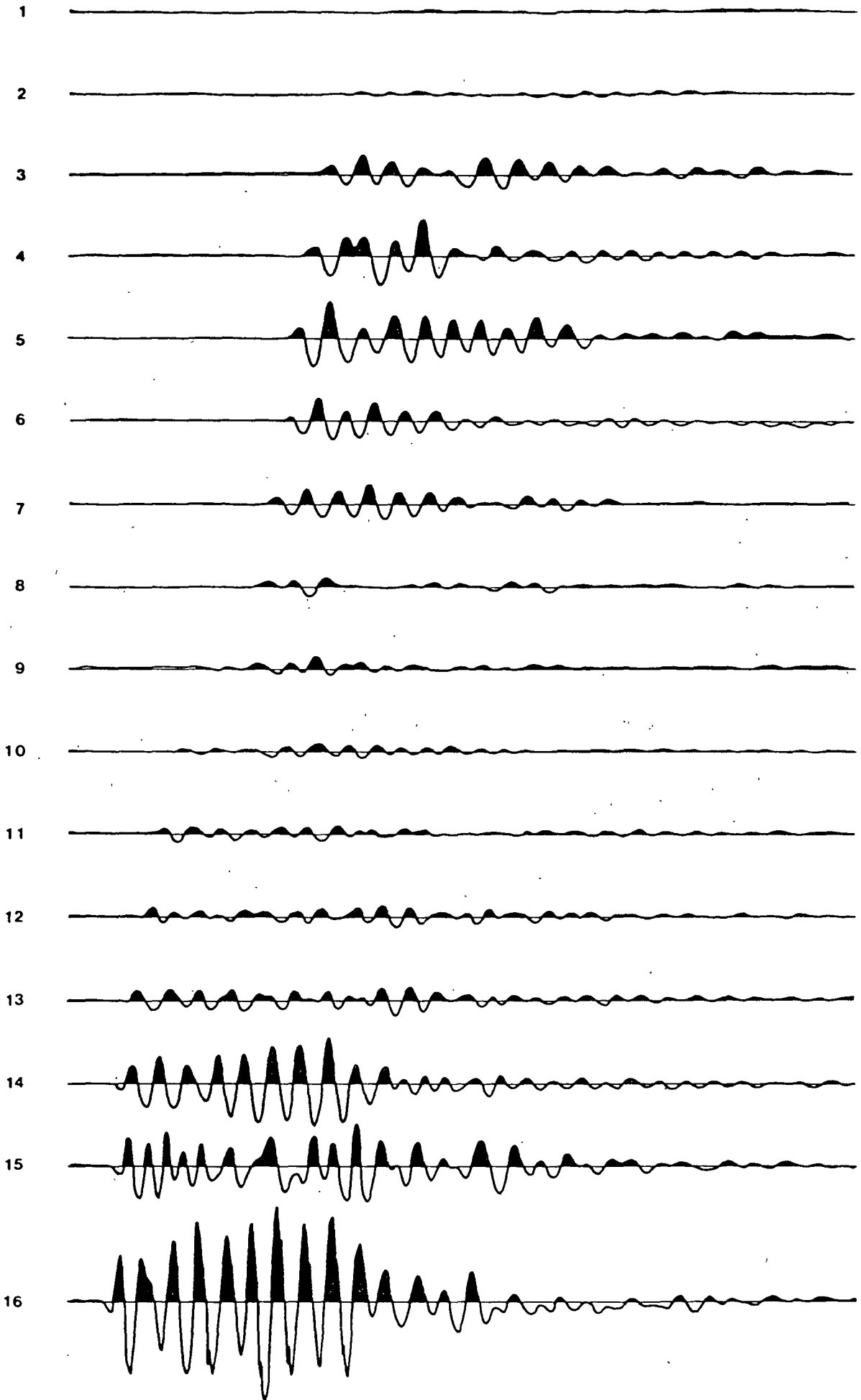


FIG. 5:1:9 COCKING SURVEY - SIGNATURES FOR SEISMIC SCAN 8/6

Depth

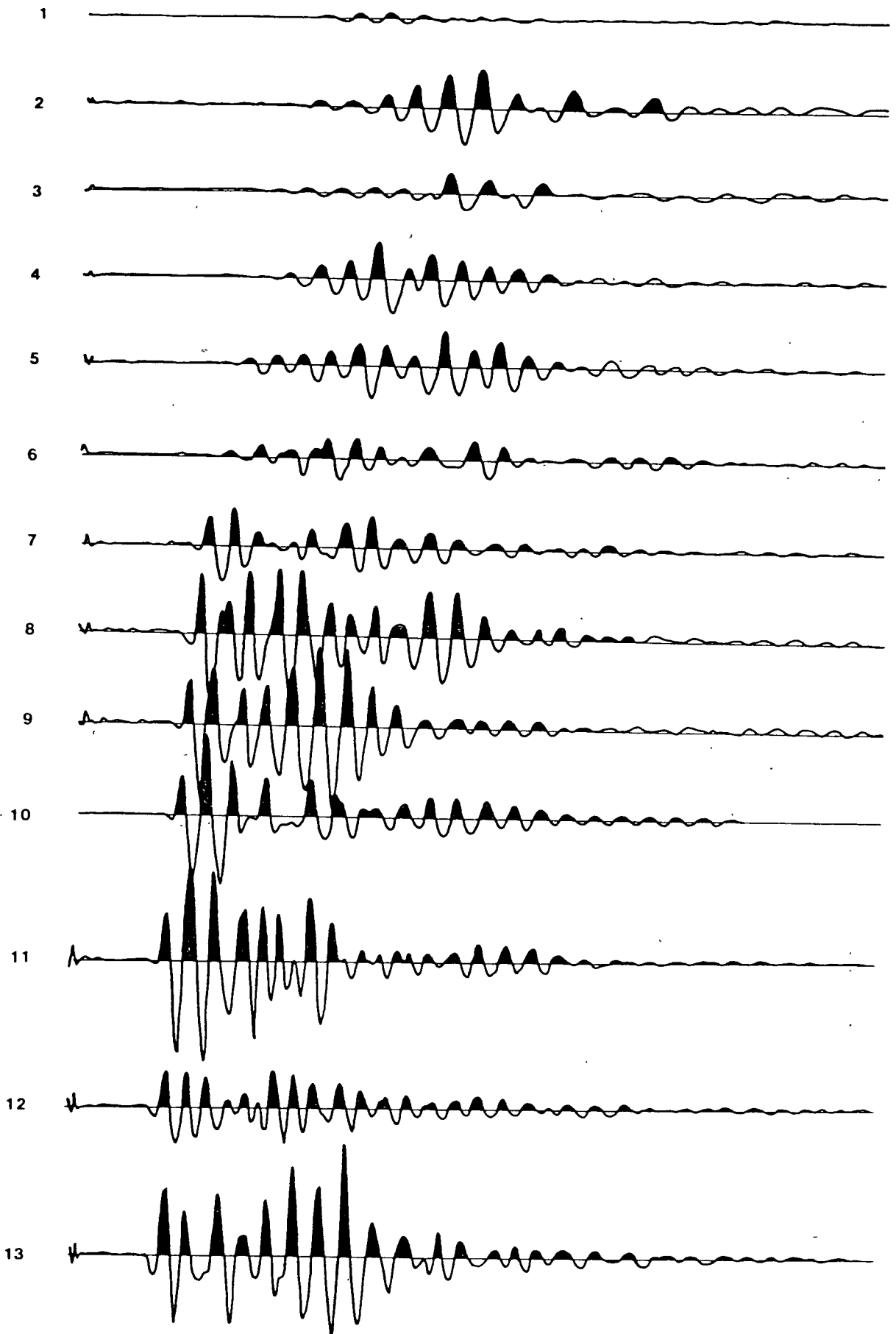


FIG. 5:1:10 COCKING SURVEY - SIGNATURES FOR SEISMIC SCAN 8/5

Hence, the presence of the cavity has a marked effect on the amplitude of the received pulse. To emphasise this point, the amplitude values from scan 8/5 (adjusted for spreading) were subtracted from the values from scan 8/6 at each depth and a plot of the amplitude difference against depth is shown Fig 5:1:11. Again, it is clear that there is an increase in the relative amplitude attenuation below 8 m when the tunnel is present between the boreholes.

5:1:3 Interborehole seismics at Maidstone

Interborehole seismic scanning was used to investigate an area of disturbed ground which was suspected to contain cavities at Norman Close, Maidstone, Kent. Subsidence at one corner of 22, Norman Close had resulted in eventual demolition of the entire building (22/24, Norman Close). The appearance of cracks in the adjacent building (26/28, Norman Close) resulted in the present investigation to look for a possible extension of the cavities.

Four boreholes were placed by South Eastern Soils Limited at the corners of this building so that an interborehole acoustic scanning survey could be performed, and their positions are shown in Fig 5:1:12.

a Geology

Norman Close is situated to the northeast of Maidstone on the side of Foley Hill near its top. The house is situated on the Folkestone Beds (Green et al 1975; Ref 114) which form part of the Lower Greensand. In this area the Beds are composed of sediments ranging from coarse sand to clayey silts, but silty fine sand predominates. At a depth of about 17 m a bed of Fullers Earth approximately 1 m thick is encountered. This is an almost pure montmorillonite clay that occurs at the base of the Folkestone Beds and was once of great economic importance. The boreholes terminate approximately 1 m below this in the Landgate Beds.

The borehole between 20/22, Norman Close proved ragstone from the Hythe Beds at about 25 m. The beds are practically horizontal at this point, being on the crest of a small anticline. The anticline is not tectonic in origin, but results from the action of the river Medway to the south. It has cut through to the incompetent Weald Clay which has subsequently

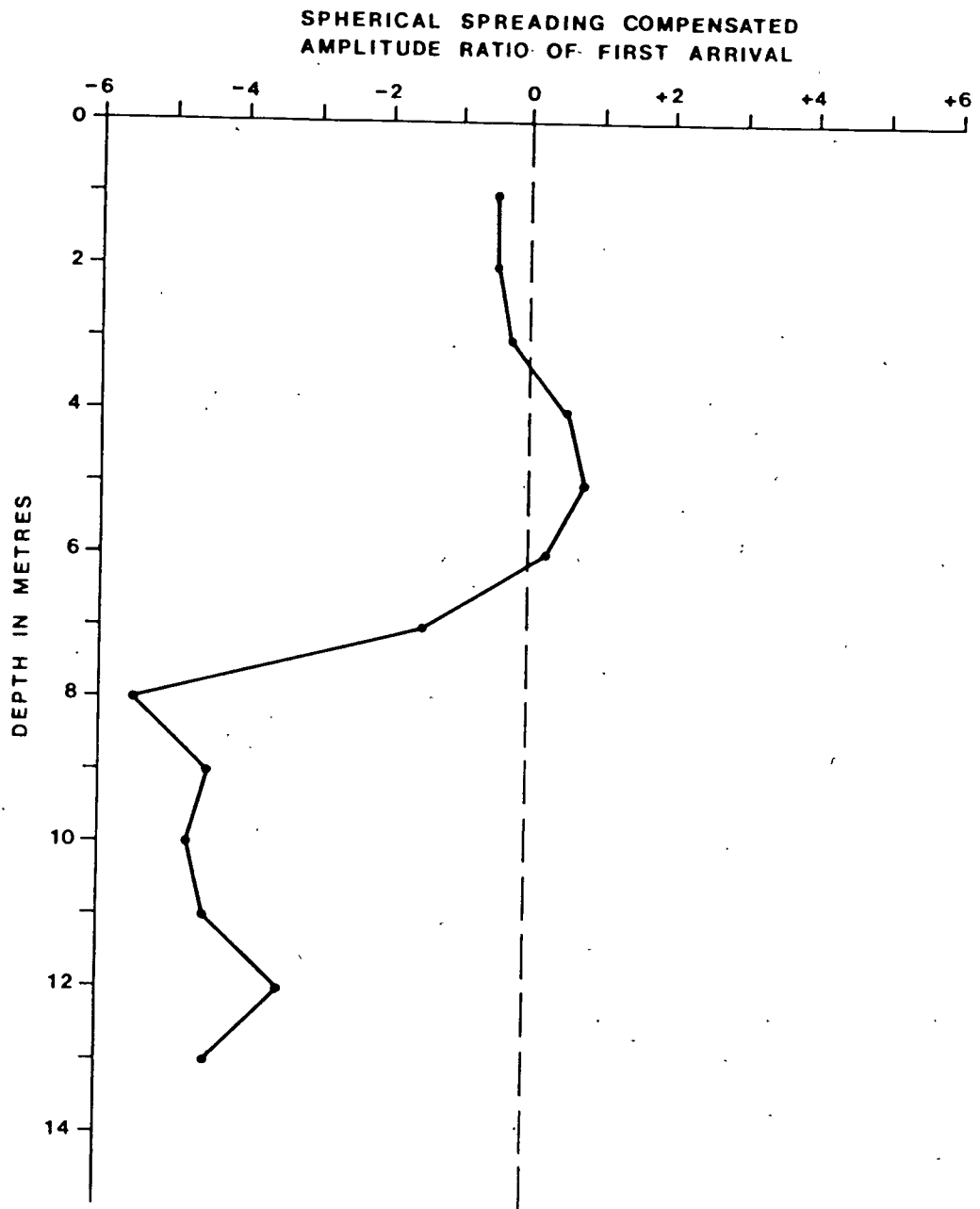
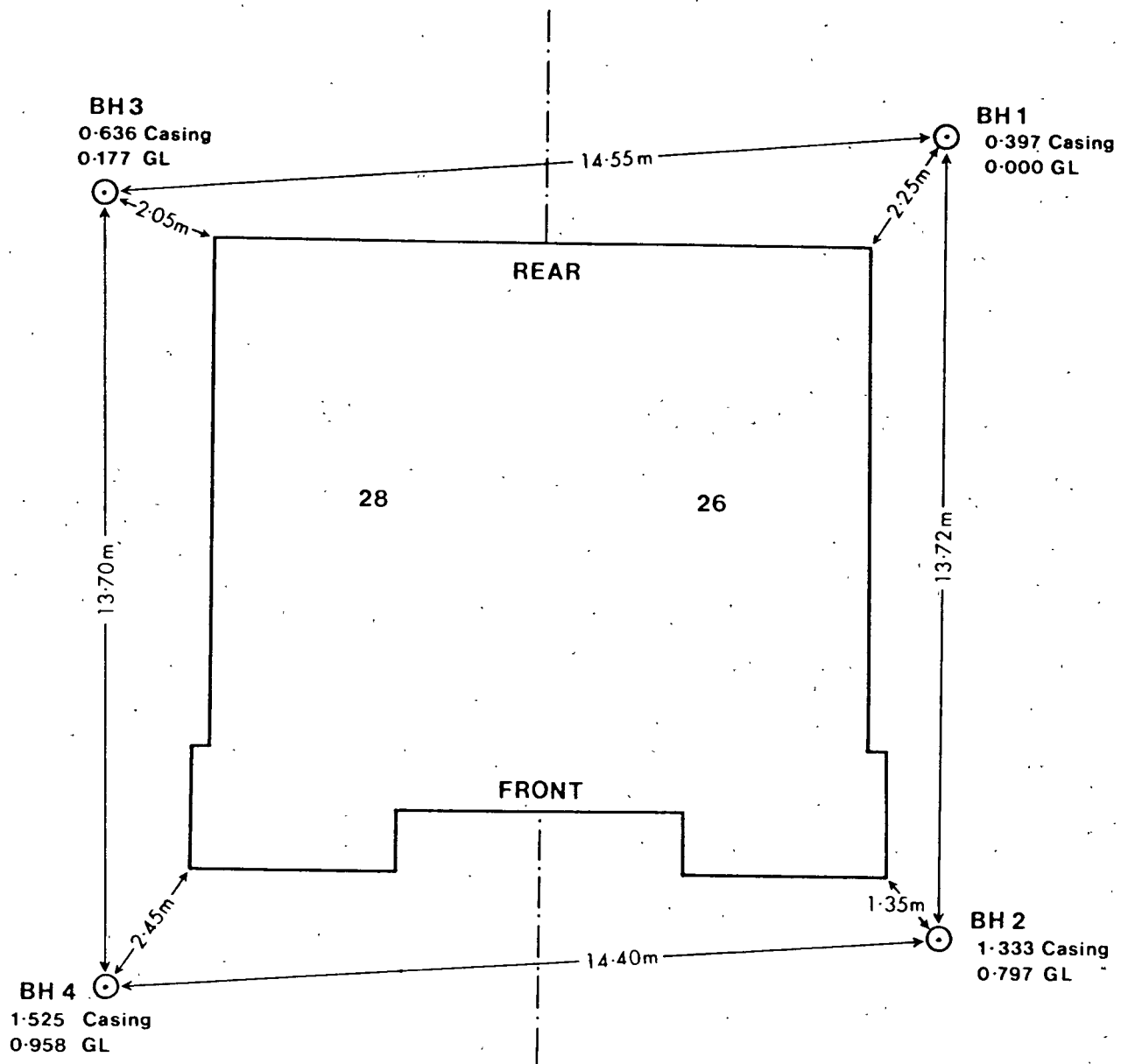


FIG. 5:1:11 COCKING SURVEY - NORMALISED AMPLITUDE RATIO
(amp. scan 8/6 - amp. scan 8/5)



BH 3	Borehole number
0.636 Casing	Height of casing top above ground level at BH3.
0.177 GL	Height of ground level above BH3.

FIG. 5:1:12 POSITIONS AND RELATIVE HEIGHTS OF BOREHOLES USED FOR THE SEISMIC SCANNING AT NORMAN CLOSE, MAIDSTONE.

flowed outwards into the river valley, causing the incompetent Greensand above to downwarp. This is termed 'cambering', and has principally affected the Hythe Beds. It has resulted in the formation of tension cracks and gulls, which can be a great hazard to the engineer. Dr A Penman (1976; Ref 121), of the Building Research Establishment, has commented on them as follows:

'Gulls can be something of a nuisance to the engineer, particularly when the loose loam is washed out by concentration of water from leaking pipes of soakaways, causing swallow holes at ground surface. The old builder got over these difficulties by spanning across the cracks with arched foundations. Unfortunately, modern buildings with shallow foundations are often damaged when these swallow holes appear.'

Cambering is also referred to, together with a detailed account of the geology, in Worssam (1963; Ref 122).

b Interborehole seismic survey

Interborehole seismic scanning was used to investigate an area of disturbed ground containing cavities at Norman Close.

The instrumentation for interborehole acoustic scanning is fully described in section 5:1:1. Measurements were taken of travel time and amplitude of the received signal at 1 m intervals between BH1 and BH2 (scan 1/2), BH4 and BH2 (scan 4/2), BH3 and BH2 (scan 3/2), and BH3 and BH4 (scan 3/4) respectively. An additional set of amplitude measurements was performed using the stationary hydrophone method by transmitting diagonally underneath the house between BH3 and BH2 (scan 3/2) and BH4 and BH1 (scans 4/1 and 1/4). It is important to recognise that these last two scans are different, since scan 4/1 had the hydrophone positioned at the bottom of BH1 and scan 1/4 had it at the bottom of BH4.

The computed values of the velocity of propagation for the seismic pulse for scan 1/2, 4/2, 3/1 and 3/4 respectively are shown in Fig

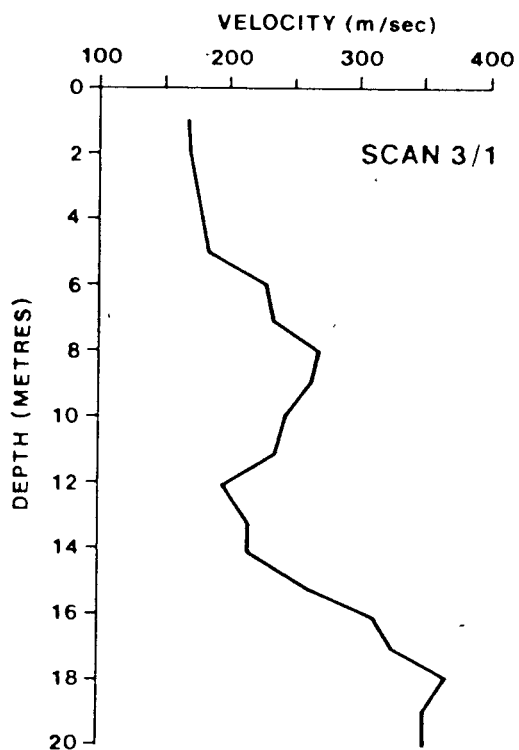
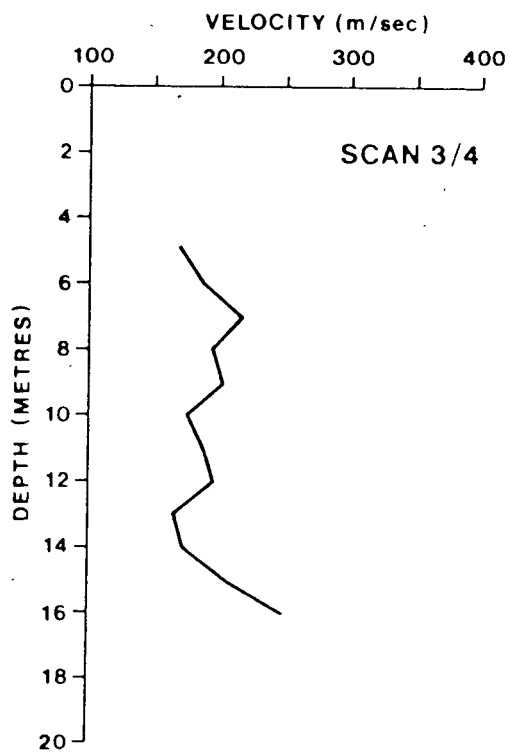
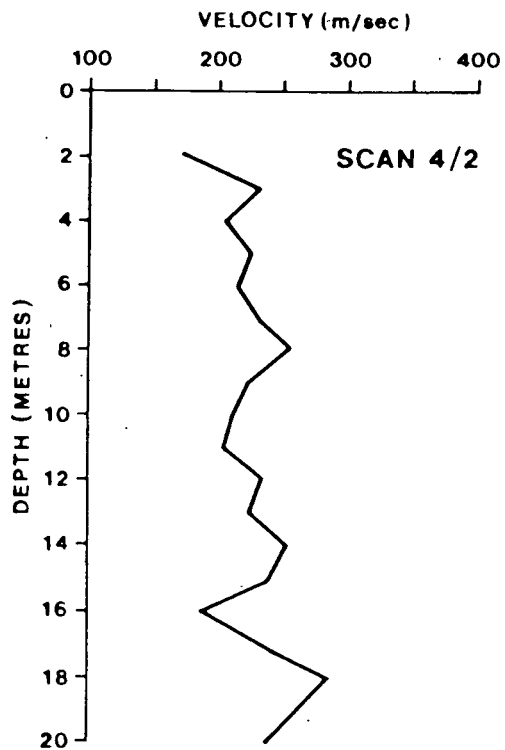
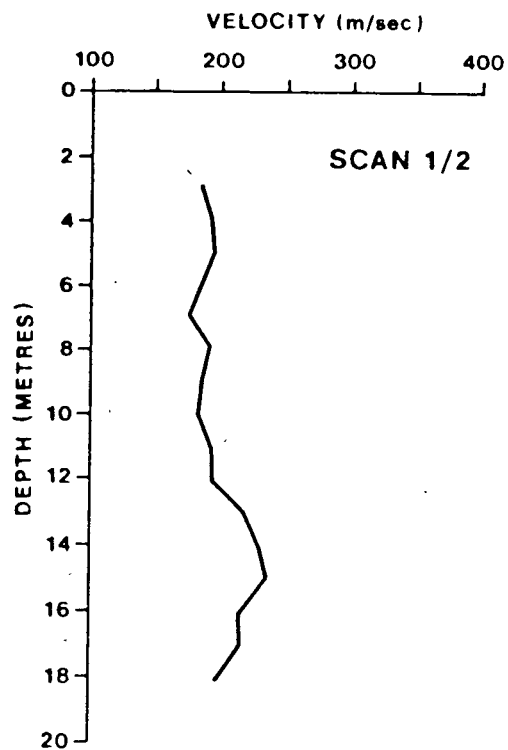


FIG. 5:1:13 MAIDSTONE SURVEY - VELOCITY SCANS

5:1:13. The velocity varies between about 160 ms to 340 ms. These values are considerably lower than expected for P waves, even for less compacted sand, and are most probably associated with Sv waves. Schultheiss (1983; Ref 123), while investigating the influence of the packing structure on the seismic wave velocity in sediments, has shown that the S wave velocity for sand in the laboratory vary from 17 ms to 149 ms. Hamilton (1975; Ref 73) reviewed what little information existed on saturated marine sediments and using the results from Cunny and Fry (1973; Ref 124), which formed bulk of the sand data, concluded that the S wave velocity varied from 53 ms to 287 ms in depth range 0.1 m to 7.2 m.

McCann et al (1984; Ref 125) used interborehole seismic measurements to determine the dynamic elastic moduli of sediments at a test site at Newborough, Anglesey. Borehole investigation at the site had indicated the presence of an extensive and fairly uniform sand body to a depth of more than 20 m with a thin gravel layer at 15 m. The result of the P and S wave velocities obtained are shown in Fig 5:1:14. The P wave velocity varied very little with depth in the top 15 m but showed small fluctuations with lithological changes in the sand mass. The S wave velocity (Sv) increases steadily with depth as the overburden pressure increases; the water table was close to the ground surface. The average P wave velocity was 1600 ms but the S wave velocity varied between 140 ms to 260 ms.

Therefore, the values of the velocity measured at Maidstone indicate that they were most probably from S waves which were mode converted to P waves at the borehole interface, for the hydrophone to detect. The absence of P wave is difficult to explain but the measured value of the velocity, which is slower than the velocity in air ie 390 ms, does agree with other field and laboratory shear wave data.

The variation of amplitudes with depth was also plotted for each of the scans above (Fig 5:1:15) and also for scans 1/4 and 4/1 (Fig 5:1:16). From the results of these scans it is possible to delineate an area of disturbed ground (Fig 5:1:17). Sediment here will have a much looser packing, with the possible existence of small cavities.

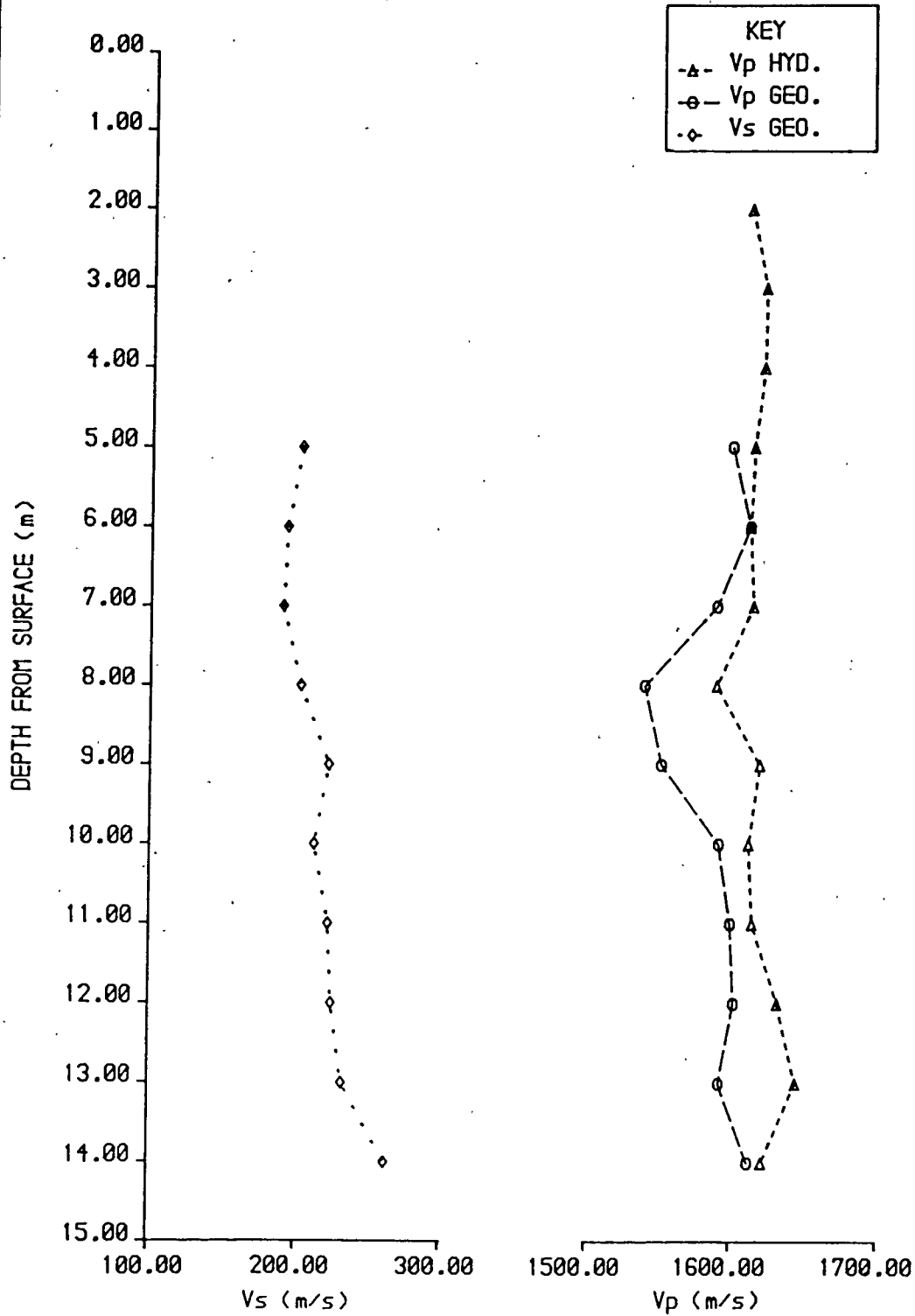


FIGURE 5:1:14 IN-SITU Vp & Vs FOR SATURATED SAND AT NEWBOROUGH ANGLESEY (after McCann et al 1984; Ref 125).

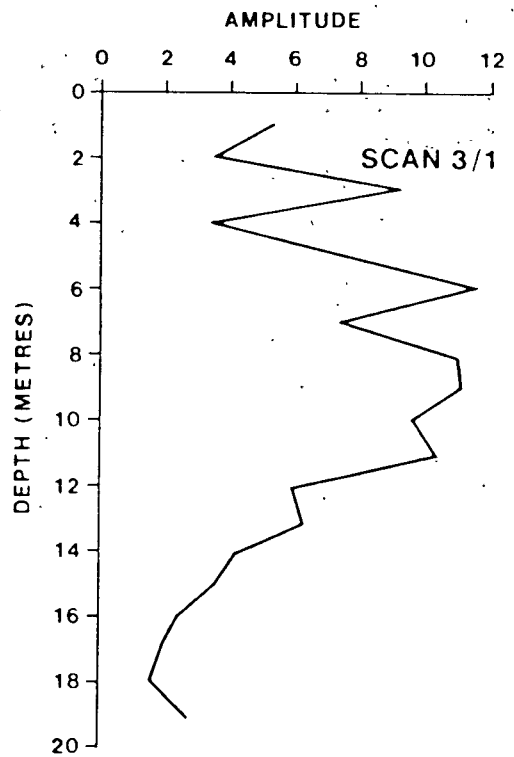
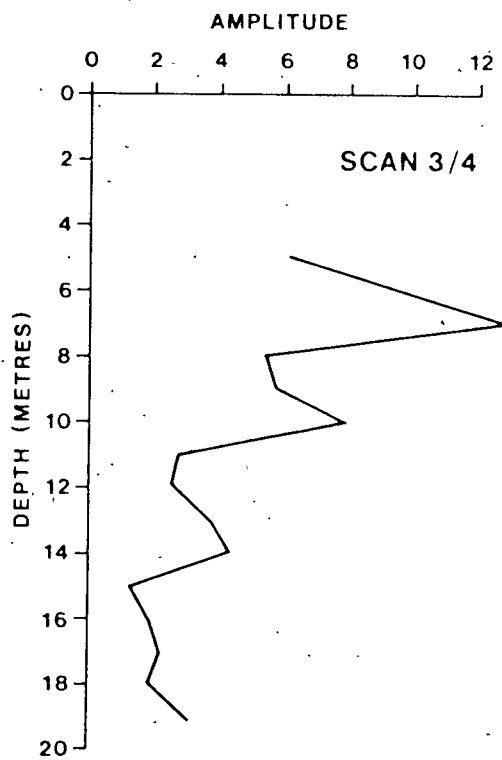
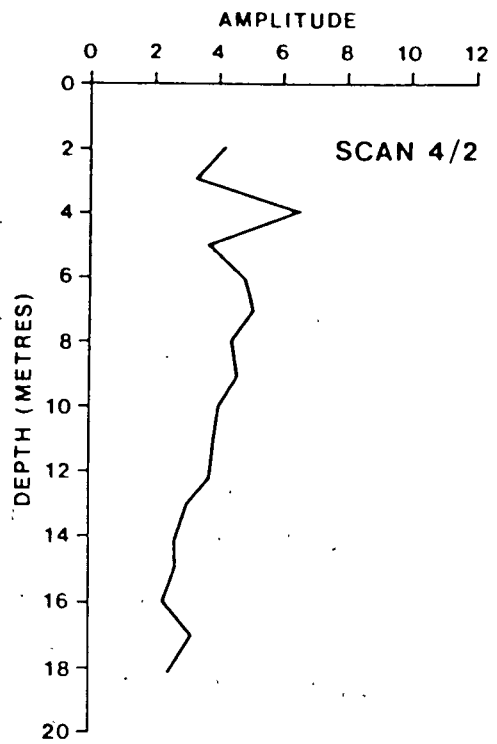
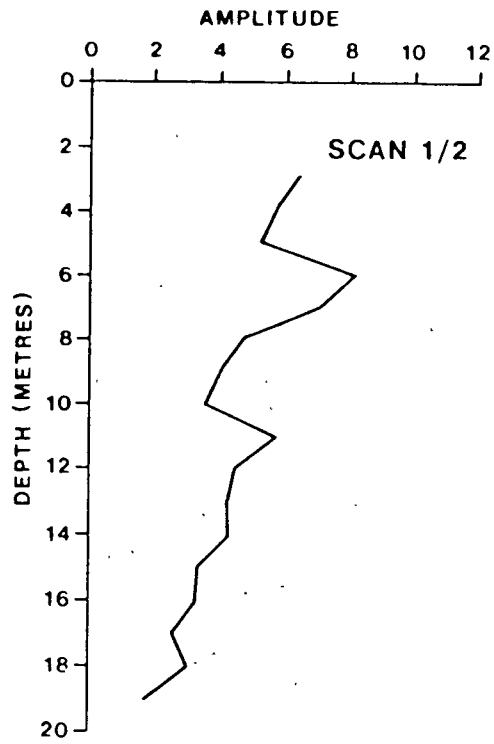


FIG. 5:1:15 MAIDSTONE SURVEY - AMPLITUDE SCANS

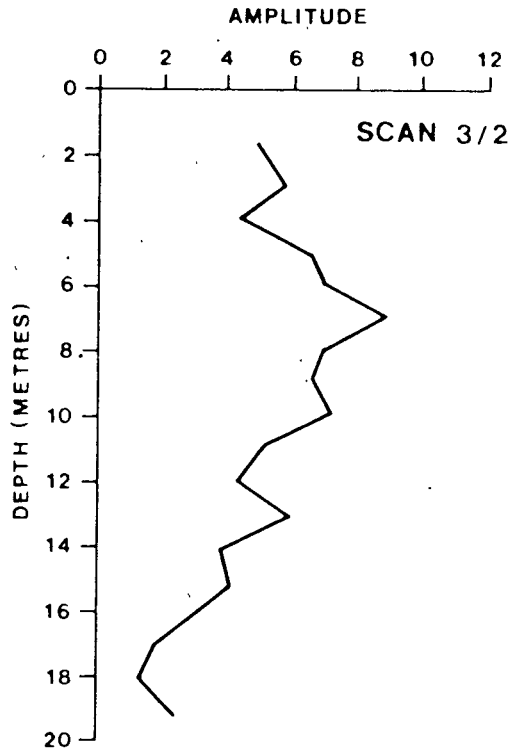
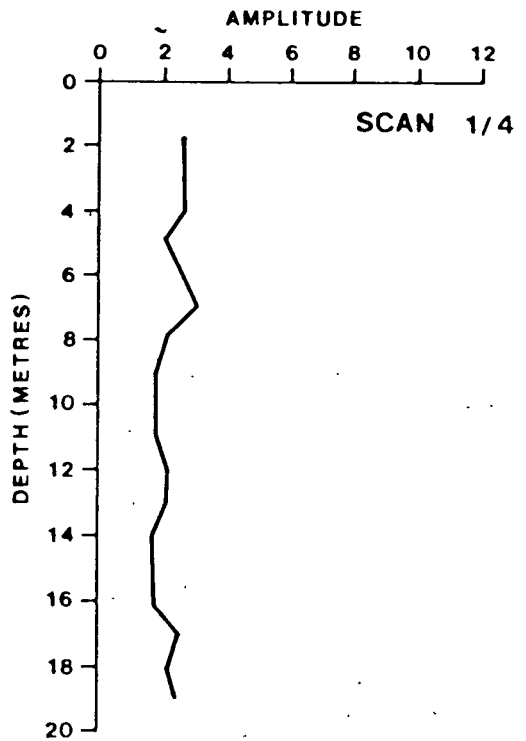
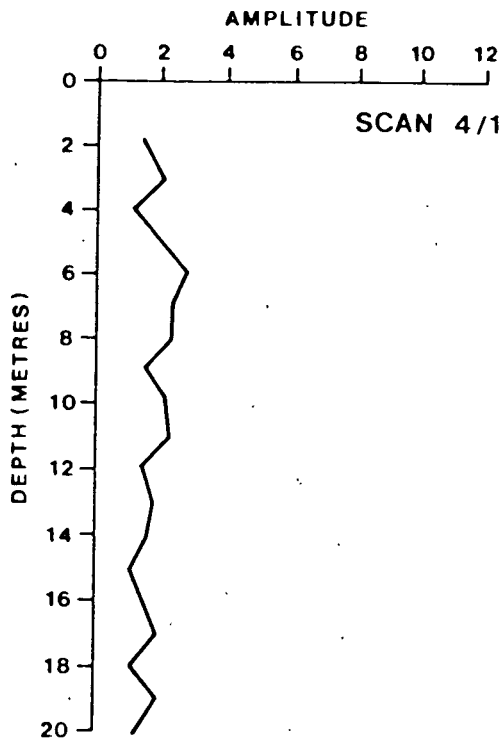
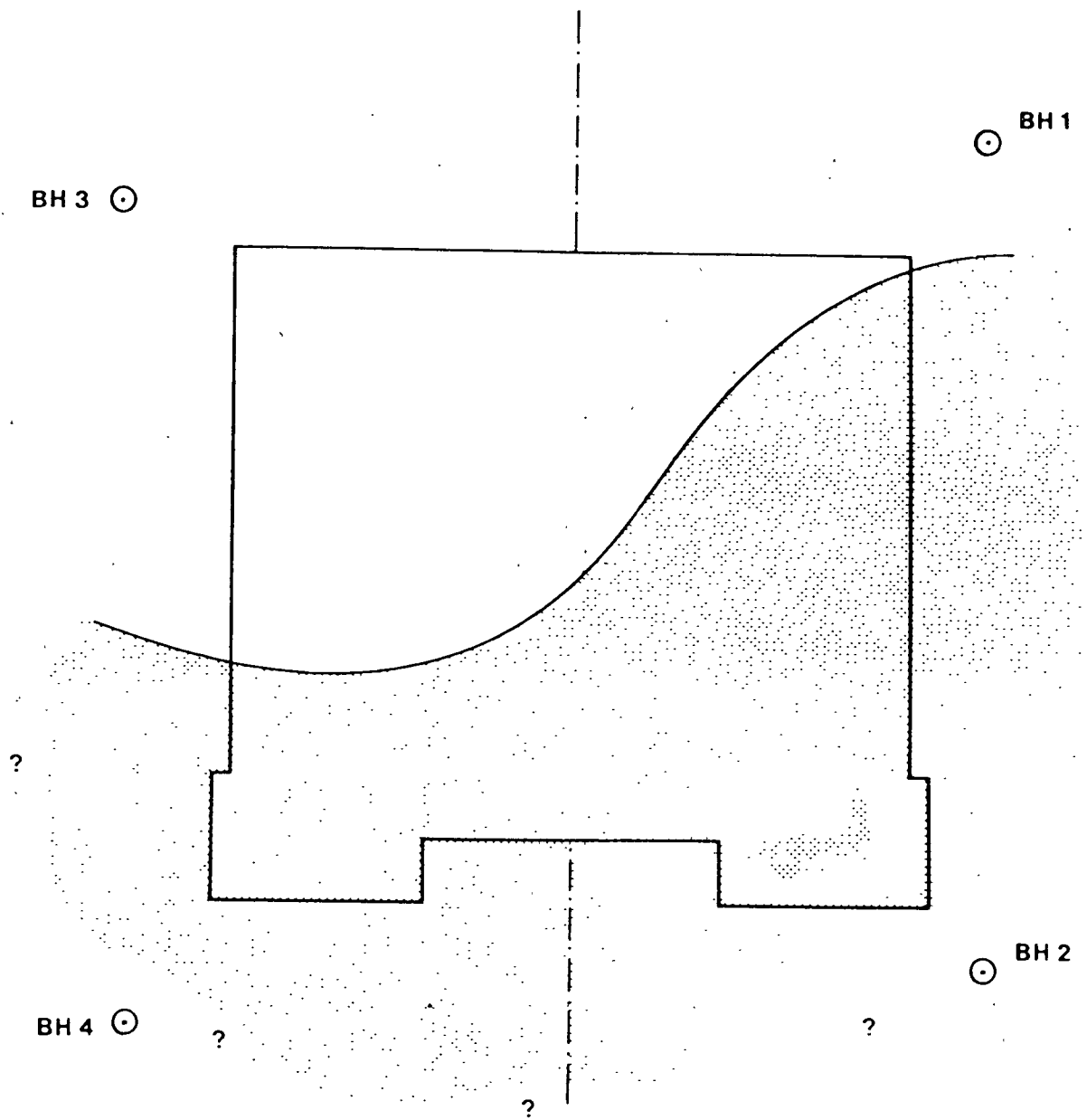


FIG. 5:1:16 MAIDSTONE SURVEY - AMPLITUDE SCANS
WITH A STATIONARY HYDROPHONE



Area in which Acoustic Anomaly lies at a depth of between 7 and 13 metres below ground level.

FIG. 5:1:17 MAIDSTONE SURVEY - AREAL EXTENT OF SEISMIC ANOMALY ZONE

The amplitude scans (Fig 5:1:15) make this anomaly apparent. There is a greater attenuation of the signal transmitted between BH1 and BH2, BH2 and BH4, and BH3 and BH4 than between BH3 and BH1. This is apparent at a depth of between 8 m and 12 m. This difference was emphasised by subtracting scan 3/1 from the other three (Fig 5:1:18). It was assumed that scan 3/1 reveals a profile through ground which was less disturbed. This is a reasonable assumption which may be on the conservative side. If ground is more disturbed between BH3 and BH1, it would only mean that the anomaly between the other boreholes is more serious than was previously thought.

Results of the velocity scanning (Fig 5:1:13) confirm the difference in acoustic properties of the material between BH3 and BH1. At a depth of between 6 m and 11 m, scan 3/1 shows a maximum apparent velocity of 270 ms. This is greater than in the other scans. Scan 2/1 has a maximum velocity of only 196 ms in this region.

Diagonal scans were also carried out to obtain more information on position and size of the disturbed ground by scanning underneath the house (Fig 5:1:16) between BH1 and BH4, and BH3 and BH2. Scans 4/1 and 1/4 show low-amplitude levels throughout, indicating poor transmitting characteristics of the ground between these two boreholes. Scan 3/2, however, is similar to the normal profile (scan 3/1), showing the ground to have better seismic properties in this area - especially near BH3.

The seismic scanning survey revealed an acoustic anomaly bounded by BH1, BH2 and BH4 at a depth of between 7 m and 13 m. This anomaly was believed to be caused by a disturbance to the sedimentary structure. This may either take the form of small cavities similar to those found in BH2 and BH8 at 22, Norman Close or a difference in packing structure sediment. The latter effect may be difficult to confirm as one cannot be certain of its existence, even if a borehole was driven right through its centre. The only evidence of such a disturbance on the borehole log may be a change from, say, a medium dense brown silty sand to a loose brown silty sand. Nevertheless, a sediment in such a condition could well have cavities form in it under the influx of a large amount of water.

It is suggested that loose packing of the sediment was probably caused

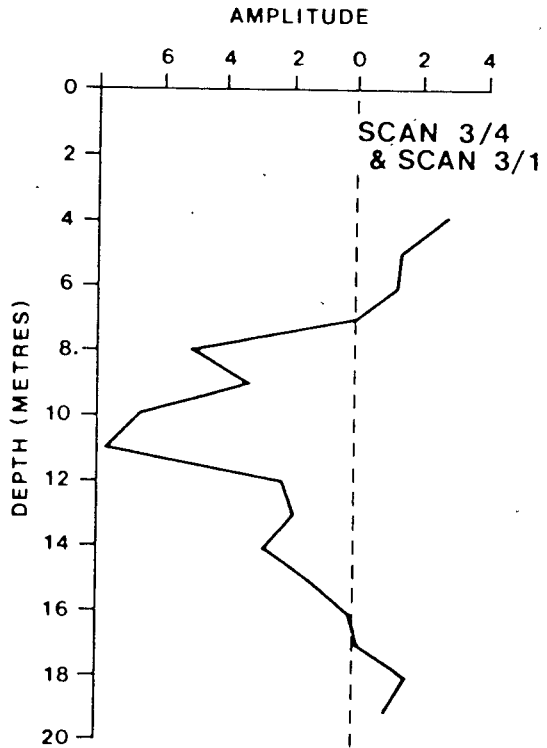
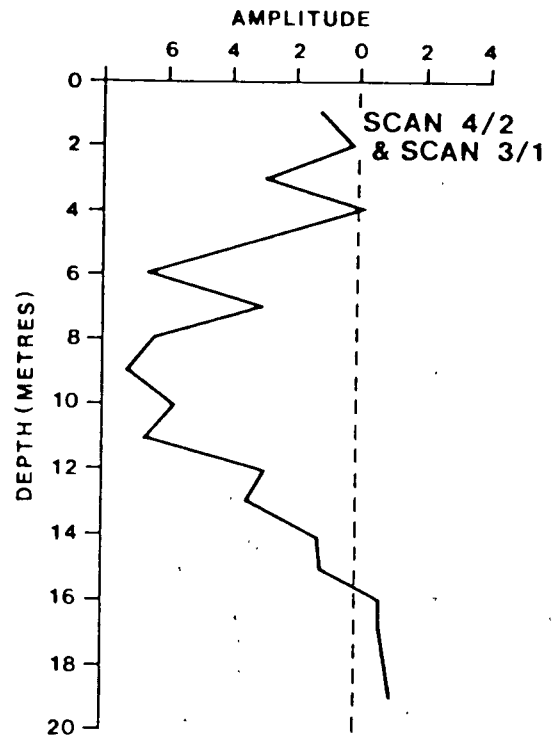
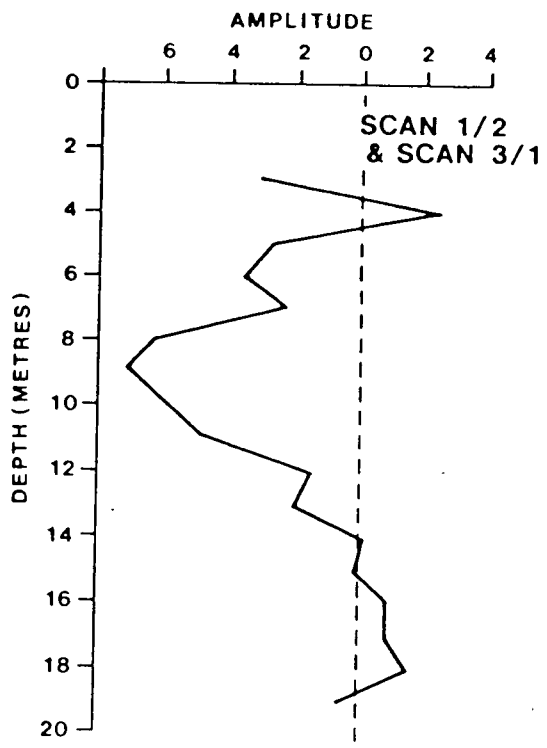


FIG. 5:1:18 MAIDSTONE SURVEY - COMPARISON OF HORIZONTAL
AMPLITUDE SCANS

by a combination of the following factors: a) cambering which primarily affects the Hythe Beds, also producing tensional forces in the overlying Folkestone Beds, and b) gravitational forces acting down the slope. Sediment in such a state of stress would then be activated by a large influx of water and caused to flow downhill. The Fullers Earth would be an impenetrable barrier to the water present, causing it to collect and have its worst effect in sediment in the area where the seismic anomaly is to be found.

It is interesting to note that a distinct refracted arrival from the upper surface of the Fullers Earth clay (band) is observed in scan 3/1 (Fig 5:1:13) between 14 m and 18 m. There is also some indication of this refracted arrival on scan 3/4, but it is not observed on either scan 1/2 or scan 4/2. It is considered that failure to observe this refracted arrival on the latter two scans is due either to the very low level signals associated with these two scans or the partial collapse of the refracting interface.

5:2 Surface to borehole seismic method

Most site investigations carried out for civil engineering structures require a few boreholes to be drilled on site to investigate in detail the changing lithological and geotechnical properties of the superficial material.

These boreholes can be used for the interborehole acoustic scanning method described above to detect the presence of a cavity or mine shaft, but the instrumentation is fairly complex and rather expensive. However, the presence of boreholes at a site does provide the geophysicist with the opportunity of making measurements between the ground surface and at any point in the borehole. Although, in theory, the position of the source and the receiver are interchangeable, very few seismic sources can be used in the boreholes without causing damage to the borehole wall.

The surface to borehole method is an extension of the Vertical Seismic Profiling (VSP) method, which is widely used in the oil industry (Kennett et al 1980; Ref 126). This consists of suspending a hydrophone or a geophone in the borehole (well) at a known depth and recording the

received pulse train from a seismic source near the borehole (Fig 5:2:1).

5:2:1 Theory and principles

The basic seismic theory described in Chapter 4 can be applied to the borehole to surface surveying method. The generation of a theoretical model, however, requires complex mathematical equations to satisfy all the boundary conditions and a computer with a fairly large storage capacity. This type of analysis where the model is compared with the field data is carried out in the oil industry but does not appear to be a practical proposition for a normal site investigation at present.

Using fairly simple instrumentation it is possible to measure the time taken for a pulse to travel from the seismic source on the surface to a receiver in the borehole. The analysis can then be concentrated on the first arrival (first time break), which can be either a direct pulse or a refracted one depending on the geology and the geometry of the source and the receiver.

The main difficulty which arises in producing a set of travel times or a given model is calculating the travel time of a direct wave between the shot point and hydrophone. Any attempt to calculate this trigonometrically indicates that:

- i It is not possible to produce a simple solution for the travel time involving an arbitrary number of layers
- ii The method of solution, even for a small number of layers, is extremely complex and becomes increasingly difficult as the number of layers is increased.

It is therefore necessary to use an approximate method of solution. A computer program based on a method of successive approximation was developed by Rouse (1981; Ref 127). This program gives results to an accuracy well within that expected from the field data with a reasonable number of iterations. In the model shown in Fig 5:2:2 there is clearly a unique direct ray path between the shot point and hydrophone for a given set of layer parameters. Subsequently, the angle at which the wave

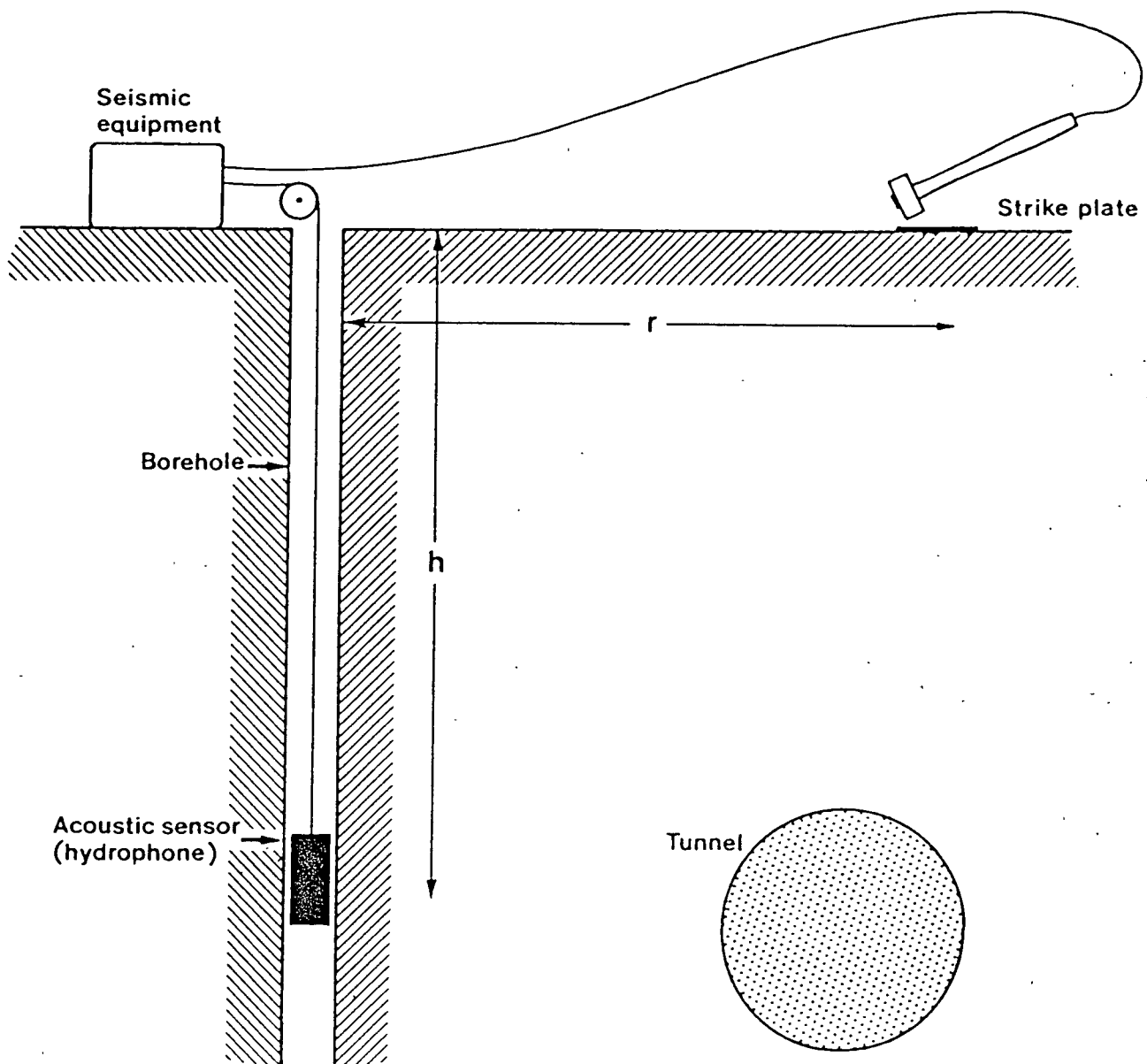


FIG. 5:2:1 SCHEMATIC DIAGRAM OF THE SURFACE TO BOREHOLE
SEISMIC TECHNIQUE

arrives at the borehole and hydrophone (angle 'A') will enable the travel time to be calculated.

It can be shown that for a given angle A, hydrophone depth X, and set of layers of thickness D and velocity V:

Direct travel time

$$T_D = \frac{X - \sum_{i=k-1}^l D_i}{V_k \cos A} + \sum_{i=k-1}^l \frac{D_i}{V_i \cos A_i} \quad - (5.1)$$

where the hydrophone lies in the kth layer and where

$$A_i = \sin^{-1} ((V_i/V_{i+1}) \sin A) \quad - (5.2)$$

Furthermore, the displacement between the shot point and hydrophone, H_D

$$H_D = \left\{ X - \sum_{i=k-1}^l D_i \right\} \tan A + \sum_{i=k-1}^l D_i \tan A_i \quad - (5.3)$$

This computer program successively approximates A so that H_D tends to the distance between the borehole and shot point at the surface.

There may also be arrivals which have travelled as head waves along interfaces below the layer in which the hydrophone is situated. The program calculates all such possible arrivals directly. The refracted arrival time for the hydrophone in the kth layer and refraction along the interface at the base of the jth layer is given by

$$T_R = \sum_{i=j}^1 \frac{D_i}{V_i \cos \theta_i} + \left\{ \frac{\sum_{i=k}^1 D_i - X}{V_k \cos \theta_k} \right\} + \frac{Y - \sum_{i=j}^1 D_i \tan \theta_i - \sum_{i=j}^1 \frac{D_i \tan \theta_i}{V_{j+1}} - \left\{ \sum_{i=k}^1 D_i - X \right\} \tan \theta_k}{V_{j+1}} \quad (5.4)$$

where Y is the borehole to shot point distance and θ_k is the critical angle at the refracting interface where

$$\theta_k = \sin^{-1}(V_j / V_{j+1})$$

and

$$\theta_i = \sin^{-1}(V_i / V_{i+1})$$

5:2:2 Experimental procedure for surface to borehole seismic method

Although, in theory, the source and receiver can be interchangeable, it is preferable to use the source on the surface with the receiver in the borehole, for the following reasons:

- i environmental noise reduces with depth below the ground surface
- ii various seismic sources including explosives can be used on the surface with little restriction on the size of the source
- iii a polarised shear wave source (SH and SV) can be used with a clamped geophone or accelerometer in the borehole.

It must be borne in mind that with the surface to borehole technique the

volume of the rock mass investigated is very limited. If, for instance, a series of measurements is taken with a source on the surface at a fixed radius from the centre of the borehole, then the volume of investigation is cone shaped, with twice the radius as the base and the distance from surface to receiver as the apex. The effective volume of investigation can be increased by using larger separations between the seismic source and the top of the borehole but this can result in a loss of resolution; alternatively the boreholes can be positioned such that the volume of investigation associated with each borehole has a substantial overlap. The receiving array and associated instrumentation identical to the one used for the inter-borehole surveys are described above and most seismic sources can be used for this method.

Various combinations of the source and receiver position can be used, but the most practical approach is to position the receiver at a known depth, and move the source either in a circle (Fig 5:2:2) or a straight line from the centre of the borehole. The measurements are repeated at various hydrophone positions down the length of the borehole.

The hydrophone array used in this case can be replaced by a three-component well geophone clamped to the borehole wall. This can provide information on the shear wave velocity, which is used to calculate the dynamic elastic properties of the rock mass. To simplify the instrumentation, the recording of the acoustic pulses can also be carried out on a standard seismic set such as the Bison Type 1575 stacking seismograph.

5:2:3 Surface to borehole seismics at Cocking

A series of surface to borehole seismic measurements were carried out above the disused tunnel at the Cocking test site. The geology, layout of the boreholes and the tunnel dimensions have been described in section 4.

At the Cocking site a drop weight (ABEM) seismic source was used. This consists of a steel base and a weight which is raised to a height of 4 m. When the weight is released it strikes a steel plate on the ground surface, and seismic energy is developed by the conversion of potential energy to kinetic energy at the point of impact. On impact, an inertia

switch mounted on the guide tube for the weight closes and produces a pulse suitable to trigger the trace on a storage oscilloscope (Tektronix type 7039). The receiving sensor was an BGS BAR IV hydrophone array and the associated instrumentation was identical to that used for the interborehole measurements. The method of monitoring the travel time and amplitude of the acoustic pulse is as described in section 5:1.

The position for the source was selected by scribing a circle of 7.5 m radius, with the borehole at the centre, and dividing the circle into eight sections, ie N, S, E, W, NE, NW, SE and SW as shown in Fig 5:2:3. The ABEM drop weight source was deployed at each of these intersecting points on the circle. The hydrophone array was placed in BH6 and the acoustic waveform was recorded on a tape recorder. This was carried out in steps of 1 m from the surface to the bottom of the borehole for each shot location.

The same procedure was also adopted for shot points on a 15 m radius circle. It became apparent that a shot point on a much larger diameter circle will be required to see the effect of the cavity on the acoustic pulse, as the angle of investigation from the vertical was very narrow. A circle with a radius in excess of 30 m will be required for the seismic pulse to intersect the tunnel. This was an impractical proposition as the site did not lend itself to such large areas of shot point coverage, due to the trees, barbed wire, farm animals etc.

a Results and discussion

The time taken for an acoustic pulse to travel from the surface to the sensor in the borehole was plotted against the depth at which the sensor was positioned down the length of the borehole. Time/depth plots for shot points on 7.5 m radius centred around BH6 are shown in Fig 5:2:4. Shot points at this distance form a very narrow cone and, therefore, the acoustic pulse does not intersect the cavity. The figure shows that there is a considerable variation in time/depth plot for each shot point. In theory, they should all be similar if the geology and the distance are kept the same, and this situation exists in this case. The variation in the time/distance plots can be associated with the heterogeneous nature of the backfill and, in this instance, the use of the computer program described above was not applicable.

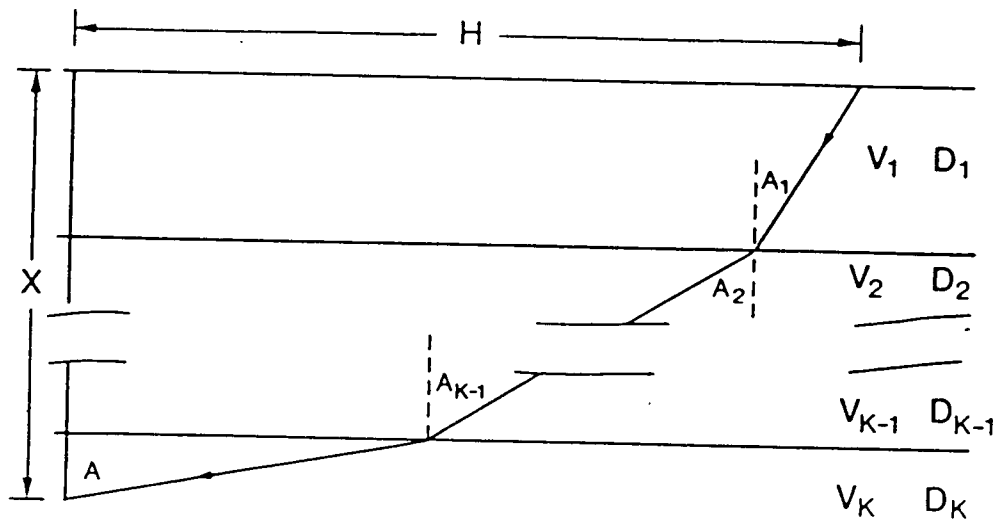


FIG. 5:2:2 MATHEMATICAL MODEL OF SURFACE TO BOREHOLE MEASUREMENTS (after Rouse, 1981; Ref 127)

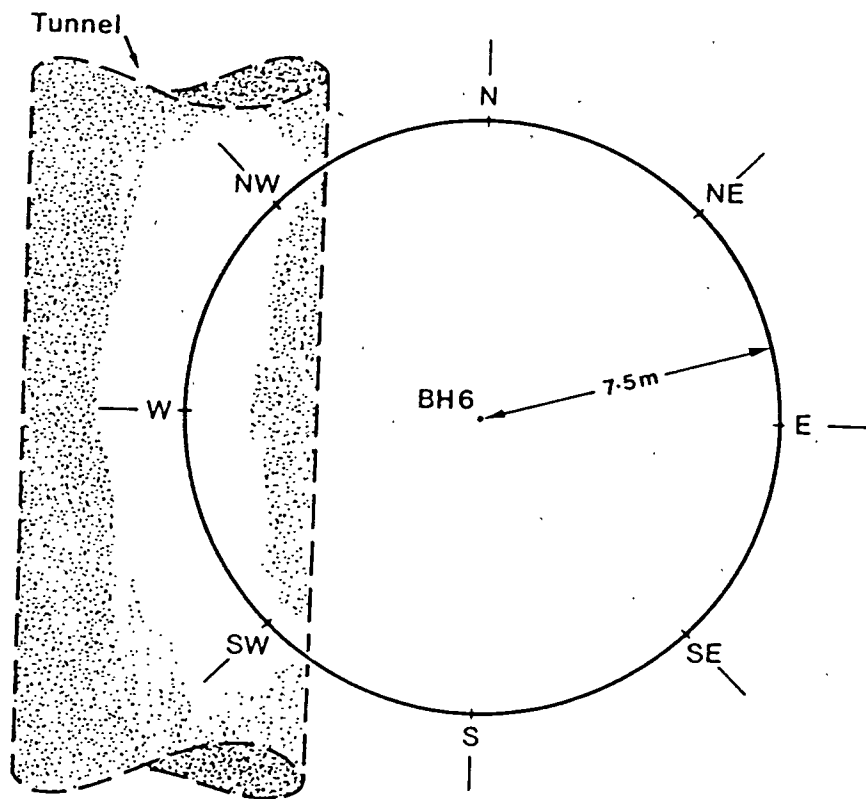


FIG. 5:2:3 COCKING SURVEY - LAYOUT OF SOURCE POSITIONS FOR SURFACE TO BOREHOLE SEISMIC MEASUREMENTS

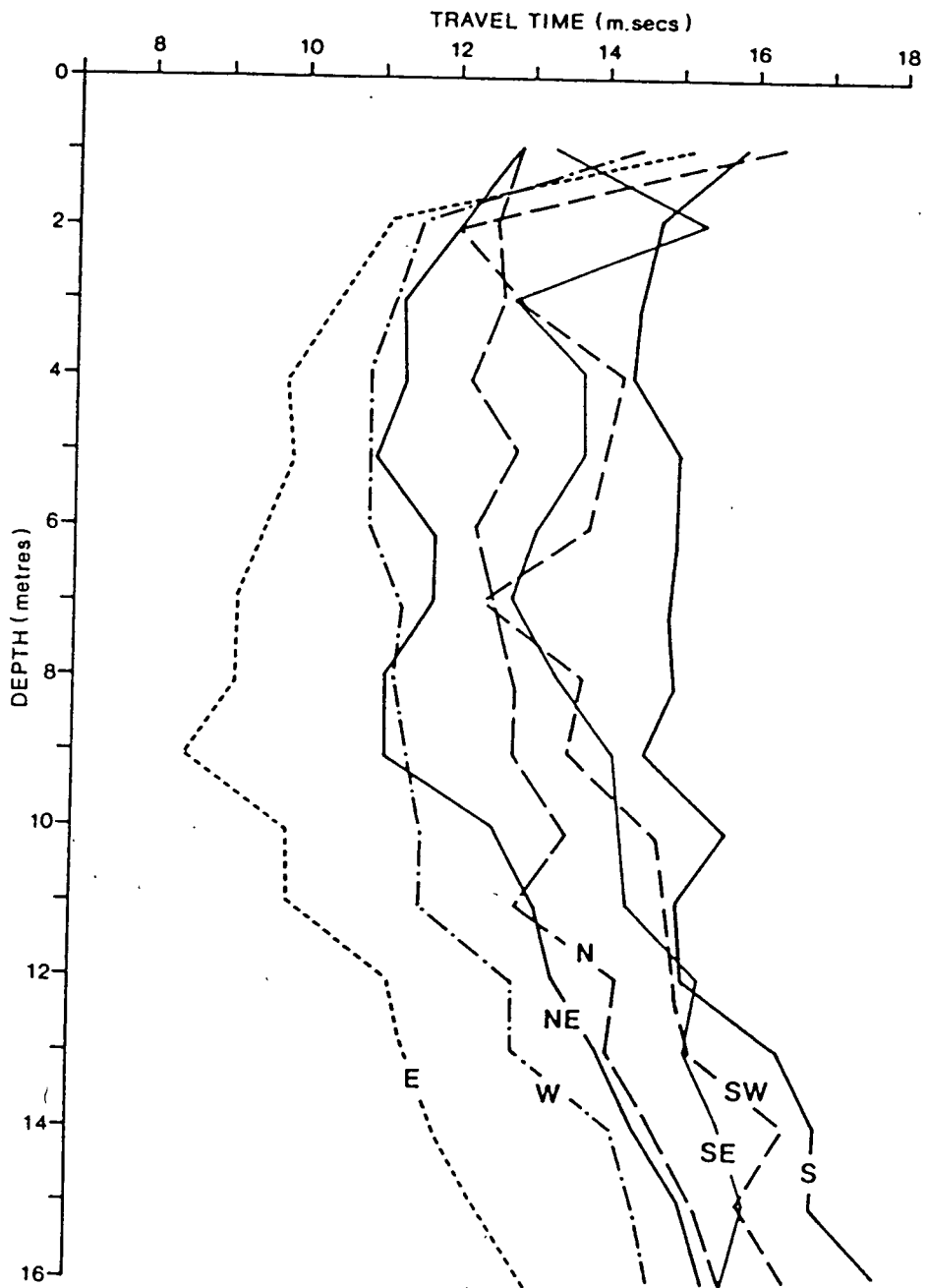


FIG. 5:2:4 COCKING SURVEY - TRAVEL TIME OF SEISMIC PULSE VS DEPTH
WITH SOURCE AT A DISTANCE OF 7.5 M FROM BOREHOLE

Fig 5:2:5 shows the time/depth plot for shot points on 15 m radius centred around BH6. The acoustic pulse from these shots is affected towards the bottom of the borehole in the depth range 12-15 m, by the presence of the cavity in the rock mass. This is apparent when the delay time is compared for a group of measurements near the cavity (W, NW, SE). These delay time measurements are plotted for the depths of 12 m, 14 m and 15 m in Fig 5:2:6. The figures indicate that the group facing the cavity show considerably more delay than the ones facing away from the cavity.

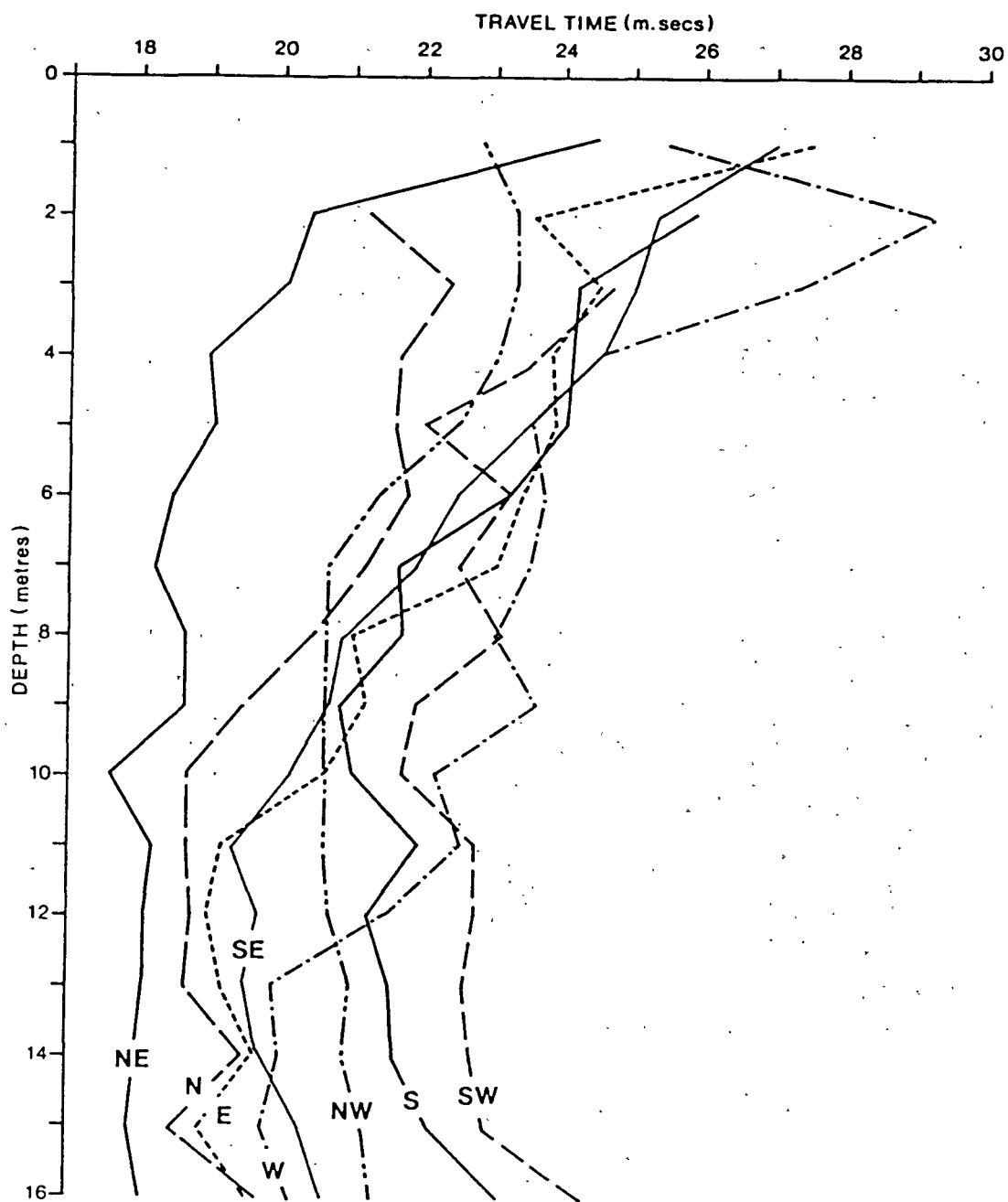
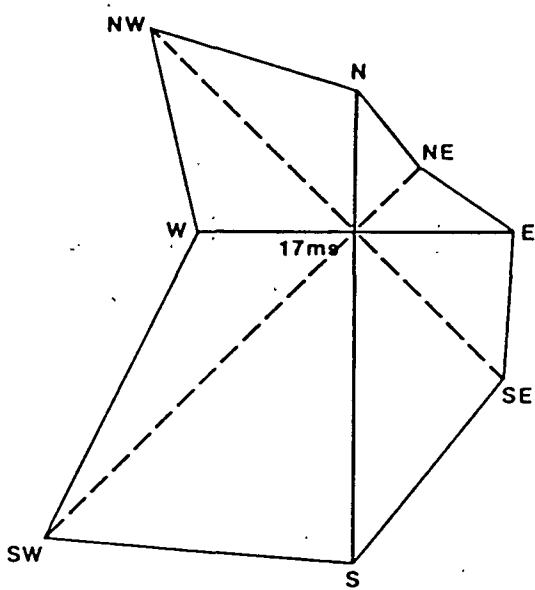
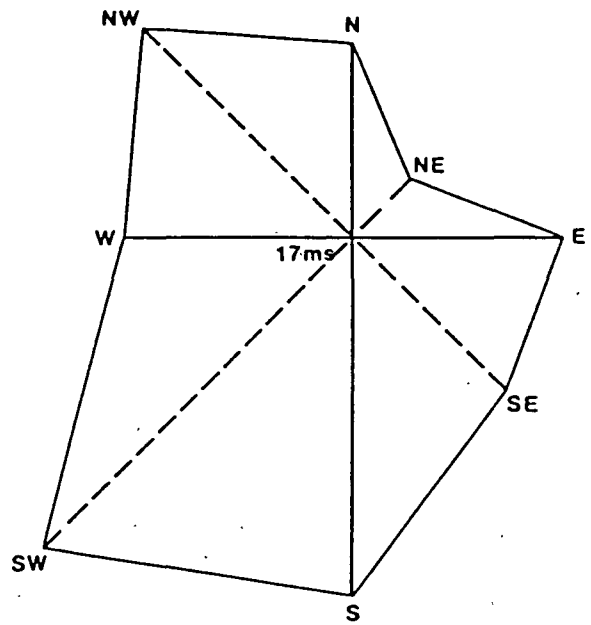


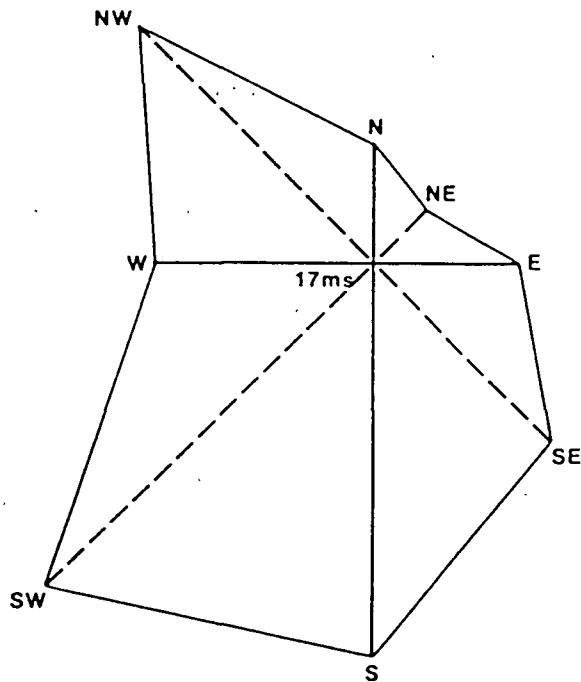
FIG. 5:2:5 COCKING SURVEY - TRAVEL TIME OF SEISMIC PULSE VS DEPTH
WITH SOURCE AT A DISTANCE OF 15 M FROM BOREHOLE



(a) 12 metres.



(b) 14 metres.



(c) 15 metres.

FIG. 5:2:6 COCKING SURVEY - DELAY TIME SECTIONS AT VARIOUS DEPTHS

6 DEVELOPMENT OF A SINGLE HOLE METHOD (ACDER)

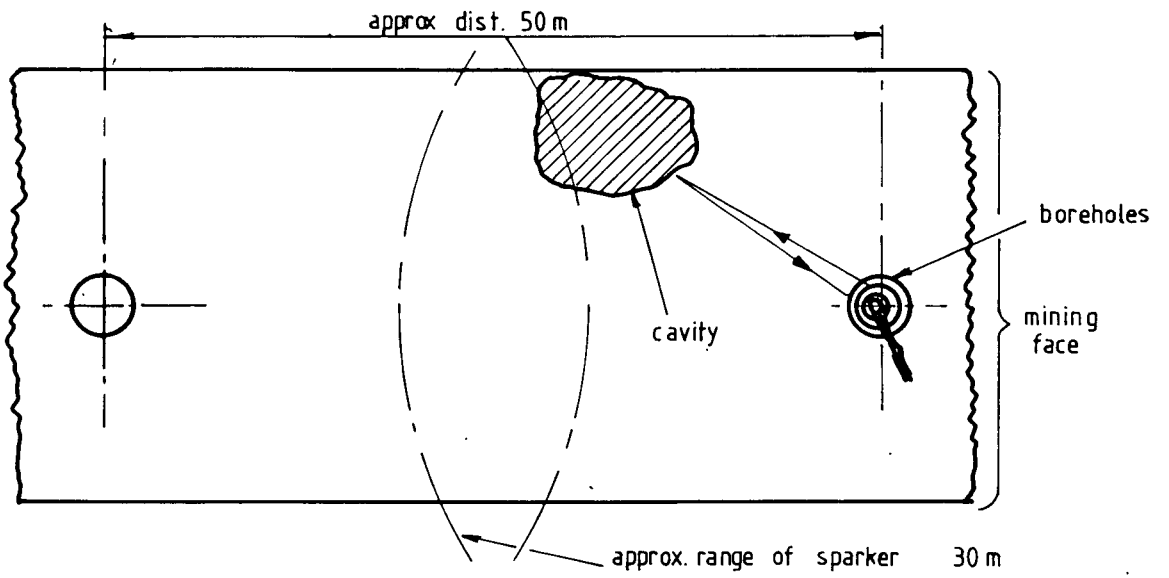
Most of the geophysical techniques available for the detection of cavities have one great disadvantage, and that is the time lag between the data acquisition and the data interpretation. Some of these techniques are only suitable for surface geophysics as the others, which are used for deep exploration, lack the resolution, range and azimuth required in a mining environment. A new technique was considered to overcome the above problems, and research was carried out to assess its feasibility.

This system is analogous to the radar system used in aircraft traffic control or guided weapon systems, and is called the ACoustic DETection and Ranging system (ACDER). ACDER uses an omnidirectional seismic pulse and a directional receiver operating from a single borehole (Fig 6:0:1). An omnidirectional seismic pulse is fired while the directional receiver is facing a known direction. If a sufficiently large discontinuity exists with a reasonable seismic impedance contrast, some of the energy would be expected to be reflected back towards the directional receiver.

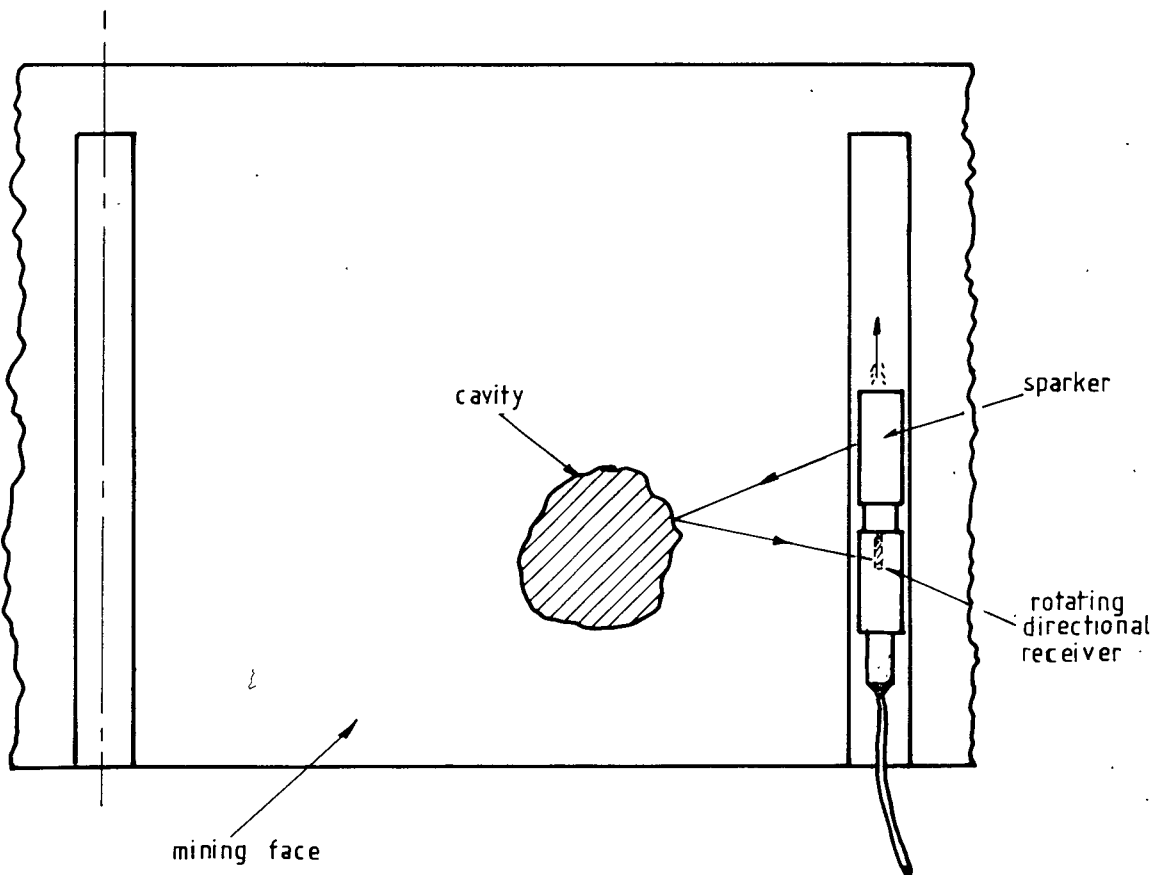
The seismic source continuously fires a seismic pulse at a specified rate while the directional receiver rotates slowly, and in this way receives reflected seismic energy pulses for different sectors. This could be programmed in such a way that, while the receiver rotates through 360° , the entire assembly moves forward gradually at a rate which provides a continuous scan of the area using a spiral mode. Knowing the direction in which the transducer faces, the time taken for the seismic pulse to be reflected back, and the position of the entire assembly relative to the mining face, the position of the cavity can be located and its size estimated.

There are three areas of uncertainty requiring investigation in order for the ACDER system to work. These are the seismic source and the radiation pattern in the borehole, the directional receiver and the display (data processing) system. Fig 6:0:2 shows the geometrical layout of the source, receiver and cavity to enable visualisation of the associated difficulties.

The maximum distance at which a cavity should be detectable is assumed



FRONT ELEVATION



PLAN VIEW

FIG. 6:0:1 SCHEMATIC DIAGRAM OF ACDER SYSTEM

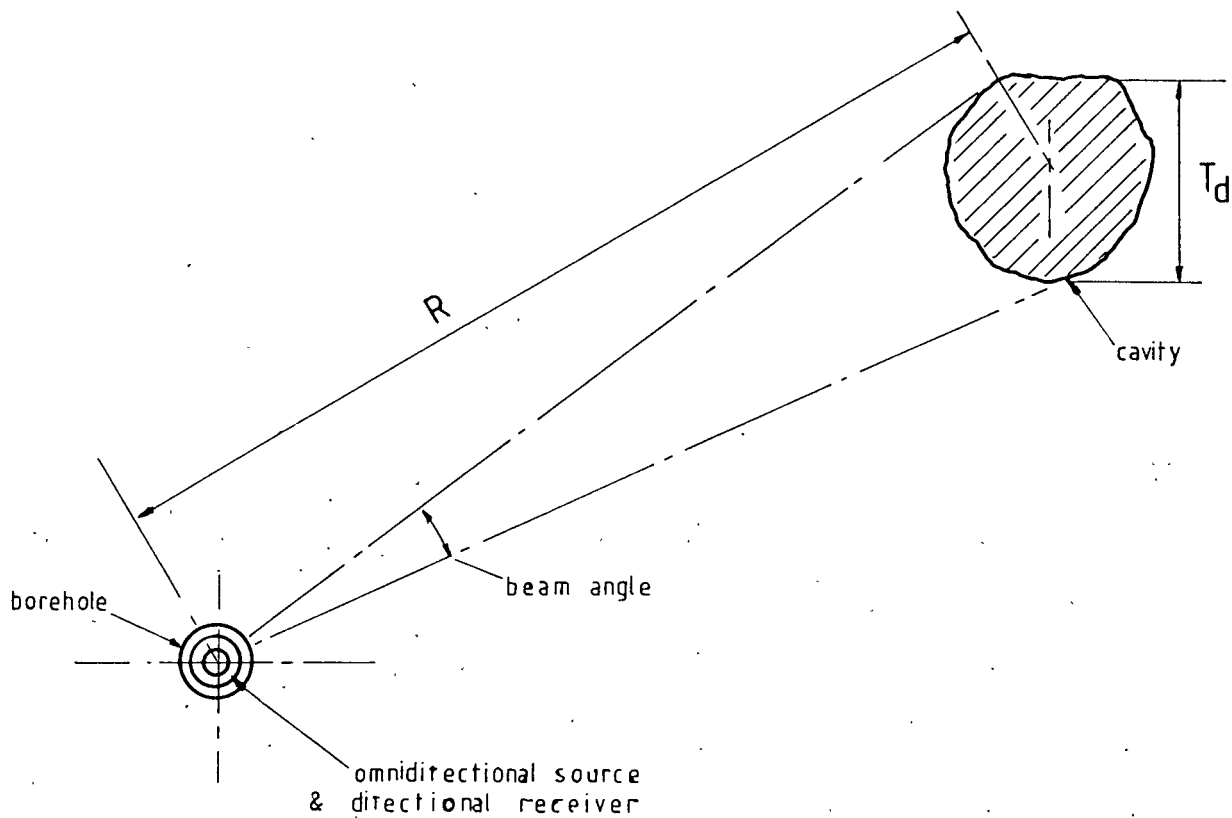


FIG. 6:0:2 GEOMETRICAL LAYOUT OF SOURCE,
RECEIVER AND TARGET

to be 30 m radius, which gives a total coverage of 60 m, ie 30 m on either side of the borehole. The smallest diameter cavity to be located is assumed to be 1 m.

The following assumptions are made:

$$\begin{aligned}
 R &= \text{maximum penetration distance} &= & 30 \text{ m} \\
 T_d &= \text{target diameter (cavity)} &= & 1 \text{ m} \\
 V_p &= \text{compressional wave velocity} &= & 2.5 \text{ km/s} \\
 f &= \text{predominant frequency of source} &= & 1000 \text{ Hz} \\
 \lambda &= \text{seismic wavelength in formation } (V_p/f) &= & 2.5 \text{ m}
 \end{aligned}$$

In order to separate a reflected pulse from a direct pulse the seismic pulse must be of sufficiently short duration, as a short seismic pulse facilitates identification of reflected pulses from several targets. Research was carried out to understand the generation of the sparker source output and to eliminate the long modulation associated with a normal metal borehole sparker.

The maximum time taken by the seismic pulse to travel to the cavity and reflect back to the directional receiver is:

$$T_r = 2R/V_p = 60/2500 = 0.024 \text{ s} \quad - (6.1)$$

To obtain a true geometrical image on the display, the beam angle of the receiver must be smaller than the angle subtended by the cavity at the maximum penetration distance. In order to calculate the beam angle, it is assumed that a 1 m arc of a circle with 30 m radius is almost a straight line.

Therefore, the beam angle required to detect a 1 m cavity at 30 m distance is given by:

$$1/2 R \times 360 = 2^\circ \quad - (6.2)$$

This shows that a beam angle of the transducer has to be 2° or less in order to obtain a reasonable geometrical image of the cavity at the 30 m range. To obtain a 2° beam angle, the diameter of the receiver would have to be considerably larger for the wavelength available (2.5 m),

because as the cavity diameter becomes smaller than the wavelength, reflection ceases and backscatter appears. It has been suggested (Wood, 1964; Ref 17) that an object size must be at least several times the wavelength in order to obtain a reasonable reflection. Details of the receiver and possible directivity of the directional transducer are discussed in section 6:1:2.

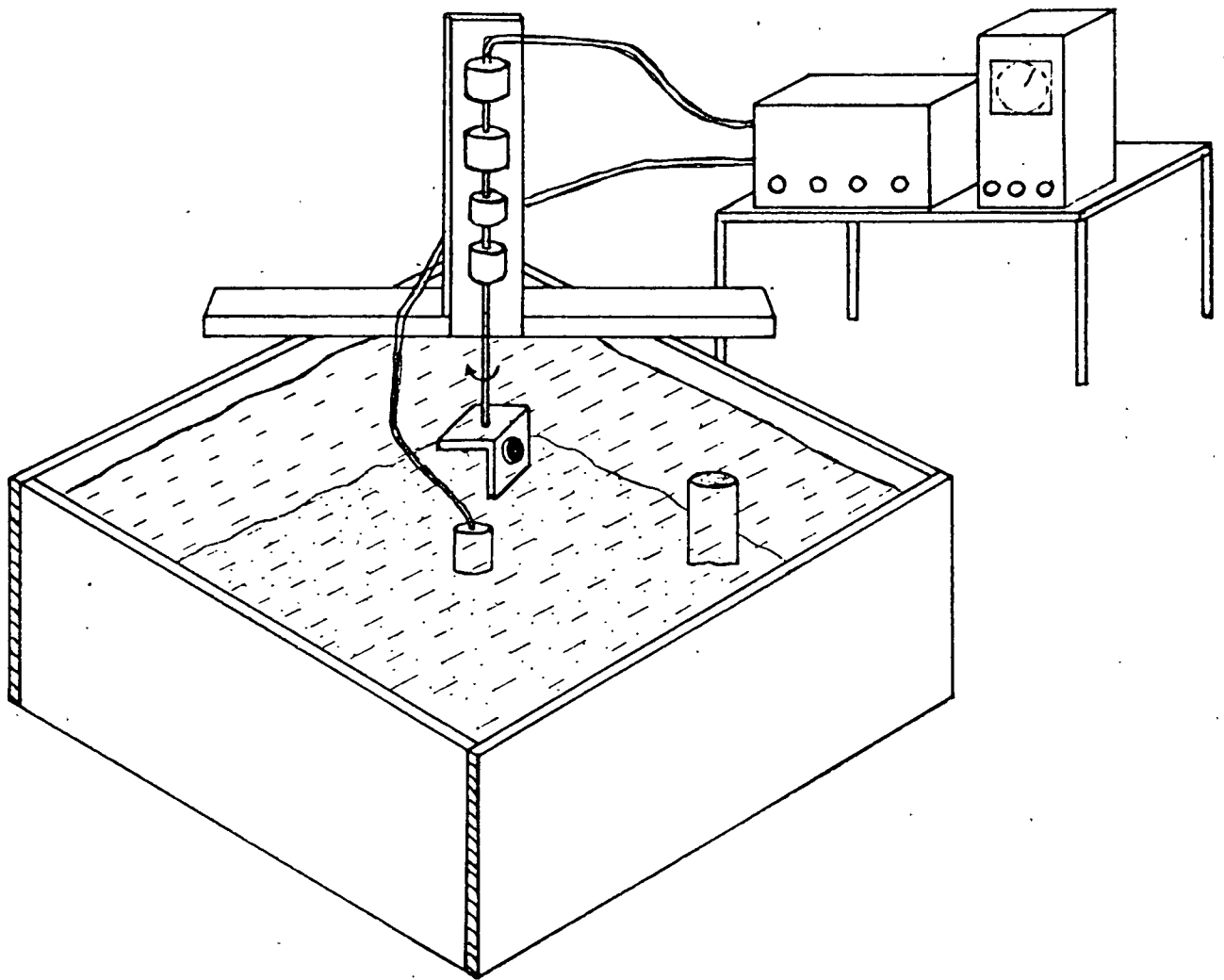
The data processing and the display system has been designed to make interpretation of the result considerably simpler, and therefore fulfil the requirement for immediate action if any danger near the working face is identified.

6:1 Laboratory model study

A laboratory model study was carried out using a mini-sparker as a source, a directional piezoelectric sensor as a receiver, a wooden tank and associated electronic instrumentation. The laboratory model set-up is shown in the schematic diagram Fig 6:1:1.

The model tank was made of wood and was 1.5 m long, 1.5 m wide and 0.6 m deep. It was filled with sand to a depth of about 0.2 m and water to a depth of about 0.5 m. Wood was selected as the material for the tank based on earlier investigations (Baria, 1974; Ref 3) using a mini-sparker and directional receiver. By observing the reflection, these experiments had shown that wood has very good acoustic damping properties compared to other materials such as, for instance, expanded polystyrene. This latter material contains over 90% of air and has very low density, which makes it an ideal reflecting surface (the coefficient of reflection at the water/air interface is practically 1), but a poor damping substance: it does not absorb and dissipate energy from the seismic pulse. Thus, a wooden panel made out of blockboard replaced the polystyrene sheet.

The reflected pulse amplitude was reduced by a factor of 5 or more. The exact value of the amplitude of the reflected seismic pulse was difficult to measure, as the reflected pulse could not be separated from the general backscatter created within the tank. Fig 6:1:2 shows a comparison of the reflections from panels of expanded polystyrene and blockboard.

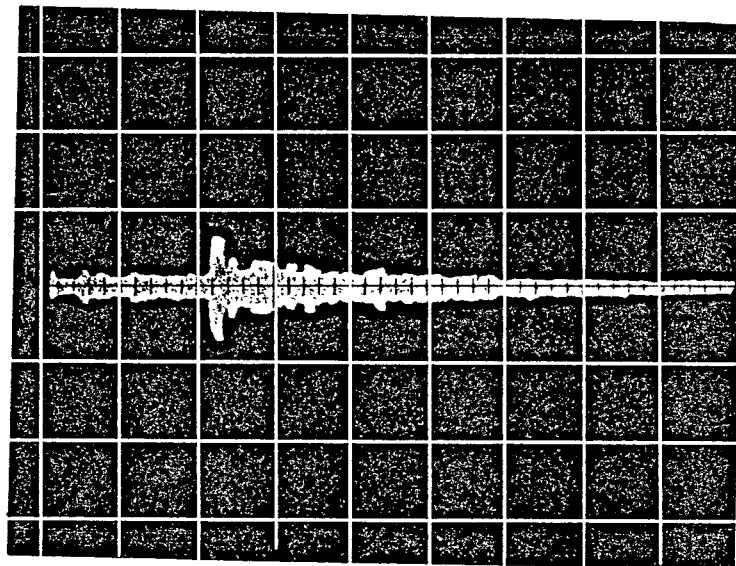


KEY

water — — —

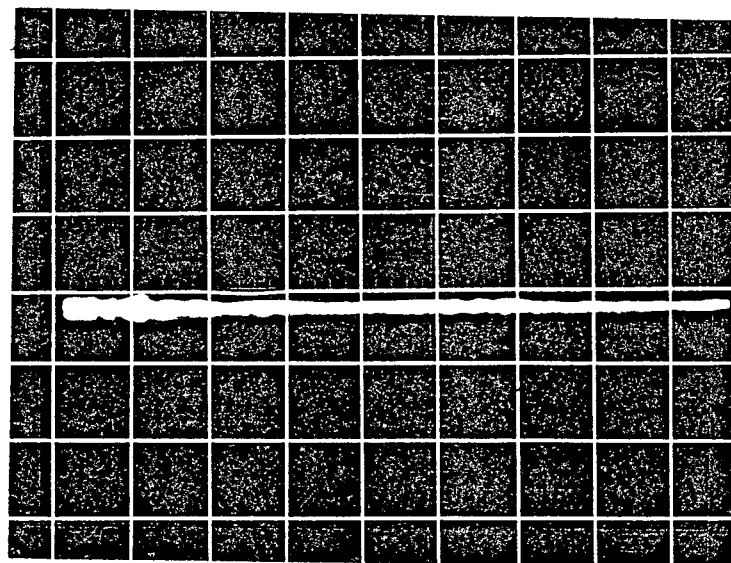
sand

FIG. 6:1:1 SCHEMATIC DIAGRAM OF THE LABORATORY SET-UP



vert. sc. = $\cdot 01V/cm$
 horz. sc = $2ms/cm$

(a) reflection from an expanded polystyrene sheet



vert. sc. = $\cdot 002V/cm$
 horz. sc = $1ms/cm$

(b) reflection from a blockboard sheet (wet)

FIG. 6:1:2 MODEL TANK DAMPING

The seismic source (the sparker) was placed on sand just below the seismic scanning platform. The platform, which is anchored to the sides of the tank, houses a directional seismic receiving transducer, a slip ring assembly, a sine-cosine potentiometer, an epicyclic gearbox and a stepper motor, all mechanically coupled as shown. Various diameters of PVC pipe were inserted into the sand as targets. All instrumentation used for the display unit, stepper motor, and acoustic source etc were placed on a nearby instrument trolley as shown.

The laboratory model could be divided into three basic groups: the seismic source, signal display unit and signal receiver and control system. The seismic source is a small sparker which transmits an seismic pulse omnidirectionally, while the receiver is a uniaxially polarised piezoelectric crystal.

The seismic source, ramp generator and stepper motor control unit are all synchronised by the clock pulse. The clock pulse causes the sparker to fire an seismic pulse and the stepper motor control unit advances the armature in the stepper motor through one step to a new position, which in turn rotates the directional receiver by a predetermined angle. The ramp generated by the clock pulse was fed into the sine-cosine potentiometer, which triggered a spot on the display unit. The spot appears to travel from the centre of the screen outwards, its brilliance (ie Z modulation) dependent on the strength of the signal received by the directional receiver. This describes the functioning of the entire model, but each of the three basic groups of instruments are described in detail below under the appropriate subtitles.

6:1:1 Seismic source

The seismic source used for the laboratory was a modified version of the electrical sparker source used by Donato (1961; Ref 128). The seismic pulse is generated by discharging a high voltage capacitor across a gap in a cylinder containing a saturated solution of sodium chloride.

Kramer et al (1968; Ref 129) describes the mechanism of the electrical discharge energy source (sparker), whereby a capacitor charged at 3000-5000V was discharged suddenly between the electrode rod and the ground frame. A heavy surge of current then begins to flow. Since the

electrode rod is insulated, and only a small end surface area is exposed to the salt water conductor, the current flow and potential field will appear as that shown in Fig 6:1:4. It is apparent that potential gradients and current densities become very high at the end surface of the electrode rod. Since the end surface is quite rough and pitted, current flow will be even more strongly concentrated at sharp points and spines on the copper surface. Since heat generation is concentrated where the electric current density is heaviest, there is in essence a flash boiler at the electrode surface. An extremely hot and incandescent plasma of steam-ionised gases, vapourised copper 'gas' and free electrons is thereby formed.

Fig 6:1:3 is a high-speed photograph of an expanding plasma bubble, taken by Prof Edgerton. Close examination reveals what appears to be a number of small metal projectiles which have been explosively ejected from the central region at velocities sufficiently high to penetrate the bubble wall.

A small sparker was used initially in the laboratory in conjunction with a thyatron discharge unit similar to that used by Donato (1961; Ref 128), when a capacitor was charged to 3-4KV and then discharged across a gap in the sparker containing sodium chloride solution. The EGU's thyatron unit discharged at the very limited rate of once about every five to six seconds. This was found to be extremely slow for the purposes of data display on the c.r.o. storage screen. Therefore, a new thyristor controlled discharge unit was designed, with a discharge rate of up to ten firings per second.

a Thyristor controlled discharge unit

The maximum operating voltage of the thyristor controlled discharge unit is 3KV, as compared with the fast-switching thyristors available at the present state of technology, which work at a maximum peak voltage of 1.5KV. This necessitates three thyristors to be connected in series to form a high voltage switch. It is essential to ensure that none of the thyristors is subjected to excessive voltage, under either static or dynamic conditions (Naik et al, 1972 (Ref 130) and Eveleigh, 1973 (Ref 131)).

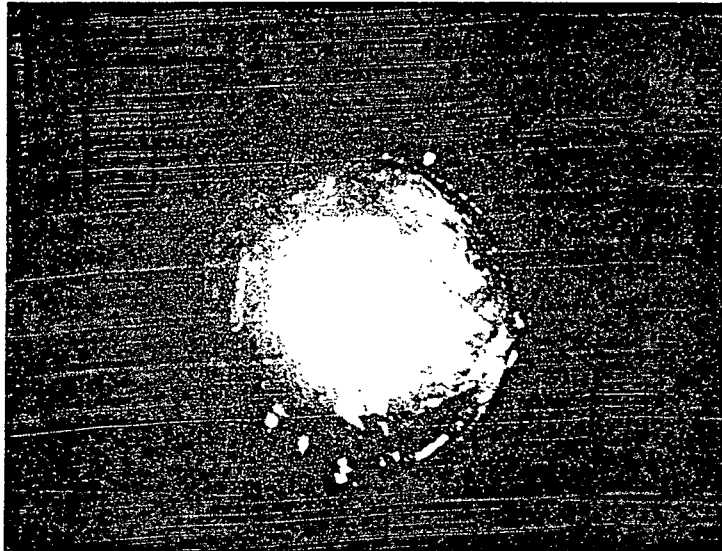


FIG. 6:1:3 HIGH SPEED PHOTOGRAPH OF A PLASMA BUBBLE
FROM AN UNDERWATER SPARKER (taken by
Professor H.E. Edgerton)

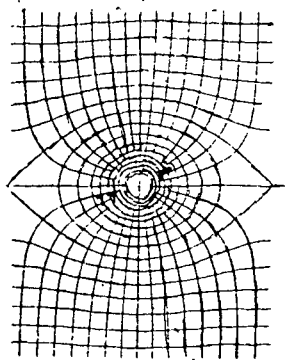


FIG. 6:1:4 CURRENT FLOW AND POTENTIAL
FIELD FOR A POINT ELECTRODE

The distribution of the static part of the switch, commutating voltage among the thyristors within the switch, is governed by the leakage resistance of the thyristors. However, this resistance differs from unit to unit as a result of the normal spread in their characteristics. Therefore, external measures must be taken to force an equal voltage distribution among the thyristors.

An usual way of achieving this is to provide a voltage dividing resistor network running in parallel with each of the thyristors. For reasons of standardisation, a common value of voltage-equalising resistors is chosen to run across each thyristor. The value is then calculated from knowledge of the variation in leakage resistance of the thyristors, and the maximum permissible voltage across a single thyristor.

Any transient voltage condition the thyristors may experience is adjusted by the discharge capacitor and the varistor transient suppressors (metal oxide) strapped to each thyristor.

The thyristors are switched off as soon as the anode current falls below their minimum holding current.

Design and detail of the thyristor-controlled unit is given in Appendix III. Briefly, these include a master pulse generator, high voltage DC power supply, pulse transformer and other associated electronics required for a complete unit.

The high voltage capacitive discharge pulse for the mini-sparker source is provided on the front panel through a UHF female connector. The trigger pulse to the oscilloscope is provided through a BNC connector. Fig 6:1:5 shows the thyristor controlled discharge unit.

b Laboratory experiments

For laboratory experimentation a source (mini-sparker) and a receiver (hydrophone) should be separated by the minimum acceptable distance in order to minimise interference from the reflectors. The criteria for the minimum distance or proximity are a function of the size and the configuration of both transducers and of the type and desired accuracy of the measurements.

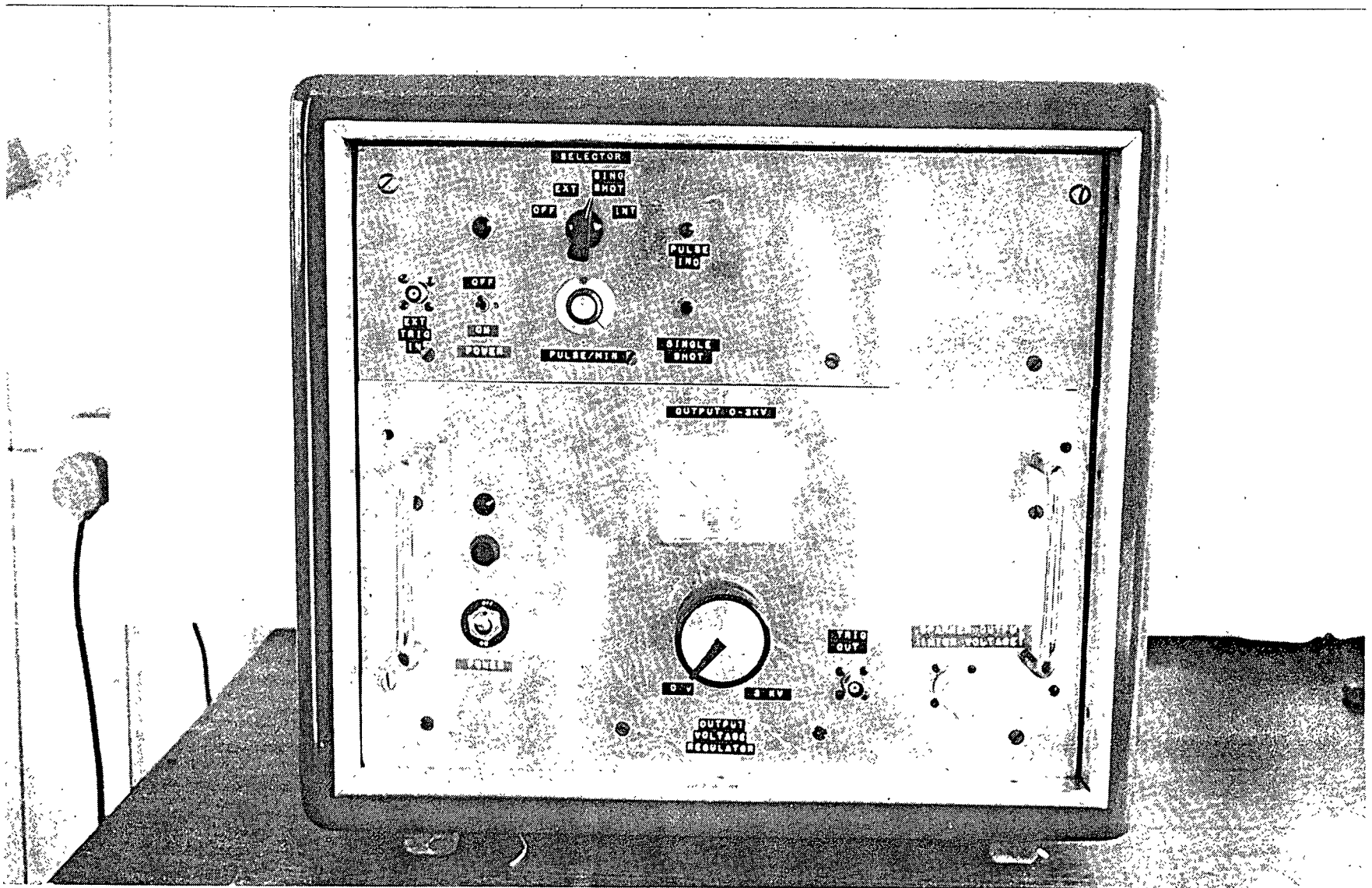


FIG. 6:1:5 THYRISTOR CONTROLLED DISCHARGE UNIT

The proximity criterion of the source alone comes from the requirement implied in the definition of the transmitting current or voltage response: that the pressure be that in a spherically diverging wave (Bobber, 1970; Ref 132). The reference distance is 1 m from the projector. If the wave is not spherically divergent at 1 m, however, the pressure must be measured at some distance and extrapolated back to 1 m by making the assumption that pressure is inversely proportional to distance.

The proximity requirement for a hydrophone comes from the definition of the free field voltage sensitivity, in which the input free field pressure is specified as that in a plane progressive wave. Plane waves can only be approximated in a free field, so that the practical requirement is that the hydrophone intercept a segment of a spherical wave that is indistinguishable from a plane wave. That is, the segment must be very small, or the radius or curvature of the wave very large.

The minimum distance between the source and the receiver can be determined experimentally. With a constant current input into the source, the output voltage of the receiver can be measured at two or more distances. If the voltage is inversely proportional to the distance, the proximity criterion is satisfied. However, if the desired proportionality is not found, the error may be due to causes other than proximity, and the reason is not answered. For such reasons, as well as for measurement design and planning, proximity criteria and an understanding of proximity effects are useful.

Proximity criteria have been discussed by H Stenzil (1939; Ref 133) and Bubmore and Hansen (1959; Ref 134) for transducers of common shapes. These criteria apply to single transmitting transducers, in that they define the distance at which the Fresnel zone or near field ends and the spherically divergent far field begins. When applied to source-receiver combinations, these criteria are valid only if the receiver is essentially a point sensor. If neither the source nor the receiver is a point, a proximity criterion for the combinations must be established. The criterion is not merely the sum of the individual criteria for the two transducers.

The proximity criteria for single transducers usually are visualised in

terms of where the spherically divergent far field of a projector begins, the criteria applying also to the transducer as a hydrophone. According to the theory of reciprocity, it is apparent that the proximity criteria for the combination of a large piston and a small point transducer, for example, must be the same, regardless of which is the source and which is the receiver.

The combination of a large circular piston and a small point receiver is a common and particularly suitable example to illustrate the theory and rationale of proximity criteria.

If the large piston is the source, the sound pressure on the piston axis, as would be measured by a point receiver, is shown in Fig 6:1:6. The dashed curve shows the inward extrapolation of the far field pressure as it meets the solid line curve very gradually, indicating that there is no exact boundary between the near field and far field. It is not surprising, therefore, that the proximity criteria of different authors do not always agree.

The minimum distance criterion for the response measurements of a piston and a line source is given by Bobber (1970; Ref 132) as

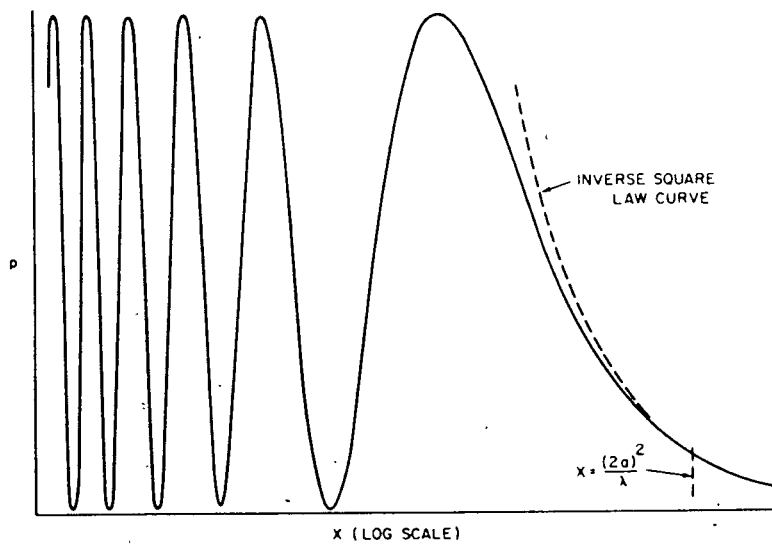
$$\text{For a piston, } x \geq (\text{maximum dimension})^2/\lambda = L^2/\lambda \quad - (6.3)$$

$$\text{For a line source, } x \geq \text{maximum dimension}/\lambda = L/\lambda \quad - (6.4)$$

where x is the distance between the source and the receiver.

With the limit on the size of the tank, in particular the depth of the tank, an optimum source receiver distance was calculated to fulfil the proximity criteria and yet give a reasonable separation of the direct pulse through the water, from the reflected pulse from the water surface and the sides of the tank.

Assuming that the criteria for the piston type source can be applied for the sparker



Relative pressure p at distance x on the axis of a circular piston projector of radius a for sound of wavelength λ . Also, the average free-field pressure over the area of a circular piston hydrophone of radius a , from a point projector at distance x on the hydrophone axis. (after Bobber, 1970)

FIG. 6:1:6

$$\begin{aligned}
 \text{ie } x &= L^2/\lambda = (L^2 \cdot f)/c \\
 &= (0.05^2 \times 70\,000)/1500 \\
 &11 \text{ cm}
 \end{aligned}$$

where L = length of the sparker (5 cm)
 f = frequency output of 2.3 cm OD x 5 cm/lg rigid PVC sparker
 c = velocity of sound through water

During most of the experiments an attempt was made to fulfil the above criteria and therefore take the measurements in the spherically divergent area, but in some cases these might have been breached due to the small size of the model tank. Some of the measurements were made on a relative basis to compare two different variables with a fixed source receiver geometry. This may not necessitate the stringent requirement of the minimum distance criterion.

Fig 6:1:7 shows a small sparker which was used for generating seismic pulses. It consists of a cylinder, with two electrodes exposed within it, containing sodium chloride solution. The material and shape of the cylinder can be used for shaping the output seismic signature (Baria, 1974; Ref 3).

Laboratory experiments were carried out to understand some of the characteristics of the mini-sparker. The mini-sparker was used in conjunction with a thyristor discharge unit to generate a seismic pulse. A small hydrophone (12.7 mm diameter) was used as a seismic pulse detector. These experiments were carried out in the model tank described earlier.

Fig 6:1:8 is a block diagram of instrumentation used for carrying out some of the experiments in the model tank. The master pulse generator fires a pulse which switches on a 0.5 μ F capacitor charged to 1.5KV across the gap in the mini-sparker containing sodium chloride solution. A trigger pulse for the storage oscilloscope is provided by the thyristor discharge unit. This is achieved by dividing the high voltage output with a series of resistor chains which give a precise trigger pulse value, since it is obtained from the high voltage energy being discharged in the mini-sparker.

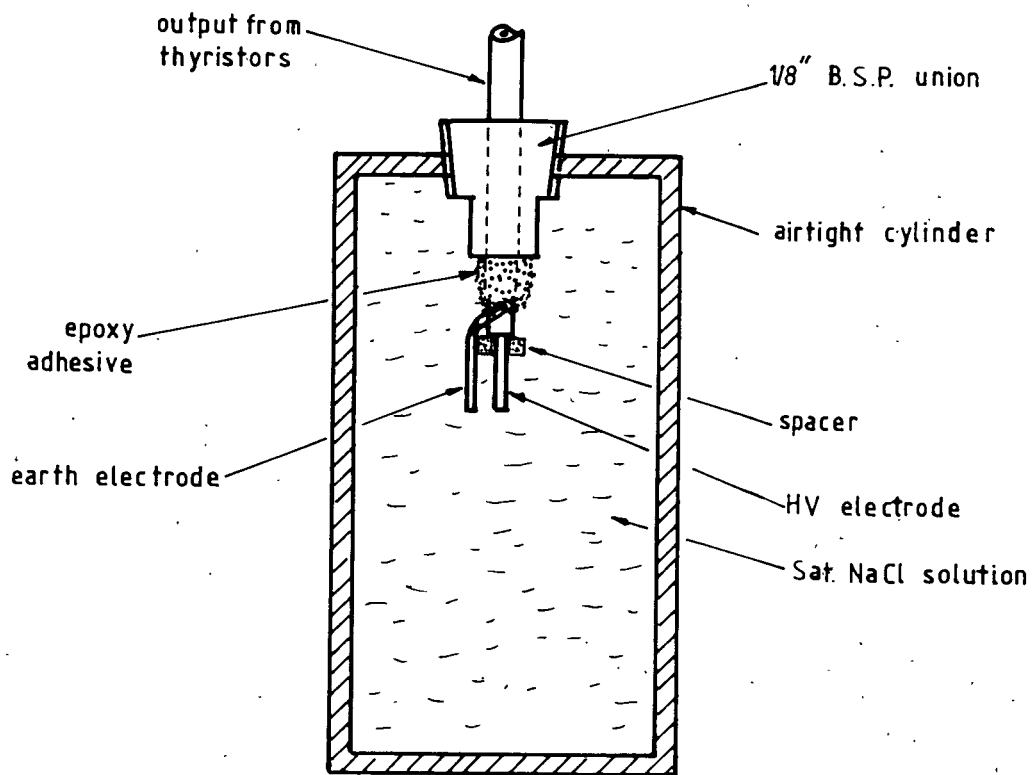


FIG. 6:1:7 MINI-SPARKER

The seismic receiver is a 12.7 mm (0.5 in) ball hydrophone with a bandwidth of 0-170 kHz and a sensitivity of 6.3V/ bar. The output from the hydrophone is fed into the Kemo filter type VB4, which is also used as an amplifier. The output from the Kemo filter is in turn fed to a Nicolet storage oscilloscope.

The Nicolet type oscilloscope is a complex digital storage oscilloscope. It stores a wave form in the digital mode, has a pair of cursors to measure time and amplitude (absolute or relative), can expand traces in an X and Y direction and store the wave form in a digital format on a 13 cm magnetic disk.

The stored wave forms were plotted later using an HP45 micro-computer and associated digital plotter.

Experiment 1: Relationship between the electrical energy input and pressure input of a mini-sparker

The experiment was carried out to establish a relationship between the electrical energy input into the source and the pressure output of the mini-sparker. Fig 6:1:9 shows the geometrical layout of the source and the receiver. The distance between the source and receiver was approximately 15 cm. The source and receiver were positioned about 20 cm deep into the water, with the centre of the source aligning horizontally with the centre of the receiver.

The source and receiver were attached firmly to thin steel rods, which in turn were clamped to a wooden frame member of the model tank. Mounting the two transducers rigidly in this way eliminates any variation in the pressure pulse arrival time due to accidental changes in path length or vibration of the source.

The mini-sparker used for the experiment was constructed from rigid PVC domestic water drainage pipe of 23 mm OD, 19 mm ID and 5 cm length. Electrical input energy to the source (mini-sparker) was varied by charging the 0.5 μ F internal capacitor of the thyristor discharge unit from 0.5kV to 2.25kV. The first negative joint peak value and the peak to peak value of the received pressure pulse were measured. Each wave form was stored on a magnetic disk.

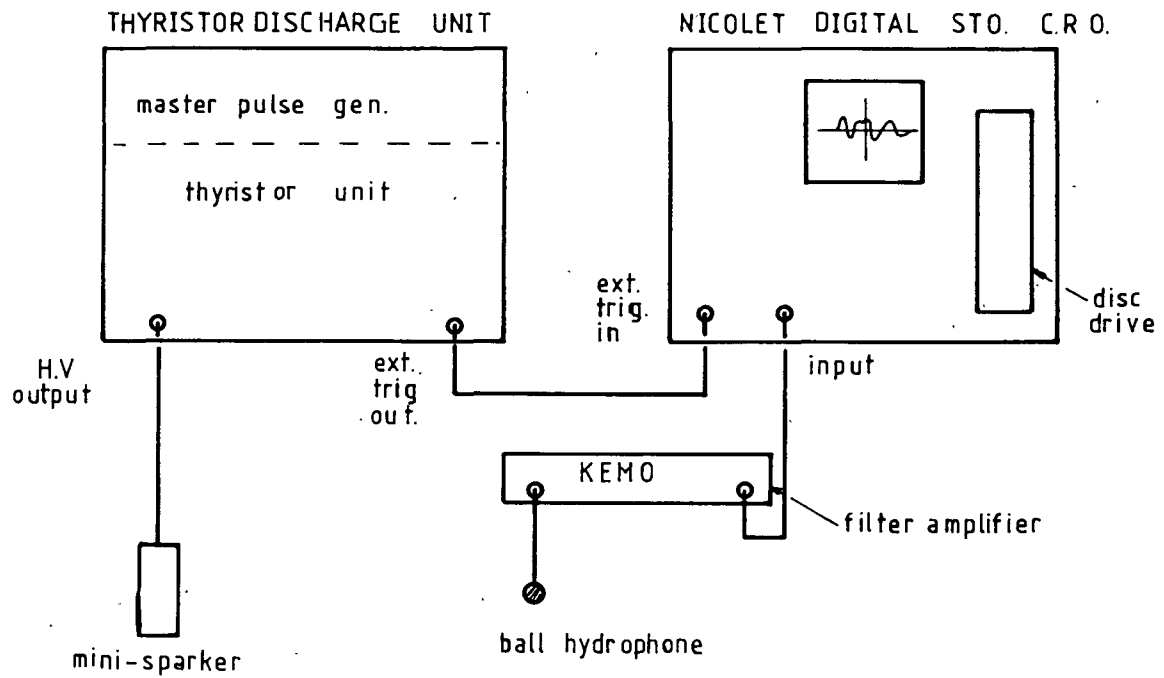


FIG. 6:1:8 BLOCK DIAG. OF THE SYSTEM USED TO MEASURE THE OUTPUT OF THE MINI SPARKER

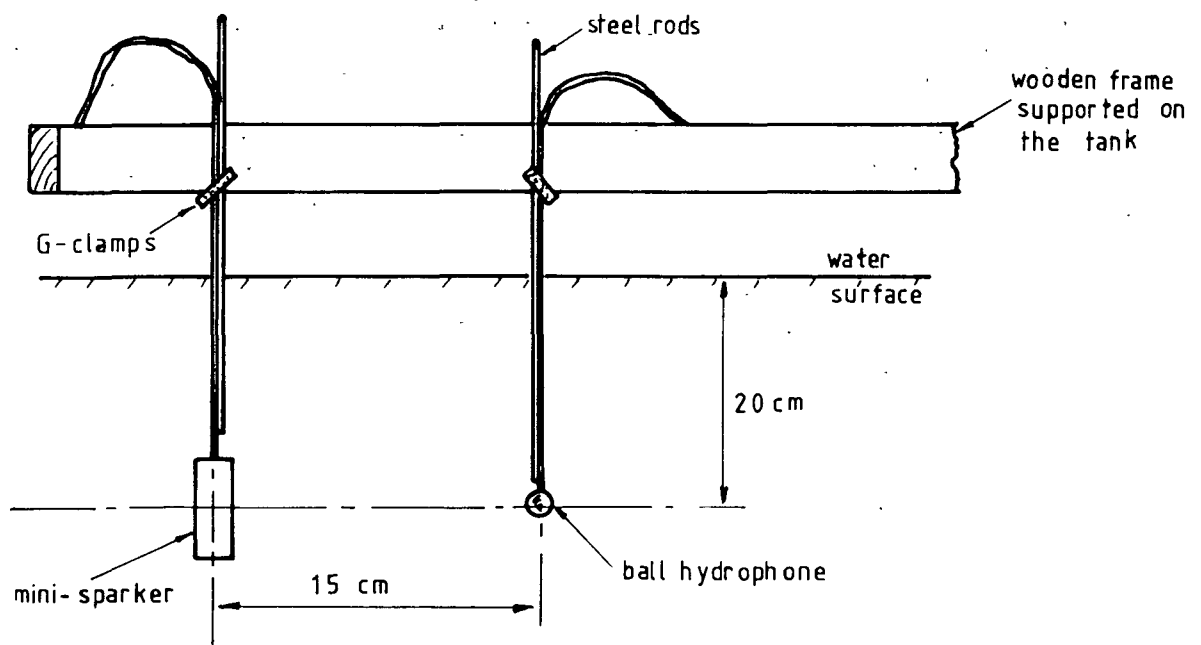


FIG. 6:1:9 GEOMETRICAL LAYOUT OF $X_r - X_t$ FOR EXP. 1

Table 6:1 shows the electrical input voltage, the input energy into the sparker, the first negative peak in mbar (which was converted into pressure values by multiplying the measured voltage output from the hydrophone by the sensitivity of the hydrophone), peak to peak value in mbars and magnetic disk on which the data is stored.

TABLE 6:1

Input voltage	Capacitance (μ F)	Input energy (Joules)	First negative peak (mbar)	Peak to peak (mbar)	Magnetic storage disk	Fig 4:1:11 trace
500	0.5	0.06	0.07	0.16	65/1	1
750	0.5	0.14	0.17	0.43	65/2	2
1000	0.5	0.25	0.31	0.78	65/3	3
1250	0.5	0.39	0.52	1.26	65/4	4
1500	0.5	0.56	0.73	1.81	65/5	5
1750	0.5	0.77	1.03	2.33	65/6	6
2000	0.5	1.00	1.36	3.04	65/7	7
2220	0.5	1.27	1.82	3.64	65/8	8

Fig 6:1:10 shows a graph of the electrical energy input into the mini-sparker against pressure output from the mini-sparker, measured at a fixed distance (15 cm). The graph shows that the first negative pressure peak was linearly dependent for the range of electrical energy input under investigation. The relationship can be expressed in the form:

$$P = 1.3923E - 0.05 \quad \dots (6.5)$$

where P = peak pressure in mbar
 E = input energy in Joules

The relationship between peak to peak pressure and electrical input is not linearly dependent, but follows a shallow curve.

Fig 6:1:11 shows the wave forms of the pressure pulses for eight electrical energy inputs, as indicated in Table 6:1. The frequency content of the source is constant for circumferential vibrations at 77 kHz, but at the high energy input there are apparent low-frequency longitudinal vibrations due to the length of the spark chamber.

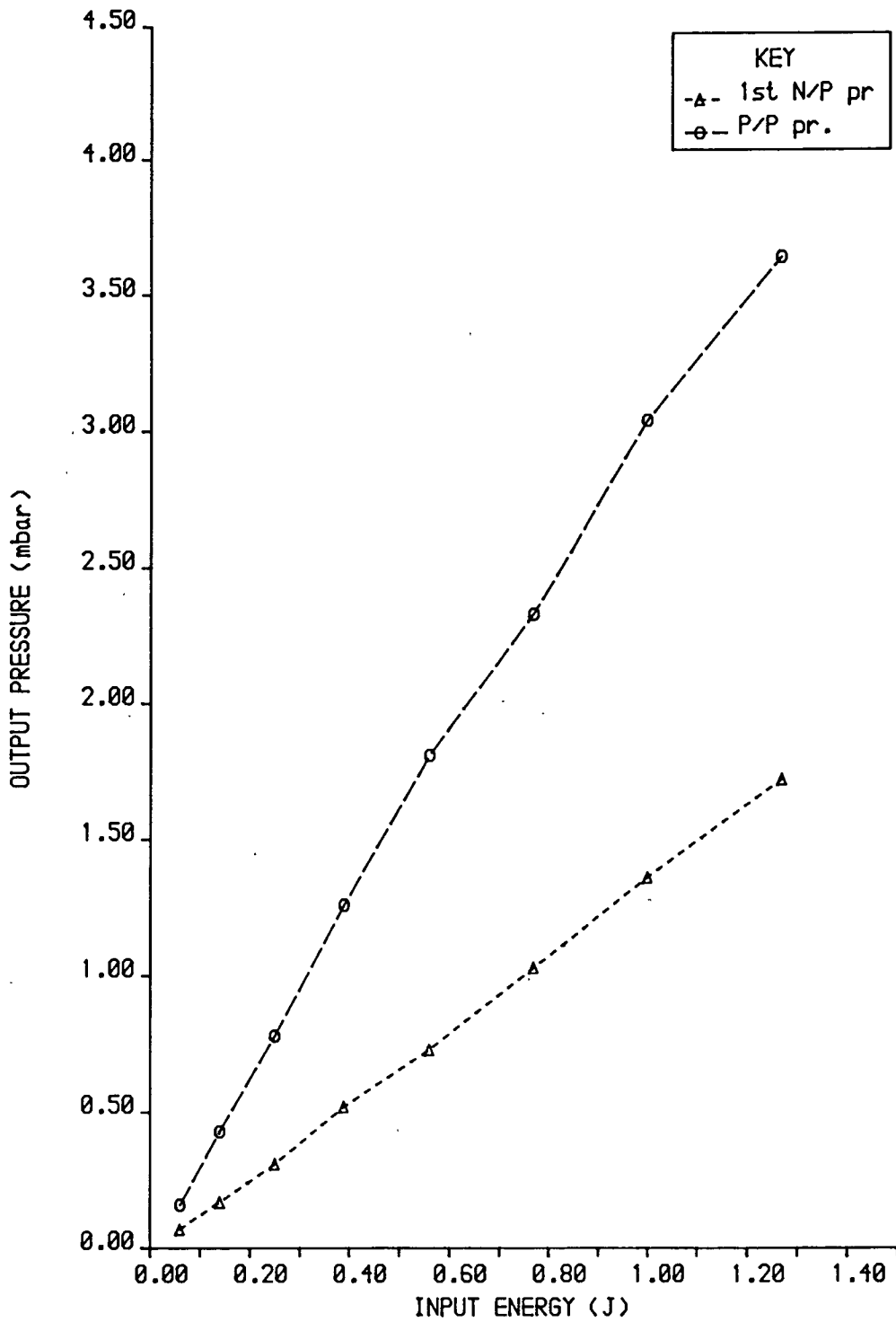
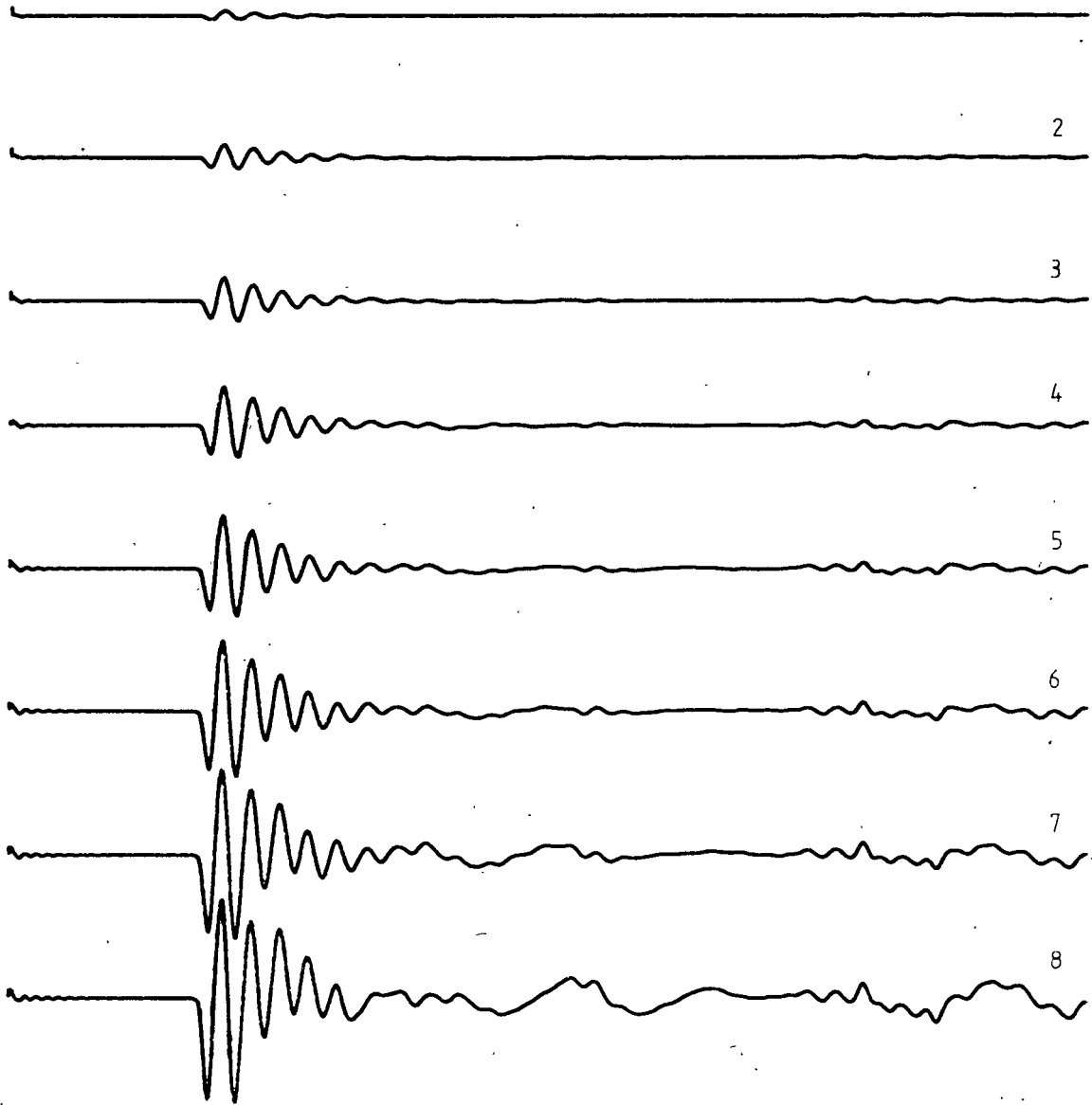


FIGURE 6:1:10 RELATIONSHIP BETWEEN ELECTRICAL ENERGY INPUT AND PRESSURE OUTPUT FROM A MINI-SPARKER

TRACE NO. 1



VERT. SCALE 1cm = 1.3 mbar

HORI. SCALE 1cm = 33.3 μ s

FIG. 6:1:11 PRESSURE SIGNATURES FOR ELECTRICAL
ENERGY INPUTS

Experiment 2: The effect of salinity on the output pulse

The original electrical discharge source (sparker) was developed for use in marine seismic surveying, and therefore the conductive solution to dissipate the electrical energy has always been sodium chloride (sea water). Subsequently, when the sparker was adapted as a seismic source for model study in the laboratory and on land for field use, the use of NaCl solution as a conductive solution was maintained. However, there is no reason why other solutions, such as zinc chloride or copper chloride, should not be used, providing the effect of these conductive solutions on the environment and the metal housing of the sparker is acceptable.

The experimental set-up to observe the effect of salinity on the output pressure pulse was similar to the one used in the previous experiment. The distance between the source and the receiver varies slightly, because the mini-sparker had to be removed from the frame to empty the saline solution and refill it with a solution of different salinity.

The electrical energy input into the mini-sparker was kept constant at 0.56 J (1500V, 0.5 μ F). The 23 mm OD rigid PVC sparker was used. The geometrical layout for this experiment was similar to the previous one.

Seven NaCl solutions were prepared, each solution doubling in salinity value. The temperature of the water was 11°C when all the solution samples were prepared. Salinity and temperature of the solution were measured using the Cambridge Instrument conductivity meter (PW9505).

Each solution was put into the mini-sparker and 15 shots were fired (0.56 J of energy being dissipated 15 times through the saline solution) in order to stabilise the pressure built up within the mini-sparker. This procedure produces a consistent pressure pulse signature for measurement. For each concentration of saline solution, a negative peak voltage and peak to peak voltage were measured. These voltage measurements were converted to pressure values in mbar. The first negative peak and peak to peak pressures are tabulated in Table 6:2.

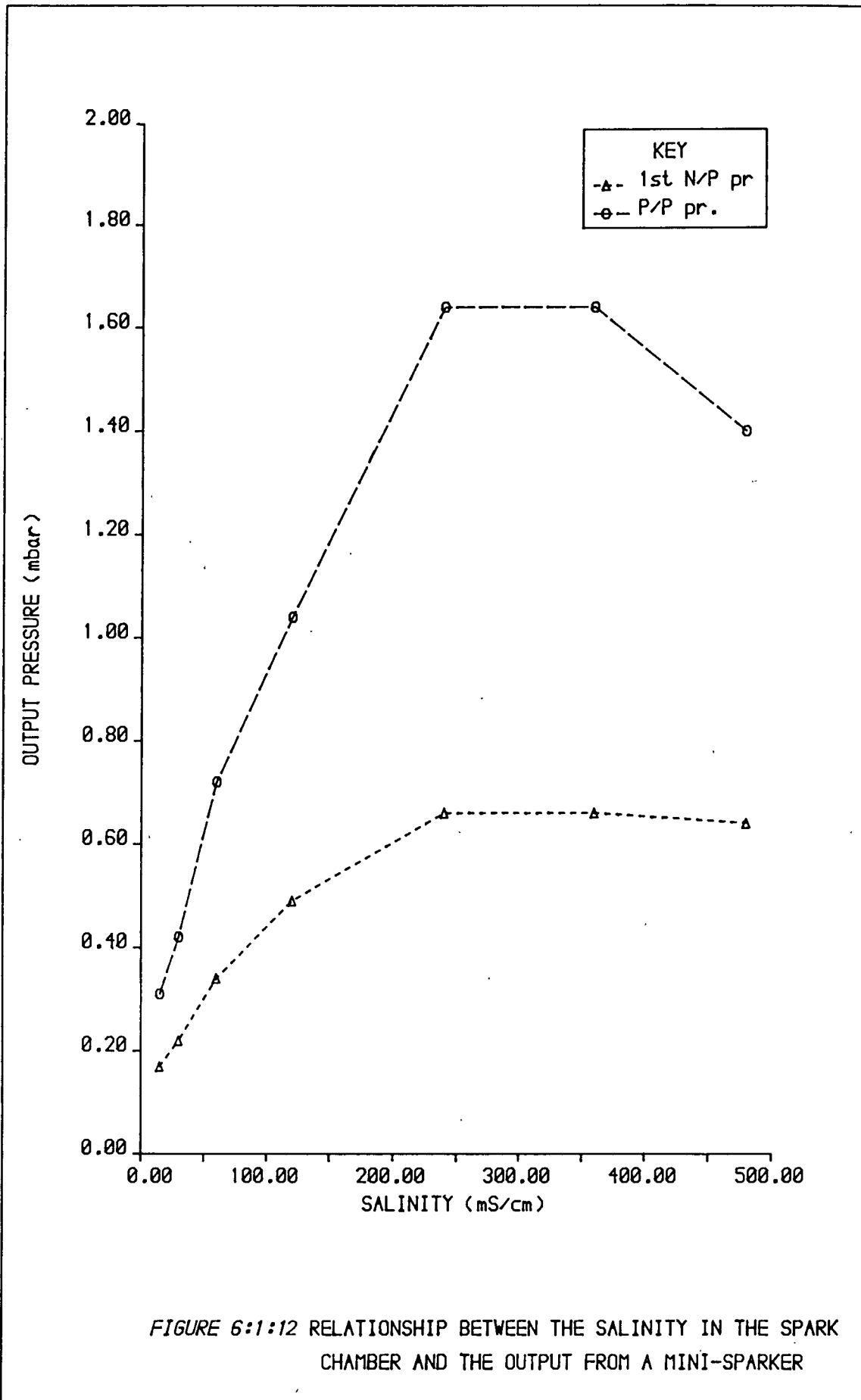
TABLE 6:2

Salinity (mS cm ⁻¹)	First negative peak (A) (mbar)	Peak to peak (B) (mbar)	Magnetic storage disk	Figure wave form number	Ratio B/A	Fig 4:1:14 trace
15	0.17	0.31	66/1	1	1.824	1
30	0.22	0.42	66/2	2	1.909	2
60	0.34	0.72	66/3	3	2.118	3
120	0.49	1.04	66/4	4	2.123	4
240	0.66	1.64	66/5	5	2.485	5
360	0.66	1.64	66/6	6	2.485	6
480	0.64	1.40	66/7	7	2.187	7

Fig 6:1:12 shows the first negative peak and peak to peak values of pressures plotted against the concentration of sodium chloride in water (salinity) as used in the mini-sparker for a constant energy input. It would appear that both first peak and peak to peak pressures initially increase considerably with increase in the concentration of NaCl solution, but begin to fall once the concentration rises above 300 mS/cm. Fig 6:1:13 is the plot of the ratio of peak to peak/first negative peak against the salinity concentration. The graph shows that the ratio increases with increase in the salinity concentration, but levels off at 300 mS/cm, and begins to fall for concentrations above this level. Fig 6:1:14 shows the pressure signatures for the various concentrations of NaCl solution, as indicated in Table 6:2.

Experiment 3: The effect of increase in diameter of a steel mini-sparker on output pressure pulse

The experimental layout and the instrument used is the same as for the previous experiment. Sodium chloride solution was prepared in a large beaker and four mini-sparkers were filled with the solution. The four steel mini-sparkers had the same length (11.2 cm) but varied in diameter. The outside diameters of the four mini-sparkers were 18 mm, 25 mm, 32 mm and 38 mm respectively. The wall thickness of the steel mini-sparkers was 1 mm.



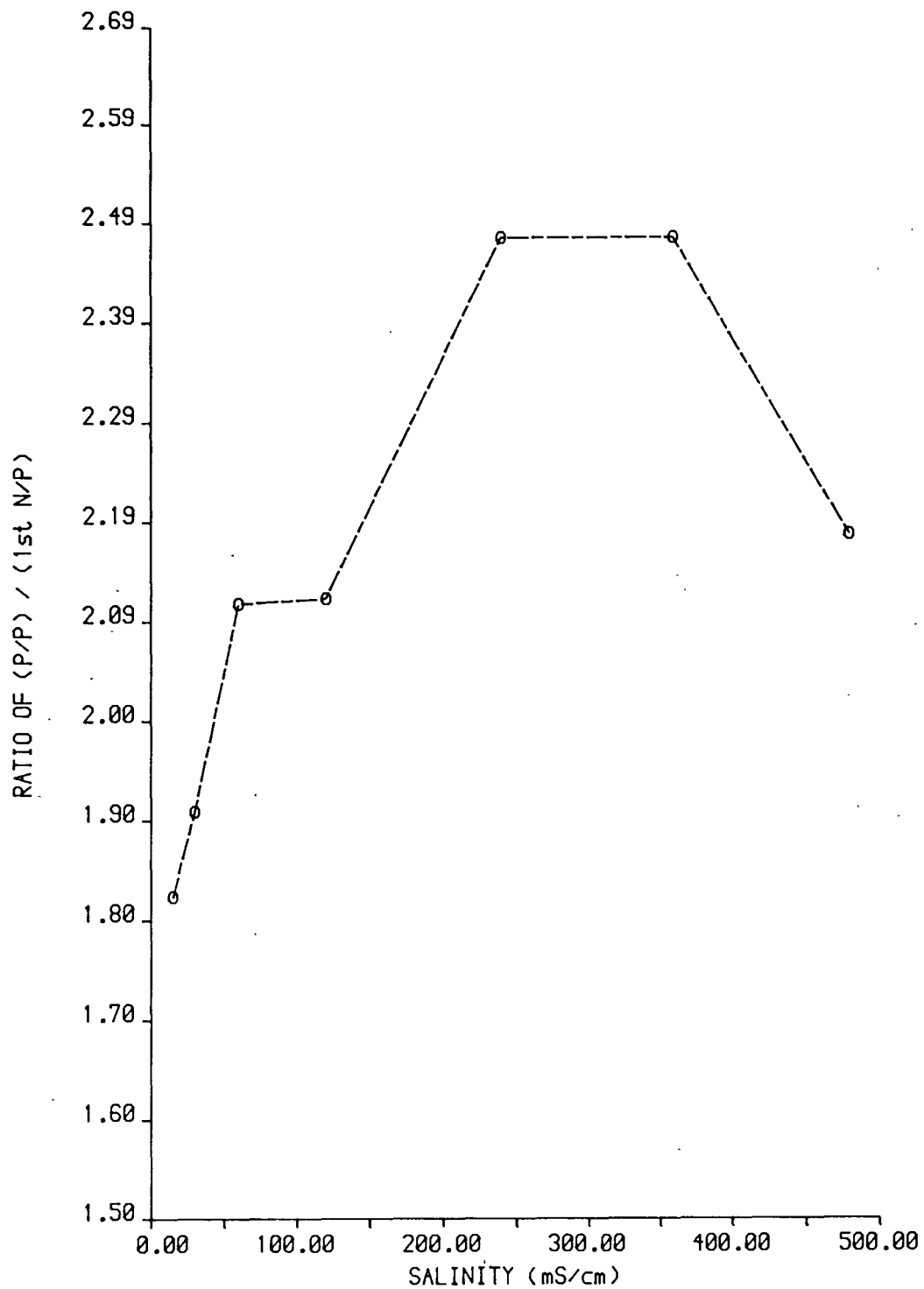
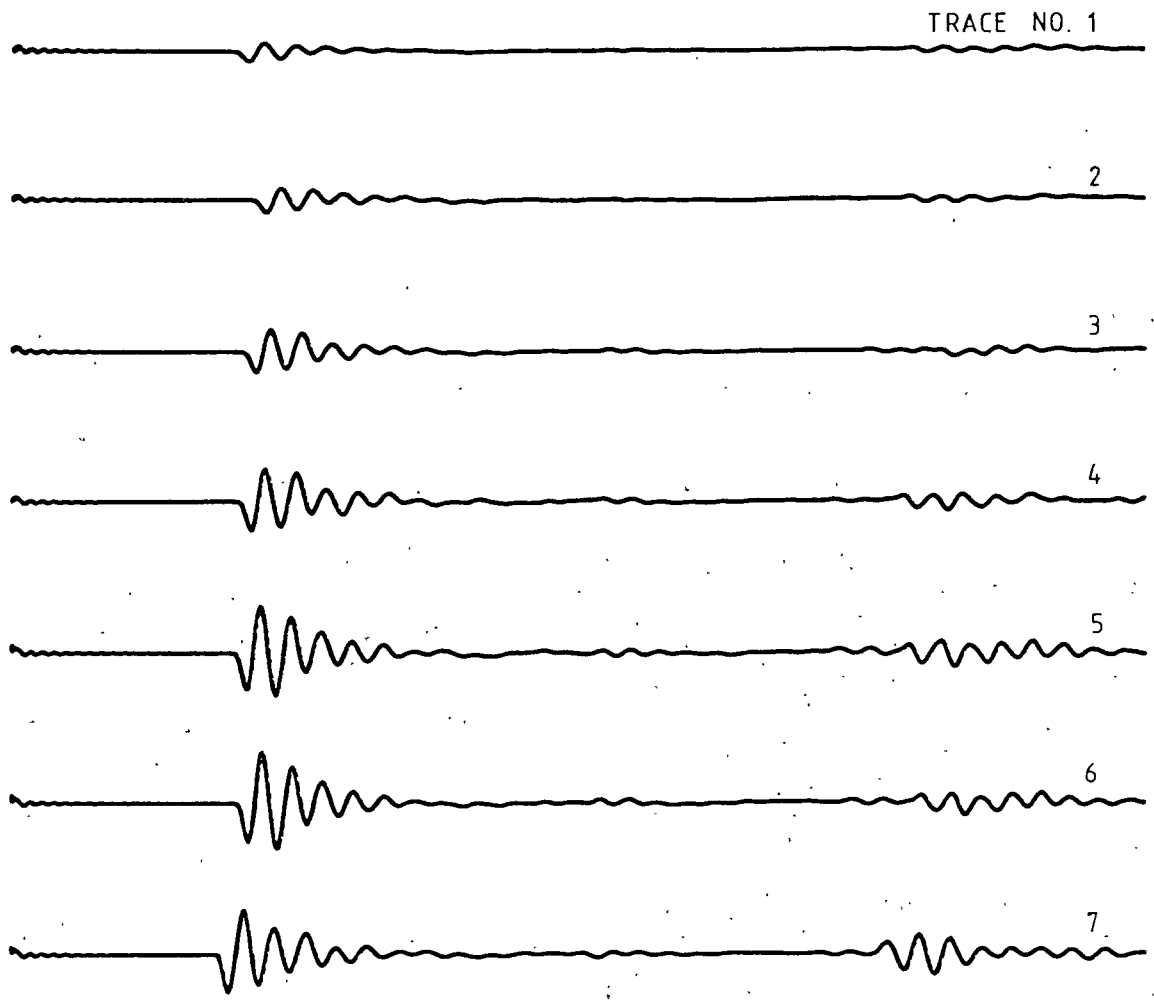


FIGURE 6:1:13 GRAPH OF (P/P) / (1st N/P) PRESSURE RATIO AGAINST SALINITY



VERT. SCALE 1 cm = 1.3 mbar
HORI SCALE 1 cm = 3.33 μ s

FIG. 6:1:14 PRESSURE SIGNATURES FOR VARIOUS SALINITY

Each steel mini-sparker was loaded into the test rig and the output pressure pulse was measured for the same electrical energy input, using a Nicolet storage oscilloscope. The energy input was 0.56 J (1500V, 0.5 μ F). Particular attention was paid to eliminating any variations of the output pressure pulse due to the increase in source-receiver distance, by keeping the time taken for the direct water wave as the same.

The results obtained are given in Table 6:3. Fig 6:1:15 shows a graph of the first negative peak and peak to peak pressure magnitude plotted against the diameter of the steel sparker.

TABLE 6:3

Sparker diameter size (mm)	First negative peak (mbar)	Peak to peak (mbar)	Magnetic storage disk	Fig 4:1:16 trace
18	0.194	0.350	72/1	1
25	0.200	0.406	72/2	2
32	0.260	0.386	72/3	3
38	0.510	0.640	72/4	4

The first negative peak pressure varies from 0.194 mbar for the smallest steel mini-sparker to 0.51 mbar for the largest. The first negative peak pressure increases as the diameter of the mini-sparker increases, and the increase is non-linear.

The peak to peak pressure curve follows the same trend as the first peak pressure curve (the pressure increases as the diameter increases), except for the 32.0 mm diameter mini-sparker. The output from this particular sparker appears to show a slight reduction in the magnitude of the peak to peak pressure. This can be attributed to several factors. They are: a) incorrect electrical energy input, b) incorrect measurement of the pressure magnitude, and c) interaction between the size of the mini-sparker and the pressure distribution within the chamber. The first suggestion can be rejected, as the magnitude of the first negative peak

is considerably greater than that of the next smaller size, ie 32 mm OD. The smoothness of the curve for the first negative peak pressure curve strongly emphasises this. The second hypothesis can be eliminated because the waveform is stored on a magnetic disk and the magnitude of the pressure was checked and found to be correct. Therefore, the only possible cause left is the third suggestion, which is the interaction of the pressure wave and the steel chamber.

Fig 6:1:16 shows the four wave forms from the four steel mini-sparkers. The shape of the first pulse of the first two wave forms is similar and the shape of the next two are similar, but when the first pulse in the second wave form is compared to the first pulse in the third wave form, the reduction in the magnitude of the second positive peak in the third and fourth wave forms, compared to the first and second wave forms, becomes apparent. This change in shape of the pulses therefore must be due to the interaction between the size of the chamber of the mini-sparker and the wavelength of the pressure pulse within the chamber. This may be similar to the interaction between the faces of a piezoelectric ultrasonic transducer, and the coupling problem on output waves discussed by Redwood (1963; Ref 135) and Redwood (1962; Ref 136).

Experiment 4: The effect of electrode and spark chamber material on the output pressure pulse

The experimental layout and the instrumentation used was similar to the previous experiment. The distance between source and receiver was approximately 25 cm. Sodium chloride solution was prepared in a large beaker, so that the salinity of the various sparkers was constant. Electrical energy input into the mini-sparker was kept constant at 0.56 J (1.5kV and 0.5 μ F).

The effect of the electrode size was investigated using a rigid PVC mini-sparker of 23 mm OD, 19 mm ID and 5 cm length. Initially, two line electrodes were used on both high voltage and earth return electrodes. The electrodes were 2 mm in diameter and 12 mm in length. Fig 6:1:17, trace 1, shows the output pressure pulse. The first negative peak was 2.58 mV, which equates to 0.41 mbar. Sensitivity of the hydrophone was 6.3 mV/mbar.

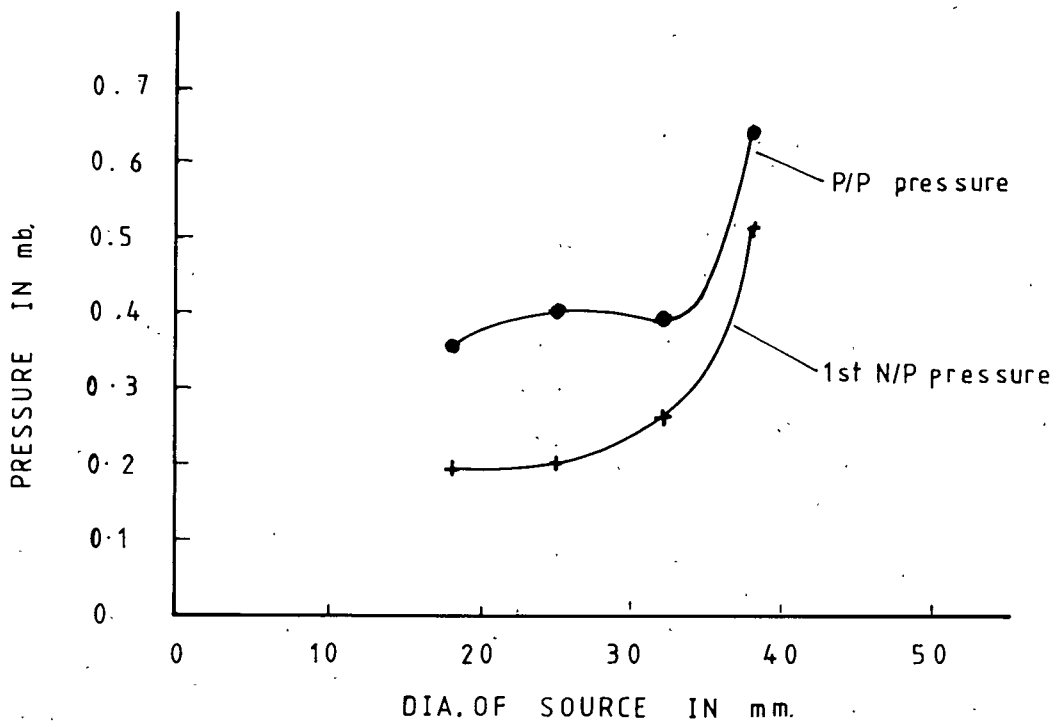


FIG. 6:1:15 PRESSURE OUTPUT FROM DIFFERENT DIA. STEEL MINI-SPARKER

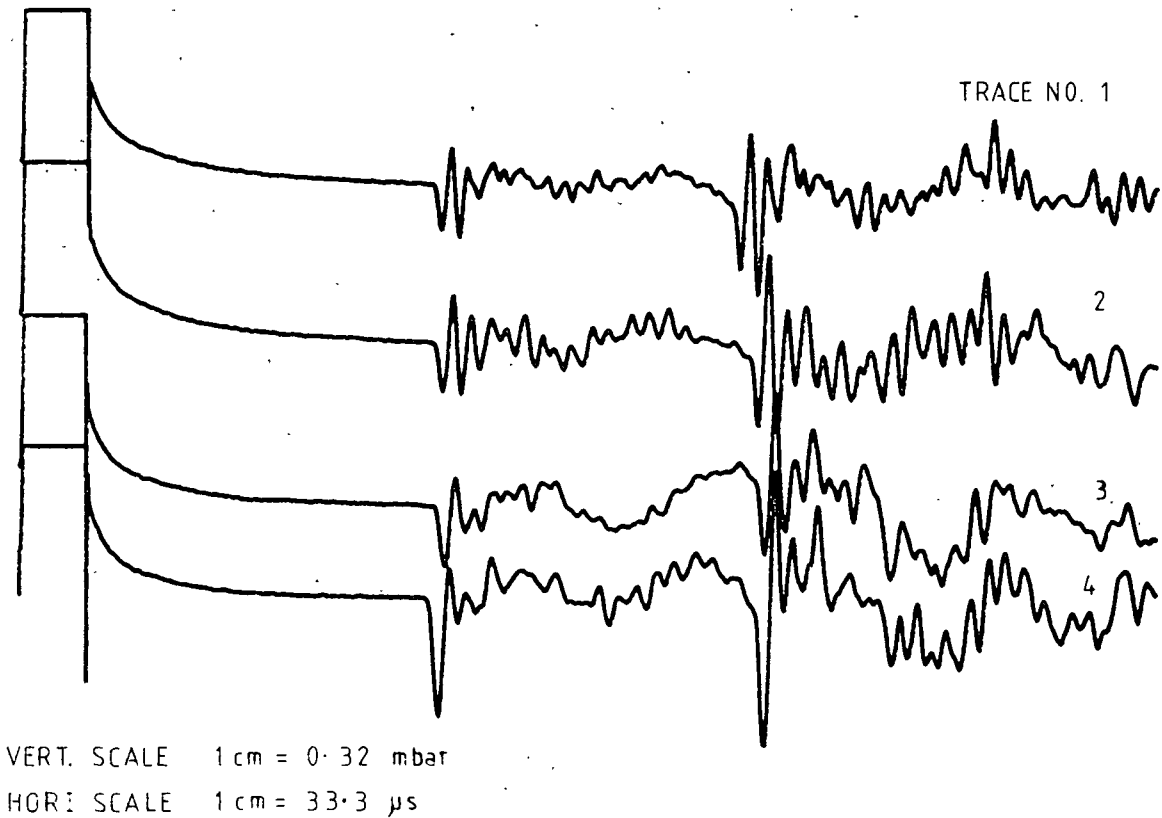
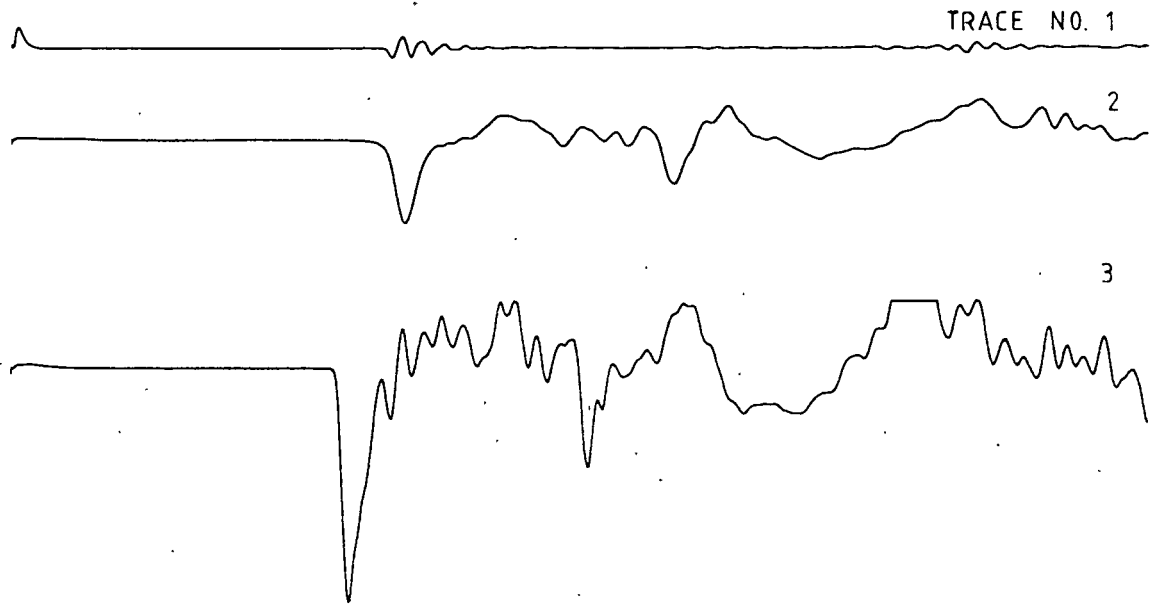
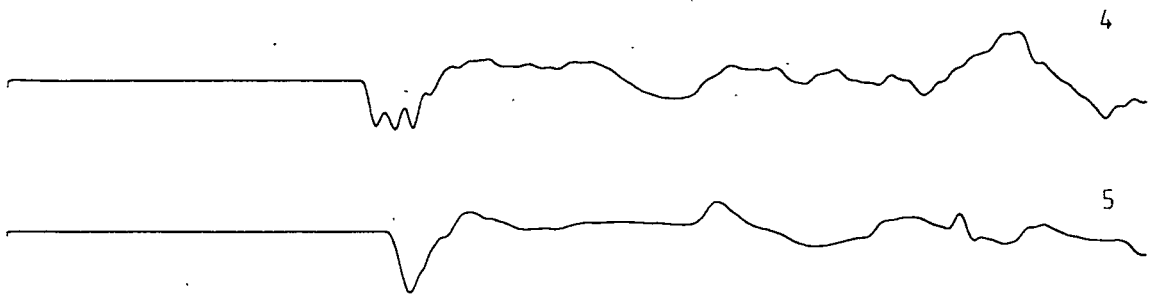


FIG. 6:1:16 PRESSURE SIGNATURES FROM STEEL MINI-SPARKERS



VERT. SCALE 1 cm = 3.3 mbar



VERT SCALE 1 cm = 33.0 mbar

HORI SCALE 1 cm = 33.3 μ s

FIG. 6:1:17 PRESSURE SIGNATURES FROM VARIOUS
ELECTRODE AND CHAMBER CONFIGURATIONS

The mini-sparker was dismantled and the high voltage line electrode removed and replaced with a point electrode, represented by trimming the central core of the coaxial cable close to the insulation. The mini-sparker was assembled and the output signature monitored. The output shape and peak pressure varied considerably. Traces 2 and 3 of Fig 6:1:17 show the mini-sparker's minimum and maximum outputs respectively. The output varies by a factor of approximately 3, from 22.3 mV to 63.1 mV.

The mini-sparker was dismantled again and both electrodes made up to represent point sources, but the separation between them was similar to the line electrodes' configuration. The mini-sparker was reassembled and the output signature monitored. Trace 4 shows the mini-sparker's output pressure signature with point electrodes. The output has gone up by a further factor of 2 mV to 121 mV (19.2 mbar).

The rigid PVC electrode chamber was replaced by a soft plastic tube, which had an outside diameter of about 20 mm and a length of 5 cm. The output pressure signature was monitored using the same input energy and the point electrode configuration. Trace 5 of Fig 6:1:17 shows the pressure signatures, with a negative peak reaching 164 mV (26.0 mbar). The signature displays a clean negative going spike with no apparent sparker chamber resonance effect and internal reverberation. The mini-sparker output has gone up by a factor of 60, due to the modification of the electrode configuration and casing material, although Roi and Frolov (Ref 137) also show that the output rises with increase in separation of the electrode.

The increase in pressure peak output can be explained by the extra plasma generation. The increase in plasma can be attributed to the higher current density obtained by effectively reducing the electrodes' surface area. Kramer et al (1968; Ref 129) have discussed the formation of high current density during plasma generation.

The above experiments show that output pressure pulse size and shape can be affected by salinity, energy input, chamber size and electrode configuration. The single spike required for the AC DER system can be achieved by the development of spark chamber housing, electrodes, etc.

6:1:2 Directional receiver

In the majority of underwater applications of seismic/acoustics there is a need for information on the direction of the object or the sound source being detected, and sometimes very high precision is required. This is usually achieved by designing a receiver transducer system which responds effectively over a small angle of space near it. In a sonar system the transmitter, which also works as the receiver, is designed in such a way that in both modes the beam generated or received is very narrow. Such systems, which respond in transmission or reception over a restricted range of directions, are called directional systems. In both the transmitting and receiving mode the sound is confined to a beam which is solid angle over which their response is effective. This property of confining response to a limited angle is called directivity. Directivity has some quantitative connotations, but does not have a quantitative definition of its own.

All transducers, except for small spherical transducers with an entirely surface motion, always have some degree of directional property. A spherical transducer with radial motion and a point transducer of infinitesimal size, which respond equally in all directions in a uniform infinite medium, are called omnidirectional.

A single transducer designed with a radiating surface of a shape designed to give desired directionality, or an array of omnidirectional transducers, can be arranged to give a particular directionality for a directional transducer system. An array of this type, requiring considerable complicated signal processing, is one of great complexity. The discussion in this section only considers the far field condition, as the results from near field (Fresnel zone) conditions are very complex and of little significance. The near field condition is defined in the area where the width of the nominal beam is less than the length of the array.

At the beginning of section 6, the requirement of a directional receiver for a ACDER system to work was introduced, and some quantitative assessments made of the size of the required beam angle for the directional receiver. Although the beam angle does give some quantitative information on what is required, it does not give any

attenuation figures to assess the rate at which directivity of the beam is formed.

The common term used for describing the directionality of the beam is called the beam width. The beam width of a directivity pattern is taken as the angular distance between the two points on either side of the principal axis, where the sound pressure level is down by a specified decibel (dB) level from its value at $\theta = 0$. Beranek (1954; Ref 138) regards 6 dB down from $\theta = 0$ as the way to define the beam width, while Urlick (1967; Ref 139) suggests the use of values of -3 dB and -10 dB to define the beam width. In view of the narrow beam width required to discriminate or resolve the target, a -10 dB figure would be more useful. The requirement for the beam width for a ACDER system would now be defined as a 2° beam width at -10 dB from the principal axis of the receiver.

An analytical approach was considered to be the best solution after the initial investigation, which suggested that the desired beam width would be impossible to achieve for an available 51 mm diameter transducer and the wavelength in question (see page 161).

A wave equation can be used to derive an equation for the directivity or the beam width of a source or a receiver. The acoustic reciprocity method states that the analytical method can be applied to either a source or a receiver, as they are virtually represented as equal.

The most elementary radiator of sound is a spherical source whose radius is small compared to one-sixth of a wavelength. Such radiators are called simple source or point source. Their properties are specified by the magnitude of velocity of their surface and by their phase relative to some reference point.

The wave equation for the sound pressure from a spherical source at distance r from its centre can be derived (Beranek, 1954; Ref 138) as

$$p(r,t) = [(\sqrt{2A+})/r]e^{j(\omega t - kr)} \quad - (6.6)$$

where

p = pressure at distance r from the centre of the source

A = magnitude at unit distance from centre of the source ($\sqrt{2}$ =rms)

k = $w/c = 2\pi f/c = 2\pi/\lambda$ = wave number

The basic principles governing the directivity patterns from a source or a receiver can be derived by combination of simple sources. This approach is similar to the consideration of Huygens wavelets in optics. Basically, the problem is to add, vectorially, at the desired point in space the sound pressure arriving at that point from all the simple sources.

Consider two simple sources in phase. The geometric solution is shown in Fig 6:1:18.

It is assumed that the distance r from the two point sources to point A at which the pressure p is being measured is large compared with the separation b between the two sources.

The spherical sound wave arriving at point p from source 1 will have travelled a distance $r-(b/2)\sin\theta$, and from equation (6.6) the sound pressure will be given by:

$$p_1(r_1, t) = (\sqrt{2}A+/r)e^{j(w, t)} e^{-j(2\pi/\lambda)[r-(b/2)\sin\theta]} \quad - (6.7)$$

The wave from source 2 will have travelled a distance $r+(b/2)\sin\theta$, so that

$$p_2(r_2, t) = (\sqrt{2}A+/r)e^{j(w, t)} e^{-j(2\pi/\lambda) r+(b/2)\sin\theta} \quad - (6.8)$$

The sum of $p_1 + p_2$, assuming $r \gg b$, gives

$$p(r, t) = (\sqrt{2}A+/r)e^{j(w, t)} e^{-j(2\pi/\lambda)r} \times (e^{j(\pi b/\lambda)\sin\theta} + e^{-j(\pi b/\lambda)\sin\theta}) \quad - (6.9)$$

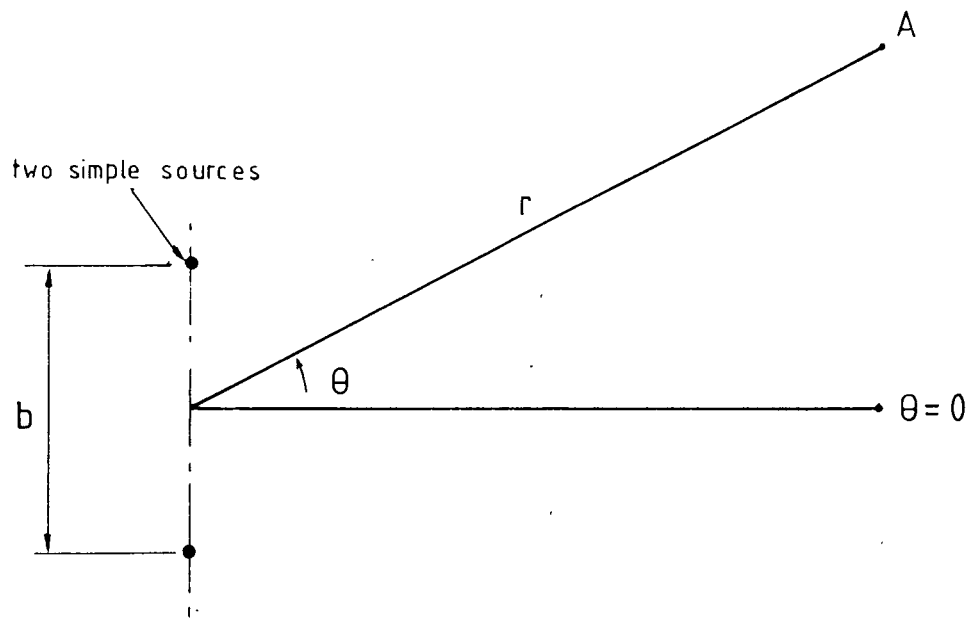


FIG. (a)

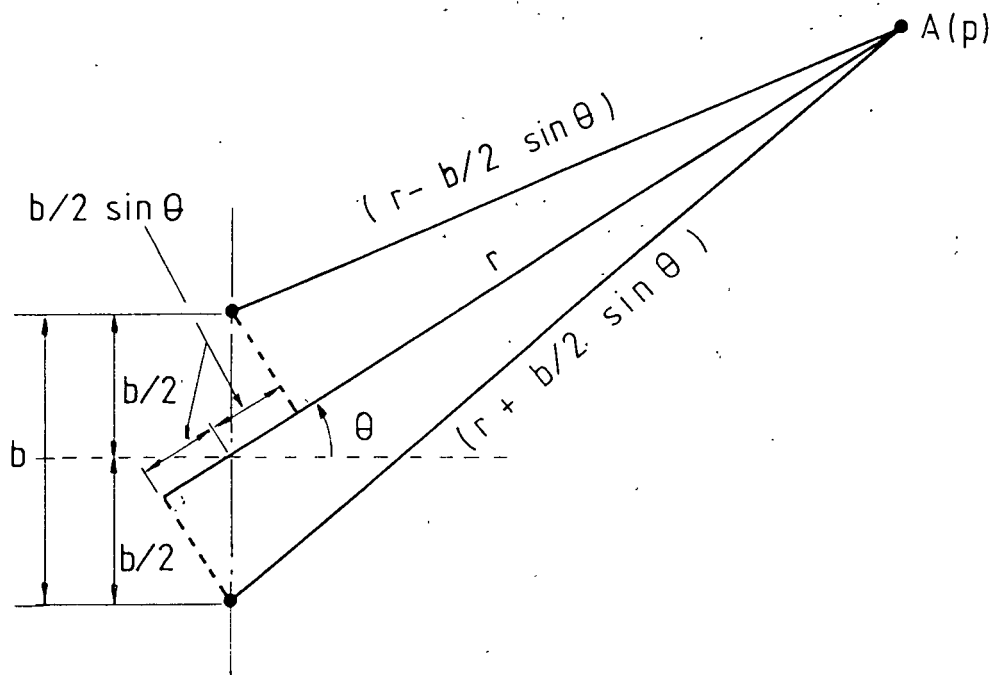


FIG. (b)

FIG. 6:1:18 TWO SIMPLE SOURCES VIBRATING IN PHASE

Multiplication of the numerator and the denominator of equation (6.9) by $\exp(j\pi b \sin\theta/\lambda) - \exp(-j\pi b \sin\theta/\lambda)$ and replacement of the exponential by sines, yields

$$p(r,t) = (\sqrt{2}A+/r)e^{j(\omega,t)} e^{-j(2\pi r/\lambda)} \times \left[\frac{\sin(2\pi b/\lambda)\sin\theta}{(\sin\pi b/\lambda)\sin\theta} \right] \quad - (6.10)$$

The equation for the magnitude of the rms sound pressure $|p|$ is

$$|p| = (2A+/r) \left| \left[\frac{\sin(2\pi b/\lambda)\sin\theta}{(2\sin(\pi b/\lambda)\sin\theta)} \right] \right| \quad - (6.11)$$

The portion of this equation within the straight line yields the directivity pattern.

With reference to Fig 6:1:18b, if b is very small compared with a wavelength, the two sources essentially coalesce and the pressure at a distance r at any angle θ is double that for one source acting alone. The directivity pattern will be a circle.

As b gets larger, however, the pressure arriving from the two sources will be different in phase and the directivity pattern will not be a circle. In other words, the sources will radiate sound in some directions better than others.

A computer program was written on an HP45 mini-computer in order to generate directivity patterns for various source dimensions and wavelengths combinations. The program is called 'DIRPAT' and is listed in Appendix IV.

Each run requires four inputs. They are

- A = amplitude at distance which is normally unity (1)
- r = distance from source to receiver, which in this case is 30 m
- b = diameter of the receiver in metres (0.051 m)
- λ = wavelength from the source, which is derived from the frequency of interest and the velocity of the compressional wave through the rock mass ($c = f\lambda$)

With each set of inputs, two pages of printouts are dumped. The first is a tabulated list of pressure magnitudes calculated from different angles θ . The pressure magnitude is calculated from 0° - 90° in steps of 2° , as shown in Fig 6:1:19. The second printout is a directional plot, as shown in Fig 6:1:20. The pressure magnitude is plotted against angle θ in degrees starting from -90° on the lefthand side, rising to $+90^\circ$ on the righthand side. A directivity pattern can be plotted by converting the pressure magnitude in relative dB loss compared to the pressure at 0° .

$$A_x(\text{dB}) = 20 \log(P_0/P_x) \quad - (6.12)$$

where

P_0	=	pressure at	$\theta = 0$
P_x	=	pressure at	$\theta = x$
$A_x(\text{dB})$	=	relative pressure loss in dB	

The tabulated result is used to convert the loss in pressure in dB and construct the directivity pattern, using polar graph paper, as shown in Fig 6:1:21.

A number of these directivity patterns were constructed. The first one uses the receiver diameter of 51 mm, which is the maximum diameter that can be incorporated in the mechanical housing. The wavelength for the velocity of 2.5 km/s and the predominant frequency of 1000 Hz was calculated to be 2.5 m. The tabulated results of these two variables is shown in Fig 6:1:22. The radiation pattern is spherical, which suggests that, with small receiver diameters, the long wavelengths involved will not facilitate the construction of a desired narrow beam.

The wavelength was reduced to 0.0625 by increasing the frequency of interest to 40 kHz. The tabulated results, direction plot and directivity pattern are shown in Figs 6:1:19, 6:1:20 and 6:1:21 respectively. Even at these high frequencies, which will be impractical for use in highly fissured environments such as coal mines, the beam width of the main beam is 60° for -10 dB criteria and 36° for -3 dB criteria. These values are significantly lower than those deemed necessary.

ANGLE θ AMPLITUDE

A= 1 R= 30
LAMBDA= .0625 B= .051

0	6.66666599913E-02
2	.066400037639
4	6.56035762113E-02
6	6.42874844453E-02
8	.062468518332
10	6.01696248297E-02
12	5.74194497037E-02
14	5.42517314777E-02
16	5.07045998457E-02
18	.046819799576
20	.042641862516
22	3.82172511333E-02
24	3.35934969123E-02
26	2.88183561335E-02
28	2.39390037809E-02
30	1.90012841652E-02
32	1.40490339858E-02
34	9.12349040727E-03
36	4.26279339627E-03
38	4.98411938553E-04
40	5.12927048447E-03
42	9.60291052407E-03
44	1.38965388902E-02
46	1.79914438349E-02
48	2.18729137187E-02
50	2.55300808568E-02
52	2.89557012989E-02
54	3.21458815727E-02
56	.03509976372
58	3.78191798047E-02
60	.040308286367
62	.042573188611
64	4.46215630877E-02
66	4.64622864897E-02
68	4.81050770507E-02
70	4.95601538043E-02
72	5.08379178433E-02
74	5.19486586473E-02
76	.052902287585
78	5.37080999337E-02
80	5.43745660037E-02
82	.05490915154
84	5.53181670863E-02
86	5.56066459227E-02
88	5.57782498913E-02
90	5.58352026677E-02

FIG. 6:1:19 DATA LIST OF AMPLITUDES FOR ANGLES

THETA, 0-90 DEG.(lambda=0.0625 m)

A= 1 R= 30
LAMBDA= .0625 B= .051
MAXIMUM= 6.6666599913E-02

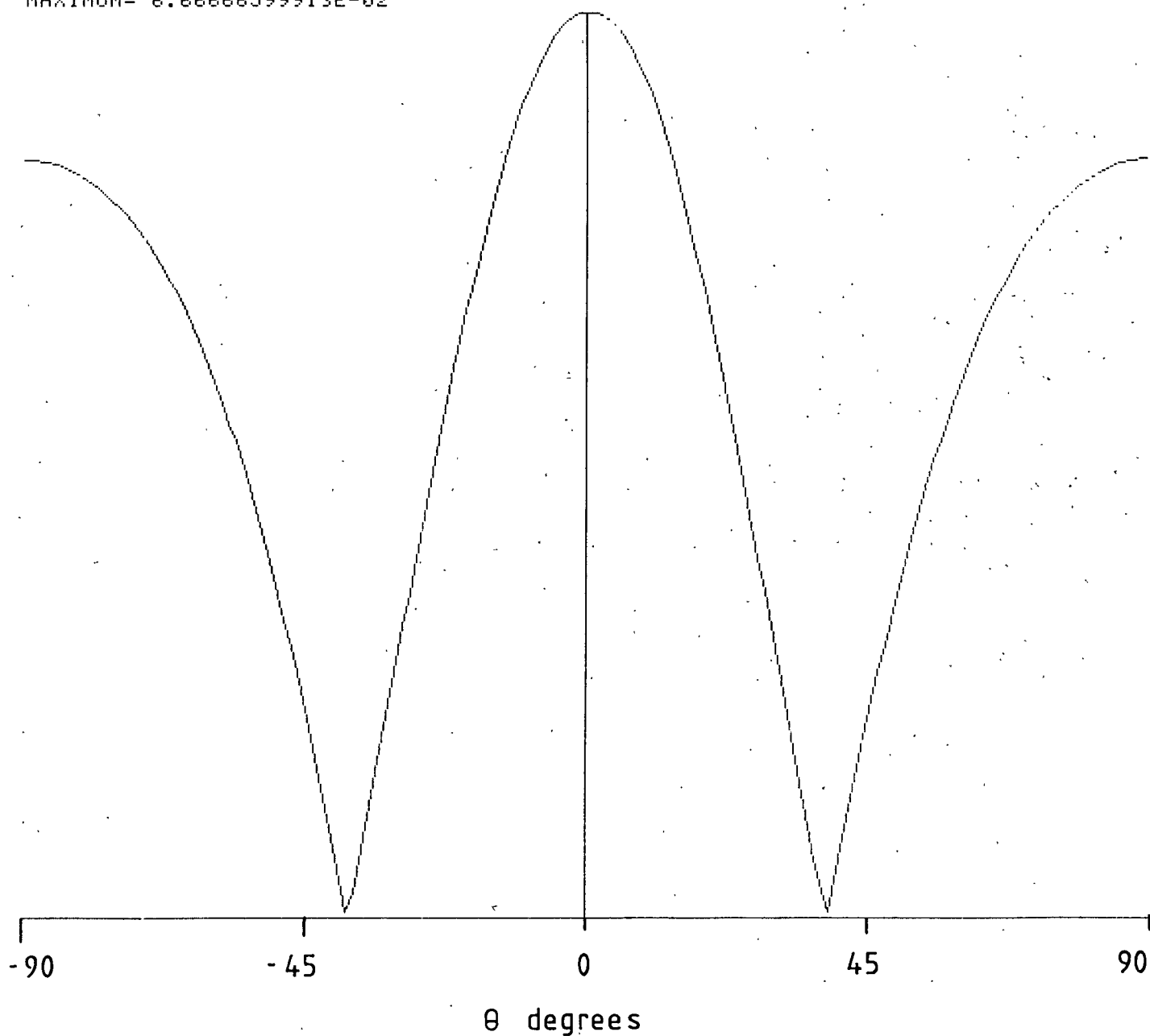


FIG. 6:1:20 DIRECTIONAL PLOT FROM THE DATA LIST

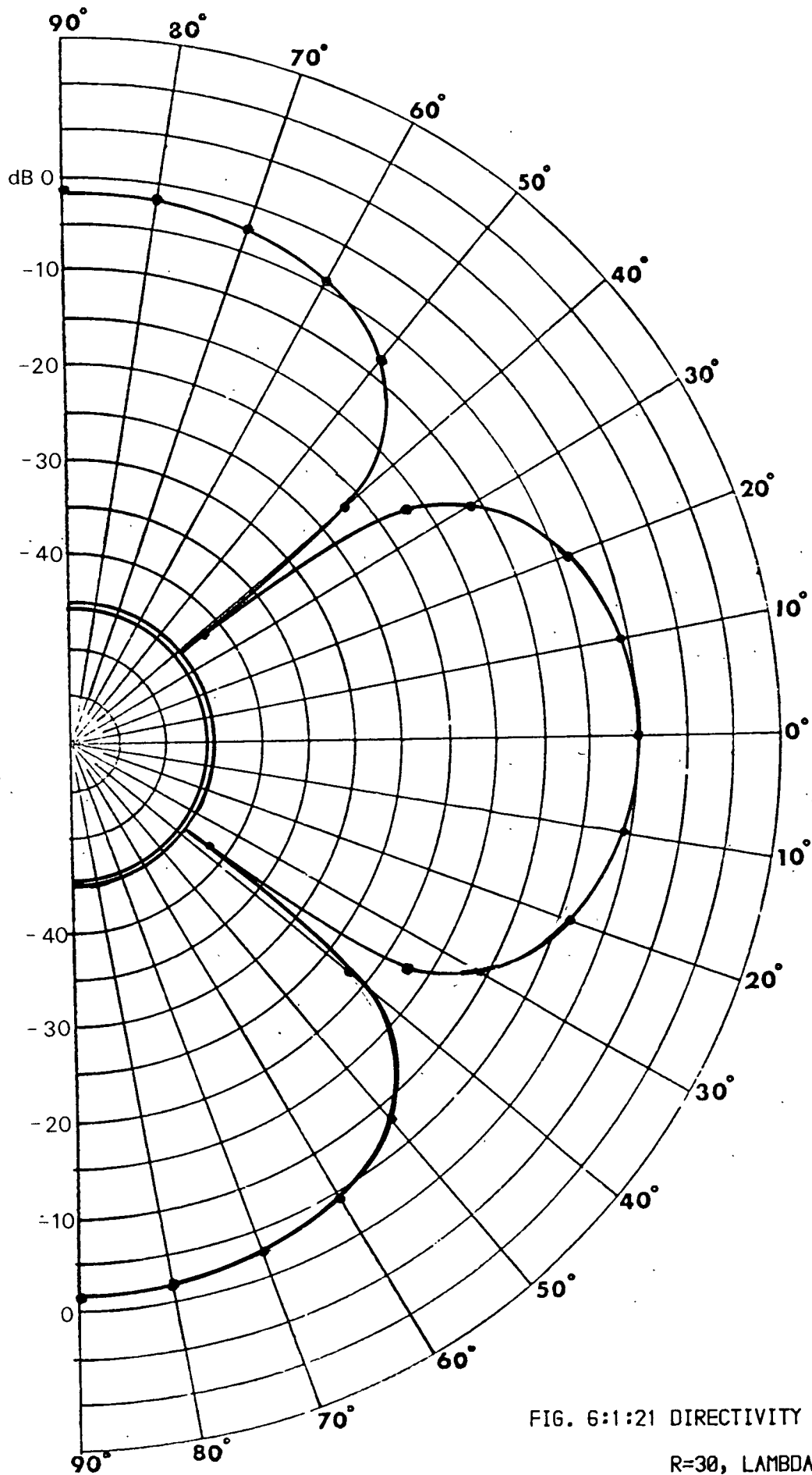


FIG. 6:1:21 DIRECTIVITY PATTERN FOR $A=1$,
 $R=30$, $LAMBDA=0.0625$ & $B=0.051$

ANGLE θ

AMPLITUDE

A= 1 R= 30
LAMBDA= 2.5 B= .051

0	.06666666666653
2	.0666666499908
4	6.66660004637E-02
6	6.66651707557E-02
8	.066664014834
10	6.66625383357E-02
12	.066660748458
14	6.66586539333E-02
16	6.66562649853E-02
18	6.66535932423E-02
20	6.66506517437E-02
22	6.66474548323E-02
24	6.66440180923E-02
26	6.66403582853E-02
28	.066636493239
30	.066632441807
32	6.66282237307E-02
34	6.66238595763E-02
36	6.66193706193E-02
38	6.6614787277E-02
40	6.66101062803E-02
42	.066605376041
44	6.66006110713E-02
46	6.65958045683E-02
48	.066591069826
50	.06658634004
52	.06658166826
54	6.6577072213E-02
56	.066572589317
58	.066568226377
60	6.65640096623E-02
62	6.65599596983E-02
64	.066556096212
66	6.65524380103E-02
68	6.65490029003E-02
70	.066545807609
72	6.65428677007E-02
74	6.65401974767E-02
76	6.65378099353E-02
78	6.65357167087E-02
80	.066533927965
82	6.65324524233E-02
84	6.65312972737E-02
86	.066530468118
88	.066529969006
90	.066529802373

FIG. 6:1:22 DATA LIST OF AMPLITUDES FOR ANGLES

THETA, 0-90 DEG.($\lambda=2.5$ m)

The other alternative is to increase the diameter of the directional receiver. Let us assume that it had been feasible to house a 1.5 m diameter piezoelectric disk as a directional receiver and still maintain the 2.5 m wavelength, as was originally intended. The directivity pattern is shown in Figs 6:1:23. The beam width appears to be approximately 80° for -10 dB criteria and 48° for -3 dB criteria. This again falls significantly short of what is required.

Two composite directional plots were constructed by initially varying the wavelength on its own, and then varying the diameter on its own. Fig 6:1:24 shows a directional plot, with the diameter of the receiver kept constant at 0.051 m, and wavelength decreasing in the following steps: 2.5 m, 0.25 m, 0.125 m, 0.0833 m and 0.0625 m. The figure illustrates that, as the wavelength increases with rising frequency, so does the directivity of the receiver increase.

Similar directional plots were constructed with the wavelength kept constant at 2.5 m, and directional receiver diameter increasing in the following steps: 0.051 m, 0.50 m, 1.0 m, 1.5 m and 2.0 m. Fig 6:1:25 is a directional plot of the various receiver diameter sizes, and illustrates that the directivity of the receiver rises with increasing diameter.

These units are also substantiated by the monogram computed by Urick (1975; Ref 139) for finding the width of the beam pattern of circular planes and line transducers, as shown in Fig 6:1:26. The dashed line indicates how the monogram is to be used. Thus, a circular plane array of 20 in diameter at a wavelength of 4 in (corresponding to a frequency of 15 kHz at a seismic velocity of 5000 ft/s) has a beam pattern of 6° width between the axis of the pattern and the -3 dB down point, and 10° width between the axis and the -10 dB down point.

For the case in question, with a velocity of 2.5 km/s (8200 ft/s), a frequency of 1000 Hz (which makes $\lambda = 2.5$ m or 8.2 ft) and a receiver diameter of 0.051 m (2.0 in), the beam width obtained from the monogram shows that it will be spherical without any directional property.

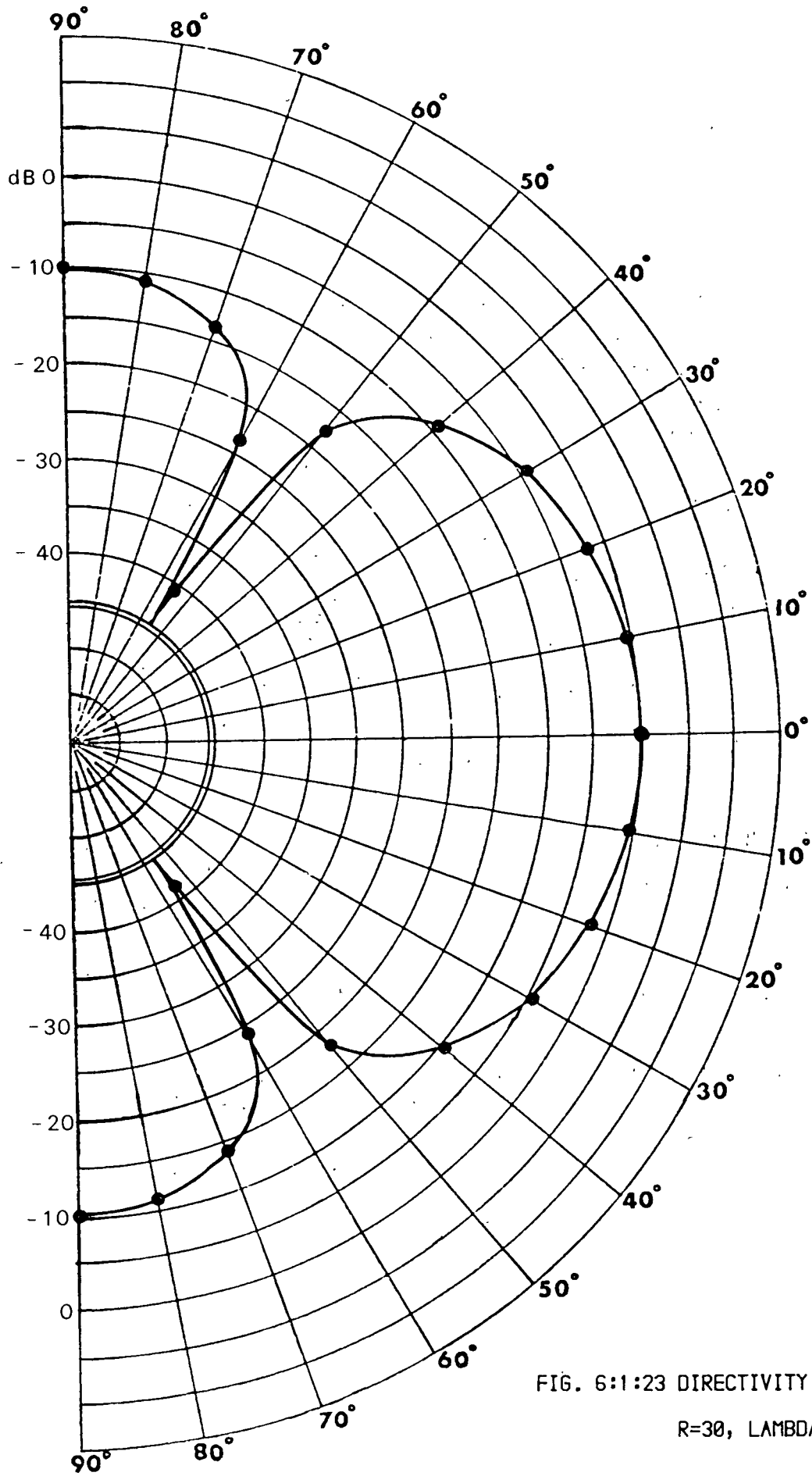


FIG. 6:1:23 DIRECTIVITY PATTERN FOR A=1,
R=30, LAMBDA=2.5 & B=1.5

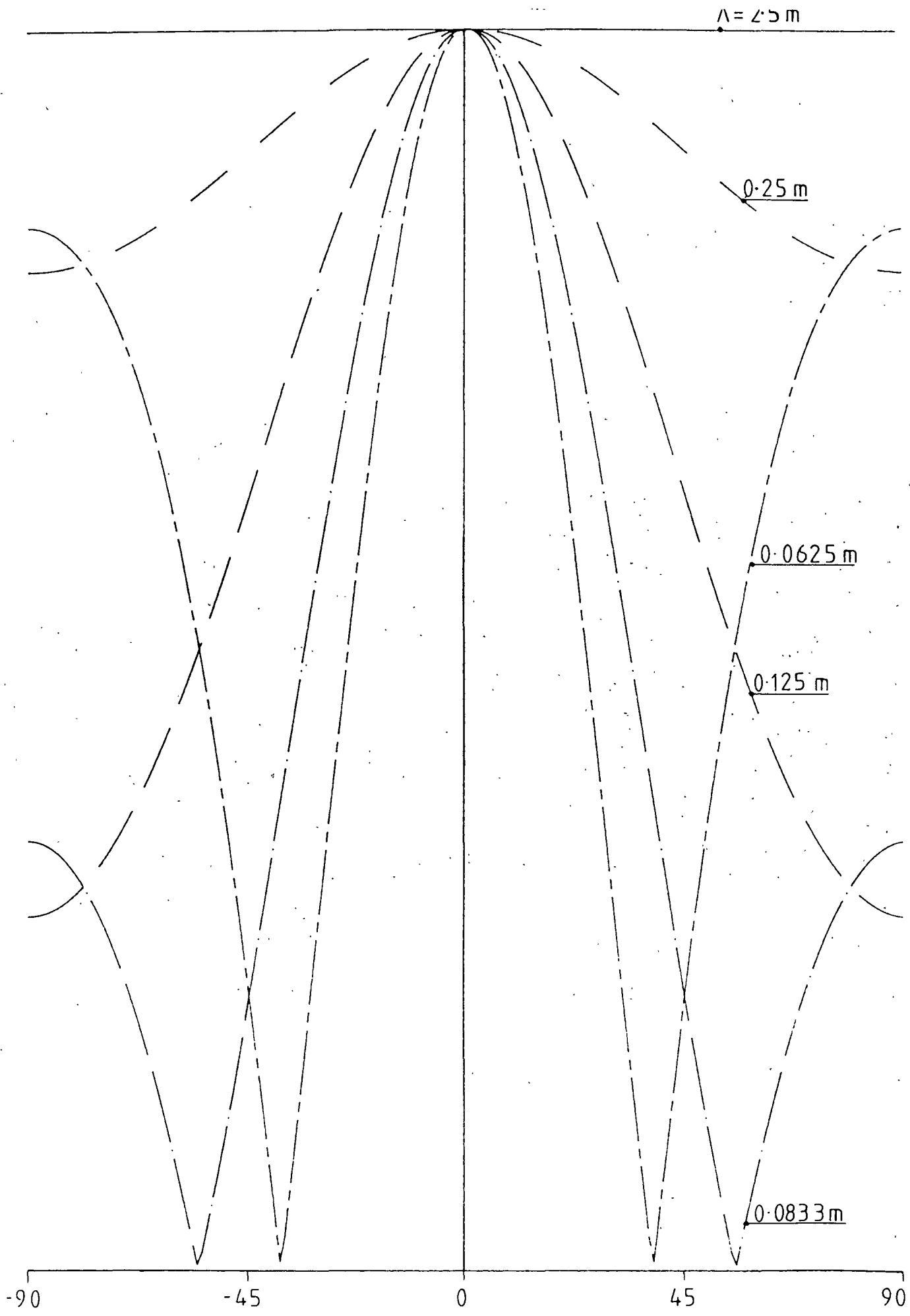


FIG. 6:1:24 DIRECTIONAL PLOTS FOR VARIOUS VALUES OF LAMBDA

RECEIVER DIA. $B = 0.051 \text{ m}$

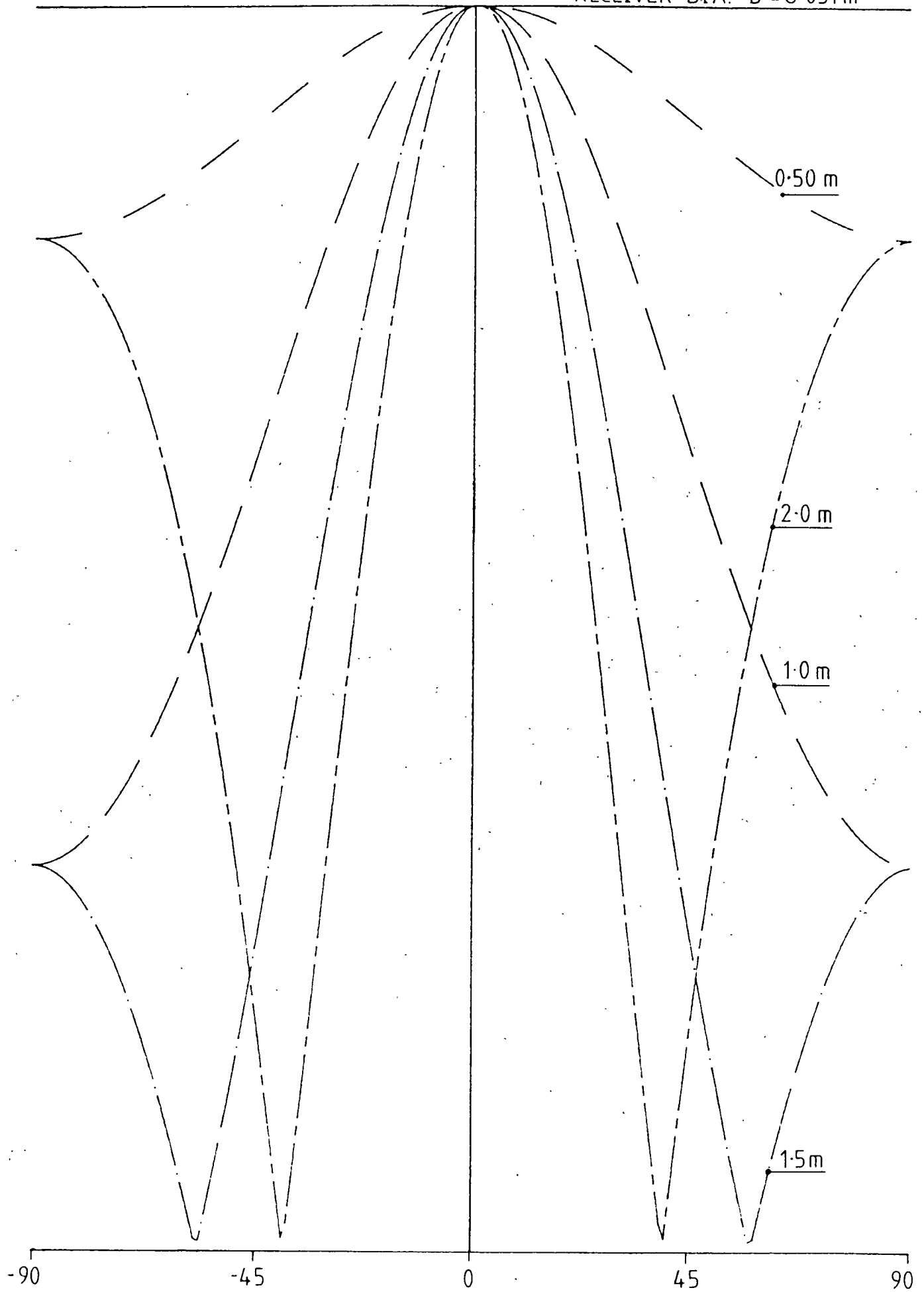


FIG. 6:1:25 DIRECTIONAL PLOTS FOR VARIOUS VALUES OF 'B'

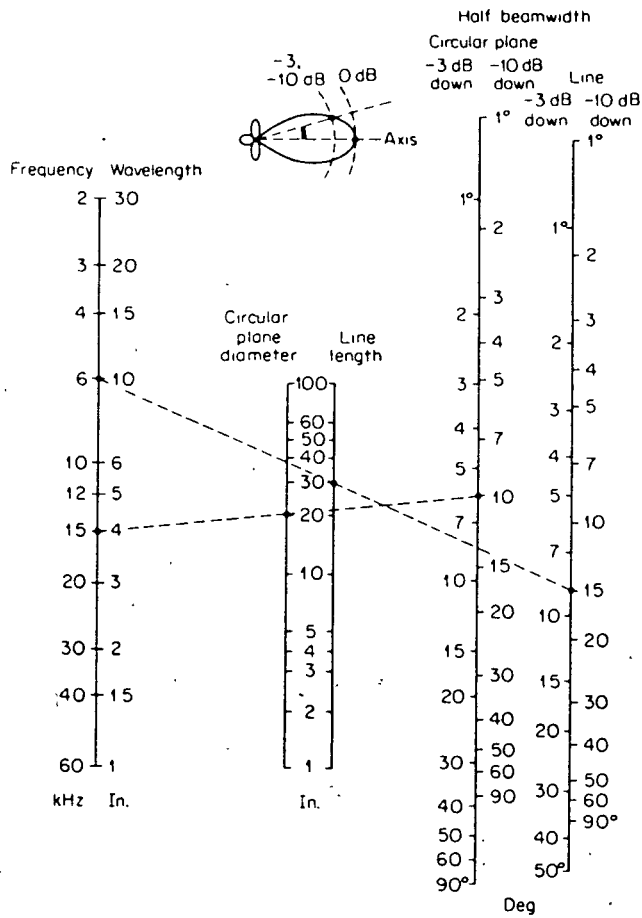


FIG. 6:1:26 MONOGRAM FOR THE FINDING THE WIDTH OF THE BEAM PATTERN OF A CIRCULAR-PLANE & LINE TRANSDUCERS (after Urick, 1967; Ref 139)

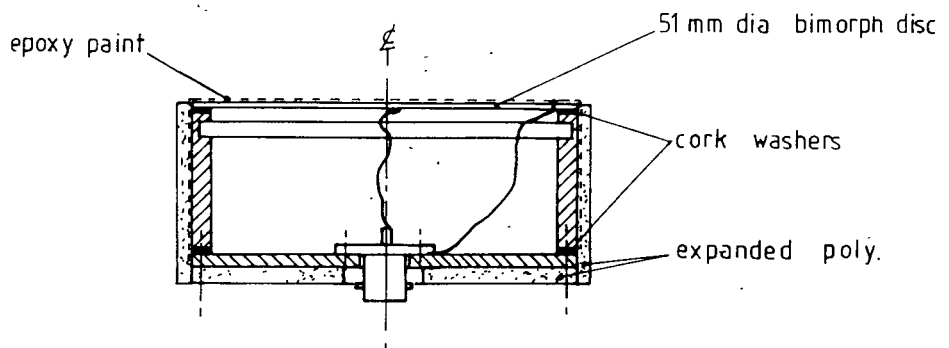


FIG. 6:1:27 RECEIVER TRANSDUCER FOR THE ACDER SYSTEM

Assuming the worst case, with a 4° beam width at -3 dB down and a directional receiver of an 0.051 m diameter disk, the wavelength required will be approximately 8.89 mm, which is equivalent to 280 kHz. At this frequency penetration into the rock mass will be in terms of tens of centimetres and not 30 m.

This demonstrates the difficulty of designing a narrow beam receiver for longer wavelengths using a single 51 mm diameter transducer. It was envisaged that a smaller diameter receiver transducer was desirable, in order to make the scanning part of the sonde relatively smaller and lighter so that it would facilitate the ease of deployment, both in vertical and horizontal boreholes. The above work indicates that the use of a single transducer to generate the desired beam pattern was not feasible and that an array will have to be considered. The use of an array to converge a beam in the direction of the axis of the borehole would not be difficult, as the convergence in this plane would be at the expense of making the receiver longer. To converge the beam in the plane normal to the axis of the borehole could be complex, especially if the narrow beam angle and the relatively smaller diameter of the sonde had to be maintained with sufficient sensitivity.

In view of the complexity of the design, construction and processing of data for such an array, a brief description is given of the various types of arrays that may be considered for further investigation in the future. The principles of these arrays are described by Urick (1975 Ref 139).

Linear or equally spaced array

This is the simplest form of array, where the elements (acoustic transducers) are arranged along a line or distributed along a plane. The acoustic axis of such an array, when unsteered, lies at right angle to the axis of the line or plane. The beam pattern of a line array may be visualised as a doughnut-shaped figure having supernumerary attached doughnuts formed by the side lobes of the pattern (Urick, 1975; Ref 139).

Arrays can be steered by introducing appropriate phase or time delays in the output of the various elements to rotate the main lobe of the

pattern in a desired direction. This changes the beam width and side lobe structure of the beam pattern. Normally, the beam width widens as the beam is steered from broadside to end-fire, the directivity index of the steered line remaining approximately the same.

Synthetic aperture line array

In a synthetic aperture line array, the multielement conventional line array is replaced by a single unit. As the single unit is towed or moved through the water, the receiver signals are windowed using electronic switching at various intervals, applying the time delays required to focus the virtual beam. The sampled data is suitably recorded or stored, and later range-gated and summed at the appropriate time intervals. The sum of the gated samples will appear equivalent to the output of a conventional focussed array of elements as the number of windowed samples. Very long virtual arrays can be realised in this way using a single transducer, but they require that the echo be coherent over the distance and time required for beam formation.

Shading and superdirectivity

Shading is a process of controlling the response or gain of each element of an array so that some control can be exercised over the beam pattern. Most arrays are shaded with a maximum response at the centre and the least response at the ends or sides of the arrays, so that the sensitivity is tapered from high value on the inside to a lower value on the outside.

Amplitude shading is a convenient way to tailor a beam pattern to some desired shape. However, with a coherent signal in uniform incoherent noise, shading results in a lower array gain than with constant element sensitivity. Therefore, heavy shading should not be used under low signal-to-noise ratio conditions where the array gain is an important consideration.

Superdirectivity is an extreme form of shading in which a narrow beam may be obtained with an array of a limited size. In a superdirective array, elements are spaced at less than one-quarter of a wavelength apart, with the signs, or polarity, of adjacent elements reversed.

Superconductive arrays suffer from low array sensitivity, due to the phase reversals of the elements and the relatively high sided lobes.

Phase shading may also be used, by varying the space between the elements to obtain the desired beam pattern. By virtue of the spacing required between elements, arrays with phase shading would be larger in size.

Multiplicative arrays

Most of the arrays discussed previously were of the linear and additive types, where the output of the acoustic elements is linearly proportional to the pressure and the array output is just a summation of individual element outputs. Instead of being added, the element output may be multiplied together so as to form a multiplicative or correlative array, generating properties different from those of linear arrays. For example, a multiplicative array of only two elements can be made to have the same beam pattern as a linear array of an arbitrary number of equally spaced elements (Dolph, 1946; Ref 140). This technique is appealing in applications where a reduction in the number of acoustic sensor elements is necessary. The reduction in the physical size or the number of elements, or both, is gained at the expense of the complexity of handling and the processing of data. The method is practical only at high signal-to-noise ratios, as the effect of noise is to destroy the beam pattern unless a long averaging time period is used.

The advantages of multiplicative processing lie in narrow beams and in the better angular resolution of closely spaced acoustic elements. Another benefit lies in the flexibility in the design that multiplicative processing provides (Tucker, 1963; Ref 141). With linear arrays, the beam width, array gain, and resolution are all interconnected, while with multiplicative arrays there is no longer any direct relationship among these array properties. These properties have to be determined mathematically for particular configurations of multipliers and averagers.

In summary, it would appear that use of multiplicative arrays would be perhaps a more suitable way of generating the beam angle required with a limited number of acoustic elements (because of the limited space in the

sonde), but the complexity of downhole processing and the reduction in the sensitivity of the array will require further research. Another parameter which has not been discussed but will require considerable work is the calibration of the array, both for sensitivity and for beam width.

Although the above analytical work carried out shows that the required beam width will not be feasible using a single element, a receiver was designed and constructed with the maximum diameter piezoelectric disk that can be incorporated into the housing. Fig 6:1:27 is a diagram of the receiver and its construction. Instead of the standard piezoelectric disk, a 51 mm disk was cut out of a bimorph plate as a receiving transducer. A bimorph plate has a higher sensitivity per unit input of pressure pulse compared to a piezoelectric disk.

6:1:3 Instrumentation and display

The instrumentation associated with the ACDER system can be explained by considering in detail the working of the system. Fig 6:1:28 shows the block diagram of the ACDER system.

When the system is activated, the trigger pulse is applied simultaneously to the thyristor control unit, the stepper motor and the external ramp generator. The thyristor control unit fires the sparker as the stepper motor control circuit advances the stepper motor by a step of $7^{\circ}13'$ angular displacement. The stepper motor is mechanically coupled to the epicyclic gear assembly, which gives an angular displacement reduction of 15:1. The epicyclic gear is then mechanically coupled to the directional receiver transducer through a sine/cosine potentiometer and a low noise slip ring assembly. The total rotation of the directional transducer is reduced to 0.48° of rotation for each firing of the trigger pulse. It is essential to realise that stepper motor, epicyclic gear, sine/cosine potentiometer, slip ring assembly and directional receiver are mechanically coupled to each other and form a borehole sonde, as shown in Fig 6:1:29.

The dual ramps generated when the trigger pulse was fired are fed into the input of the sine/cosine potentiometer, and the output from the potentiometer is fed into the vertical (y) and horizontal (x) deflection

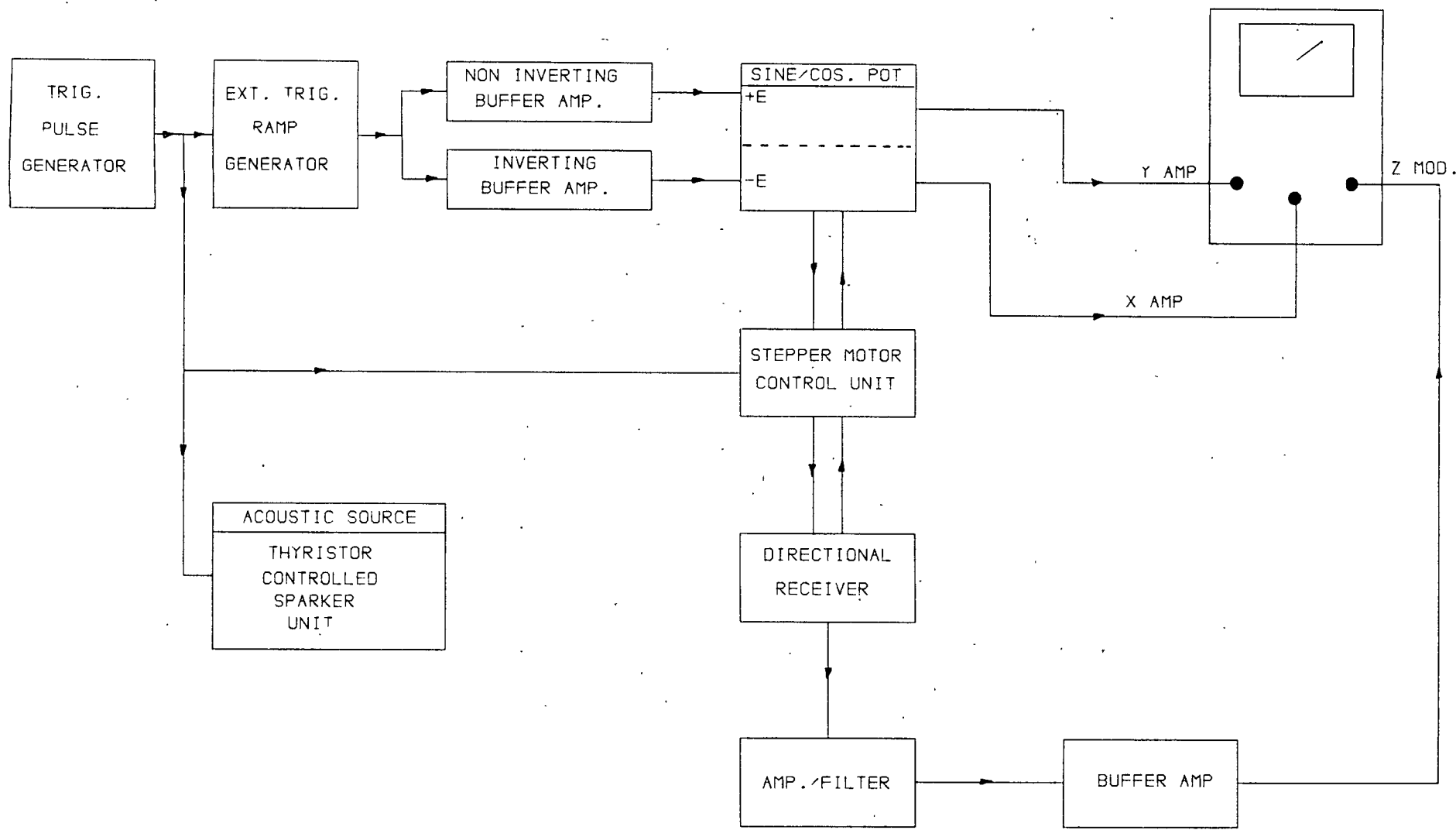


FIG. 6:1:28 BLOCK DIAGRAM OF THE LABORATORY MODEL OF AC/DC SYSTEM

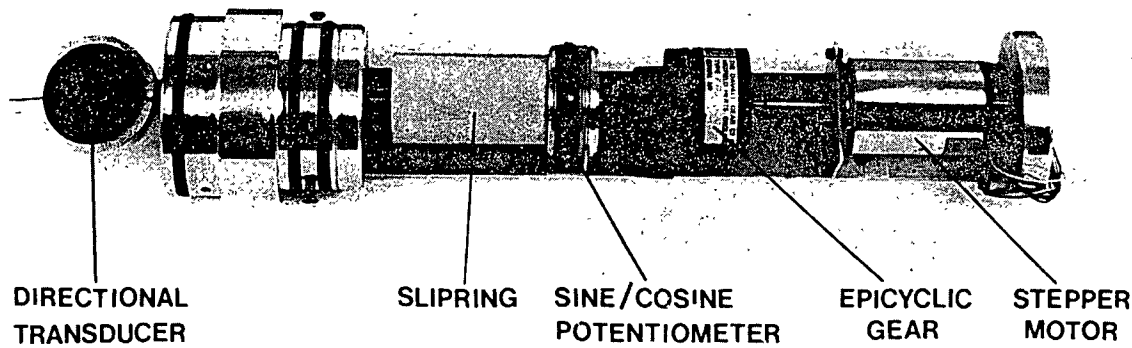
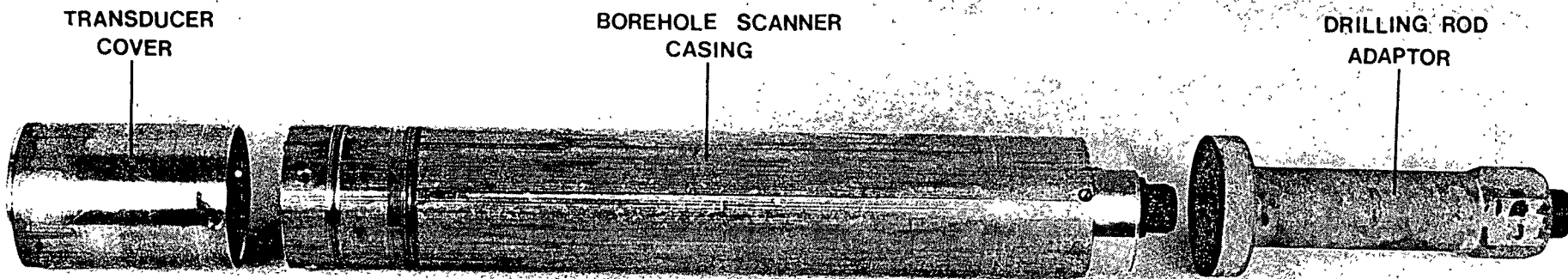


FIG. 6:1:29 ACDER BOREHOLE SONDE

control circuit of a storage c.r.t., which causes the electron beam to scan from the centre of the screen and track outward towards its periphery. Any reflection pulse detected by the directional receiver is filtered, amplified, processed and fed into the z modulation of the storage c.r.t. through a buffer amplifier.

The display unit and other associated instrumentation is described below in detail.

The display unit's screen image appears as a faint spot, which has an apparent motion from the centre of the screen towards its periphery in a specific direction. If any reflections are detected, the faint electron beam becomes more intense and leaves as a trace on the display a bright image or short line, during the period the reflected seismic pulse is detected by the receiver. The process of increasing the intensity of the electron beam by a signal wave is called z modulation.

a **Display unit**

During the introduction of section 6, it was stressed that the data display should be such that there is no appreciable time lag between signal capture and data interpretation. This was achieved by using a technique similar to that involved in radar tracking of an aerial object. A beam on the radar cathode ray tube (c.r.t.) appears to rotate in the same direction as the radar dish, and whenever it encounters a large object in the sky, within the range of the signal, a part of the transmitted signal is reflected back to the radar dish (aerial) and in turn appears on the c.r.t. as a bright spot.

The beam, which appears to rotate on the display unit, is in fact a continuous scan of a small spot of electron beam travelling from the centre of the screen to its periphery at a set rate. On reaching the periphery it returns to the centre of the screen and begins travelling across once again, but in the meantime has moved through a small angle predetermined by the radar dish rotation. In so doing, a very small sector is scanned for reflections from any aerial objects.

The data display technique can also be illustrated by visualising the display screen as four quadrants, shown in Fig 6:1:30. Horizontal and

vertical axes are represented by x and y respectively, with 0 as their origin.

Consider a point P at a distance r from origin. Point P can be represented in Cartesian coordinates as x , and y , on the x and y axes respectively, such that

$$x_1 = r \sin \theta \quad - (6.13)$$

and
$$y_1 = r \cos \theta \quad - (6.14)$$

Point P can be generated on a cathode ray oscilloscope (c.r.o.) by applying a fixed level of DC voltage across the x and y inputs. Alternatively, a line can be generated by varying voltage inputs from zero to a set DC level. This will cause the dot on the screen to move from origin (the centre of the screen) to the periphery, depending on the rate of change of the voltage. Changing the voltage linearly from zero to a fixed value is called a ramp. When a ramp is applied to the two inputs (x and y), the beam will move from its origin to the periphery of the display screen.

If scanning beams are required to start at angle $\theta = 0^\circ$ and gradually move towards $\theta = 90^\circ$, the input ramps must be processed to take angle into consideration. This was achieved by using the function derived for point P in Cartesian coordinates (equations (6.13) and (6.14)), so that when a linear ramp is applied to the input of a dual gauge sine/cosine potentiometer, output voltage from the potentiometer is represented by sine and cosine .

When output from the sine/cosine potentiometer is applied to inputs x and y of the c.r.o., the scanning beam moves in relation to the shaft of the potentiometer. This rotation of the beam in relation to the shaft of the sine/cosine potentiometer will hold for angles $\theta = 0^\circ-90^\circ$ only. Referring to Fig 6:1:30, it can be seen that a negative DC potential will be required if the electron beam is to be deflected into the other three quadrants. Therefore, instead of a single positive ramp, a dual ramp is produced, one positive going and one negative going, as shown in Fig 6:1:31. If the positive going ramp is applied to the +E terminal on the sine/cosine potentiometer and the negative ramp is applied to the -E

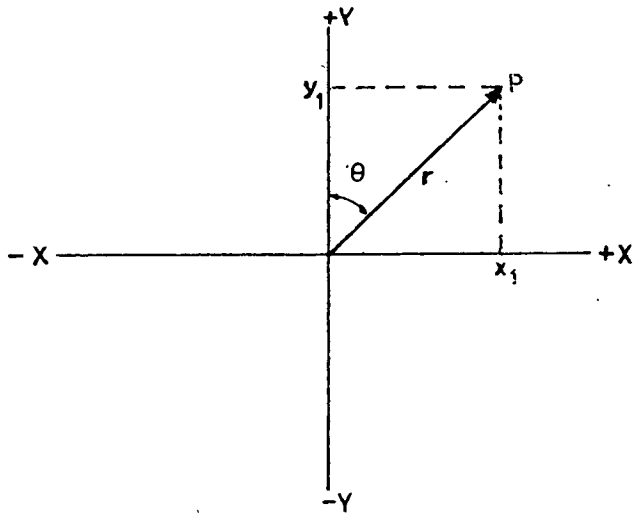
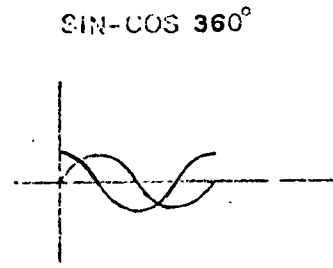


FIG. 6:1:30 POLAR DIAGRAM OF THE DISPLAY SCREEN



$$\frac{e}{E_1} = \sin \alpha$$

$$\frac{e_2}{E} = \cos \alpha$$

$$0^\circ \leq \alpha \leq 360^\circ$$

$$0^\circ \leq \theta \leq \theta_1$$

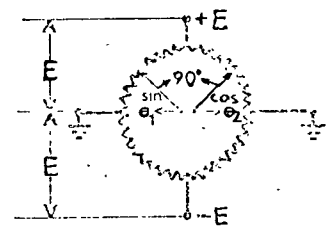
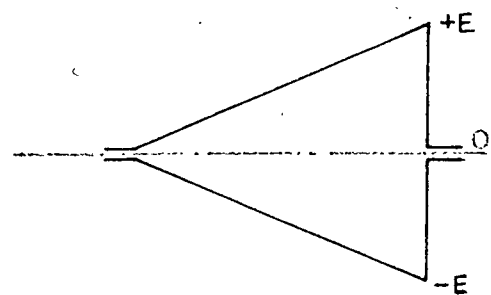
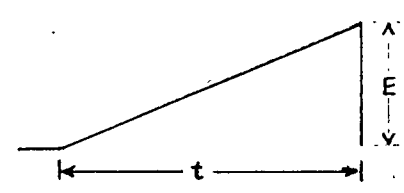


FIG. 6:1:32 SCHEMATIC DIAGRAM OF THE SINE/COSINE POTENTIOMETER



(A)
DUAL RAMP



(B)
LINEAR RAMP

FIG. 6:1:31 RAMPS REQUIRED FOR THE DISPLAY

terminal, as shown in Fig 6:1:32, the electron beam deflects from the centre of the screen to its periphery and rotates in sympathy with the rotation of the potentiometer for all four quadrants, ie $\theta = 0^\circ - 360^\circ$.

The above technique was adopted to display all reflections detected by the directional receiver of the ACDER system, rotating continuously in a borehole.

b Externally triggered dual ramp generator

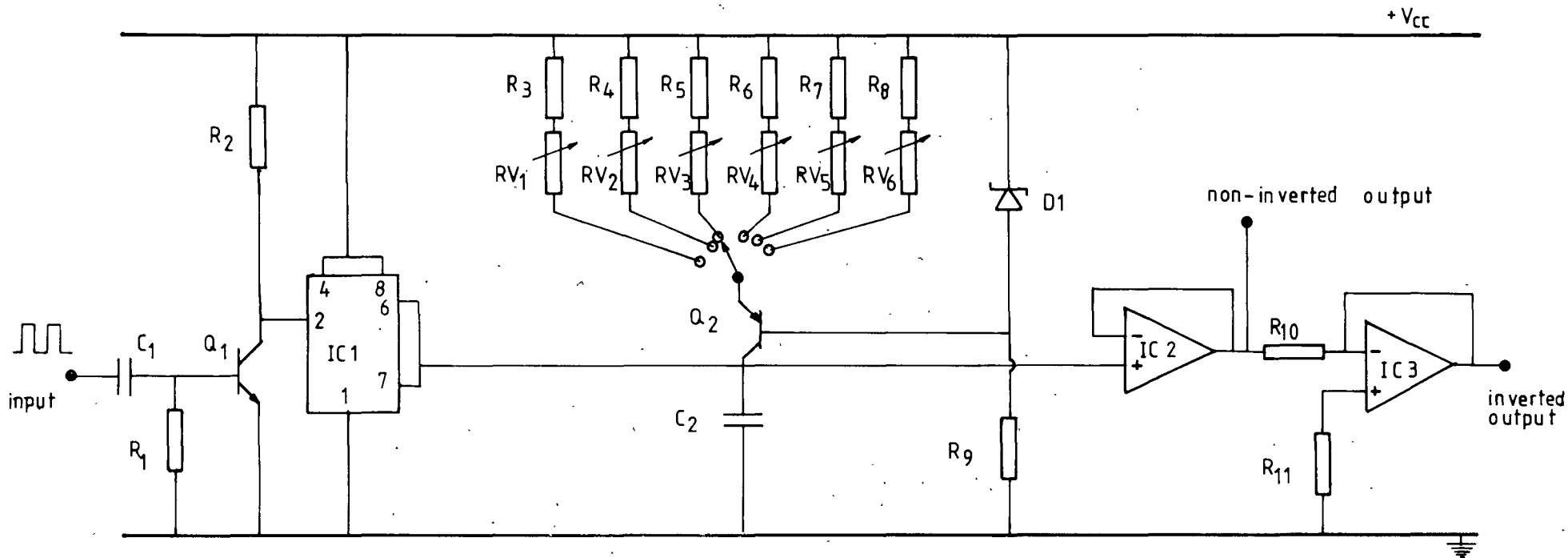
The need for the dual ramp to generate the display unit beam rotation was discussed in section 6:1:3a.

A Farnell pulse generator was used as a master pulse generator to trigger the ACDER system. The same output pulse was also applied to the input of the dual ramp generator circuit.

Fig 6:1:33 shows the dual ramp generating circuit. At the heart of the circuit is the CMOS version of the BIPOLAR 555 timer integrated circuit referred to as ICM 7555. The 7555 is used to initiate and terminate a triggered sweep. Normally the discharge FET (pin 7) is in the on position, and so C1 is shorted to ground. When a trigger is applied to the input, the collector of Q₂ momentarily goes low, which sets pin 7 of the 7555 into its off position. Q₁, R₁, R₂ and D₁ form the current generator that drives C1. Once the discharge FET has been turned off, the voltage on C1 rises linearly. When it reaches $\frac{2}{3} V_{CC}$, the threshold comparator sets the discharge FET into its on state, and so C1 is shorted to ground. IC1 is used to buffer the voltage on C1 to produce a positive going ramp, which the negative going ramp is generated by feeding the output of IC1 through an inverting amplifier using IC2, thus producing positive and negative going ramps with a single pulse input. The sweep generator is not retriggerable and is only initiated on fast positive going inputs. The sweep rate can be altered by varying C1 and/or R₂, but R₂ was found to be more practical.

The sweep time T relationship is given by

$$T = (V_{CC} \times \frac{2}{3} \times C1) / iC \quad - (6.15)$$



RESISTORS

- R1 = 10k Ohm
- R2 = 47k "
- R3 = 2.2k "
- R4 = 7.5k "
- R5 = 18k "
- R6 = 33k "
- R7 = 47k "
- R8 = 91k "
- R9 = 22k "
- R10 = 100k "
- R11 = 10k "

PRESETS

- RV₁ - RV₆ = 2k Ohm

CAPACITORS

- C1 = 0.1μF
- C2 = 0.1μF

TRANSISTORS

- Q1 = BC182L
- Q2 = BC212L
- D1 = BZY88 2V7

I.C.

- 1 = CMOS 7555
- 2 = 741 OP-AMP
- 3 = 741 OP-AMP

FIG. 6:1:33 CIRCUIT DIAGRAM OF DUAL-RAMP GENERATOR

where

$$iC = (2.7 - 0.7)/R_2 \quad - (6.16)$$

$$V_{CC} = 15 \text{ volt}$$

$$C1 = 0.1 \mu F$$

Seven selectable ranges of sweep time were selected, which were 2 mS, 5 mS, 10 mS, 15 mS, 20 mS, 50 mS and 100 mS, with theoretically calculated resistor (R_2) values (in kiloohms) of 4, 10, 20, 30, 40, 50 and 200 respectively. The actual resistors used (values in kiloohms) were 2.7, 7, 14.4, 21.8, 30 and 70 respectively, to obtain the sweep time of the ramp using the delayed time base facility of the Tektronix 7000 series storage oscilloscope. The difference between the theoretical and actual value of R_2 must be due to the leakage current of the capacitor, which was not included in the calculations.

Using 2.5 kms^{-1} as a typical velocity of the formation in question, each millisecond of sweep time represents 1.25 m of the travel path between source and target. Therefore 2 mS, 5 mS, 10 mS, 15 mS, 20 mS, 50 mS and 100 mS sweep time represents a target range radius of 2.5 m, 6.25 m, 12.5 m, 18.75 m, 25 m, 62.5 m and 80 m respectively.

6:1:4 The effect of a cylindrical obstruction/target on a propagating seismic pulse

The model tank set-up for studying the characteristics of a mini-sparker gave an opportunity to observe and possibly determine the relationship between the diameter of the obstruction/target and the output pressure pulse of a mini-sparker. Cylindrical shaped obstructions/targets were selected because they are easy to construct, and the physical construction of mines and tunnels could actually be regarded as cylindrical in shape.

a The effect of a cylindrical obstruction on a direct pulse between source and receiver

An experiment was carried out to investigate the effect of a cylindrical obstruction in the path of a seismic pulse propagating from a source to a receiver. Obstructions consisted of seven hollow plastic tubes with outside diameters as close to the various wavelengths selected as possible. The wavelengths selected for diameters were 0.25λ , 0.5λ , 0.80λ , 1.0λ , 2.0λ , 3.0λ and 4.0λ respectively. All the obstructions

were hollow, and therefore were filled with air to provide a maximum acoustic impedance mismatch between the water/air interface.

The source was a rigid plastic mini-sparker with a 23 mm outside diameter and a 19 mm inside diameter. The sparker was 5 cm long. The receiver was a 12.7 mm diameter small ball hydrophone.

The layout and instrumentation was similar to the experiments described earlier in section 6. The distance between source and receiver was 23 cm. The depth of the source and receiver was 18 cm from the water surface. They were both rigidly attached to the frame, as discussed earlier. All obstructions were positioned in the middle of the source and receiver in such a way that the centre of the source, obstruction and receiver were in a straight line. The electrical energy input into the mini-sparker was kept constant, at 0.56 joules (1500V, 0.5 μ F). All measurements were taken after the mini-sparker had been fired 15 times, to make sure that sparker energy output was consistent. The output frequency of the sparker was 70 kHz.

Obstructions were placed in turn between the source and receiver. The amplitude of the first negative going pulse and the peak to peak seismic pulse were measured. The results are tabulated, as shown in Table 6:4.

TABLE 6:4

Obstruction diameter (wavelength)	First negative peak (A) (mbar)	Peak to peak (B) (mbar)	Pressure ratio A (without obstruction)	Pressure ratio B (without obstruction)	Magnetic storage disk	Fig 4:1:38 trace
0	0.53	1.19	-	-	67/1	1
0.25	0.48	0.99	0.91	0.84	67/2	2
0.50	0.48	0.97	0.90	0.88	67/3	3
0.80	0.32	0.62	0.60	0.53	67/4	4
1.25	0.30	0.58	0.57	0.49	67/5	5
2.00	0.14	0.26	0.26	0.22	67/6	6
3.30	0.13	0.22	0.24	0.18	67/7	7
4.17	0.05	0.04	0.05	0.03	67/8	8

Fig 6:1:36 shows a graph of the first negative peak and the maximum peak to peak pressure pulse in mbar, plotted in wavelengths against the diameter of cylindrical obstructions.

The graph shows that both the first negative peak and the maximum peak to peak pressures diminish as the diameter of the obstruction increases. The first negative peak and the peak to peak pressure converges to almost the same amplitude as the diameter of the obstruction becomes greater than 4 .

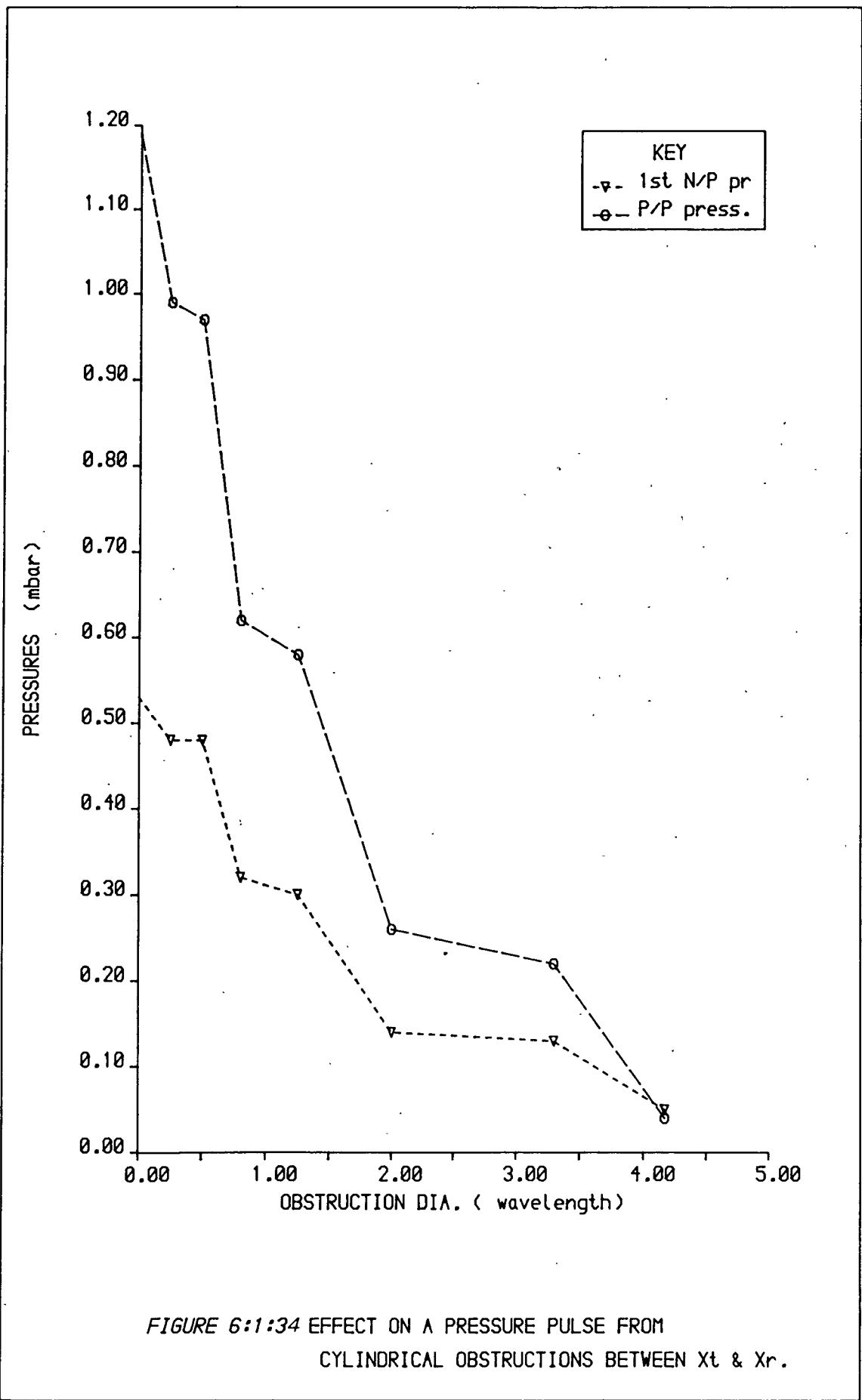
Fig 6:1:35 is the graph of the ratio of the negative peak pressure with obstruction divided by the negative peak pressure without obstruction, and gives a similar ratio for the peak to peak pressures. The graph shows that there is a reduction in amplitude of the first negative and peak to peak pressure pulse by approximately 10%, 40%, 75% and 95% for obstructions with a diameter of 0.5, 1.0, 2.0 and 4.25 wavelengths respectively. The waveforms associated with the above obstructions are shown in Fig 6:1:36.

The experiment shows that both the first negative peak and peak to peak pressure amplitudes are very sensitive to an obstruction in the path of a propagating pulse. The graph (Fig 6:1:35) also shows that there may be a constructive and destructive interference between the pressure pulse bypassing the obstruction and the pressure pulse reflected from the obstruction by a divergent wave (by the convex shape of the outside of the cylinder), giving a rather 'staircase' shape of decay of the pressure pulse rather than a smooth decaying response.

b Reflections from a cylindrical target using a mini-sparker source

An experiment was carried out to observe a possible reflected pulse from a cylindrical target. These targets consisted of seven hollow rigid plastic tubes of finite length, as described in the previous experiment (section 6:1:4a).

The layout of the source (mini-sparker), receiver (a 12.7 mm ball hydrophone) and target is shown in Fig 6:1:37. The distance between source and receiver was approximately 10 cm. The target was positioned



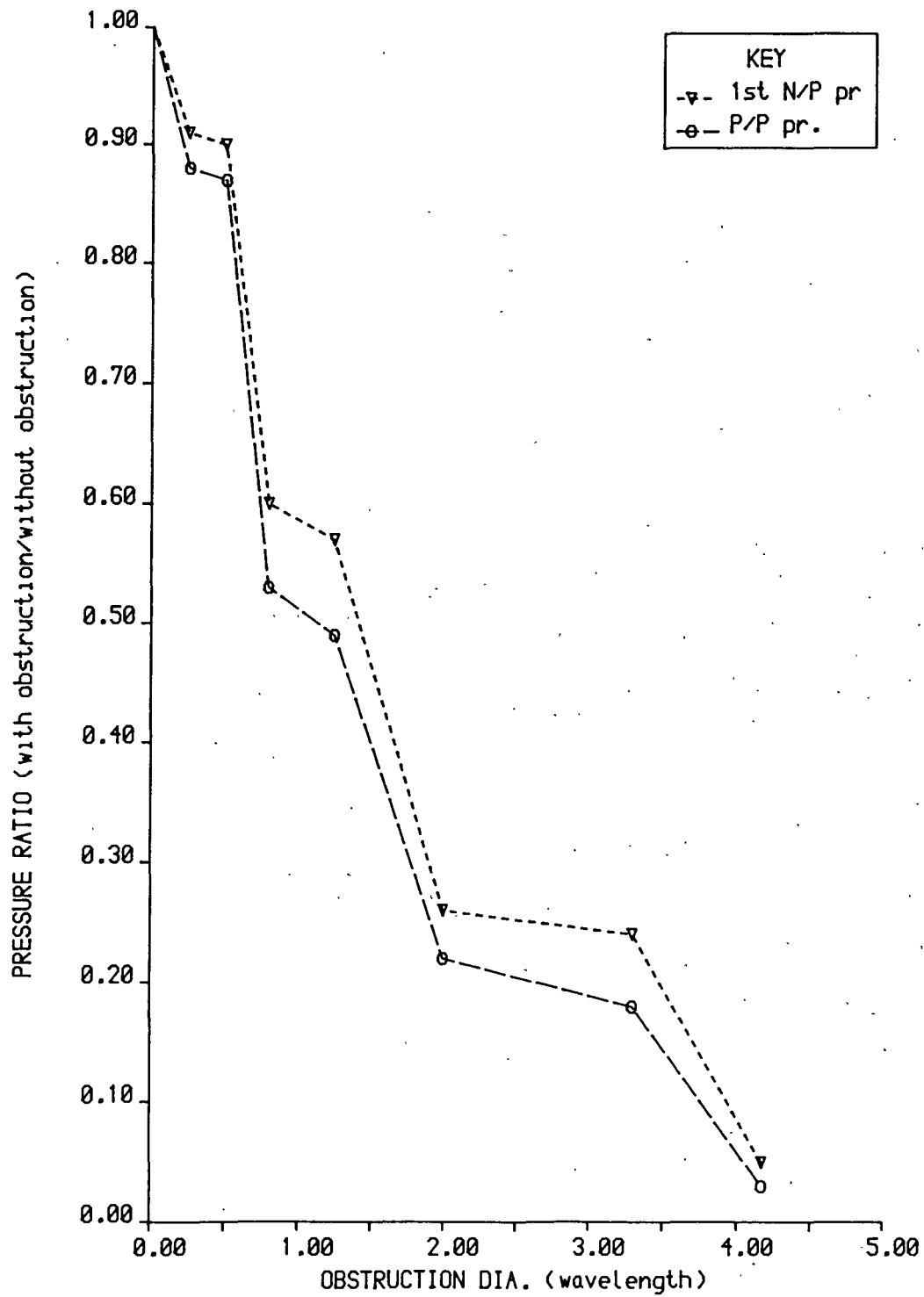
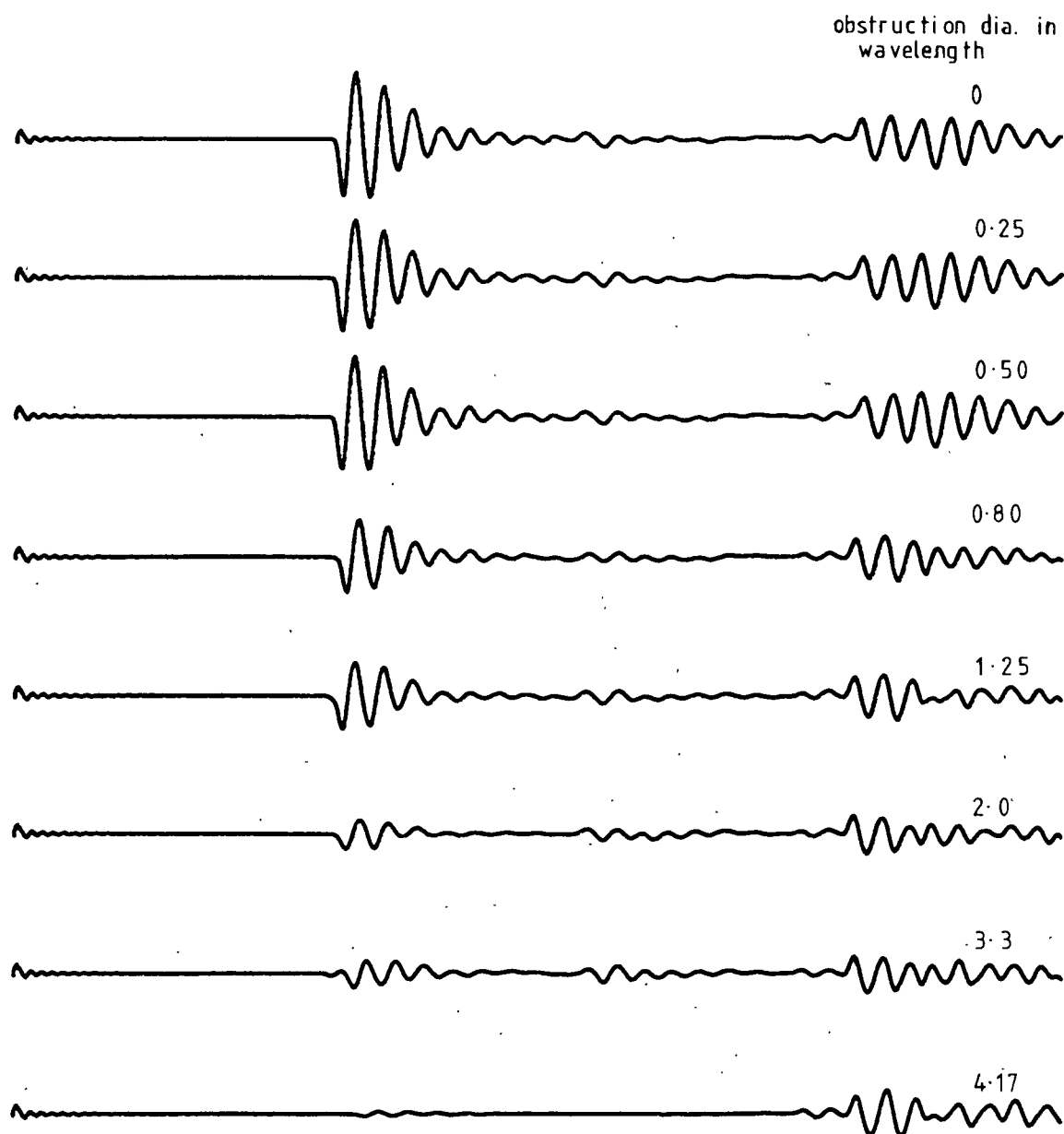


FIGURE 6.1.35 RATIO OF PRESSURES WITH OBSTRUCTION / WITHOUT OBSTRUCTION, FOR 1st N/P & P/P VALUES.



VERTICAL SCALE 1cm = 0.625 mbar

HORIZONTAL SCALE 1cm = 33.3 μ s

FIG. 6:1:36 EFFECT ON PRESSURE SIGNATURES FROM CYLINDRICAL
OBSTRUCTIONS BETWEEN X_t & X_r

about 21.5 cm from the source/receiver centre line, and all three units were positioned horizontally about 19 cm from the water surface. This was found to be the best position to obtain a fairly clean 100 mS span of waveform to observe any reflection.

The mini-sparker used was the 23 m outside diameter x 5 cm long rigid PVC housing, with 2 mm diameter x 12 mm long electrodes. The electrical energy input was 0.56 joules. Targets of varying size were positioned, and a waveform for each target was received. Fig 5:1:38 shows the wave train for eight cylindrical targets and one co-planar target, which consisted of a flat piece of wood (7.5 cm wide x 20 mm thick).

The reflection from the cylindrical target should arrive in the middle of the trace at about 288 mS from the beginning of the trace. The trace length is 150 mm, which represents 500 mS.

There is a slight indication of a possible reflector on the trace for a target diameter of 1.25 wavelength, but it does not become apparent until the target diameter increases to 3.3 times the wavelength. The bottom trace shows a reflection from a flat piece of wood: a piece of plywood 3.6 wavelength wide and approximately 1 cm thick. The reflection is quite apparent in the middle of the trace, and when compared with an equivalent cylindrical diameter target, it is clear that the energy reflected back from a convex surface is considerably less than that of a flat plane.

It may be possible to increase the amplitude of the reflector by increasing the output energy of the source, but it is apparent that a curved target such as a tunnel or mineshaft would be relatively difficult to detect using reflection techniques, compared with a co-planar target like a fault. The reflection from the flat sides of the tank can be seen towards the ends of the traces, which emphasise the point under discussion.

6:2 Borehole sparker source

Interborehole seismic measurements have been used by many authors (Bois et al, 1971, Ref 109; Bois et al, 1972, Ref 110; McCann et al, 1975, Ref 113; Auld, 1977, Ref 142; Hall et al, 1979, Ref 143; and Butler and

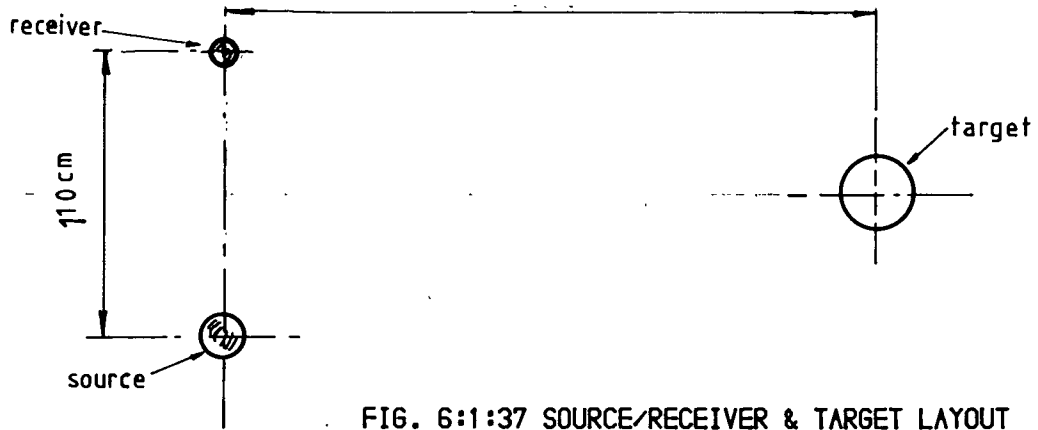


FIG. 6:1:37 SOURCE/RECEIVER & TARGET LAYOUT
TO OBSERVE REFLECTION

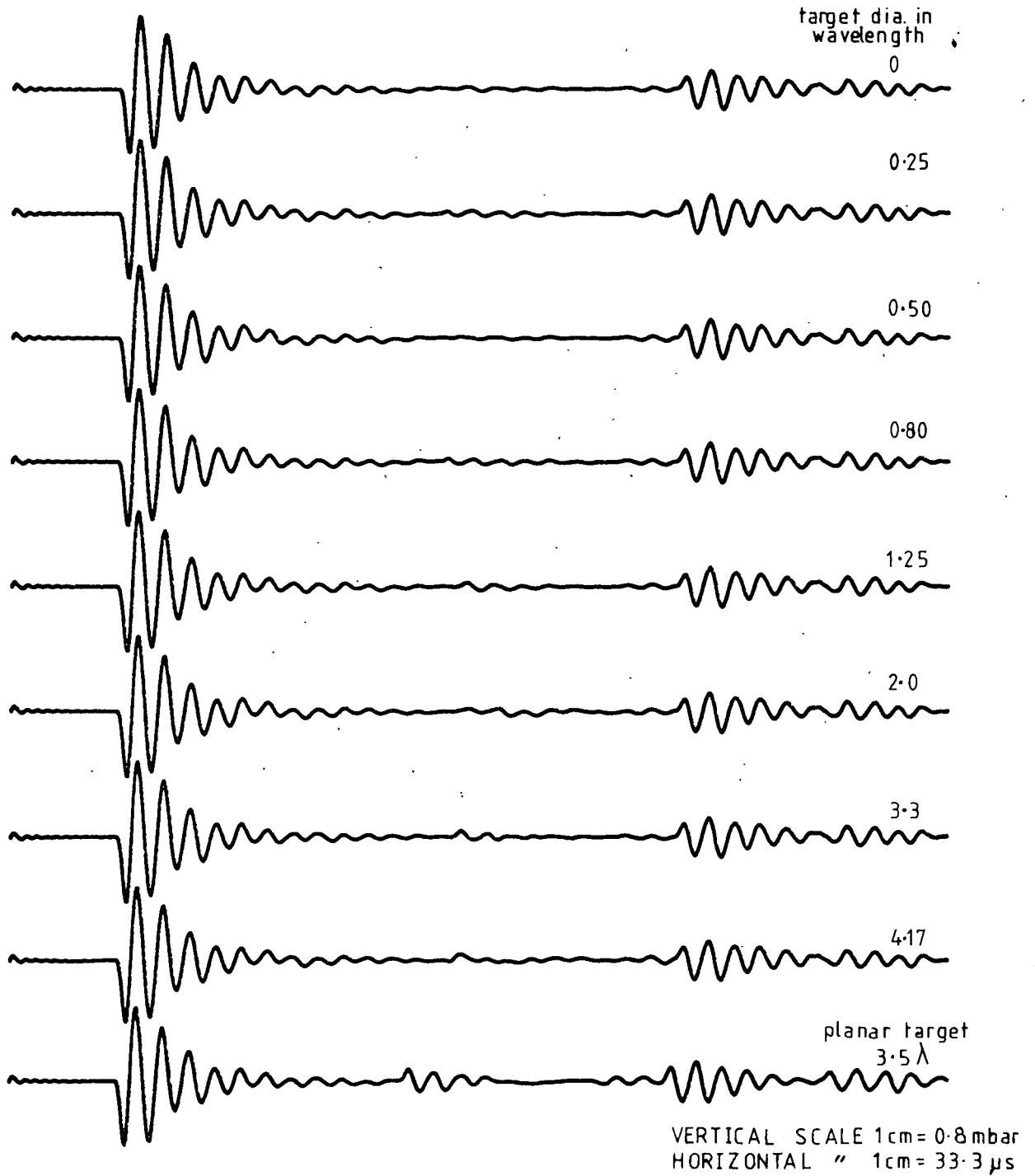


FIG. 6:1:38 PRESSURE SIGNATURES TO SHOW REFLECTIONS
FROM VARIOUS DIA. TARGETS

Curro, 1981, Ref 144) to determine elastic properties of the rock mass in the boreholes for civil engineering and other applications.

The use of a sparker as borehole tool was developed by McCann et al (1975; Ref 113). This consisted of a 7.5 cm internal diameter Duralumin tube of a length of 75 cm with two chambers, separated by a PVC plate. The lower chamber contained the electrolyte and the sparker electrode, while the upper chamber consisted of a high voltage cable termination in an air-tight inner PVC chamber.

The Duralumin sparker probe had been successfully used in many site investigations for civil engineering purposes, but the high stress generated by the expanding gas bubble within the lower chamber had produced quite a few failures of the probe, by either the shearing of the top or bottom end caps or leakage of the electrolyte into the PVC insulation in the upper chamber.

The output signature of a metal borehole sparker was found to be very complex, due to the various resonances in the chamber generated by the impulse pressure pulse of the expanding gas bubble.

Hall et al (1979; Ref 143) simplified the mechanical construction of the borehole sparker by using the standard RG 58A/V coaxial cable with an inner cage of perforated aluminium tube, to house electrode and sodium chloride solution. The entire assembly was enclosed in a bicycle tube and its ends sealed using hose clamps. Input energy to the sparker was quoted as 128-384 joules.

Although the borehole sparker designed by Hall et al (1979; Ref 143) appears to have produced the desired result, the use of the system for higher electrical energy input would have generated considerable losses in the cable. Exposure of the coaxial braid into the sparking chamber causes the saline solution to travel up the braid by capillary action, and was also assisted by the pressure built up in the chamber. This could create a dangerous hazard if the saline solution were to bridge the gap between high tension output and earth return.

There is no discussion in the paper by Hall et al (1979; Ref 143) on the output shape of the pulse from the sparker. The only trace which appears in the paper shows the signature through granite at a depth of 58 m and a source/receiver separation of 58 m. The signature displays a predominant wave period of approximately 0.25 ms.

The concept of the ACDER system makes use of reflection from the target to display discontinuities, and therefore a short seismic pulse would enhance the process of discrimination between direct pulse from the transmitter and received pulse from various targets. A borehole seismic source was developed to produce a pressure pulse spike during gas bubble expansion, and a damped output during bubble collapse. The sparker was identified as a high resolution borehole sparker probe, as the two mechanisms which generate the seismic pulse (ie, gas bubble expansion and collapse) can be identified on the sparker output signature. This was accomplished by development of the borehole sparker probe designed by McCann et al (1975; Ref 113).

6:2:1 High resolution sparker probe (HRSP)

Fig 6:2:1 is a simplified drawing of the high resolution sparker probe. It can be divided into four sections consisting of cable clamp assembly, high voltage chamber, spark chamber and pressure release end cap.

Heavy duty coaxial cable was used for transferring energy from the discharge capacitor to the spark chamber high voltage electrode. The HRSP was attached to the coaxial cable using a cable clamp. The inner core and insulation of the coaxial cable were terminated in the high voltage chamber, which consisted of a PVC insulator with 'O' rings to isolate the high voltage chamber from the spark chamber. The chamber was filled with transformer oil, to eliminate any high voltage arcing generated by the presence of damp air or moisture in the high voltage chamber.

The spark chamber consists of a cotton braid reinforced rubber tube housing enclosing a high voltage electrode and an earth return electrode. The spark chamber was filled with sodium chloride solution. The rubber tube was attached to the high voltage chamber using hose clamps and sealed at the bottom to a pressure release end cap with

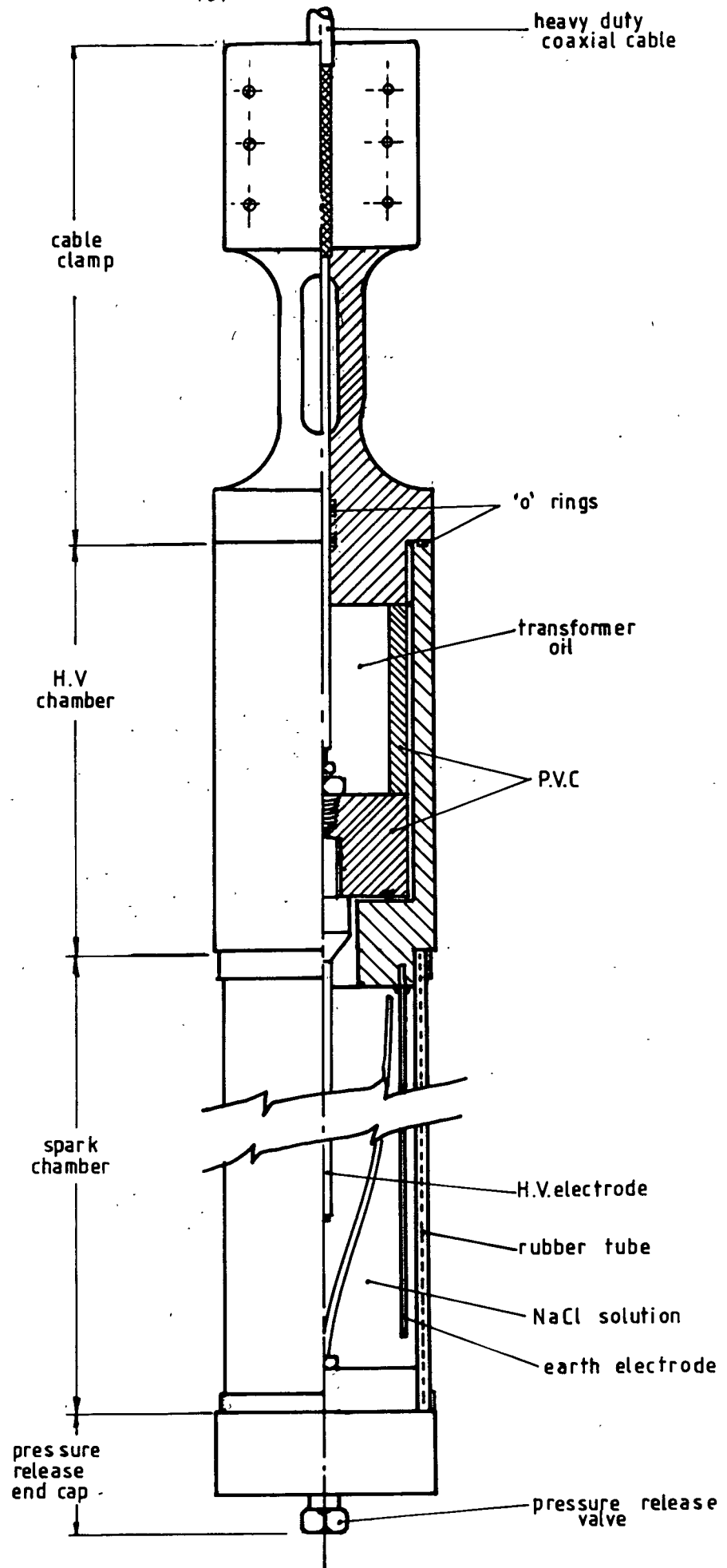


FIG. 6:2:1 H.R.S.P. BOREHOLE SOURCE

another hose clamp. The pressure release end cap contains a pressure release valve to prevent pressure build-up within the chamber during operation. The pressure release valve is attached to a thin nylon tube which is open at the top of the spark chamber, so that only residual gases and not electrolyte are expelled. This technique prolongs continuous use of the sparker over several days by not vacating the electrolyte from the chamber.

The HRSP (Fig 6:2:2) was developed in early 1976 and is very easy to assemble. It has been successfully used to a depth of 300 m for several days in mapping a geothermal reservoir (Ref 73).

The desired shape of the output pressure pulse was achieved by using a cotton braid reinforced rubber tube as a spark chamber. The chamber expands when a gas bubble is formed and contracts when the bubble collapses, without the continuous oscillation associated with metallic chamber resonance. The cotton braid acts as a damper to stop the chamber from oscillating when secondary bubble collapse occurs.

6:2:2 Free field measurements

Free field output signatures and borehole sparker directivity have always been unknown parameters, especially in diagonal scanning or in any other configuration where transmitter and receiver are not horizontally in line. In order to establish a sparker source free field signature and directivity pattern, free field measurements were carried out at sea in the Menai Straits off Anglesey.

Three sparkers were investigated for their directivity pattern and signature. Two sparkers were made of aluminium alloy, the first (large) with an outside diameter of 89 mm and the second (small) with an outside diameter of 70 mm. The third sparker (HRSP) had its spark chamber constructed from cotton reinforced rubber tube. Construction and operation of aluminium sparkers have been described by McCann et al (1975; Ref 113). Construction of HRSPs has already been discussed in section 6:2:1.

Sarker and receiver were suspended from the starboard side of the ship (Prince Madog) into sea water. The receiver consisted of a single

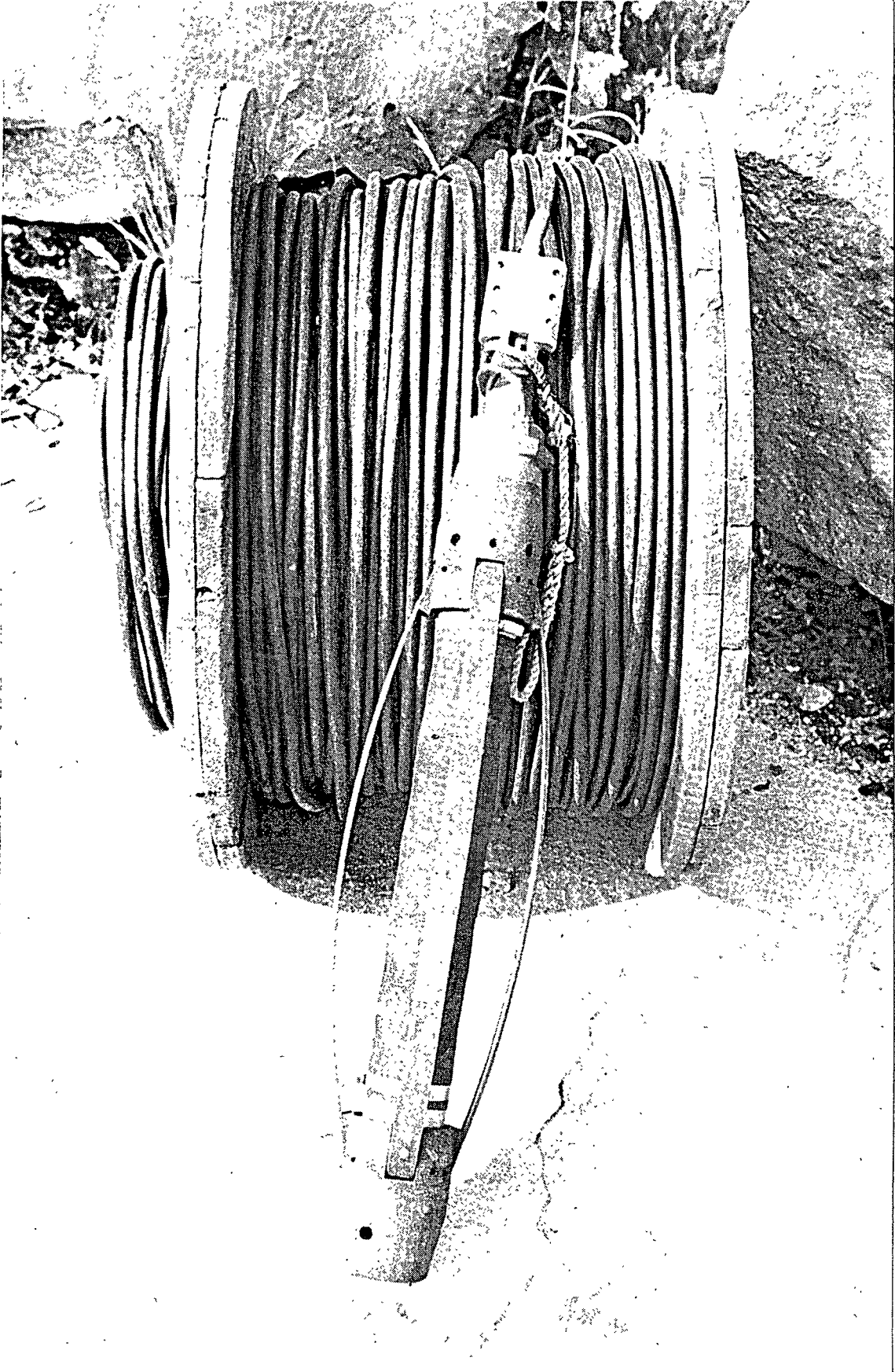


FIG. 6:2:5 H.R.S.P BOREHOLE SOURCE

omnidirectional ball hydrophone, with a directivity of up to 60 kHz in receiver mode. The ship was anchored in approximately 20 m of water. The sparker source was kept fixed at halfway depth between the water surface and sea bottom. The receiver was made to move past the sparker in steps of 1 m from sea surface to bottom. An attempt was made to keep the sparker source and hydrophone separated by about 5 m by tying a 5 m long rope with a loop at the end to the sparker source cable, and allowing the hydrophone cable to slide within this loop. Subsequent attempts to keep the source receiver vertical include suspending heavy lead weights on two separate ropes 5 m apart, and making source and receiver slide up and down on the weighted ropes.

For each position of the hydrophone, direct arrival was timed using the delayed time base facilities of a Tektronix oscilloscope, and a photograph was taken of the complete pulse train using a Polaroid camera. In the initial survey it was not possible to record any sparker signals on a magnetic tape recorder, as the sparker source emitted pulses in the region of 7 kHz, while the Fenlow tape recorder was limited to a bandwidth of 0-2.5 kHz. On subsequent surveys, however, a Racal Store 7DS tape recorder was used to overcome the above problems.

Fig 6:2:3 shows the four output pressure signatures of the two aluminium sparkers. Figs 6:2:3a and 6:2:3b represent the output pressure signature from the large aluminium sparker. Fig 6:2:3b shows an expanded time base trace of Fig 6:2:3a to emphasise the detail within the first pulse train. This was achieved using the delayed time base facility of the Tektronix oscilloscope. Figs 6:2:3c and 6:2:3d depict the output pressure signature of the smaller diameter aluminium sparker, displayed in the two time bases as described earlier.

The output signatures of both aluminium sparkers show complex waveforms. A possible explanation of complex waveform generation is discussed here. When electrical energy is discharged into sodium chloride solution within the chamber, an explosion is created which initially releases a primary gas bubble. The sharp expanding pressure pulse hits the spark chamber (housing) and sets the chamber resonating. The gas bubble then reaches its maximum size and begins to collapse, causing a negative going pressure, as shown by Kramer et al (1968; Ref 129). Interaction of the metal housing resonance and the pressure perturbations within the

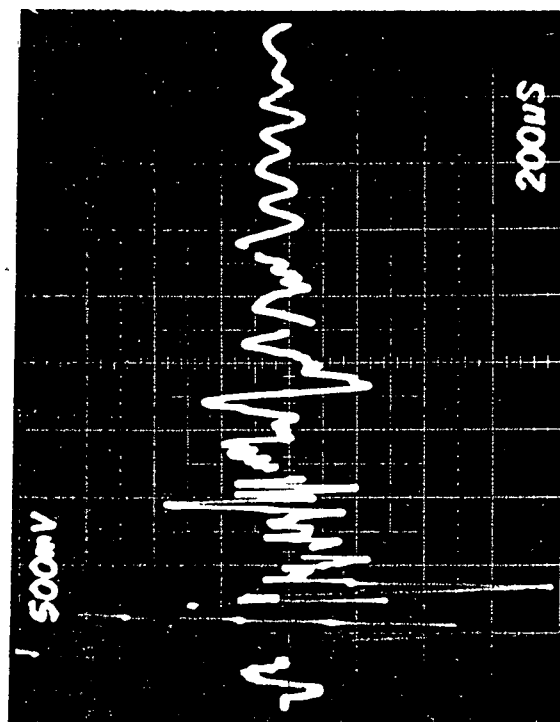
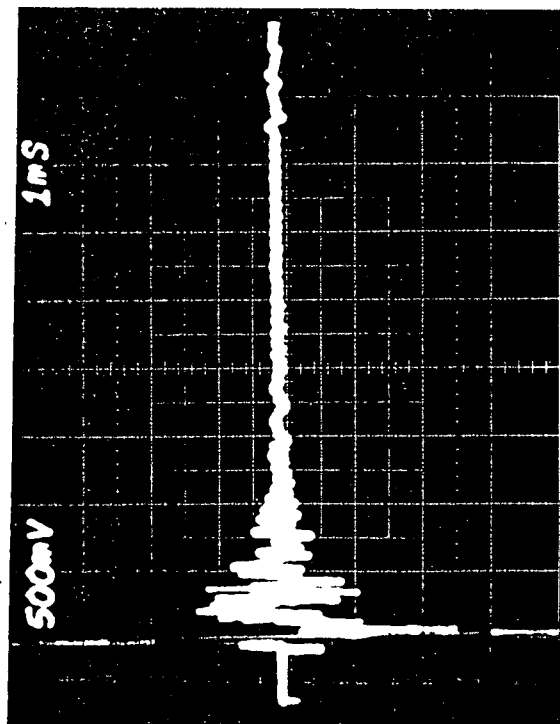
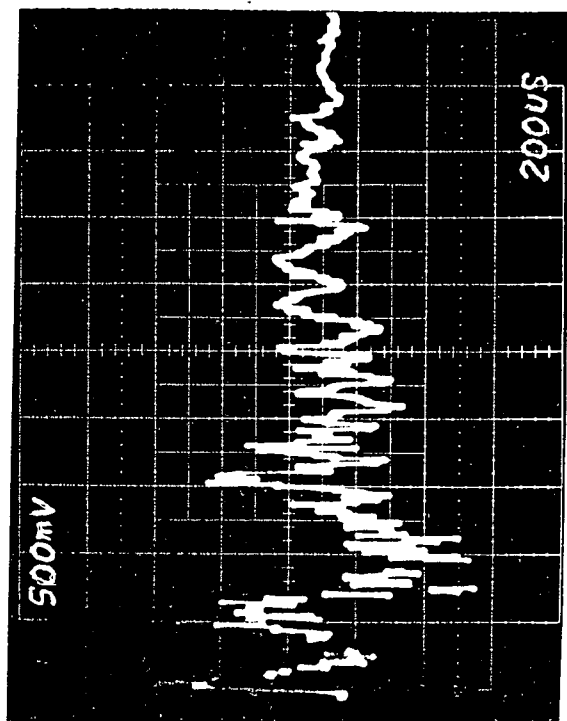
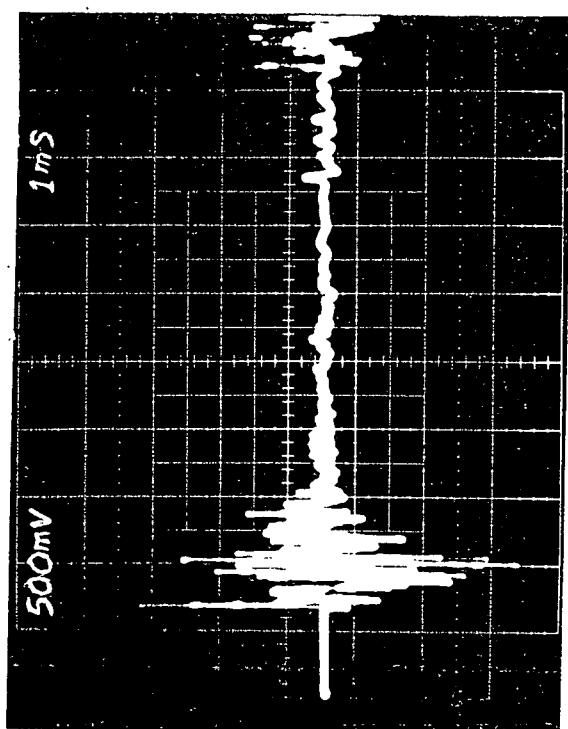


FIG. 6:2:3 OUTPUT SIGNATURES OF METAL SPARKERS

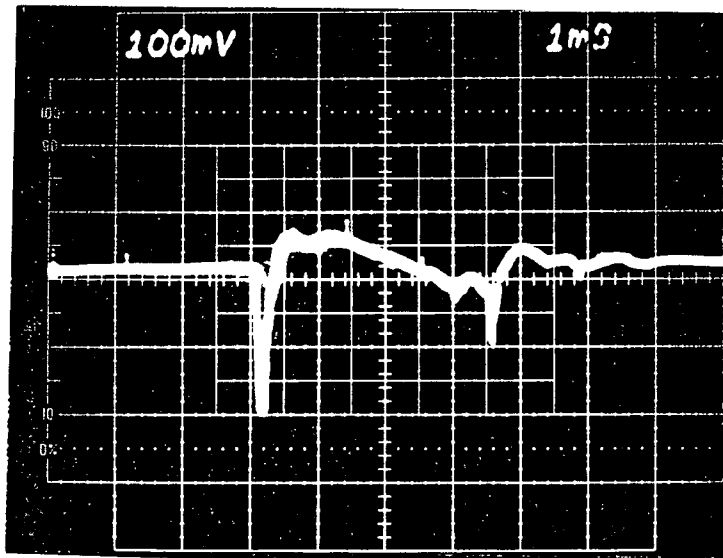
chamber results in a complex waveform, which is in effect a resultant displacement of the metal housing, generated by the metal housing resonance and the constructive/destructive effect of pressures generated within the chamber.

If the above postulation is correct, a borehole sparker source without a metal spark chamber should produce an output signature which is close to the true signature of a spark discharge source pressure pulse, as shown by Roi and Frolov (1961; Ref 137). This was evident from free field measurements of the output pressure signature from a high resolution sparker probe (HRSP), as shown in Figs 6:2:4a and 6:2:4b. Fig 6:2:4b is an expanded time base picture of Fig 6:2:4a. Fig 6:2:4a gives the compressive pressure pulse output of the HRSP, followed by the rarefaction effect due to collapse of the bubble. The expanded trace in Fig 6:1:4b shows the effect on output signature of pressure perturbations within the chamber, as the initial expansion of the chamber ceases and its contraction begins. Development of the spark chamber to provide a single predominant pressure spike output, as required by the ACDER system concept, has therefore been achieved.

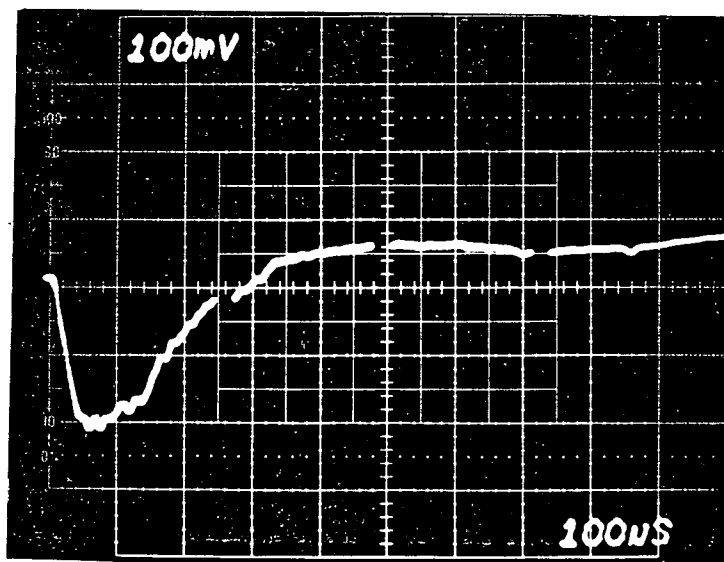
Spectral analysis was carried out on a time history of HRSP output to determine the predominant frequency. Fig 6:2:5a shows the HRSP output signature with three pressure pulse spikes. The first is a large negative going spike representing an expansion of the chamber, followed by a small in phase spike which represented the sea bottom reflection, and the last is a 180° phase reversed spike from the surface water/air interface.

The power spectrum of the pressure pulse of interest was carried out by windowing the time history in such a way so that only compression and rarefaction portions of the spike were present, as shown in Fig 6:2:5b. The power spectrum of the windowed pulse is shown in Fig 6:2:5c, and displays a predominant frequency of 570 Hz, representing the lower frequency output energy during the rarefaction stage, or chamber contraction. However, energy for the spark chamber expansion lies near 2000 Hz, which can be seen as a lobe near the main power spectrum.

Attempts to determine the directivity pattern of the three sparkers were less successful, since the source/receiver geometry did not lend itself



(A)



(B)

FIG. 6:2:4 OUTPUT SIGNATURES FROM HRSP SPARKER

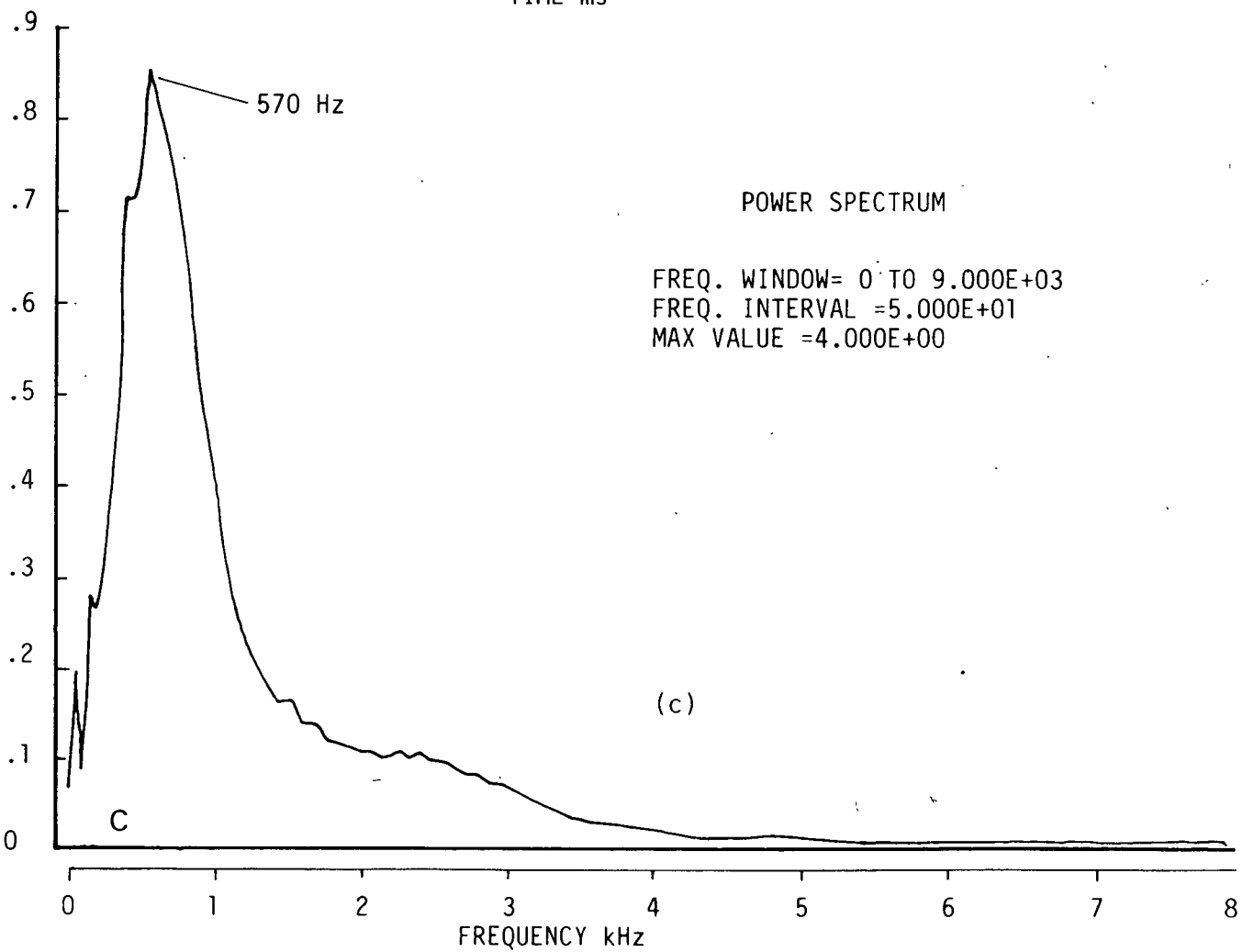
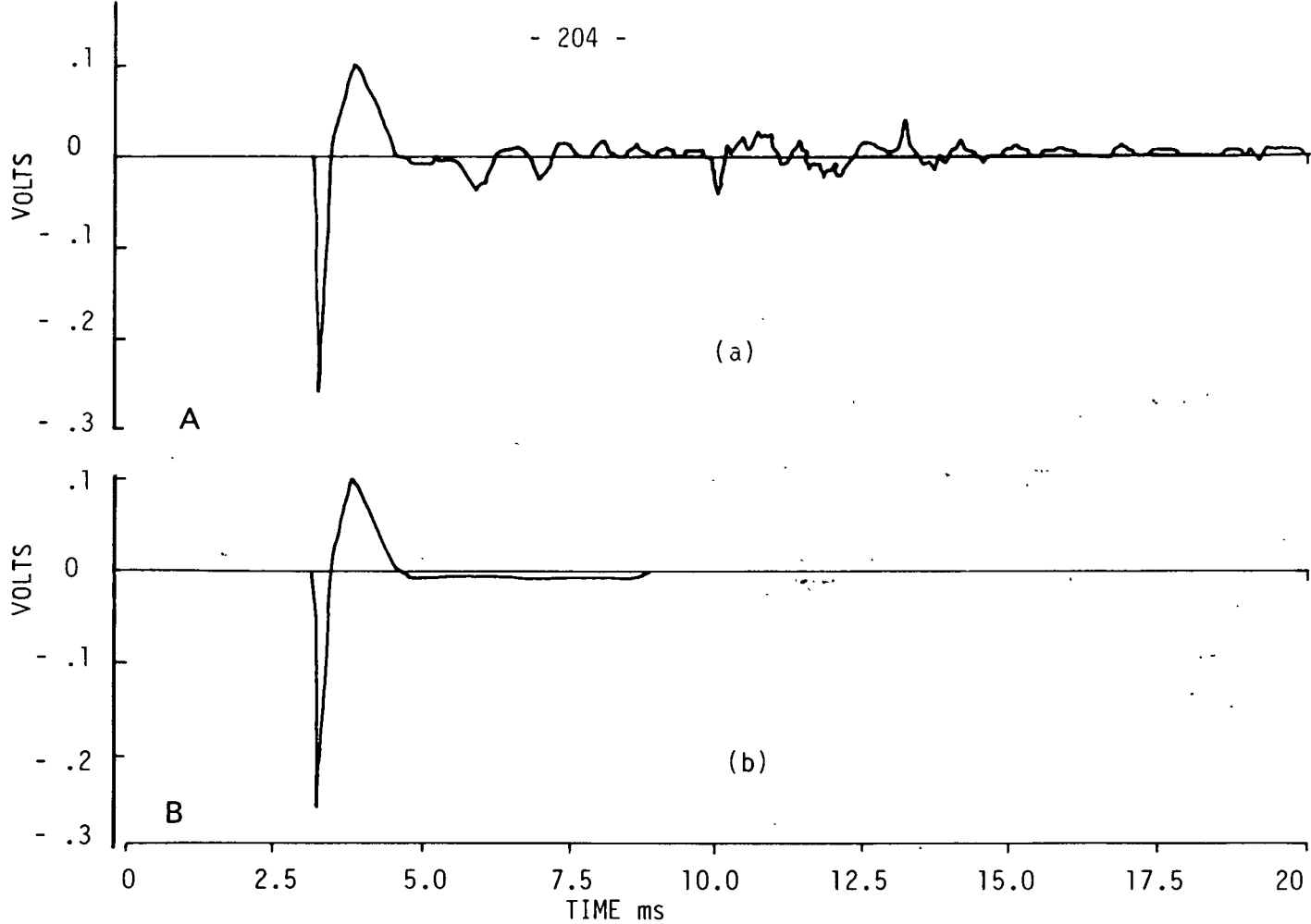


FIG. 6:2:5 TIME HISTORY & POWER SPECTRUM OF
HRSP BOREHOLE SOURCE

to total circular coverage of the source in the vertical direction. The source was kept stationary at about mid-depth between surface and sea bottom, while the receiver was made to move from surface to sea bottom on a vertical line parallel to the source axis. The distance between the vertical axis of source and receiver was approximately 5 m.

There were two basic problems. The first was the difficulty in keeping source and receiver axes vertical due to the incoming tide, which caused source and receiver to drift up to an angle of 45° from vertical. The second was that the depth was insufficient to obtain a complete 180° vertical coverage of the source. The angular coverage obtained for directivity measurements was between 120° and 140° . The increase in distance between source and receiver as they move apart to cover an angular increment has been compensated in the calculation, by using the spreading correction.

Figs 6:2:6, 6:2:7 and 6:2:8 show the directivity pattern of the large aluminium, small aluminium and HRSP borehole sparker sources respectively. These are only quantitative measurements due to the uncertainty discussed above. To obtain a more precise measurement of the directivity would require a deep artificial pool or deep lake, as discussed by Bobber (1970; Ref 132), and the appropriate mechanical framework to move the receiver in a 180° arc around the source, keeping the source/receiver distance constant.

Fig 6:2:6 shows that the directivity pattern for the large aluminium sparker is constant (within a few dB) for a measured angle of approximately 120° , ie 60° in the vertical direction from the horizontal centre line of the source.

Figs 6:2:7 and 6:2:8 show a similar trend as above, and the variations could be accounted for by the uncertainty of the source/receiver geometry.

It is reasonable to conclude that the directivity pattern is reasonably constant for a total angle of 120° in the vertical direction.

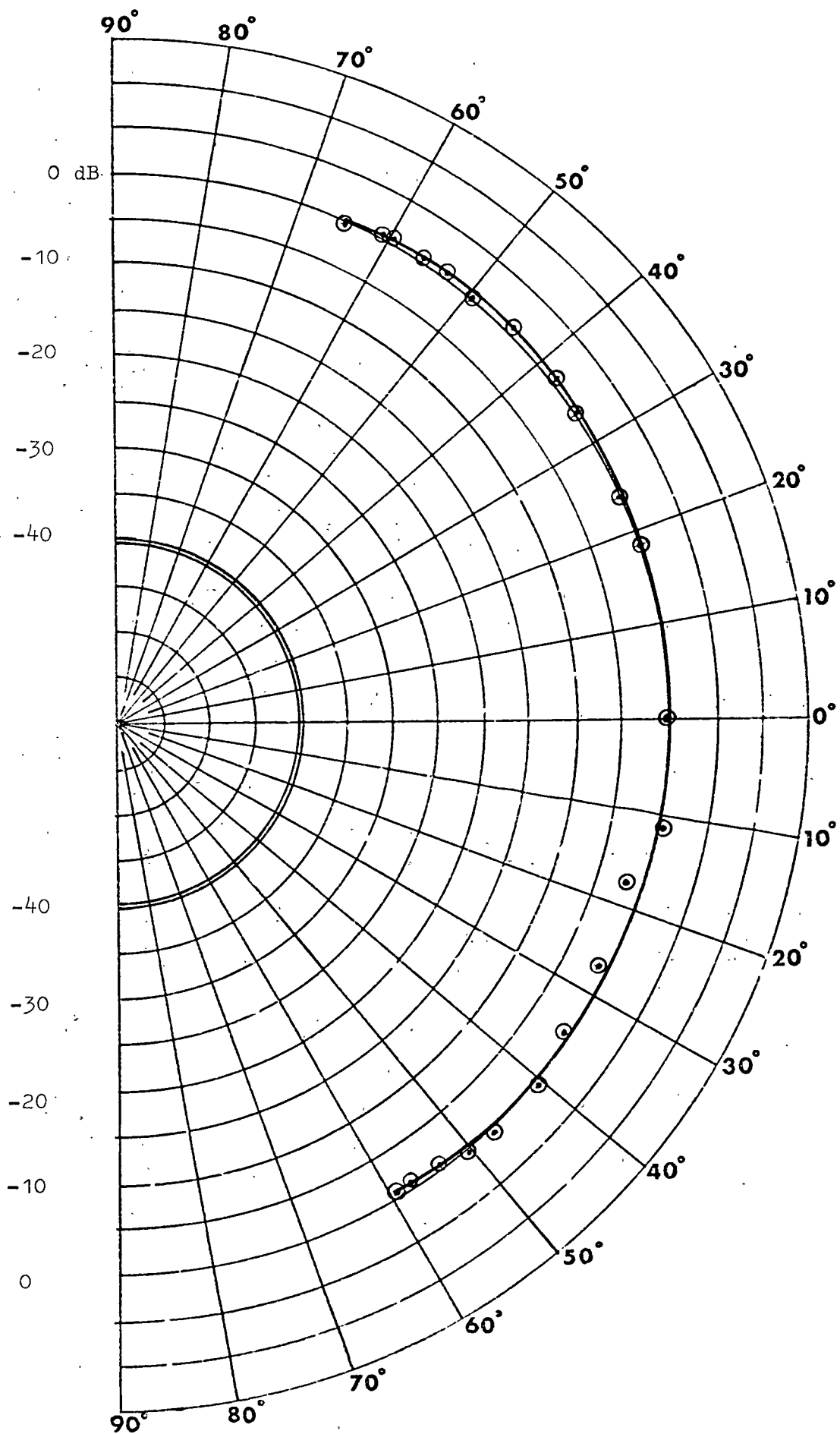


FIG. 6:2:6 DIRECTIVITY PATTERN OF THE LARGE METAL SPARKER

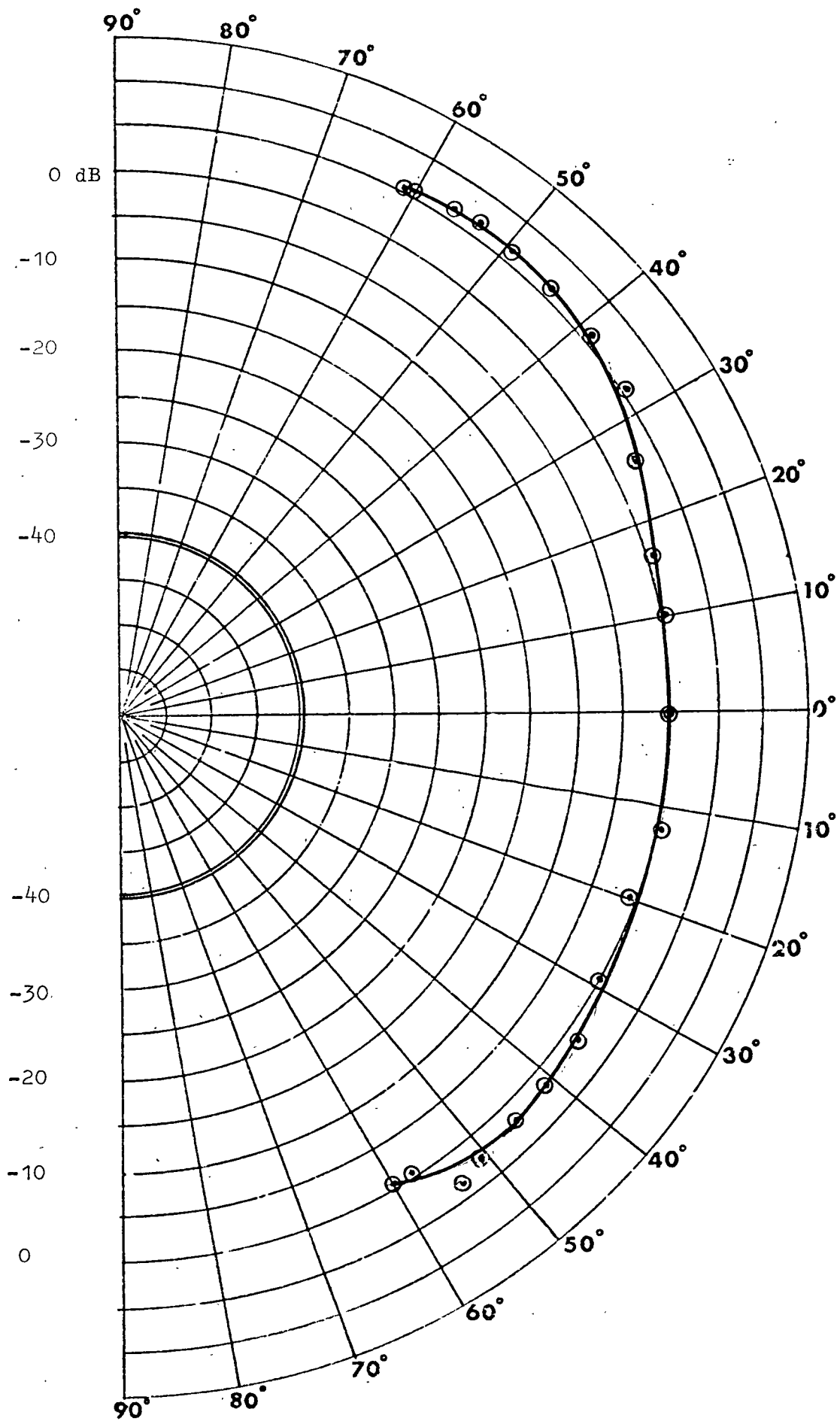


FIG. 6:2:7 DIRECTIVITY PATTERN OF THE SMALLER METAL SPARKER

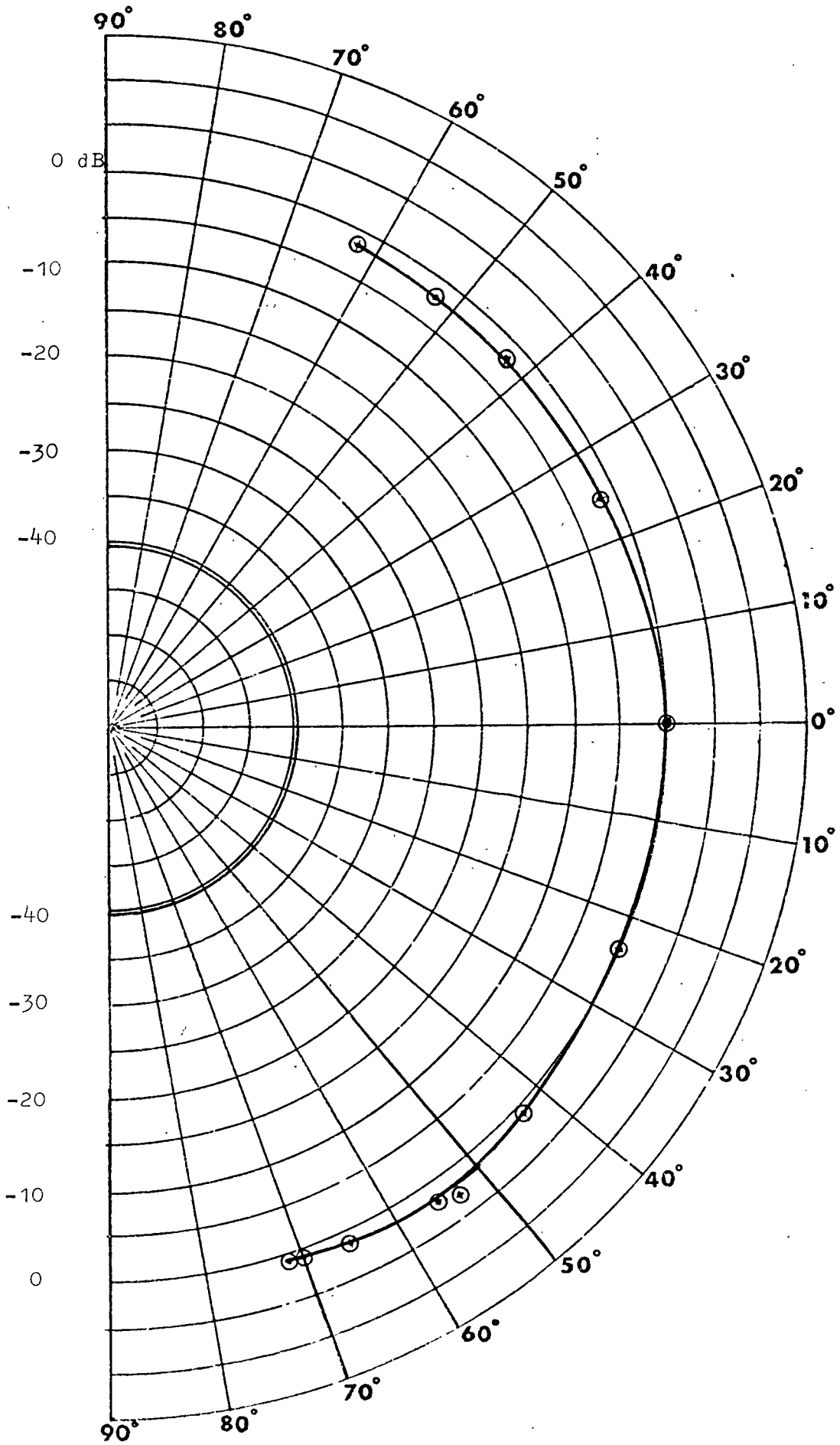


FIG. 6:2:8 DIRECTIVITY PATTERN OF THE HRSP SPARKER

6:2:3 Radiation patterns from a seismic source in a borehole

A rigorous treatment of the linear and non-linear interactions between waves generated from a seismic source in a fluid-filled borehole, induced borehole motions and radiation patterns is beyond the scope of this thesis. However, general consideration permits some statements to be made.

Free field radiation patterns from a HRSP borehole source were discussed earlier in the chapter, but the usefulness of the source depends on the far field seismic wave radiation patterns from a fluid-filled borehole. Other factors which may also influence the shape of the radiation pattern would include travelling tube waves inside the hole, which have been observed to generate a very high amplitude body wave in the surrounding medium when the tube wave is reflected at the bottom of a fluid-filled hole (White and Sengbush, 1963, Ref 145; Parrott, 1980, Ref 146).

Heelan (1953; Ref 147) discussed compressional (P) and shear (S) wave radiation patterns from an empty borehole, while White and Sengbush (Ref 145) formulated the effect of fluid in a borehole by combining Heelan's solution with an elementary tube wave propagating along a source hole. Ingram (1963; Ref 148) discussed the effect of waves due to a point-dilational source on the axis of a fluid-filled hole using contour and numerical integration. Peterson (1974; Ref 149) investigated elastic wave propagation from a point source located in a fluid-filled borehole. His main consideration was normal P wave propagation.

Lee and Balch (1982; Ref 150) carried out investigations into theoretical seismic wave radiations from a fluid-filled borehole. Far field radiation patterns for compressional and shear waves from a fluid-filled borehole in an infinite medium were constructed using low-frequency approximations. Two kinds of sources were considered: a volume displacement point source acting on the axis of a borehole and a uniform radial stress source acting on the walls of a borehole.

White (1965, Ref 14; 1983, Ref 151) has carried out extensive analytical work on seismic wave characteristics in boreholes, and in particular waves travelling along cylindrical boreholes.

Radiation patterns from a seismic source in a borehole were also investigated by Fehler and Pearson (1981; Ref 152), and their work is very similar to that dealing with seismic source operation, such as a sparker in a borehole. Far field radiation patterns for P and S waves, due to a seismic source located in a fluid-filled borehole, were calculated by initially assuming that the source caused a small increase in borehole diameter over some finite length along the borehole axis. The displacement field amplitude outside the borehole was obtained by Fehler and Pearson (1981; Ref 152) from the seismic moment tensor, M_{pq} , and the elastodynamic Green's function, G_{np} , using (Aki and Richards, 1980; Ref 153).

$$U_n = M_{pq} * G_{np,q} \quad - (6.17)$$

where U_n = displacement parallel to the nth coordinate axis, x_n
 $*$ = convolution operator
 $G_{np,q}$ = derivative of Green's function with respect to the x_q variable

Far field terms were evaluated by Aki and Richards (Ref 153) using the Green's function for an infinite, isotropic, homogeneous, elastic medium, from equation (6.11) as

$$U_n = (\gamma_n \gamma_p \gamma_q / 4 \rho a^2) (1/R) \dot{M}_{pq}(t-r/a) - (\gamma_n \gamma_p - \delta_{np} / 4 \pi \rho \beta^2) (\gamma_q / R) \dot{M}_{pq}(t-r/\beta) \quad - (6.18)$$

where λ_i = directional cosines of line joining source and receiver location
 a = P wave velocities
 β = S wave velocities
 ρ = rock density
 R = distance between source and receiver

The first term in equation (6.18) represents the P wave and the second term represents the S wave.

Fehler and Pearson (Ref 152) have used the above equation to derive a radiation pattern for P and S waves. The amplitude of the radiated compressional wave was defined by

$$A_p(\Phi, R) = K_p/R \left\{ (\gamma + \mu) - \cos^2\Phi \right\} e^{-(\pi f R / Q_p V_p)} \quad - (6.19)$$

and the shear wave amplitude by

$$A_s(\Phi, R) = (K_s/R) \sin\theta \cos\theta e^{-(\pi f R / Q_s V_s)} \quad - (6.20)$$

where

- A_p, A_s = amplitudes of compressional and shear waves at distance R from the borehole
 Φ = angle between borehole axis and line joining source and receiver
 K_p, K_s = constants depending only on source parameters
 μ, λ = elastic Lamé parameters
 Q = seismic quality factor
 f = frequency
 V = propagation velocity

From the field study, Fehler and Pearson (Ref 152) concluded that P and S wave amplitudes from borehole seismic sources are related to the source receiver distance R and the dip of the ray path measured from the wellbore axis by

$$A_p \sim (2 - \cos^2\Phi) / R e^{-(\pi f R / Q_p V_p)} \quad - (6.21)$$

$$A_s \sim (\sin\Phi \cos\Phi) / R e^{-(\pi f R / Q_s V_s)} \quad - (6.22)$$

The computed radiation pattern and field measurements are shown in Fig 6:2:9. The figure shows that the radiation pattern for a P wave source in a vertical borehole was horizontal in direction, while that of the shear wave was polarised approximately at 45° to the axis of the borehole. This shows that a sparker operating in a vertical borehole would have a radiation pattern which is predominantly normal to the axis of the borehole with higher attenuation towards the axis of the borehole.

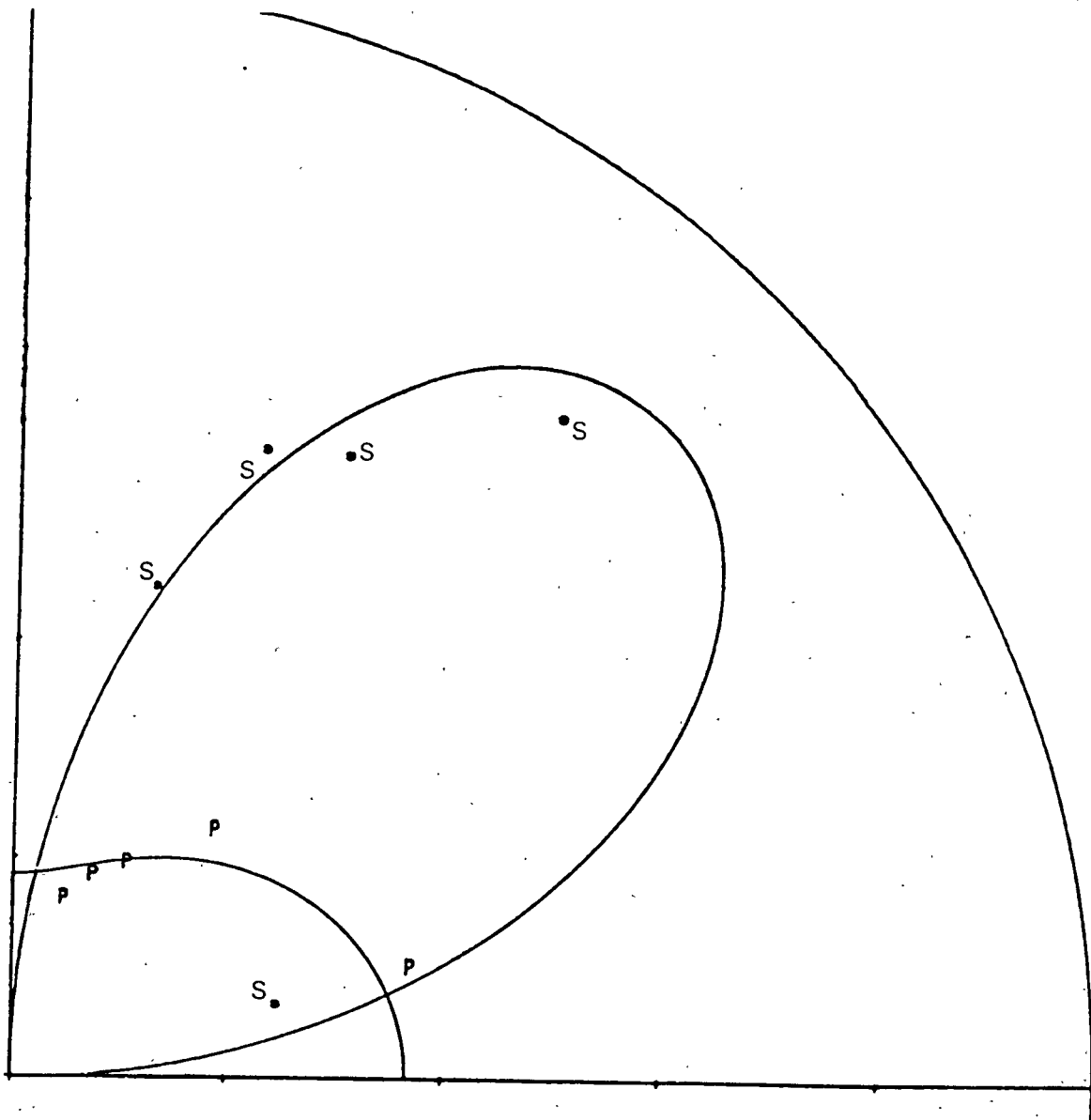


Figure 6:2:9 Amplitudes of P and S waves due to small explosions in one borehole as measured in a neighboring borehole. Amplitudes have been corrected for geometrical spreading ($1/R$). Solids lines represent angular dependence of radiation pattern predicted by eqns. 6.19 and 6.20 without anelastic losses. (After Fehler and Pearson, 1981; Ref 152)

6:3 Field trial of the single hole method

After initial development of the ACDER system, a field trial was carried out in December 1979 to assess the system and other problems associated with the practical use of the concept. The field assessment was carried out at a test site located on a Ministry of Defence firing range at Tidmoor Point, East Fleet, Dorset. The site has been used in the past by the British Geological Survey and the Department of Physical Oceanography, University College of North Wales, for geophysical surveys.

The proposal was to simulate a vertical tunnel as a target for the ACDER system by drilling a large borehole and casing it with a rigid PVC liner (38 cm diameter), sealed at both ends. Various other shallow boreholes were drilled adjacent to the large one in order to deploy the ACDER borehole probe and assess its performance.

6:3:1 Geology and borehole configuration

The geology near the test site at East Fleet consists of Oxford Clay outcropping, which forms part of the Weymouth anticline. It is estimated that Oxford Clay reaches a maximum thickness of 150 m in the Dorset region. Oxford Clay is relatively homogeneous in character, although the sequence is occasionally interrupted by thin, localised fossil bands. Davis (1982; Ref 154) mentions that X-ray diffraction indicates a clay mineral content of predominantly hydrous mica, together with a large amount of chlorite and a lesser quantity of quartz and calcite. Davis (1982; Ref 154) also states that Oxford Clay is heavily overconsolidated, as formerly it was buried below several tens of metres of overburden which, combined with tectonic activity, has produced structural features such as fissures, minor faults, etc, and contributes to in situ bulk sediment properties.

The geometrical layout of the boreholes is shown in Fig 6:3:1. The largest borehole attainable in the centre of the borehole layout acts as the target area. It was cased using 5 m long by 38 cm (15 in) outside diameter rigid PVC pipe.

A total of fourteen other boreholes were drilled to a depth of

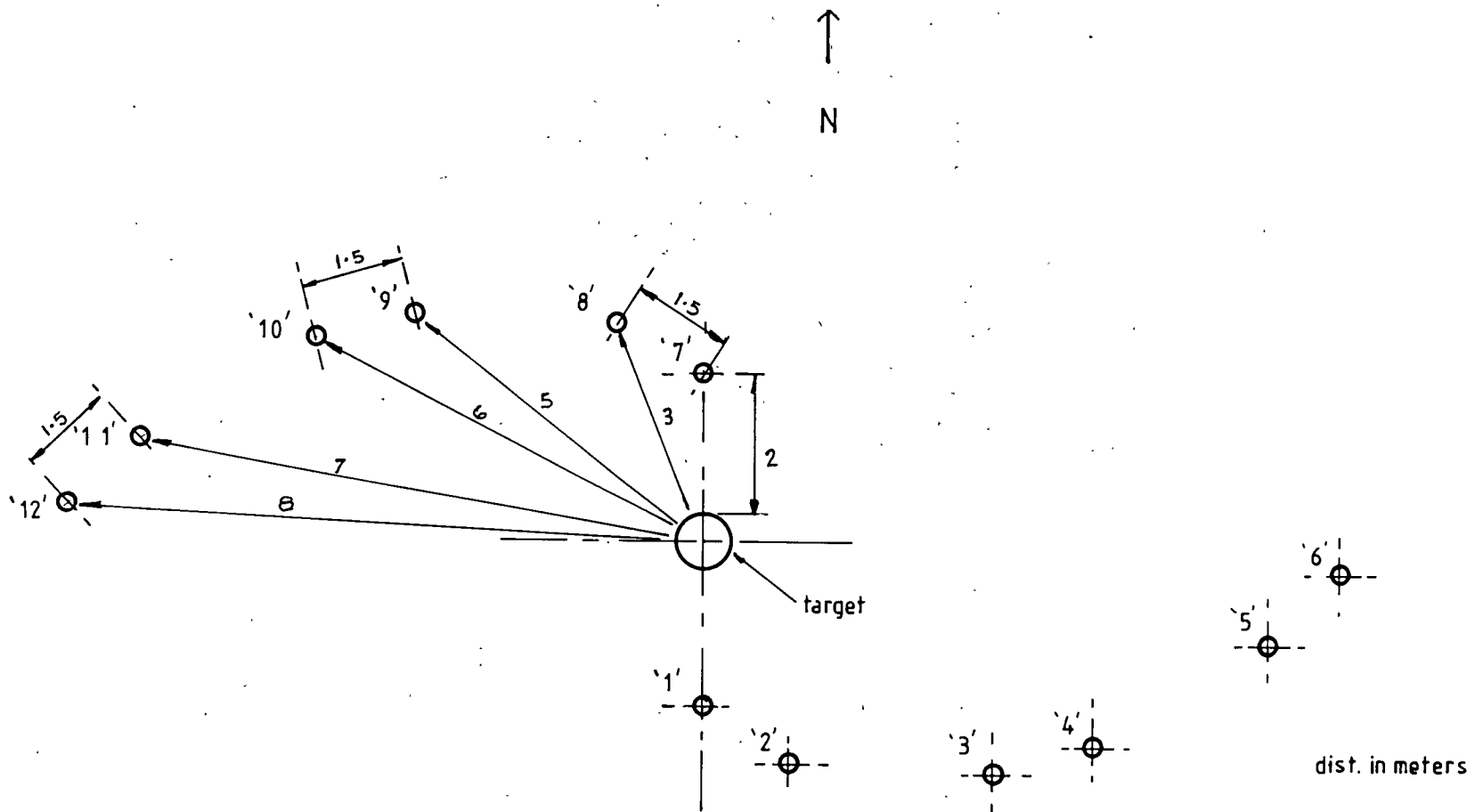


FIG. 6:3:1 EAST FLEET SURVEY - BOREHOLE LAYOUT

approximately 5 m depth and lined with 10 cm internal diameter rigid PVC casing. These boreholes were used to deploy the seismic source and receivers. The borehole layout was planned to provide an increasing distance between the large borehole and each subsequent 10 cm diameter borehole. Increasing the distance between a pair of boreholes and the target provides a useful source/receiver geometry to verify reflecting pulses from the target. The water table was just over a half metre below the surface.

6:3:2 In-situ compressional wave velocity structure

In order to be able to identify reflections from the target, the in situ compressional wave velocity structure was measured. This was done using a brass mini-sparker as a source. On this occasion a thyatron capacitor discharge unit was used to deliver 2.25 J (3kV, 0.5 μ F) of electrical energy into the mini-sparker. A 2.54 cm ball hydrophone with a resonant frequency of 80 kHz was used as the receiver. Signals were fed into a Kemo filter with the bandwidth limited to 1-20 kHz, and a gain of x 10.

Velocity scans were carried out between boreholes 5 to 6 and 5 to 4, with the source in borehole 5. Measurements were taken at 0.25 m intervals, with both source and receiver moving up from the bottom of the boreholes in parallel. Fig 6:3:2 shows the velocity profile for scans between boreholes 5 and 6 and 5 and 4 respectively. The velocity profile for the two scans appears to vary as much as 100 m/s at similar depths. This may be associated with the uncertainty in the position of the source and receiver in the borehole and the measured distance between the boreholes.

Initially the velocity appears to decrease slightly with an increase in the depth, showing a minimum at depths between 3 m and 3.5 m. The velocities increases on average with the increase in depth. The velocity measurements obtained in scan 5 to 4 were used for most of the calculations associated with assessing the possible position of the reflected pulse on the received wave form.

6:3:3 Field trial of the ACDER system

The detailed working of the ACDER system has been discussed earlier in

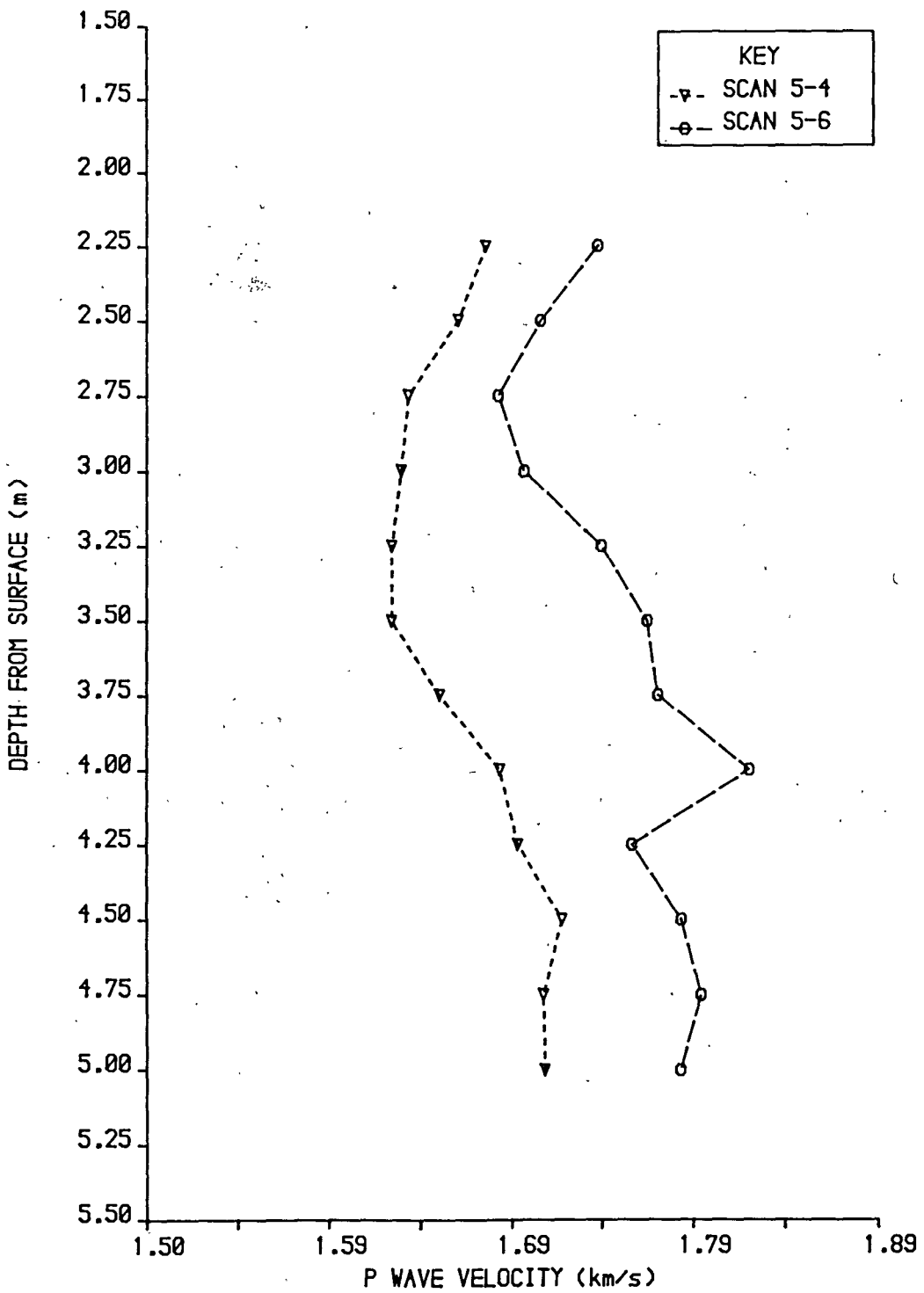


FIGURE 6:3:2 EAST FLEET SURVEY - P WAVE VELOCITY
SCANS 5-4 AND 5-6

this chapter but a summary is given here to assist in the understanding in its operation in the field.

Initially, both HRSP source and ACDER borehole sonde were deployed in a single borehole, but this arrangement was found to be impractical due to the shallowness of the borehole (only 5 m deep). Subsequently, two adjacent boreholes were used to deploy source and receiver.

The HRSP source was deployed in borehole 3, with the ACDER probe in borehole 4, at an approximate depth of 4 m. The system was assembled and wired as shown in the block diagram in Fig 6:3:3. A master pulse generator produces a 10V pulse, which is applied simultaneously to a capacitor bank, a stepper motor control circuit and a c.r.t. control box. With the application of a pulse, a capacitor bank was discharged through the sodium chloride solution in the HRSP to generate a shock wave.

When the master pulse is applied to the stepper motor control unit, it advances the stepper motor in the ACDER sonde by one step and thus rotates the directional receiver through 0.48° . At the same time a pair of ramps (one positive, one negative) are generated and fed to the sine/cosine potentiometer in the ACDER sonde. The period of the ramp determines the range of the scan.

The output from the sine/cosine potentiometer is buffered and fed into the X and Y inputs of a Tektronix storage oscilloscope. The electron beam of the oscilloscope is positioned in the centre of the screen. X and Y gains on the oscilloscope were set at the same level, in such a way that when ramps are applied to the input, the beam moves from the centre of the screen to its periphery.

Signals received on the directional receiver were transmitted to the surface through a set of slip rings, filtered through a Kemo filter, amplified, buffered and then fed into the Z modulation of the Tektronix storage oscilloscope. The beam's brilliance control is reduced in such a way that a bright spot only appeared on the screen when a seismic signal was present.

After setting up the ACDER system as described above, surveys were

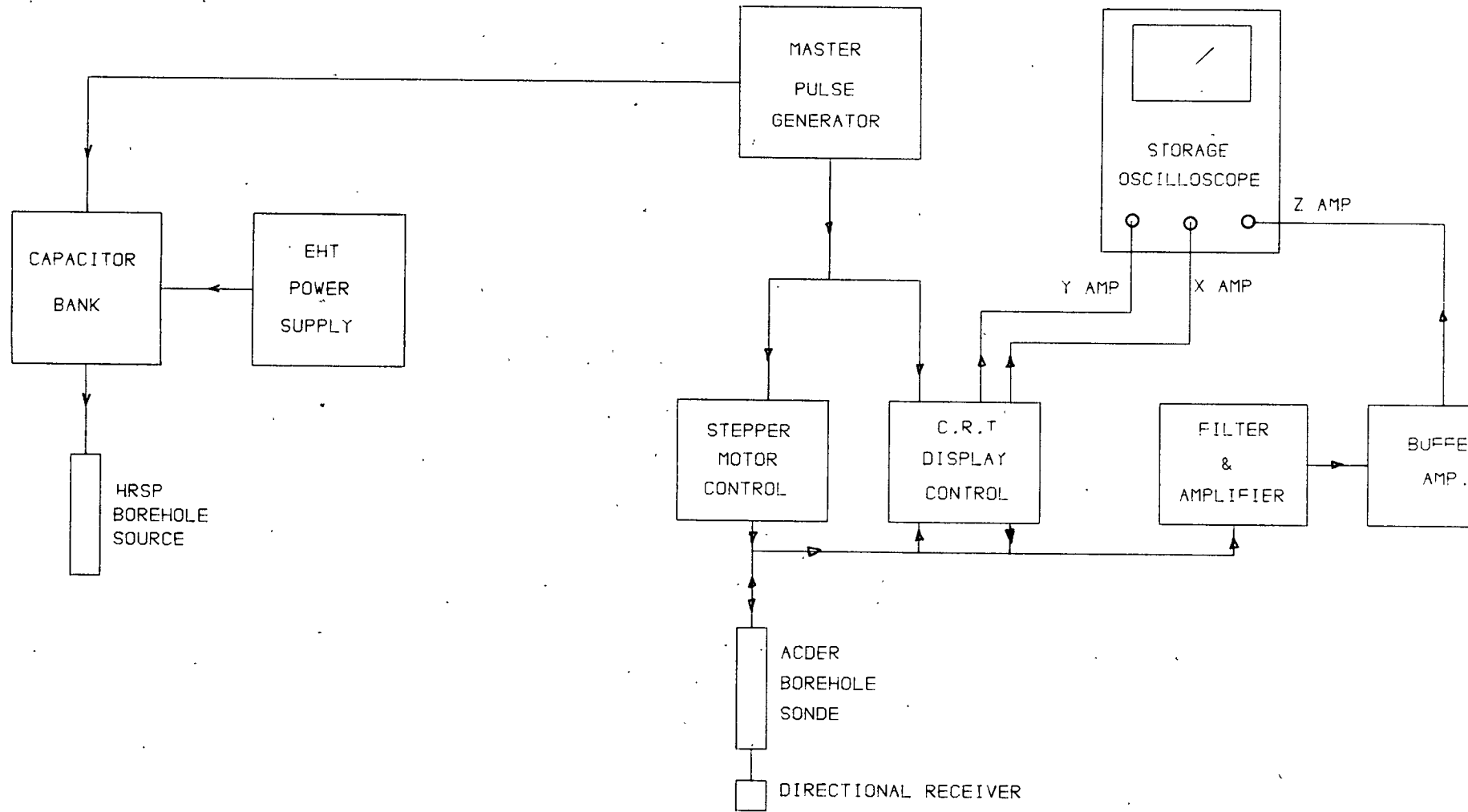


FIG. 6:3:3 BLOCK DIAGRAM OF THE FIELD ACDER SYSTEM

carried out using a pair of adjacent boreholes. Results showed that there were no identifiable reflections from the target, and that the receiver acted omnidirectionally for the wavelengths being propagated. This was further emphasised when the first arrival from the borehole sparker was displayed on the oscilloscope screen as a thick bright circular band instead of just a short bright line, when the directional receiver was facing the source. Field trial of the ACDER system was abandoned because of poor directivity of the receiver sonde and the operation difficulty in making the electronic equipment function reliably in the continuous heavy rain. The above harsh conditions caused the magnetic tape recorder to malfunction and record intermittently. The data presented below are from the field log book and Polaroid photographs.

6:3:4 Interborehole measurements

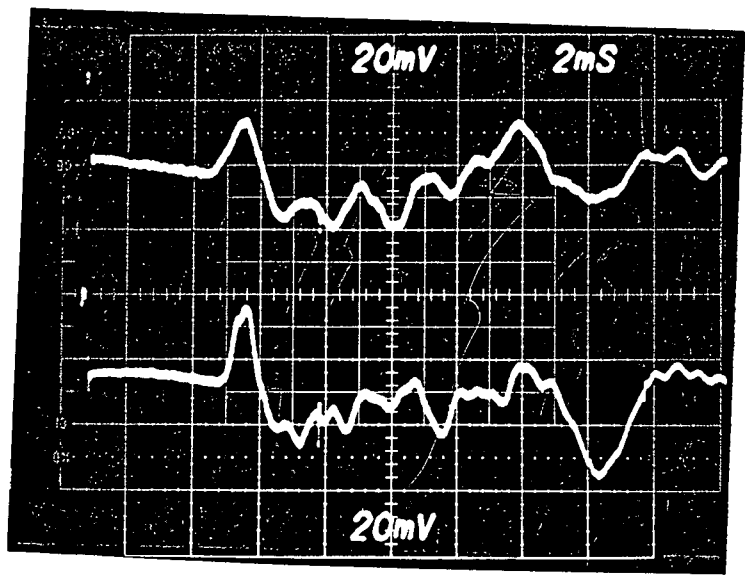
Seismic measurements were carried out using the interborehole method to observe the presence of the large PVC pipe on the amplitude of a direct pulse and to identify a possible reflected pulse.

Interborehole measurements were carried out using ball hydrophones as receivers and the sparker as a source. Two sets of scans were carried out. In the first set the sparker was deployed in borehole 2 and the ball hydrophones in boreholes 5 and 8. In the second set the sparker was deployed in borehole 4 and the ball hydrophones in 6 and 10. In the two sets of scans, scans 2-8 and 4-10 represented paths with the target between the source and the receiver.

For the first set of scans (2-5 and 2-8), the distances between the seismic source and the receivers were about equal and therefore no spreading corrections were necessary. Fig 6:3:4 shows the signatures from the two ball hydrophones at various depths, with the upper trace representing scans 2 to 8 and the lower trace scans 2 to 5. Figs 6:3:4a, b and c were recorded at depths of 2 m, 3.25 m and 4.5 m respectively. Reflectors from the target should appear on the lower trace at about 6.5 ms with a phase reversal (due to the hollow, air-filled target), but it could not be identified on any of the signatures. The comparison of the amplitude of the first peak for the two scans 2-5 and 2-8 are shown in Fig 6:3:5. The amplitudes of scan 2-5, without the pipe in its path,

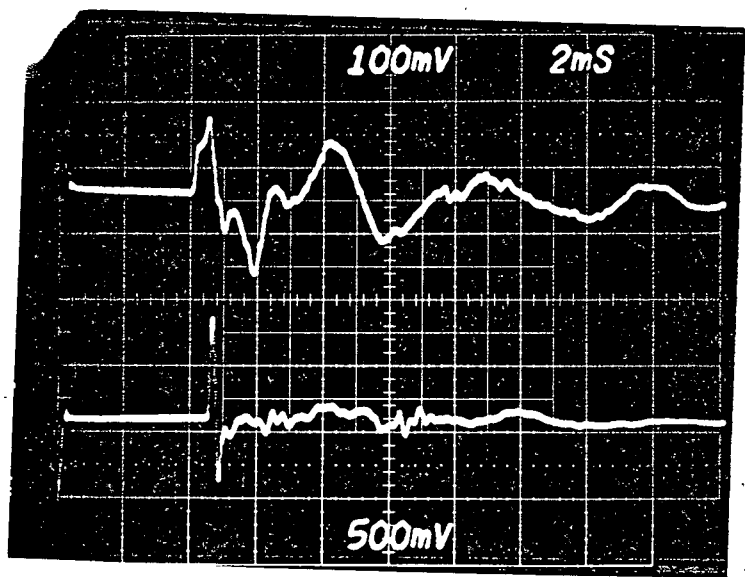
Trace

(a)



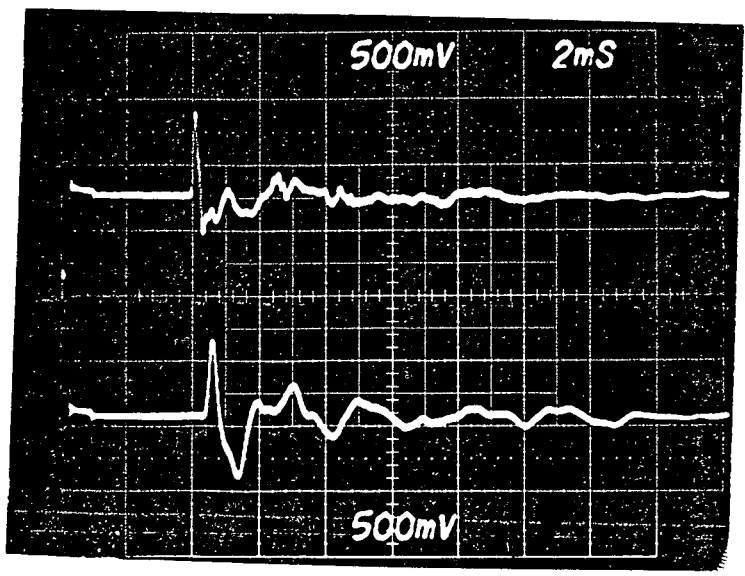
1
2

(b)



3
4

(c)



5
6

FIG. 6:3:4 EAST FLEET SURVEY - SIGNATURES FROM SCANS 2-8 & 2-5

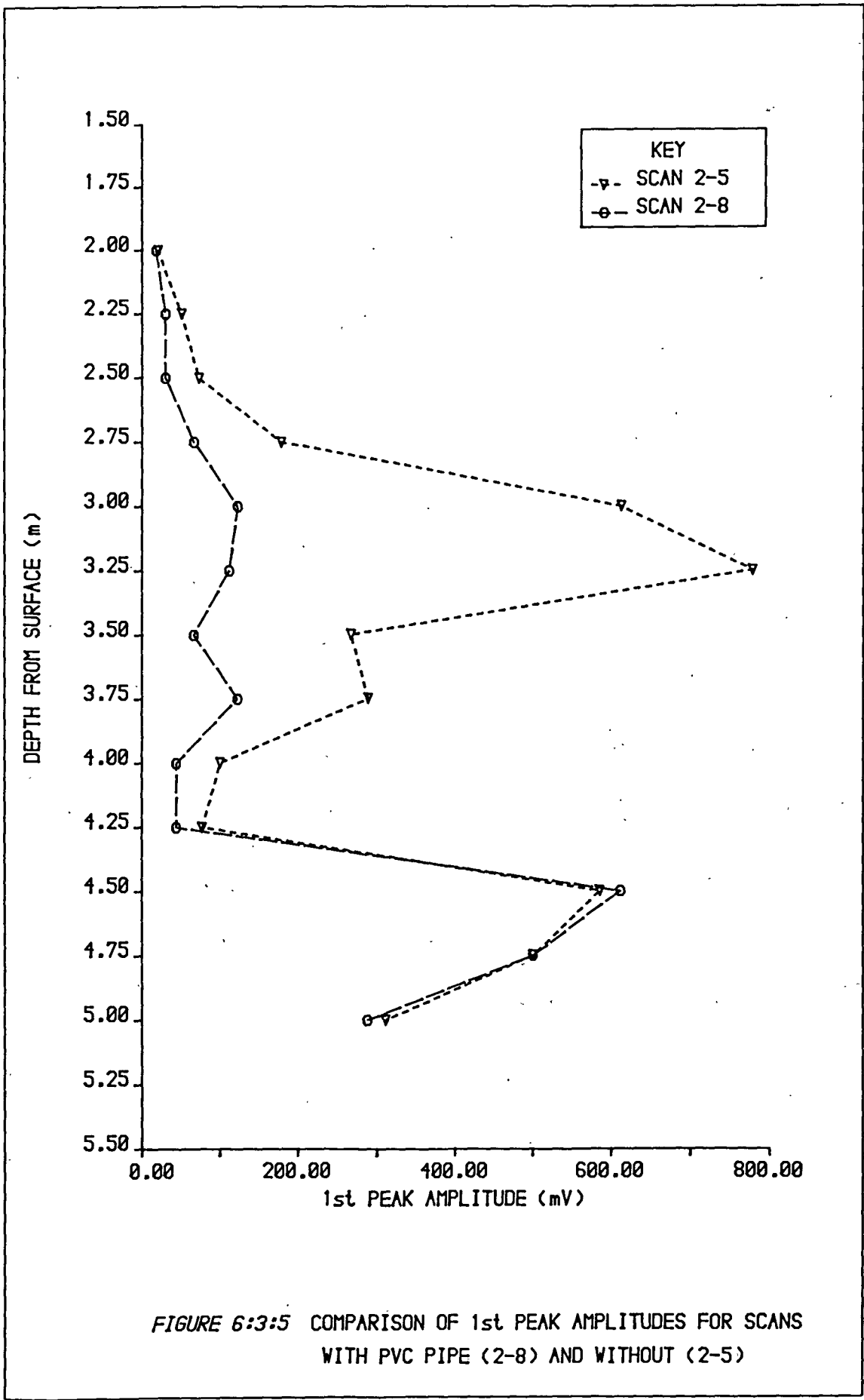


FIGURE 6:3:5 COMPARISON OF 1st PEAK AMPLITUDES FOR SCANS WITH PVC PIPE (2-8) AND WITHOUT (2-5)

are relatively greater than that of scan 2-8 at depths between 2.5 m to 4.25 m.

The signatures from the second set of scans (4-6 and 4-10) did not indicate the presence of a reflected pulse from the target either. A comparison of the amplitude of the first peak for the two scans 4-6 and 4-10 are shown in Fig 6:3:6. The amplitudes of scan 4-6, without the target in its path, are relatively greater than that of scan 4-10 at depths between 2.25 m to 4.25 m. The amplitudes of scan 4-10 have been corrected for spreading losses.

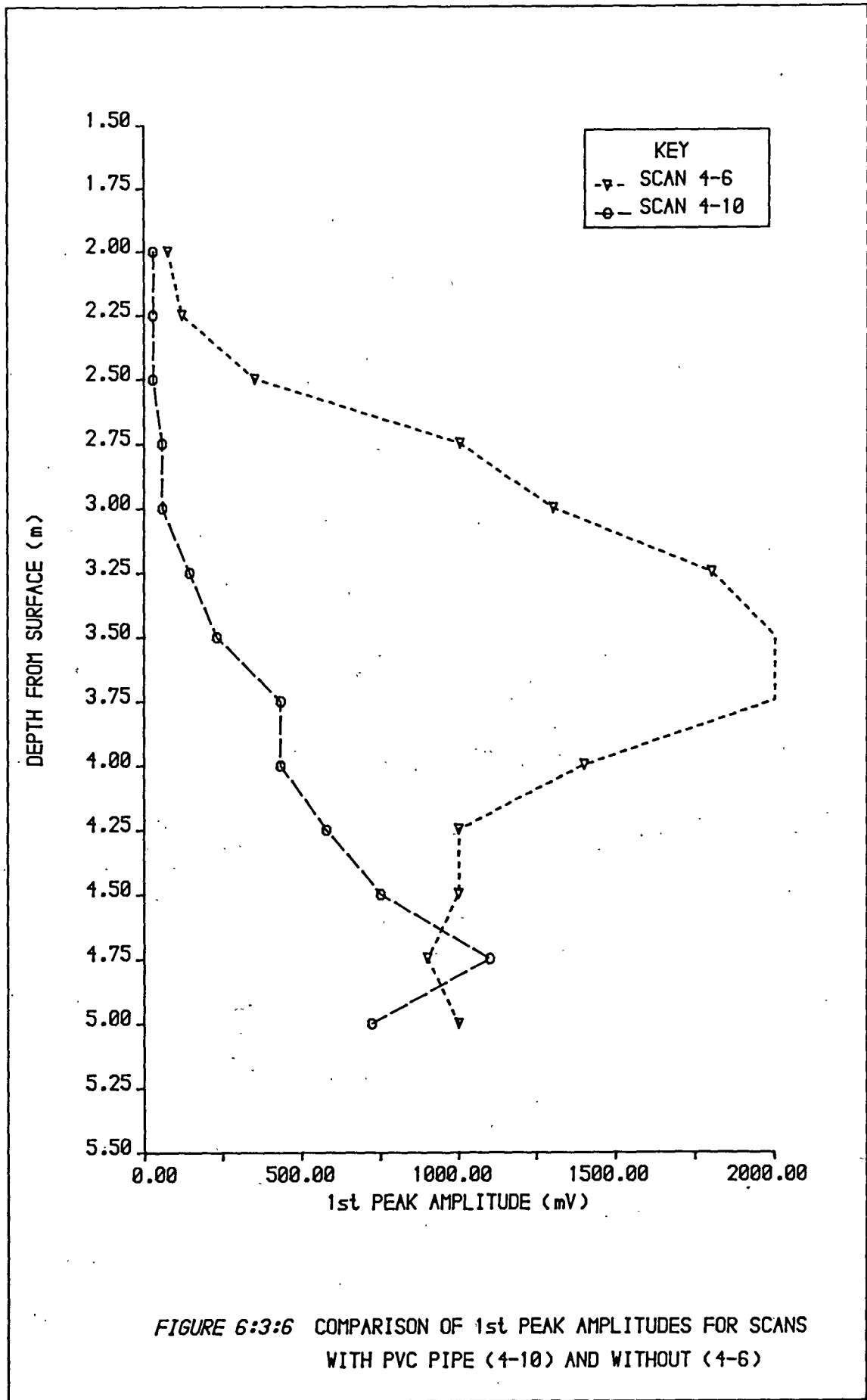
The absence of a reflected pulse from the target can be explained by the relatively smaller size of the target compared to the predominant wavelength of the source and the cylindrical shape of the target. Laboratory study (section 6:1:4) had shown that the amplitude of a reflected pulse from a cylindrical shaped target was considerably less than from a planar target, and that the diameter of a cylindrical target had to be considerably greater than a wavelength for a reflected pulse to be identified; assuming there are no changes in other parameters such as the geology, the source output energy, source/receiver layout etc. The predominant frequency represented in the spike on trace 6 can be estimated to be approximately 2000 Hz, which represents a wavelength of about 0.8 m. The target diameter was 0.38 m, which is less than half the wavelength; therefore, it is not surprising that there are difficulties in identification of a reflector from the target.

The comparison of the amplitudes for two paths, one with a PVC pipe in between the source and the receiver and the other path without, from the two scans, suggests that the former shows considerably more attenuation. The difference in the attenuation between the two paths appears to be large when compared to the laboratory experiment (Fig 6:1:35). The laboratory experiment indicated that a target with a diameter of about half the wavelength would attenuate the amplitude by about 10%. The target would have to be about a wavelength in diameter to produce an appreciable reduction in amplitude (about 40%). This suggests that there may be other extraneous geological conditions which might have a considerable influence.

The in situ P wave velocity profile (Fig 6:3:2) shows that the velocity varies with depth and there is an indication of a probable slower P wave velocity layer at a depth of about 3 m, although the lack of a number of these measurements over a larger separation makes the positive identification of the layer difficult. Davis (1983; Ref 154) and McCann and McCann (1975, Ref 113), who carried out seismic investigation of the site, suggest that the first few metres of the Oxford Clay were highly weathered with some anisotropy. McCann and McCann (1969; Ref 57), while investigating the in situ P wave properties of the sediments, concluded that the clay was layered and there were high velocity layers consisting of fossil bands which considerably influenced the amplitude, depending on the frequency, thickness of the layer and the separation of the source and receiver.

With a limited number of measurements and in a cohesive sedimentary formation which can exhibit anisotropic behaviour, the results were not conclusive. A significant number of interborehole measurements are required to obtain an in situ P wave velocity structure, both with depth and azimuth.

In conclusion, the development of the ACDER system has been partially successful. A borehole source has been developed which produces a single spike shaped pulse, as shown in Fig 6:3:4c. The instrumentation to capture and display the data functioned satisfactorily, but the design of a directional receiver that could work in a 100 mm borehole requires further work. This was highlighted during the model study and has shown to be present in the field study as well.



The application of the major seismic methods to delineate geological hazards associated with the presence of cavities during site investigation have been investigated and reviewed in some detail. Some of the geological hazards that may be encountered have been discussed and the effect of these on the seismic properties have been investigated.

Prior to the embarkation of any geophysical site investigation it is prudent to carry out a comprehensive desk study. The desk study of historical documents, maps, local church records, aerial photographs, local newspapers, etc may yield information for the civil engineers to assess the risk of civil engineering hazards. This may lead to the identification of the type of cavity, mine working and ground condition that might be present in the area so that consideration may be given to selection of the most suitable geophysical method for locating the anomalous zones associated with the presence of a cavity. McCann et al (1982; Ref 95) emphasise the choice of selecting the correct geophysical method for the type of hazard in order to maximise the success of the survey and to prevent the waste of time, effort and money. Close collaboration between the site geologist, civil engineer and geophysicist is also emphasised to achieve a successful survey, since it is usually the combination of all the available information that helps the site geophysicist to finally interpret the data and identify the hazard.

Most of the case histories and investigations have been orientated towards the detection of anomalous zones down to a depth of 50 m only, as this appears to be the main area of interest in most site investigations. Some of the relatively shallower cavities result in some disturbance at the surface which assists in the detection of cavities using the geophysical method, because it effectively enlarges the area of disturbed ground and presents itself as a much bigger discontinuity. However, it must be emphasised that this anomalous ground condition must be sufficiently different from the surrounding material for it to be able to be resolved using seismic techniques.

The chances of being able to identify an anomaly associated with

hazardous ground conditions using seismic methods are influenced by the physical dimension, shape and depth of burial of the cavity, the properties of the surrounding rock mass and the drainage conditions. These physical and geological constraints are in addition to the seismic controlling factors, namely the source characteristics, with sufficient energy to be able to penetrate and resolve the changes in the physical properties with an adequate signal to noise ratio. However, with the advent of microcomputers, it is feasible to increase the signal to noise ratio by stacking and thus produce an image of the gross variations in the physical properties using a computer processing technique such as tomography.

7:1 Surface seismic methods

The use of standard seismic refraction methods for the determination of depth to bedrock and the velocity of the materials is well established in the site investigation procedure. The method is capable of delineating large discontinuities relatively near the surface, such as faulting in the rock mass. These are normally large features and therefore represent a significant anomaly beneath the seismic survey line.

The collapse or the disturbance caused by a near surface cavity may produce a geomorphological feature such as dolines, which are often characterised by a surface depression. Seismic refraction lines crossing such a feature will appear as anomalous readings, but a very close geophone spacing is required for details to be highlighted, assuming that there are no other geological complications. A detailed refraction survey of this type can become prohibitively expensive in most cases.

The seismic refraction method has been applied with varying degrees of success for the actual detection of cavities. The success of detection depends, as discussed earlier, on the size of the cavity as a function of the wavelength, shape, geology, and other properties. Normally, the drop-weight, hammer, etc are used as the seismic sources, which produce source wavelengths considerably greater than the diameter of the cavity. This is particularly accentuated by surface deposits such as dry sandy soil or peat, which absorb high frequency components.

The seismic refraction survey at the Cocking site showed that it is feasible to identify the presence of a cavity, including the disturbed ground associated with it, by the delay caused by the wave travelling from the source to the receiver. The geophone spacing used was considerably shorter than that in normal refraction surveys used for site investigations. The TIDE method developed was a good way of representing these delays as a map and may form a useful tool in the future to look at these types of variations. However, it must be stated that a number of field studies with different geologies is necessary before any conclusive evidence of the success of this method is established. On the other hand, most writers stress that the refraction method is most suitable for detecting changes in the superficial deposits associated with the presence of voids or cavities.

The seismic reflection method has been used in several cases to attempt the location of cavities and tunnels. The major difficulty with the method is its lack of resolution, which is associated with the type of seismic source used and the attenuation of high frequencies caused by the surface layer, since when the wavelength of the incident seismic energy is greater than the cavity diameter, very little energy will be reflected back to the surface. The shape of the cavity is another factor which will affect the amplitude of the reflected pulse. The laboratory experiment carried out in the tank has shown that the size and the shape of the cavity as a function of the wavelength are also the limiting criteria for the reflection technique to succeed.

In a shallow survey, reflections from near surface interfaces are often completely obscured by the large amplitude of surface wave arrivals and consequently are difficult to identify. The use of a high frequency source, such as a sparker, might well improve the situation if it is combined with modern data processing techniques and an understanding of the basic wave-cavity interaction mechanism. The high frequency energy will be attenuated, so that under normal circumstances the reflected energy would be small and probably lost in the environmental and source generated noise. The use of multiple geophone or accelerator arrays combined with digital stacking should reduce this problem. It may well be that the seismic reflection method will become more widely used in the future as improved systems become available for shallow engineering surveys. It is concluded that a high frequency seismic source

(700-1500 Hz bandwidth), used in conjunction with common depth point reflection processing, does have considerable potential for cavity location, but a practical system for shallow depths down to 5 m has yet to be developed.

The phenomenon of cavity resonance has been reported by Godson and Watkins (1968; Ref 104), and a theoretical relationship was developed from Biot (1952; Ref 102) for an idealised condition of a cylindrical tube in an infinite solid, although Richtien and Stewart (1975; Ref 105) were not able to identify any events associated with cavity resonance on their seismic records when investigating for cavity resonance. Godson and Watkins (1968; Ref 104) did obtain better resonance with near surface explosive charges, which were associated with the generation of Rayleigh waves. These waves are of fairly large magnitude and could well be the triggering mechanism for the resonance of the cavity. Richtien and Stewart (1975; Ref 105) were of the opinion that surface waves of both the Love and Rayleigh type are the most effective for the detection and delineation of cavities.

The conflicting reports on the observation and the use of the seismic resonance method indicates that the resonance phenomenon is not well understood and that the theoretical model is for an ideal condition but not for a practical situation. For instance, it is seldom possible to find a cavity without some jointing present on its walls and with a uniform diameter, which means that each segment of the cavity will have a unique resonance frequency with the joints acting as nodes. Another parameter to consider is the possibility of different stresses on the walls because the overburden stress may not be equal to the horizontal stress and in some cases the two horizontal stresses may not be equal either, particularly for deeper cavities, in which case the radiation pattern may also be affected. Finally, the amplitude of the resonant frequency will also be affected by an infill, making it more difficult to identify.

Therefore, it is not surprising that there is difficulty in the observation of cavity resonance because unless an ideal condition exists, the chance of observation may be minimal.

7:2 Borehole seismic methods

The interborehole seismic method allows an access to the seismic waves into the rock mass without the influence of the superficial sediment. This improves the resolution, as relatively higher frequency and energy are imparted into the rock mass.

Most site investigations require the drilling of a few boreholes which can be used to carry out interborehole seismic measurements. The rock mass between the boreholes can be assessed for the dynamic moduli and a possible engineering hazard by making careful seismic measurements down the length of the boreholes. The advantage of the method is that the chances of detecting hazardous zones are greater, provided that the geology and possible variations in in situ seismic properties are well established. The best results are obtained with a repetitive high frequency source having a well defined signature and reliability, such as the High Resolution Sparker Probe (HRSP) developed during this research, combined with the digital stacking technique.

A field experiment was carried out during the research programme to assess the use of the interborehole method for detecting a cavity, represented by a 5 m diameter disused tunnel at Cocking. The results show, in this case, that the tunnel forms a significant discontinuity and affects both the overall travel time and the amplitude of the received signal. A practical example of the use of this method in a site investigation is the survey of a suspected cavity beneath a house in Maidstone. In this case, interborehole seismic scanning was the only possible geophysical method that could be applied to this difficult situation. The results indicate that the presence of a gull in the Hythe Beds did affect the overlying beds and this was characterised by significant changes in the seismic properties, particularly the signal amplitude. McCann et al (1975; Ref 113), while carrying out interborehole work, using a pair of boreholes in the vicinity of an infilled sinkhole chalk, relates the changes in the seismic velocity as an indication of the presence of the sinkhole.

The interborehole seismic method is probably the most suitable seismic method that can be used for detection of civil engineering hazards during site investigations. The separation of the boreholes will depend

on the local geology, the depth of the water table, etc, but a separation of about 25 m when trying to delineate a discontinuity of about 5 m diameter seems reasonable, provided there is an adequate seismic impedance contrast between the discontinuity and the surrounding rock mass. It should be noted that, for smaller discontinuities to be resolved, the borehole separation may have to be reduced. In some cases, when the diameter of the cavity is smaller than the wavelength, it is possible for the seismic energy to be diffracted around the cavity, and it is then extremely difficult to observe the effect of the cavity on the received seismic signal. The above figures are only given as a brief guide, since there are no definite rules regarding the resolution which might be obtained without other considerations discussed above.

One of the points highlighted by this investigation is the use of a comparative method, whereby the seismic properties of two paths are compared, one with a cavity and the other without. This technique appears to be extremely useful because it reduces the effect of the boreholes and highlights the local variations in the seismic properties. Ideally, two seismic sensors ought to be used simultaneously in two separate boreholes, with the source in a third borehole, to account for a possible variation in the output of the seismic source.

The surface to borehole seismic method is another useful method for identifying local variations in the seismic properties caused by the presence of a cavity. The surface to borehole seismic method is basically a combination of the surface and borehole seismic methods. In its most advanced form it is known as vertical seismic profiling, a method which is widely used in the oil industry. The method used at the Cocking site illustrates the use of the method for a shallow site investigation. By moving the seismic source around a borehole at several different distances, it is possible to investigate a cone shaped volume of the rock mass.

The borehole can be positioned in such a way that there is reasonable overlap of the volume of investigation and, hence, it is possible to determine fracturing and anisotropy of the rock mass and the presence of cavities, provided that the travel path of the seismic pulse does intersect the cavity or geological discontinuity. The relationship between the wavelength of the incident seismic energy and the cavity

size is again critical since, for a falling weight source, a small diameter cavity would probably have very little effect on the travel time and amplitude. It should be noted that the presence of the cavity does affect the properties of the surrounding rock mass, and it is this that may affect the seismic signal rather than the cavity itself.

7:3 Single hole method

The concept of a single hole method (ACDER) for the detection of cavities is very attractive, because a considerable volume of the rock mass around a borehole could be investigated using a single hole. The development of the ACDER method can be divided into three basic groups: the source, the receiver and the instrumentation/display.

Laboratory experiments were carried out to investigate the characteristics of the sparker source and the receiver, and to observe the effect of the cavity on a seismic pulse.

Laboratory experiments showed that the output energy from a sparker source is a function of a number of variables, such as the conductivity of the solution in the spark chamber, electrode separation, shape of the electrodes, energy input, the material used for the chamber, etc. All of the above variables can be grouped into two basic mechanisms in the functioning of the sparker source, which are: the efficient conversion of the electrical energy in a plasma bubble (which produces the shock wave) and the maximum transfer of this energy from the spark chamber into the surrounding rock mass, with the desired shape of seismic pulse. The efficient generation of the plasma bubble is related to the current density produced between the two electrodes in the conductive fluid, i.e. the greater the current density, the larger the plasma bubble. The final output energy and the pulse signature are affected by the material used in the construction of the sparker chamber. Chamber resonance associated with the metal sparker was eliminated by using soft plastic or cotton reinforced rubber tube. This produced a sharp pressure spike, as required for the seismic source in the concept of the ACDER system.

A borehole sparker was subsequently developed with an output signature showing a sharp and short pressure pulse. This borehole sparker source is referred to as the HRSP, and it fulfills the original design criteria

for a borehole seismic source required for the ACDER concept. The reason for the difference in shape of the output signature between a metal sparker and the HRSP, and possible mechanisms associated with it, is discussed in section 6:2:2. Free field measurements carried out at sea show that a directivity pattern can be regarded as reasonably constant for a total angle of 120° in the vertical direction, ie 60° from the horizontal plane centred in the middle of the sparker.

Directional properties of a small single disk shaped receiver transducer which can be housed in the ACDER receiver sonde were investigated using theoretical modelling. The theoretical modelling of a single receiver transducer directivity shows that a directivity of 2° required for the ACDER concept to work, could not be attained at the frequency of interest (1000 Hz). The difficulty of generating the required directivity was emphasised in the directivity monogram by Urick (1975; Ref 139). In light of this, the possible use of arrays was considered and a brief description of the various types of arrays and their main advantages and disadvantages was discussed. The design of a directional array that can be housed in the ACDER receiver sonde appears to be one of the main topics that need further development.

Laboratory model experiments were carried out to assess the effect on the amplitude of the pressure pulse when cylindrical obstructions of differing diameters were placed in the path of the source and receiver. The result showed that the pressure amplitude parameters are very sensitive to the presence of obstructions. An obstruction with the diameter of a wavelength reduces the amplitude by approximately 40%, which is a very good indication of a discontinuity.

Laboratory experiments to identify reflections from cylindrical targets with varying diameters showed that a reflected pulse from a curved surface became noticeable when a cylindrical target was just over three times the wavelength, but a reflection from a planar target of similar width was clearly identifiable. This demonstrates that reflections from a curved surface comparable to the wavelength will be difficult to identify.

The field trials of the ACDER system at East Fleet were not successful in terms of the overall concept, due to the lack of the directivity associated with the receiver, but the HRSP sparker and the display unit worked as per the design criteria.

8 CONCLUSIONS

- a A comprehensive desk study of historical documents, maps, local church records, aerial photographs, local newspapers, etc, is essential to identify local geological and mining conditions, as it will ultimately save time and money.
- b The seismic refraction method is most suitable for detecting changes in the superficial deposits and drainage conditions associated with the presence of voids or cavities; the TIDE method may assist in the representation of these subtle changes. A survey of this type would require geophones to be spaced very closely and thus become prohibitively expensive.
- c The seismic reflection method comes closer than most geophysical techniques to providing a picture in cross-section of the geological structure that can be readily interpreted. The failure of the method, at present, is caused by the lack of resolution associated with inadequately high frequency seismic sources due to the attenuation of high frequencies caused by superficial deposits.
- d The phenomenon of cavity resonance has been observed and a theory has been postulated for an ideal condition, but its practical application in locating cavities is in doubt without considerably more research, especially when the cavity is partially filled with slurry or infill.
- e The interborehole method was the most successful of all the seismic methods for the detection of hazardous ground conditions associated with cavities. The limiting factors are the complexity of the system, the relative slowness of a survey and the necessity of boreholes, which may make the interborehole method rather expensive. The size of a cavity that may be identified will depend predominantly on the wavelength of the seismic source in a particular geology, the saturation condition, the attenuation characteristics of the material and the separation of the boreholes. The attenuation of the amplitude of the seismic wave is the most sensitive parameter to

the presence of a discontinuity. The comparison of amplitudes between two wave paths, one path with a discontinuity between a source and a receiver and another without the discontinuity, forms a very useful method of identifying a discontinuity.

- f The surface to borehole method is also a useful technique, but is limited by the cone shaped volume of the ground investigated and suffers from a lack of resolution caused by surface deposits. It is a simple method and is less time consuming and expensive than the interborehole method. One of its main advantages is that variation of the seismic properties with depth and azimuth can be measured with relative ease.

- g The concept of the single hole method for site investigation is perhaps the most exciting technique proposed in recent years. It offers the advantage of improving the resolution of detection by moving the source and the receiver away from the surface deposits, using the interborehole method, and the potential to investigate considerably more volume of ground away from a borehole. The final presentation and interpretation of the data could be relatively easy, and comes very close to the concept of an on-line cavity detection method. The method has been partially developed but requires further research in terms of the development of a directional receiver followed by field trials in various geological conditions to evaluate its limitations.

- h The successful development of the high resolution sparker probe (HRSP) is encouraging, as the main reason why the interborehole technique is not used in the oil industry is the lack of a reliable downhole seismic source which can be operated using a standard wireline logging cable. In future, the HRSP could be further developed so that a power supply and a trigger unit could be included to form a single unit to be operated using a wireline logging cable. The experience and the knowledge gained during this research can be applied to convert efficiently the electrical energy into a shock wave with the desired output signature to produce a reliable downhole seismic source for use in the oil industry.

9 RECOMMENDATIONS

- a The submission of detailed plans of mine workings and shafts was not made compulsory until 1872, and in view of the amount of mining carried out prior to this date and the present need for building land, it seems essential that comprehensive mapping of all disused workings and shafts should be carried out, either by local authorities or by central government.
- b Further investigations are required to assess the usefulness of imaging techniques such as the TIDE method, and possible adaptations of the technique for three dimensional imaging using refraction surveys.
- c Further research is required to adapt the seismic reflection technique for site investigation by the use of high energy, high frequency sources to improve the resolution.
- d Imaging techniques can be used in interborehole seismics, in which variations in velocity and amplitude are applied to generate images (tomography).
- e More theoretical and laboratory studies are necessary to observe the effect of different cavity shapes on direct and reflected waves, and diffraction and scattering associated with it.
- f A feasibility study is required to assess the generation of a directional receiver beam using a number of horizontal boreholes on a vertical plane, with each borehole containing a phase array receiver. Receiver arrays operate together to form a horizontal directional beam, which might be able to detect a reflected pulse from a large discontinuity.
- g The HRSP sparker has been used successfully in geothermal research, to identify fractured zones in a granite rock mass to a depth of 300 m. It was used continuously over a period of days without the necessity to refill the chamber. Further research is still necessary to quantify or derive a relationship between the various parameters associated with generation of a seismic pulse

from a sparker. Some of these parameters were discussed qualitatively in this thesis, but a quantitative assessment would enhance sparker efficiency and output signature shaping.

h The use of high frequency shear waves in interborehole surveys with three component clamped sondes may be another method for identifying cavities, particularly those filled by slurry or water, as the shear wave will not propagate through these infills.

10 ACKNOWLEDGEMENTS

I would like to thank Dr F Goldspink and Dr D M McCann for their continual support and assistance during this research.

I would also like to thank Mr C R Cratchley and Dr P D Jackson for their encouragement and many scientific discussions; the British Geological Survey for financial assistance; the Marine Science Laboratory of the University College of North Wales for making available the Prince Madog; and Dr A S Batchelor for enabling use of facilities of the Camborne School of Mines.

The field work on land and at sea required considerable group effort, and I would like to extend my thanks to J Hallam, A Green, P Schultheiss, M Culshaw, A Foster and other members of the Engineering Geology Unit for their cooperation.

Finally I would like to express my thanks to my wife Joyce for all the support and encouragement she gave to me, and to Mrs J Pye for typing the thesis.

11 REFERENCES

- 1 HUBERT, M KING. 1934.
Results of earth-resistivity surveys on various geologic structures in Illinois.
Geophysical Prospecting, 1934, Trans Am Inst Mining Met Engrs, Vol 110, pp 9-39.
- 2 WEATHERBY, B B. 1940.
The history and development of seismic prospecting.
Geophysics, Vol 5, pp 215-230.
- 3 BARIA, R. 1974.
Location of underground cavities with seismic techniques.
Final year project. Middlesex Polytechnic, Queensway, Enfield.
Unpublished.
- 4 LITTLEJOHN, G S. 1979.
Surface stability in areas underlain by old coal workings.
Ground Engng, Vol 12, pp 22-30.
- 5 MAXWELL, G N. 1971.
Geophysical investigation of subsurface hazards due to abandoned coal mines.
PhD thesis, Strathclyde University. Unpublished.
- 6 MAXWELL, G N. 1975.
Mining Engineer. March 1975, p 277.
- 7 JACKSON, P D and SUDDABY, D L. 1979.
Detection of hidden workings using magnetic and electrical conductivity surveying - measurements near a proposed bypass route at Dalton in Furness, Cumbria.
IGS Eng Geol Unit, Rep Set 79/16, 20 pp.
- 8 COLLINS, J F N. 1969.
Salt: a policy for the control of salt extraction in Cheshire.
Cheshire County Council report.
- 9 HORNER, P C. 1971.
Subsurface waste disposal by injection methods.
MSc thesis, Imperial College, London.
- 10 COLLEY, G. 1963.
Geophysical Prospecting. Vol 13, p 1.
- 11 WALLER, D R. 1972.
Geophysical report on the DHSS Rehabilitation Centre, Stormy Down, near Bridgend, Glamorgan.
Geophysics Division, George Wimpey and Co Ltd.
- 12 SNOWDOWNE, J B. 1968.
A gravity survey for the detection of incipient sinkholes beneath a proposed building site.
MSc thesis, Imperial College, London.

- 13 TELFORD, W M, GELDHART, L P, SHERIFF, R E and KEYS, D A. 1976.
Applied geophysics.
Cambridge University Press.
- 14 WHITE, J E. 1965.
Seismic waves - radiation, transmission and attenuation.
McGraw-Hill, New York.
- 15 DOBRIN, M B. 1976.
Introduction to geophysical prospecting.
McGraw-Hill, New York.
- 16 GRANT, F S and WEST, G F. 1965.
Interpretation theory in applied geophysics.
McGraw-Hill, New York.
- 17 WOOD, A B. 1964.
A textbook of sound.
G Bell and Sons Ltd, London.
- 18 URICK, R J. 1947.
A sound velocity method for determining the compressibility of
finely divided substances.
J. Appl. Phys. 18, pp 983-987.
- 19 URICK, R J. 1948.
The absorption of sound in suspensions of irregular particles.
J. Acoust. Soc. Am. 20, pp 283-289.
- 20 URICK, R J and AMENT, W S. 1949.
The propagation of sound in composite media.
J. Acoust. Soc. Am., 21, pp 115-119.
- 21 HAMILTON, E L. 1956.
Low sound velocities in high-porosity sediments.
J. Acoust. Soc Am., 78, pp 16-19.
- 22 EPSTEIN, P S, 1941.
On the absorption of sound waves in suspensions and emulsions.
In: Theodore von Karman Anniversary Volume, pp 162-188, California
Institute of Technology, Pasadena, California.
- 23 SEWELL, C T J. 1910.
The extinction of sound in a viscous atmosphere by obstacles of
cylindrical and spherical form.
Phil. Trans. R. Soc. Lond., A210, pp 239-270.
- 24 LAMB, H. 1945.
Hydrodynamics.
Dover Publications, New York, 6th Edition.
- 25 AHUJA, A S. 1974.
A review of the derivations of the formulas for the acoustical
properties of liquid-solid mixtures.
In: Physics of Sound in Marine Sediments (Ed. L. Hampton). pp 1-17,
New York: Plenum.

- 26 BUCHAN, S, DEWES, F C D, McCANN D M and TAYLOR SMITH, D. 1967.
Measurements of the acoustic and geotechnical properties of marine sediment cores.
In: Marine Geotechnique (Ed. A.F. Richards), pp 65-92, University of Illinois Press.
- 27 McCANN, C. 1969.
Compressional wave attenuation in concentrated clay suspensions.
Acustica, 22, pp 252-356.
- 28 GULTEPE, M A B, EVERETT, D H and GULTEPE M E. 1977.
The influence of interparticle forces on acoustic attenuation in marine sediments.
Proc. Inst. Acoust. Conf. Papers, 4/6 April, 1977, Bath.
- 29 RAYLEIGH, LORD. 1878.
The theory of sound.
Volume II. Reprinted by Dover Publications, New York.
- 30 MORSE, P M and BOLT, R H. 1944.
Sound waves in rooms.
Rev. Mod. Phys., 16, 69-150.
- 31 SCOTT, R A. 1946.
The absorption of sound in a homogeneous porous medium.
Proc. Phys. Soc. London, 58, pp 165-183.
- 32 BERANEK, L L. 1947.
Acoustical properties of homogeneous, isotropic rigid tiles and flexible blankets.
J. Acoust. Soc. Am., 19, pp 556-568.
- 33 ZWIKKER, C and KOSTEN C W. 1949.
Sound absorbing materials.
Pub. Elsevier, Amsterdam.
- 34 BIOT, M A. 1956a.
Theory of propagation of elastic waves in a fluid-saturated porous solid: I - Low-frequency range.
J. Acoust. Soc. Am., 28, pp 168-178.
- 35 BIOT, M A. 1956b.
Theory of propagation of elastic waves in a fluid-saturated porous solid: II - Higher-frequency range.
J. Acoust. Soc. Am., 28, pp 179-191.
- 36 GEERTSMA, J, and SMITH, D C. 1961.
Some aspects of elastic waves propagation in fluid-saturated porous solids.
Geophysics, 26, pp 169-181.
- 37 WYLLIE, M R J, GARDNER, G H F and GREGORY, A R. 1962.
Study of elastic waves in porous media.
Geophysics, 27, pp 569-589; with addendum, *Geophysics*, 28, 1074.

- 38 HSIEH, L, and YEW, C H. 1973.
Wave motions in a fluid saturated porous medium.
J. Appl. Mech., 40, pp 873-878.
- 39 MENGI, Y and McNIVEN, H D. 1977.
Response of a fluid-filled porous media to a transient input.
J. Acoust. Soc. Am., 61, pp 84-94.
- 40 GASSMANN, F. 1951.
Elastic waves through a packing of spheres.
Geophysics, Vol 16, pp 673-685.
- 41 FAUST, L Y. 1951.
Seismic velocity as a function of depth and geological time.
Geophysics, 16, pp 192-206.
- 42 WHITE, J E and SENGBUSH, R L. 1953.
Velocity measurements in near surface formations.
Geophysics, 28, pp 54-69.
- 43 DUFFY, J, and MINDLIN, R D. 1957.
Stress-strain relationship and vibrations of a granular medium.
J. Appl. Mech., 24, pp 585-593.
- 44 BRANDT, H. 1955.
A study of the speed of sound in porous granular media.
J. Appl. Mech., 22, pp 479-486.
- 45 BRANDT, H. 1960.
Factors affecting compressional wave velocity in unconsolidated marine sediments.
J. Acoust. Soc. Am., 32, pp 171-179.
- 46 WHITE, J E. 1966.
Static friction as a source of seismic attenuation.
Geophysics, 31, pp 333-339.
- 47 HAMILTON, E L. 19071a.
Prediction of in situ acoustic and elastic properties of marine sediments.
Geophysics, 36, pp 266-284.
- 48 HAMILTON, E L. 1971b.
The elastic properties of marine sediments.
J. Geophys. Res, 76, pp 579-604.
- 49 HAMILTON, E L. 1972.
Compressional-wave attenuation in marine sediments.
Geophysics, 37, pp 620-646.
- 50 LAUGHTON, A S. 1954.
Laboratory measurements of seismic velocities in ocean sediments.
Proc. R. Soc. London, 222, pp 336-341.
- 51 LAUGHTON, A S. 1957.
Sound propagation in compacted ocean sediments.
Geophysics, 22, pp 233-260.

- 52 HUNTER, A N, LEGGE, R and MATSUKAWA, E. 1961.
Measurements of acoustic attenuation and velocity in sand.
Acustica, 11, pp 26-31.
- 53 MORGAN, N A. 1969.
Physical properties of marine sediments as related to seismic velocities.
Geophysics, 34, 529-545.
- 54 SHUMWAY, G. 1960a.
Sound speed and absorption studies of marine sediments by resonance method - Pt I.
Geophysics, 25, pp 451-467.
- 55 SHUMWAY, G. 1960b.
Sound speed and absorption studies of marine sediments by resonance method - Pt II.
Geophysics, 25, pp 659-682.
- 56 HAMPTON, L D. 1967.
Acoustic properties of sediments.
J. Acoust. Soc. Am. 42, pp 882-890.
- 57 McCANN, C and McCANN, D M. 1969.
The attenuation of compressional waves in marine sediments.
Geophysics, 34, pp 882-892.
- 58 McCANN, D M. 1972.
Measurement of the acoustic properties of marine sediments.
Acustica, 26, pp 55-66.
- 59 BUCHAN, S, McCANN, D M and TAYLOR SMITH, D. 1972.
Relations between the acoustic and geotechnical properties of marine sediments.
Q. Jnl. Eng. Geol., 5, pp 265-284.
- 60 AKAL, T. 1972.
The relationship between physical properties of underwater sediments that affect bottom reflections.
Marine Geology, 13, pp 251-266.
- 61 HAMILTON, E L. 1970b.
Sound velocity and related properties of marine sediments, North Pacific.
J. Geophys. Res., 75, pp 4423-4446.
- 62 HAMILTON, E L. 1976.
Sound attenuation as a function of depth in the sea floor.
J. Acoust. Soc. Am., 59, pp 528-535.
- 63 JACKSON, P D, BARIA R and McCANN D M. 1980.
Geotechnical assessment of superficial marine sediments using in situ geophysical probes.
Oceanology Int., 80, pp 33-46.
- 64 SHUMWAY, G. 1956.
A resonant chamber method for sound velocity and attenuation measurements in sediments.
Geophysics, 21, pp 305-319.

- 65 HARDIN, B O and RICHART, F E Jnr, 1963.
Elastic wave velocities in granular soil.
J. Soil Mech Fdns Div Am Soc Civ Engrs, 89, pp 33-65.
- 66 GARDNER, G H F, WYLLIE, M R J and DROSCHAK, D M. 1964.
Effects of pressures and fluid saturation of elastic waves in sands.
J. Petrol. Technol., 16, pp 189-198.
- 67 HAMILTON, E L. 1968.
Sound velocity, elasticity and other mass physical properties of marine sediments, North Pacific (Abstract).
Trans. Am. Geophys. Un., 49, pp 221.
- 68 McCANN, C. 1968.
An investigation of the acoustic properties of the natural materials.
Ph.D. thesis, University of N. Wales, pp 308. Unpublished.
- 69 SCHREIBER, C B. 1968.
Sound velocity in deep sea sediments.
J. Geophys. Res., 73, pp 1259-1268.
- 70 HORN, D R, HORN, B M and DELACH, M N. 1968.
Correlation between acoustical and other physical properties of deep-sea cores.
J. Geophys. Res., 73, pp 1939-1957.
- 71 ANDERSON, R S. 1974.
Statistical correlation of physical properties and sound velocity in marine sediments.
In: Physics of Sound in Marine Sediments (Ed. L. Hampton), pp 481-518, New York: Plenum.
- 72 TAYLOR SMITH, D. 1974.
Acoustic and mechanical loading of marine sediments.
In: Physics of sound in Marine Sediments (Ed. L. Hampton), pp 41-61, New York: Plenum.
- 73 HAMILTON, E L. 1975.
Acoustic properties of the sea floor: A review.
Oceanic acoustic modelling, Pt 4, Conference proceedings No 17, October 1975, Saclant ASW Res. Centre, La Spezia, Italy.
- 74 SUTTON, G H, BERCKHEMER, H and NAFE, J E. 1957.
Physical analysis of deep-sea sediments.
Geophysics, 22, pp 779-812.
- 75 HUNTER, A N, LEGGE, R and MATSUKAWA, E. 1961.
Measurements of acoustic attenuation and velocity in sand.
Acustica, 11, pp 26-31.
- 76 HALL, J R and RICHART Jr, F E. 1963.
Dissipation of elastic wave energy in granular soil.
J. Soil. Mech. Fdns. Div. Am. Soc. Civ. Engrs., 89, pp 27-56.

- 77 MARKO, G M and NUR, A. 1979.
Wave attenuation in partially saturated rocks.
Geophysics, 23, pp 421-439.
- 78 TOKSOZ, M N, JOHNSTON, D H and TIMUR, A T. 1979a.
Attenuation of seismic waves in dry and saturated rocks: I.
Laboratory measurements.
Geophysics, 44, pp 681-690.
- 79 TOKSOZ, M N, JOHNSTON, D H and TIMUR, A T. 1979b.
Attenuation of seismic waves in dry and saturated rocks: II.
Mechanics.
Geophysics, 44, pp 691-711.
- 80 BLACK, R A, FRISEHKNECHT, F C, HAZLEWOOD, R M and JACKSON, W M.
1962.
Geophysical methods of exploring for buried channels in Monument
Valley area, Arizona and Utah.
US Geological Survey, Bulletin 1083-F.
- 81 BUSH, B O and SCHWARZ, S D. 1965.
Seismic refraction and electrical resistivity measurements over
frozen ground.
National Research Council of Canada, Associate Committee on Soil and
Snow Mechanics, Technical Memorandum No 86, Ottawa, Ontario.
- 82 HOBSON, G D. 1970.
Seismic methods in mining and groundwater exploration.
Mining and Groundwater Geophysics, 1967, Geological Survey of
Canada, Economic Report No 26, Ottawa, Ontario.
- 83 GRAINGER, P, McCANN, D M and GALLOIS, R W. 1973.
The application of seismic refraction techniques to the study of
middle chalk at Mundford, Norfolk.
Geotechnique, Vol 23, No 2, pp 219-232.
- 84 CRATCHLEY, C R, McCANN, D M and ATES, M. 1976.
Application of geophysical techniques to the location of weak
tunnelling ground, with an example from the Foyers Hydroelectric
Scheme, Loch Ness.
Trans IMM, Section A, Vol 85, pp A127-A135.
- 85 MUSGRAVE, A W. 1967.
Seismic refraction prospecting.
Society of Exploration Geophysicists, Tulsa, Oklahoma, USA.
- 86 THORNBURGH, H R. 1930.
Wave-front diagrams in seismic interpretation.
Bull Am Assoc Petroleum Geologists, Vol 14, No 2.
- 87 GARDNER, J W. 1939.
Aerial plan of mapping subsurface structure by refraction shooting.
Geophysics, Vol 4, pp 247-259.
- 88 BARTHELMES, A J. 1946.
Continuous profiling and refraction shooting.
Geophysics, Vol 11, pp 24-42.

- 89 SLOTNICK, M M. 1950.
A graphical method for interpretation of refraction profile data.
Geophysics, Vol 15.
- 90 BAUMGARTE, J. 1955.
Konstruktive Darstellung von Seismisch Horizonten unter
Berücksichtigung der Strahlenbrechung in Raum.
Geophysical Prospecting, Vol 3, pp 126-162.
- 91 HALES, F W. 1958.
An accurate graphical method for interpreting seismic refraction
lines.
Geophysical Prospecting, Vol 6, pp 285-294.
- 92 TARRANT, L H. 1956.
A rapid method of determining the form of line profile results.
Geophysical Prospecting, Vol 4, pp 131-139.
- 93 HAGEDOORN, J G. 1959.
The plus-minus method of intersecting seismic refraction sections.
Geophysical Prospecting, Vol 7, pp 158-182.
- 94 WARD, W H, BURLAND, J B and GALLOIS, R W. 1968.
Geotechnical assessment of a site at Mundford for a large proton
accelerator.
Geotechnique, 18, pp 399-421.
- 95 McCANN, D M, BARIA, R, JACKSON, P D, CULSHAW, M G, GREEN, A S P,
SUDDABY, D L, and HALLAM, J R. 1982.
The use of geophysical methods in the detection of natural cavities,
mineshafths, and anomalous ground conditions.
IGS Eng. Geol. Unit, Report No. 82/5. Unpublished.
- 96 ANDREW, E M. 1979.
A comparison of seismic sources for a shallow reflection profile at
Onley, near Rugby.
IGS Appl. Geophys. Unit, Report No. 83. Unpublished.
- 97 McCANN, C and McCANN D M. 1982.
Wide angle seismic reflection profiling on inland waterways.
IGS Report No. 82/3.
- 98 COOK, J C, 1965.
Seismic mapping of underground cavities using reflection amplitude.
Geophysics, 30, pp 527-538.
- 99 MEISSNER, R and STEGENA, L. 1977.
Praxis der Seismischen Feldmessung und Auswertung.
Berlin, Gebruder Borntraeger.
- 100 BORTFELD, R. 1972.
Seismic imaging and seismic modelling.
Proc 34th meeting Europ Ass Exploration Geophys, Paris.
- 101 WATKINS, J S, GODSON, R H and WATSON, K. 1967.
Seismic detection of near-surface cavities.
Geol Survey Am, Prof Paper 559-A, US Government Printing Office,
Washington, DC, USA, 12 pp.

- 102 BIOT, M A. 1952.
Propagation of elastic waves in a cylindrical bore containing fluid.
VI App Physics, Vol 23, No 9, pp 997-1005.
- 103 KINSLER, L G and FREY, A R. 1962.
Fundamentals of acoustics. 2nd ed.
Wiley, London, 521 pp.
- 104 GODSON, R H and WATKINS, J S. 1968.
Seismic resonance investigations of a near-surface cavity in Anchor Reservoir, Wyoming, USA.
Bull Assoc Eng Geol, Vol 5, pp 27-36.
- 105 RICHTIEN, R D and STEWART, D M. 1975.
A seismic investigation over a near-surface cavern.
Geoexploration, Vol 13, pp 235-246.
- 106 BALLARD, R F. 1982.
Cavity detection.
Int. Geoscience and Remote Sensing Symp. (IGARSS'82), IEEE, Geoscience and Remote Sensing Society, 1-4 June, Munich.
- 107 BARIA, R. 1977.
Evaluation of 'SHRIMP' system for site investigation.
IGS Special Surveys Div, Eng Geol Unit, Report No 77/5. Unpublished.
- 108 ARROWSMITH, E J and RANKILOR, P R. 1981.
Dalton bypass: site investigation in an area of abandoned haematite mine workings.
Quart Jnl Eng Geol, London, Vol 14, pp 217-218.
- 109 BOIS, P, LA PORTE, M, LAVERGNE, M and THOMAS, G. 1971.
Essai de determination automatique des vitesses seismiques par mesures entre puits.
Geophysical Prospecting, Vol 19, pp 42-83.
- 110 BOIS, P, LA PORTE, M, LAVERGNE, M and THOMAS, G. 1972.
Well-to-well seismic measurements.
Geophysics, Vol 37, pp 471-480.
- 111 LA PORTE, M, LAKSHMANAN, J, LAVERGNE, M and WILLM, C. 1973.
Seismic measurement by transmission - applications to civil engineering.
Geophysical Prospecting, Vol 21, pp 147-157.
- 112 STOKOE, K H and WOODS, R D. 1972.
In situ shear waves velocity by crosshole method.
Journal of Soil Mechanics and Foundations Division, American Society of Civil Engineers, Vol 98, No SM5, Proc Paper 8904, pp 443-460.
- 113 McCANN, D M, GRAINGER, P and McCANN, C. 1975.
Interborehole acoustic measurements and their use in engineering geology.
Geophysical Prospecting, Vol 23, No 1, pp 50-69.
- 114 GREEN, A S P, BARIA, R and McCANN, D M. 1975.
Interborehole acoustic measurements at Norman Close, Maidstone, Kent.
IGS Eng Geol Unit, Report No 77/8. Unpublished.

- 115 BARIA, R, GREEN, A, McCANN, D M and SUDDABY, D. 1978.
Acoustic studies in the Carnmenellis granite at the Holman experimental mine near Troon, Camborne.
IGS Eng Geol Unit, Report No 78/2. Unpublished.
- 116 ALBRIGHT, J M and HAROLD, R J. 1976.
Seismic mapping of hydraulic fractures made in basement rocks.
Proc ERDA Symp on Enhanced Oil and Gas Recovery, V2-Gas, Tulsa, Oklahoma, September 9-10.
- 117 DRESSEN, L. 1973.
Sinkholes and subsidence engineering geology problems related to soluble rock.
Symp Int Assoc Eng Geol, Hanover, Germany.
- 118 BARIA, R, McCANN, D M and HALLAM, J R. 1978.
Assessment of rock mass conditions using geophysical techniques.
IGS Eng Geol Unit, Report No 78/6. Unpublished.
- 119 BARIA, R, HEARN, K H and DYER, B. 1983.
Mapping of explosive and hydraulically stimulated areas in a potential hot dry rock reservoir.
(in press)
- 120 BARIA, R. 1976.
Detection of cavities by seismic techniques - report on data collected at Cocking.
IGS Eng Geol Unit, Report No 76/96A. Unpublished.
- 121 PENMAN, A D M. 1976.
Cambering and valley bulging in the Gwash Valley at Empingham, Rutland, by P Horswill and A Horton, p 462.
Phil Trans Roy Soc, London, Vol A283. pp 427-462.
- 122 WORSSAM, B C. 1963.
Geology of the country around Maidstone.
Mem Geol Surv Gt Brit.
- 123 SCHULTHEISS, P J. 1983.
The influence of packing structure on seismic wave velocities in sediments.
PhD thesis, Dept. of Phy. Oceanography, University College of N. Wales. Unpublished.
- 124 CUNNY, R W and FRY, Z B. 1973.
Vibratory in situ and laboratory soil moduli compared.
J. Soil. Mech. Found. Div., ASCE. 99, SM12, pp 1055-1076.
- 125 McCANN, D M, BARIA, R, JACKSON, P D and GREEN, P D. 1985.
Application of cross-hole seismic measurements in site investigation surveys.
(in press)
- 126 KENNETT, P, IRESON, R L and CONN, P J. 1980.
Vertical seismic profiles: their application in exploration geophysics.
Geophysical Prospecting, 28, pp 676-699.

- 127 ROUSE, P. 1981.
A program to model surface to borehole seismic data.
IGS, Eng Geol Unit Report No. 81/7. Unpublished.
- 128 DONATO, R J. 1961.
Experiments on the propagation of ultrasonic waves through layered media.
PhD thesis, University of London. Unpublished.
- 129 KRAMER, F S, PETERSON, R A, WALTER, W C. 1968.
Seismic energy source handbook.
Bendix United Geophysical Corporation. Presented at 38th annual meeting of Society of Exploration Geophysicists, Denver, Colorado, USA.
- 130 NAIK, K R and HAY, J L.
Series connected thyristors for HVDC valves.
Direct Current, Vol.2, No 4.
- 131 EVELEIGH, R D. 1973.
Series sharing of diodes and thyristors.
AEI Publications.
- 132 BOBBER, R J. 1970.
Underwater electroacoustic measurements.
Naval Research Laboratory, Washington, DC, USA.
- 133 STENZEL, H. 1939.
Leitfaden zur Berechnung von Schallvorgängen.
Julius Springer, Berlin. Handbook for the Calculation of Sound Propagating Phenomena, English translation by A R Stickley. Naval Research Laboratory, Translation No 130.
- 134 BUKMORE, R W and HANSEN, R C. 1959.
Antenna power densities in the Fresnel region.
Proc IRE, Vol 47, p 2119.
- 135 REDWOOD, M. 1963.
A study of wave forms in the generation and detection of short ultrasonic pulses.
Applied Materials Research, April 1963.
- 136 REDWOOD, M. 1962.
Coupling between two modes of vibration in a piezoelectric resonator.
Journal of Acoustic Society of America, Vol 34, pp 895-902.
- 137 ROI, N A and FROLOV, D P. 1961.
The electroacoustic efficiency of a spark discharge in water.
RAF Farnborough Library, Translation No 795.
- 138 BERANEK, L L. 1954.
Acoustics.
McGraw-Hill Book Company.
- 139 URICK, R J. 1975.
Principles of underwater sound.
McGraw-Hill Book Company.

- 140 DOLPH, C L. 1946.
A current distribution of broadside arrays which optimizes the relationship between the beam width and side-lobe level.
Proc. Inst. Radio Eng., 34, pp 335-342.
- 141 TUCKER, D G. 1963.
Sonar arrays, system and displays, in V.M. Albers (ed).
Underwater Acoustics, Plenum Press, New York.
- 142 AULD, B. 1977.
Crosshole and downhole V_s by mechanical impulse.
Journal of the Geotechnical Engineering Division, American Society of Civil Engineers.
- 143 HALL, J, MILLER, F and SIMMONS, G. 1979.
A technique for the precise measurement of acoustic velocity in, and between, boreholes with a sparker source.
Geoprospection, Vol 17, No 3.
- 144 BUTLER, D K and CURRO Jr, J R. 1981.
Crosshole seismic testing - procedures and pitfalls.
Geophysics, Vol 46, No 1, pp 23-29.
- 145 WHITE, J E and SENGBUSH, R L. 1963.
Shear waves from explosive sources.
Geophysics, Vol 28, pp 1101-1119.
- 146 PARROTT, K R. 1980.
An investigation of the interior of a salt structure using the vertical profiling technique.
Masters thesis, Colorado School of Mines, 133 pp.
- 147 HEELAN, P A. 1953.
Radiation from a cylindrical source of finite length.
Geophysics, Vol 18, pp 685-696.
- 148 INGRAM, J. 1963.
On the elastodynamic response of a fluid filled borehole.
Presented at 33rd annual international meeting of Society of Exploration Geophysicists, New Orleans, Louisiana, USA.
- 149 PETERSON, E W. 1974.
Acoustic wave propagation along a fluid-filled cylinder.
J Applied Phys, Vol 45, pp 3340-3350.
- 150 LEE, M W and BALCH, A H. 1982.
Theoretical seismic wave radiation from a fluid-filled borehole.
- 151 WHITE, J E. 1983.
Underground sound application of seismic waves.
Elsevier Scientific Publishing Company Inc, New York.
- 152 FEHLER, M and PEARSON, C. 1981.
Acoustic radiation patterns from borehole sources.
Presented at 22nd logging symposium of SPWLA, June 23-26.
- 153 AKI, K and RICHARDS, P. 1980.
Quantitative seismology: theory and methods.
Freeman, New York.

- 154 DAVIS, A M. 1982.
Dynamic-static properties of sedimentary materials.
PhD thesis, Department of Physical Oceanography, University College
of North Wales. Unpublished.
- 155 HINGORANI, N G and JAVAID, A. 1967.
Firing of series connected thyristors in HVDC converters.
IEEE summer power meeting. Paper 31, CP 67-496.

TEST	WATER LEVEL	DRILLING & CASING PROGRESS	DISCONTINUITIES	FRACTURE SPACING INDEX m	POINT LOAD INDEX MN/2500	CORE SIZE RUNS DEPTH m	CORE RECOVERY %	SAMPLING	DESCRIPTION OF STRATA	OD LEVEL	B.H. No. :		
											MC %	SC %	LO
100									IGS 907 4000 10/73				
						12			white/grey blotchy chalk Staining and spotting decreasing in extent with depth.		17.0	92.9	
						13			Proportion of natural fracture decreasing, drilling induced fractures increasing.		17.9	92.9	
						14			A more massive appearance. Some shelly fossils present at 13.40 m, 13.70 m.		18.1	90.9	
						15					18.5	88.4	
						16					18.2	87.2	
			CORE LOST			17			10cm thick band of putty chalk inclined at 60° irregular 1cm band of brown clay at interface. Suggestive of slickensides		17.5	98.0	
						18			2cm band of brown clay filling 45° induced fissure		17.2	92.3	
						19			white/grey blotch chalky Staining spotting decreasing with depth.		18.5	91.0	
						20			Natural fractures and drilling induced fractures present in about equal numbers.		17.5	86.1	
						21			1cm horizontal band of putty chalk		18.2	88.9	
						22					15.8	93.5	
						23			Blotchy grey/white chalk. Staining and spotting slight and intermittent. Spotting shows dendritic form in places.		17.4	88.8	
						24			occasional sub horizontal dark grey wispy structures.		19.3	84.0	
						25							

MARKS

APPENDIX II

SEISMIC RESONANCE SURVEY

The only commercially available system in the UK based on the seismic resonance method is known as the SHRIMP system. The system consists of a P wave sweep generator and a matrix of accelerometers mounted on steel spikes as receivers. These accelerometers were laid out within a 20 m radius of the sweep generator and any vibrations within the vertical direction directly below the accelerometer will be detected by it. As the P waves are swept through the frequency range (3-200 Hz), they propagate downwards and outwards hemispherically. If a different structural impedance from that of the surrounding media is encountered, this surface begins to participate in the induced surface motion (resonate), requiring less driving force to maintain the acceleration at that particular frequency. In other words, on reaching the resonance frequency of the cavity, it oscillates with increased amplitude which can be easily detected.

The SHRIMP system uses two vehicles: one vehicle houses the transmitting (vibrator) equipment and the second contains the signal receiving instruments (Fig B:1). Once on site, the two vehicles are placed 20 m apart. The vibrator is positioned with the appropriate weights loaded on it to generate the required energy. The vibrations of the mass are coupled to the ground by a circular steel plate (50 cm diameter). On hard and dry ground, the coupling plate would have to be anchored to the surface with some sort of fixture (rawbolts for example), but on soft and wet ground, the plate would bury itself and provide a good coupling.

On the signal detection side, holes are made in the surface of about 40 cm diameter and 25 cm deep, to suppress the larger Rayleigh wave interfering with low frequency signals from a possible inclusion in ground. These holes are positioned to form a coarse matrix of about 5 m between holes. Steel spikes are driven into these holes and the accelerometers are mounted on the spikes. These accelerometers are covered with plastic spherical shells which act as windshields.

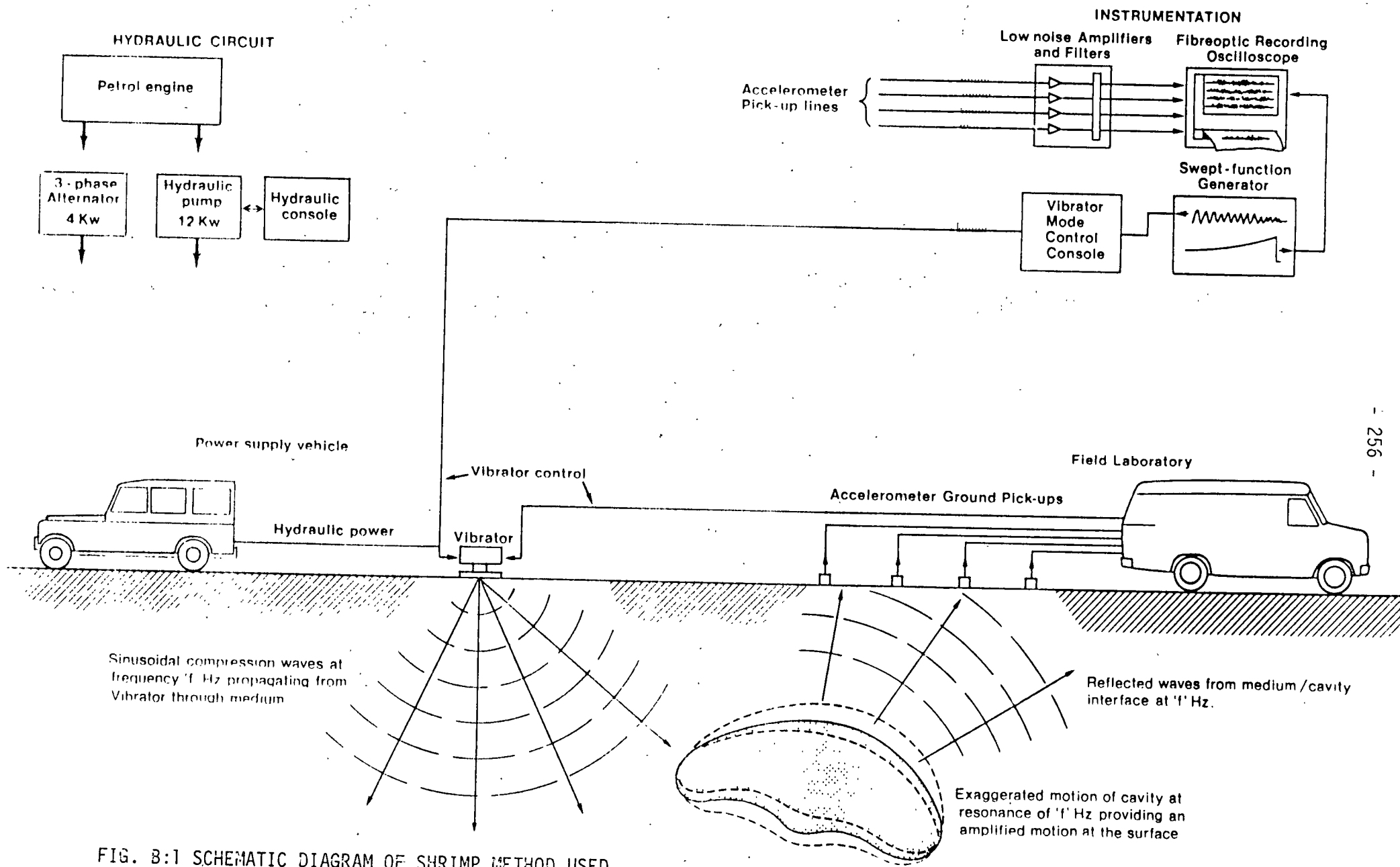
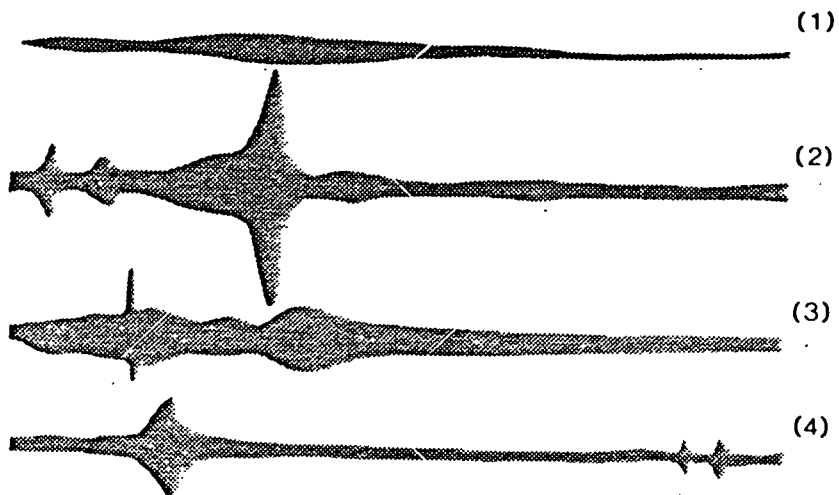
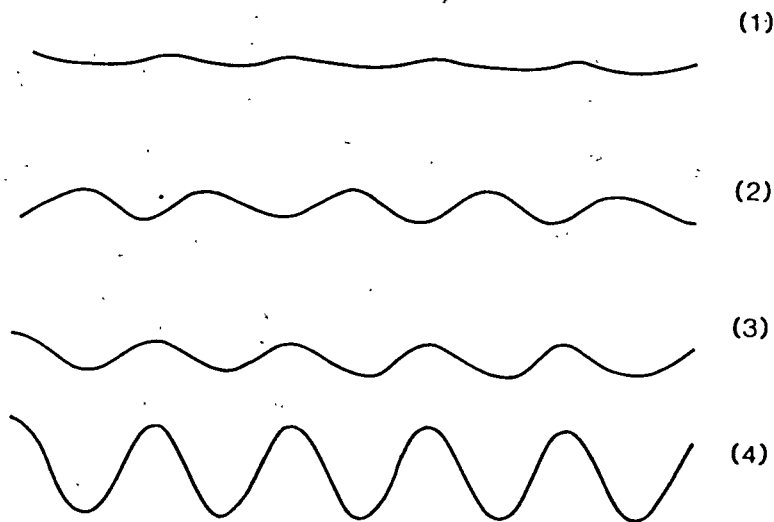


FIG. B:1 SCHEMATIC DIAGRAM OF SHRIMP METHOD USED TO DETECT THE PRESENCE OF CAVITY

The vibrator's sweep frequency is controlled by the function generator. As the vibrator sweeps from 3-200 Hz, signals from each accelerometer are examined in turn to see if there is a resonance at any particular frequency (Fig B:2). Initially, a coarse grid map is drawn showing areas of significant resonance, and following this these areas are examined in detail by repeating the whole procedure with a fine matrix of about 1 m separation over the areas. This last detailed survey would give some indication to the size of the cavity looking down at it from the surface (plan view), but not the depth. The depth of the cavity and the distance of the cavity from the surface would have to be investigated by the normal drilling process.



(a) Signals from 4 Accelerometers with Vibrator in Sweep Mode (3 - 120 Hz)



(b) Signals from the Same 4 Accelerometers with Vibrator Tuned to Resonant Frequency of No. 4 Accelerometer (28 Hz)

FIG. B:2 TYPICAL FIELD RESULTS FROM THE SHRIMP SYSTEM

DESIGN OF A HIGH VOLTAGE CAPACITOR DISCHARGE UNIT

Introduction

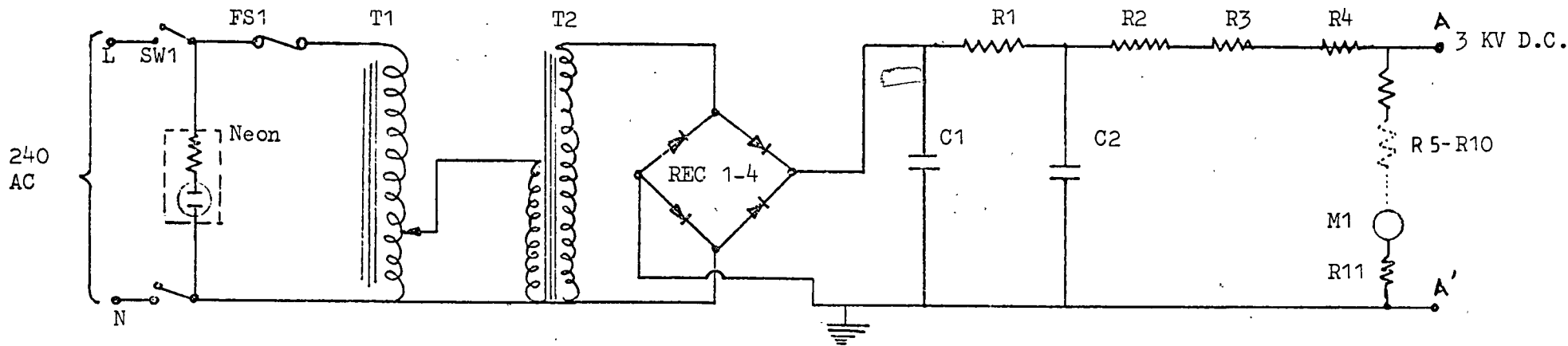
The seismic pulse is generated by discharging a high voltage capacitor across a gap in a cylinder containing a saturated solution of sodium chloride. High voltage is selected because the energy stored in a capacitor is $\frac{1}{2}CV^2$, ie the energy stored goes up by the square of the voltage increased. This also reduces the size of the capacitor that would have to be used to store the same amount of energy at a lower voltage. Stored energy in the capacitor is discharged across the sparker gap, using a series string of thyristors as a switch.

A unijunction transistor is used as a relaxation oscillator. The pulse from the unijunction transistor is shaped using a Schmitt Trigger and then applied to the base of a high gain Darlington pair. The primary of the pulse transformer is connected between the positive rail and the collector of the Darlington pair. The three secondaries of the pulse transformer are connected across the gate and cathode of the three thyristors, thus triggering all three thyristors simultaneously when a pulse is applied to the primary winding of the pulse transformer.

High voltage DC supply (0-3 KV)

The 240V AC supply is applied to a variable autotransformer (T1) through a double pole switch SW1 and a 250 mA fuse (FS1), as shown in Fig A:1. the wiper of the autotransformer is connected to the primary of the step-up transformer (T2). The output from the transformer is rectified by LA60 rectifiers, and after smoothing by C1, R1 and C2 is passed to the positive output terminal. Resistors R2, R3 and R4 limit the output current under short circuit conditions to 20 mA. Meter M1, in the divider chain R5-R11, indicates the voltage at the output terminal of HV DC supply.

All the components are mounted on a good quality resin board and a minimum air gap of 5 mm is allowed between the components and HV and the earth. All the interconnections between HV components are made by HT cable (red).



- SW1 2 Pole single throw 1 Amp
- FS1 250 mA Cartridge fuse
- T1 Variable auto transformer 1 Amp
- T2 Step-up transformer Input 240V AC
Output 3000V AC
- M1 100 μ A F.S.D. meter
(R.S.-MR 22S)

- REC 1-4 High voltage rectifiers LA 60
(International Rectifiers)
- C1 0.1 μ F 4KV D.C. WKG
- C2 1 μ F 4KV D.C. WKG
- R1 - R4 50K Ω , 15W, 5% W/W
- R5 - R11 4.3M Ω , $\frac{1}{2}$ W, 5%

FIG. A:1 H.V. D.C. SUPPLY

Capacitor bank and trigger unit

Capacitor C3 in Fig A:2 is used as the stored energy to be discharged across the spark gap. Although the term capacitor bank does not apply in these circumstances, the initial hopes were to have a set of capacitors which could be switched into the circuit depending on the amount of energy required. The lack of space in the instrument case and the difficulty in obtaining high voltage rotary switch made this impractical.

The maximum voltage across the capacitor is 3000V, while the maximum voltage rating of the thyristors is 1400V. This would require three thyristors to be connected in series.

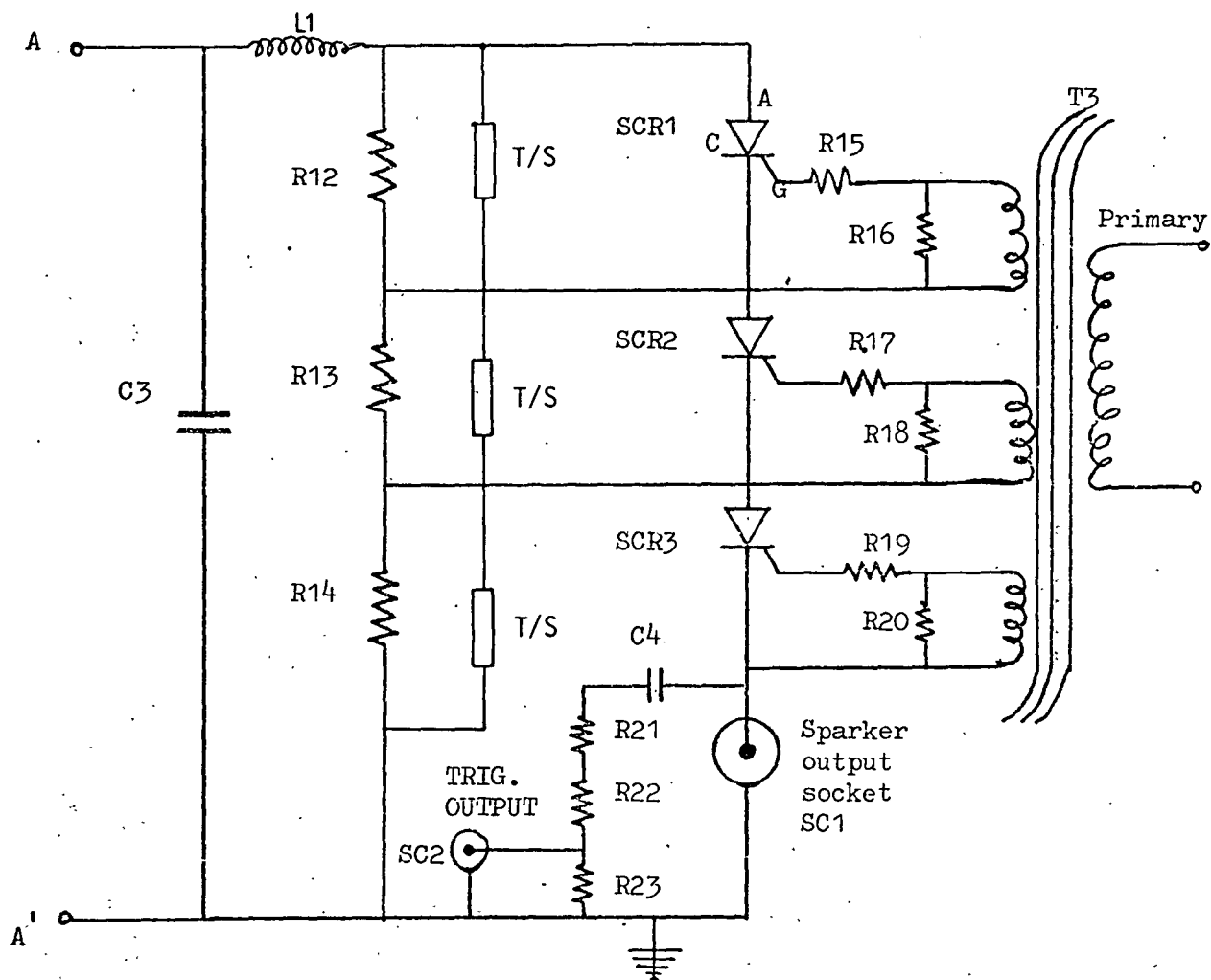
When thyristors are connected in series to form a high voltage switch, it is essential to ensure that no thyristor is subjected to excessive voltage under either static or dynamic conditions (Refs 37, 38). The distribution of the static part of the switch commutating voltage among the thyristors within the switch is governed by the leakage resistance of thyristors. However, this resistance will differ from unit to unit, due to the normal spread in their characteristics. Therefore, external measures have to be taken to force equal voltage distribution among the thyristors. A common method of achieving equal voltage distribution is to provide voltage dividing resistors in parallel with each of the thyristors. For reasons of standardisation, a common value of voltage equalising resistor (12, 13, 14) is chosen across thyristors, and the value is calculated from knowledge of variation in the leakage resistance of thyristors, and the maximum permissible voltage across a single thyristor.

Values of the shunt resistors can be calculated from the equation

$$R_s = (N_s V_A - V_{1N}) / (N_s - 1) I_R \quad - (A:1)$$

where

- R_s = shunt resistor
- N_s = number of devices in series
- V_A = rated device voltage
- V_{1N} = voltage across series string
- I_R = leakage current (see Note 1)



C3 0.25 uF 4KV WKG D.C.

C4 0.47 uF 100 V WKG MICA

R12-R14 100KΩ 10W W/W 5%

R15 2.2Ω ½W 5%

R17 1.1Ω ½W 5%

R19 2.2Ω ½W 5%

R16, R18, R20 1KΩ ½W 5%

R21, R22 470KΩ ½W 5%

R23 5KΩ ½W 5%

L1 100μH

T/S Transient suppressor
1400 V

SCR1 - SCR3 A.E.I. CR6/1403 RBA Thyristors
(See Appendix 4 for details)

SC1 U.H.F. Socket

SC2 B.N.C. Socket

FIG. A:2 CAPACITOR DISCHARGE UNIT

Note 1

I_R is the value of forward or reverse leakage current, whichever is the greater. This value can be modified to cover only the range of expected leakage current at the voltage the device is required to withstand, I_R .

Substituting values $N_S = 3$, $V_A = 3000V$, and $I_R = 5 \text{ mA}$ yields $R_S = 120 \text{ K}$ and a power rating of $I^2R = 10 \text{ W}$. The nearest available value is 100 K, 10 W.

Any transient voltage condition that the thyristors may experience is taken care of by capacitor C3 (which provides an AC path to earth), and the transient suppressors (TS) across each thyristor.

The thyristors are switched off as soon as the anode current falls below the minimum holding current of the thyristors.

In a series chain, since each thyristor is at a different potential level, it is obvious that their adoption presents difficulties of firing. The firing pulses, which are generated by the control circuit near ground potential, have to be transmitted to the gate-cathode terminals, which are elevated at high potential. One of the methods to achieve this isolation is to use a pulse transformer (Ref 77).

Transformer T3, shown in Fig A:2, is such a pulse transformer. The construction detail is described later in this chapter. The resistance R15 (R17 and R19) is chosen such that maximum current in it, assuming thyristor input resistance to be zero, is within the rating of the thyristor gate, transistor Q5 in Fig A:3 and the power supply to Q5.

R16, R18 and R20 are chosen to limit interference to a safe level. The most common interference source is the thyristor power circuit. When the main supply switch is closed, there is a sudden change of voltage on the thyristor cathode. This causes current to flow through the interwinding capacitance of the pulse transformer.

If there are variations in output of the secondary winding of the pulse transformer, R15, R17, R19 and R16, R18 and R20 can be adjusted to give the same output from each of the secondary windings of the thyristors, so that all the thyristors are fired at the same voltage and power.

A 10V pulse is provided through a series chain C1, R21, R22 and R23 to trigger the cathode ray oscilloscope externally.

Pulse transformer construction

A pulse transformer was required with one primary and a secondary to fire the three thyristor gates, which were at different potentials.

Most commercial pulse transformers did not have the high insulation required between the windings. The insulation between the primary and the secondaries had to withstand a potential of 3000V DC, and the maximum potential between the secondaries' windings was 2000V DC.

The only ferrite rings available were Mullard FX 1588. Two of these ferrite rings were used. They were taped together in four places by $\frac{1}{2}$ in P.V.C. insulation tape, and then a few layers of P.T.F.E. tape were wound on top of the P.V.C., followed by a few turns of P.V.C. insulation tape on top of the P.T.F.E. tape, as shown in Fig A:3.

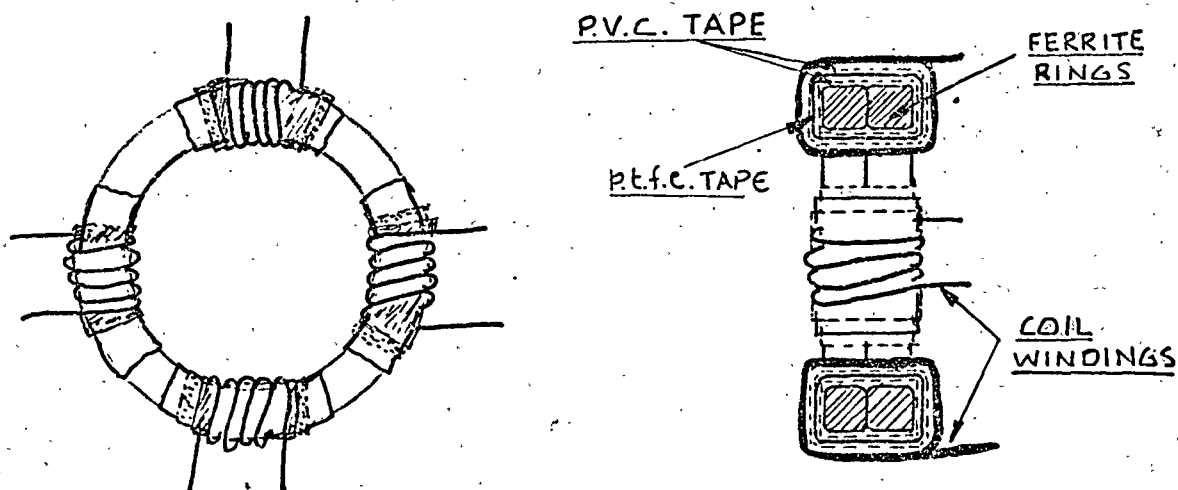


FIGURE A:3 PULSE TRANSFORMER

Thirty turns of 30 S.W.G. enamelled copper wire were wound on top of the P.V.C. tape, making sure that the coils were lightly wound and the direction of windings was the same for all the four windings.

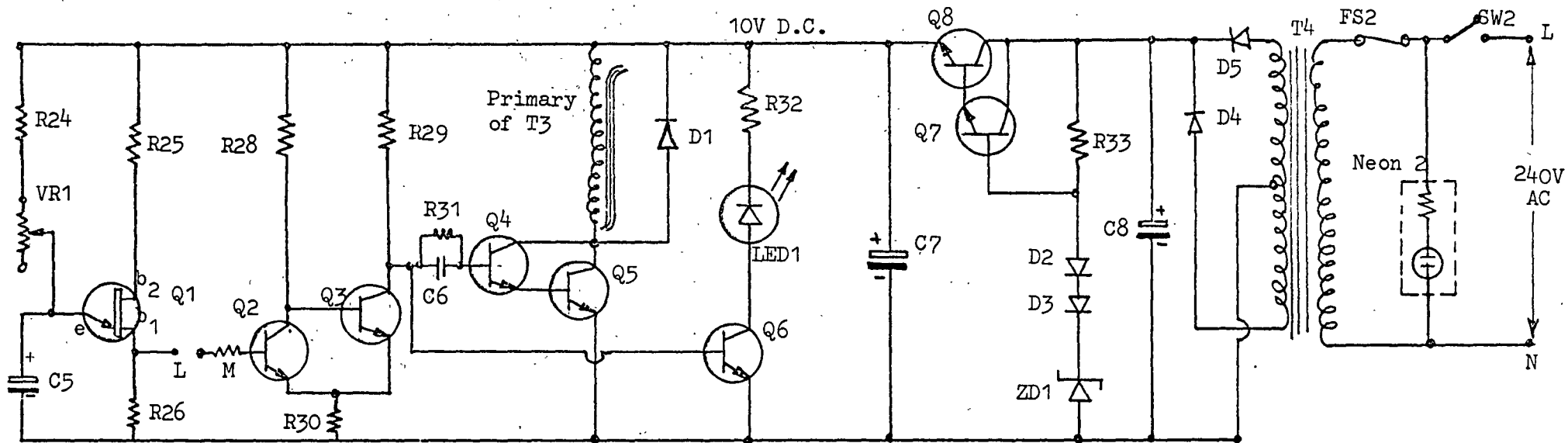
The entire assembly was potted in Araldite.

Pulse generator

Unijunction transistor Q1 is used as a relaxation oscillator, as shown in Fig A:4. When a voltage is applied to the circuit, capacitor C5 starts to charge up through R24 and VR1. Initially the emitter of Q1 will be at earth potential, but as capacitor C5 charges, the voltage at this point rises. When it reaches a certain point (about 4.5V in this case), b1 and b2 are virtually short-circuited and current will pass through R25, R26 and Q1. At the same time, C5 will discharge through R26 and the device will become open circuit again. The same process will start all over again, so that a series of pulses appears across R26. The output is in the form of a positive going pulse. If a negative going pulse is required, the output can be taken from b2 through a 0.1 F capacitor. A sawtooth wave form is available from the emitter, but it should only be connected to a high impedance load; otherwise operation of the relaxation oscillator will be affected.

The frequency of the pulses depends on the relationship of the resistance made up from VR1, R24 and capacitor C5. Larger values of capacitor will increase the time interval between the pulses, while smaller values of capacitor will decrease intervals between the pulses (ie, increase the frequency). Resistor R24 limits the current through the emitter, so that it cannot be connected directly to the positive rail; this would cause damage to the device.

Output from the unijunction transistor is applied to the base of Q2, through the selector switch SW3. Q2, Q3, R28, R29 and R30 form a Schmitt Trigger. In the normal state no input is provided and Q2 is therefore in the off state, and since $V_{C2} = V_{CC}$ Q3 is switched into hard saturation. When a positive voltage is gradually increased at the input terminal, a point will be reached when Q2 will switch on. The circuit current in the off state of Q2 is given by



R24 22K 1/2W 5%
 R25 2.2K 1/2W 5%
 R26 100Ω 1/2W 5%
 R27 5.6K 1/2W 5%
 R28 10K 1/2W 5%
 R29 5.6K 1/2W 5%
 R30 50Ω 1/2W 5%
 R31 1K 1/2W 5%
 R32 560 1/2W 5%
 R33 1K 1/2W 5%

C5 10 uF 16V D.C. Elec.
 C6 0.068 25V
 C7 3000 uF 16V Elec.
 C8 1250 uF 16V Elec.
 VR1 1M LOG. POT.

D1-D5 1N4003
 ZD1 10V Zener 400 mW
 LED Ind. R/S
 Q1 2N2646
 Q2-Q4, Q6 BC 149
 Q5, Q8 2N3055
 Q7 BC149

T3 Pulse transformer (Fig.A3)
 T4 240V AC - 9V AC out
 FS2 100 mA
 SW2 Single pole
 Single throw

FIG. A:4 PULSE GENERATOR

$$I_{C3 \text{ sat}} = V_{CC}/(R29+R30) \quad - (A:2)$$

as only 0.1V is dropped by $V_{CE3 \text{ sat}}$. From this the triggering voltage to switch Q2 into the on state may be determined by

$$V_{\text{trig (on)}} = (V_{BE2} + R30.V_{CC})/(R29+R30) \quad - (A:3)$$

When Q2 switches on, V_{C2} drops to $V_{CE2 \text{ (sat)}} + V_{R30}$. There is not sufficient voltage to support V_{BE3} , and thus Q3 is cut off, causing a positive going output at B, with a corresponding negative going output at the collector of Q2. Since both transistors share the same emitter resistor, during the actual switching operation, as the input pulse causes the Q2 collector to go negative, I_{C3} starts to reduce at the same moment that I_{C2} starts to increase. The reduction of emitter current in Q3 encourages the current to be transferred to the emitter which is now opening up, that of Q2. A regenerative effect thus occurs, the switching off of Q3 speeding up the switching on of Q2. Q2 will stay in the conducting state for as long as a positive voltage is applied at the input. If this voltage is reduced, Q2 will switch off as soon as its V_{BE} is not supported. The switching off of Q2 speeds up the switch on of Q3 and again fast edges are realised.

Output from the Schmitt Trigger is applied to the base of Q4 through R31 and C6. Q4 and Q5 form a high gain Darlington pair. The primary coil of the pulse transformer T3 is connected across the positive rail and the collector of Q5. When a positive pulse is applied to the base of Q4, Q5 conducts heavily and is saturated. This energises the primary of T3 and causes a positive pulse output on the three secondaries of the pulse transformer. D1 chops the negative going pulse when Q5 is turned off.

Light emitting diode LED 1 acts as a visual indicator every time a pulse is fired. Q6 drives LED 1 and R32 is the stand-off resistor to take the excess voltage.

Power to the pulse generator is provided by step-down transformer T4. The low voltage AC output is rectified and smoothed by D4, D5 and C8. This unregulated output is stabilised by using a series regulator. Q7, Q8, R23, D2, D3 and ZD1 form the series regulator. ZD1 is the reference element and D2 and D3 are used to compensate for the increase in V_{BE} of

Q7 and Q8 due to temperature rise. C7 provides the energy required during the conducting cycle of the primary of the pulse transformer T3.

External triggering and single shot facility

The external triggering facility is provided by inserting a rotary switch SW3 between output 'L' of the Q1 and input 'M' of the Schmitt Trigger, as shown in Fig A:5. Any external pulse will have to be from medium to low impedance output.

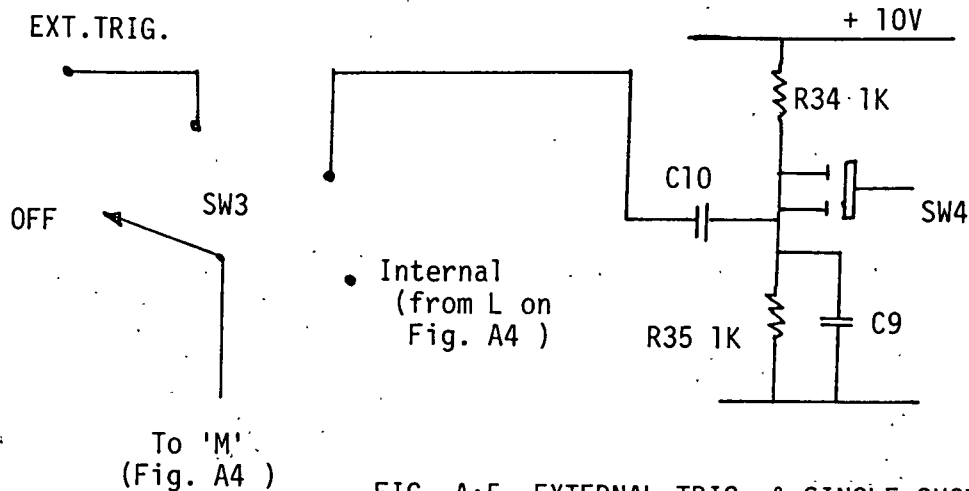


FIG. A:5 EXTERNAL TRIG. & SINGLE SHOT FACILITY

When push button switch SW4 is pressed, C9 charges through R34, giving a positive pulse out through C10 and SW3 to the input of Schmitt Trigger 'M'. The height of the pulse is the same as that from the unijunction transistor, ie 5V. R35 discharges the capacitor as soon as the push button switch is released.

APPENDIX IV

```

10  OPTION BASE 1
20  COM A,B,R,Lamda,Theta,P(300)
30  !
40  BEEP
50  INPUT "Input A, R, B and Lambda",A,R,B,Lamda
60  !
70  RAD
80  Mx=0
90  X=PI*B/Lamda
100 N=0
110 FOR I=0 TO 90
120     N=N+1
130     Theta=I*PI/180
140     Y=SIN(X*SIN(Theta))
150     IF Y=0 THEN Theta=Theta+.01*PI/180
160     P(N)=2*A*(SIN(2*X*SIN(Theta))/(2*SIN(X*SIN(Theta))))/R
170     P(N)=ABS(P(N))
180     IF P(N)>Mx THEN Mx=P(N)
190     ! GOTO 270
200     IF I>0 THEN 250
210     OUTPUT 0 USING "10/"
220     OUTPUT 0;"A=";A;" R=";R
230     OUTPUT 0;"LAMBDA=";Lamda;" B=";B
240     !
250     IF I MOD 2=0 THEN OUTPUT 0;I,P(N)
260     IF I=90 THEN OUTPUT 0 USING "#,B";12
270     NEXT I
280     PLOTTER IS "GRAPHICS"
290     GRAPHICS
300     SCALE -90,90,0,Mx
310     MOVE 90,0
320     PLOT -90,0,-1
330     MOVE 0,0
340     PLOT 0,Mx,-1
350     MOVE -90,P(N)
360     K=N
370     FOR I=-89 TO 0
380         K=K-1
390         PLOT I,P(K),-1
400     NEXT I
410     K=0
420     FOR I=1 TO 90
430         K=K+1
440         PLOT I,P(K),-1
450     NEXT I
460     OUTPUT 0 USING "12/"
470     OUTPUT 0;"A=";A;" R=";R
480     OUTPUT 0;"LAMBDA=";Lamda;" B=";B
490     OUTPUT 0;"MAXIMUM=";Mx
500     DUMP GRAPHICS
510     OUTPUT 0 USING "#,B";12
520     END

```